**Quasi-static dispersion of dusts for the measurement of safety characteristics of hybrid mixtures**

**Dissertation**
zur Erlangung des akademischen Grades

**Doktoringenieur**
**(Dr.-Ing.)**

von Zaheer Abbas

geb. am 01.08.1985 in Peshawar, Pakistan

genehmigt durch die Fakultät für Verfahrens- und Systemtechnik) der Otto-von-Guericke-Universität Magdeburg

Gutachter/innen:

Prof. Dr. -Ing. habil. Ulrich Krause

Prof. Dr. Jordan Hristov

Dr. -Ing. Arne Krietsch

Promotionskolloquium am 17.02.2025

## ABSTRACT

Knowledge of the explosion limiting concentrations of explosible materials is necessary for the design of explosion protection measures. Currently employed methods of testing the minimum explosible concentration (MEC) of a dust cloud or the lower explosion limit (LEL) of a hybrid mixture are based on arbitrary assumptions and possess technical limitations that often lead to values of MEC/LEL which are unrealistically low or poorly reproducible. The lack of reliable experimental data of the LEL of hybrid mixtures has led to the development of theoretical models that, as a quick solution, calculate the LEL of hybrid mixtures based on single component data.

This research work presents a state-of-the-art method for the experimental determination of the MEC of a combustible dust cloud or the LEL of a hybrid mixture. The new setup operates under laminar flow conditions and allows a uniform suspension of dust particles in an open top acrylic glass tube. Dust cloud is ignited in a quasi-static state to eliminate the influence of the flow regime on the ignition and combustion propagation. The dust concentration is measured with the help of infrared sensors installed a few centimetres above and below the ignition source.

In order to evaluate the possible influence of flow velocity and ignition energy, the LEL of hybrid mixtures of lycopodium and titanium with methane have been measured at four and two flow front velocities, respectively, and three ignition energies. The results suggest small variations in the LEL, which, under the consideration of measurement uncertainties, have been regarded negligible.

Based on the mass balance of the fuel mixture and the enthalpy balance of the whole system, a simple mathematical model for the calculation of the LEL of hybrid mixtures has been derived. The theoretically calculated values of the LEL of hybrid mixtures agreed well with the experimental data. By analyzing the modelled as well as the experimental values, it can be concluded that the LEL values of the individual components in a hybrid mixture set the upper and lower limit for the LEL of a hybrid mixture, provided that the results are presented in molar units. How the LEL of a hybrid mixture changes within these limits with respect to the change in the mixture composition depends on the interaction of dust and gas during the combustion.

The ignition and combustion propagation mechanism in lean hybrid mixtures has been investigated utilizing high-speed videos. The analysis of the videos revealed that in lean hybrid mixtures of volatile dusts the ignition kernel does not develop into an autonomously growing reaction zone, but rather serves as an ignition source for the rest of the fuel. Contrary to the general perception, in hybrid mixtures at their LEL, the combustion propagation speed does not increase by increasing the relative amount of gas in the system.

## ZUSAMMENFASSUNG

Die derzeit verbreiteten Methoden zur Bestimmung der unteren Explosionsgrenze (UEG) einer Staubwolke oder eines hybriden Gemisches beruhen auf unrealistische Annahmen und weisen technische Beschränkungen auf, die häufig zu ultrakonservativen oder schlecht reproduzierbaren Werten der UEG führen. Der Mangel an zuverlässigen experimentellen Daten der UEG hybrider Gemische führte zur Entwicklung empirischer Modelle, welche zur Vereinfachung die UEG der hybriden Gemische auf Grundlage der UEG der einzelnen Komponenten berechnen.

In dieser Forschungsarbeit wird eine dem Stand der Technik entsprechende Methode zur experimentellen Bestimmung der UEG einer brennbaren Staubwolke eines hybriden Gemisches vorgestellt. Der neue Versuchsaufbau arbeitet unter laminaren Strömungsbedingungen und ermöglicht eine gleichmäßige Verteilung von Staubpartikeln in einem freibelüfteten Acrylglasrohr. Die Staubwolke wird in einem quasi-statischen Zustand entzündet, um den Einfluss der Strömungsverhältnisse auf die Zündung und die Flammenausbreitung zu verhindern. Die Staubkonzentration wird mit Hilfe von Infrarotsensoren gemessen, die einige Zentimeter über und unter der Zündquelle angebracht sind.

Um den Einfluss von Strömungsgeschwindigkeit und Zündenergie zu bewerten, wurde die UEG von Hybridgemischen aus Lycopodium und Titan mit Methan jeweils bei vier und zwei Strömungsgeschwindigkeiten und drei Zündenergien gemessen. Die Ergebnisse deuten auf geringe Schwankungen der UEG hin, die unter Berücksichtigung der Messunsicherheiten als vernachlässigbar angesehen werden können.

Auf Grundlage der Massenbilanz des Brennstoffs und der Enthalpiebilanz des gesamten Systems wurde ein einfaches mathematisches Modell für die Berechnung der UEG von Hybridgemischen abgeleitet. Die vom Modell berechneten Werte der UEG von Hybridgemischen stimmten gut mit den experimentellen Daten überein. Die Analyse der modellierten und der experimentellen Werte lässt den Schluss zu, dass die UEG-Werte der einzelnen Komponenten im Hybridgemisch die Ober- und Untergrenze für die UEG des Hybridgemischs festlegen, sofern die Ergebnisse in molaren Einheiten dargestellt werden. Wie sich die UEG von Hybridgemischen innerhalb dieser Grenzwerte bei wechselnder Gemischzusammensetzung verändert, hängt von der Wechselwirkung von Staub und Gas während der Verbrennung ab.

Die Zündung und Flammenausbreitung in mageren Hybridgemischen wurde mit Hilfe von Hochgeschwindigkeitsvideos untersucht. Die Analyse der Videos ergab, dass sich in mageren Hybridgemischen aus flüchtigen Stäuben der Zündkern nicht zu einer eigenständig wachsenden Flamme entwickelt, sondern vielmehr als Zündquelle für den Rest des Brennstoffs dient. Entgegen der allgemeinen Auffassung nimmt die Flammengeschwindigkeit in hybriden Gemischen bei ihrer UEG nicht zu, wenn die relative Gasmenge im System steigt.

## TABLE OF CONTENTS

## LIST OF FIGURES

## LIST OF TABLES

## ABBREVIATIONS

| | |
|---|---|
| Approx. | approximately |
| ASTM | American Society for Testing and Materials |
| BAM | Federal Institute for Materials Research and Testing |
| DAQ | Data acquisition |
| DIN | German Institute for Standardization |
| EN | European standard |
| ISO | International Organization of Standardization |
| LEL | Lower explosion limit |
| MEC | Minimum explosible concentration |
| Mol. | Mole |
| ms | millisecond |
| NFPA | National Fire Protection Association |
| NI | National Instruments |
| SEM | Scanning Electron Microscopy |
| SKG 5 | dust concentration meter |
| VDI | Association of German Engineers |

# 1 Introduction

In industries that manufacture, process, or use combustible materials (dusts, gases, solvents and/or their mixtures), an accurate assessment of the explosion risk associated with the use of these materials is a major challenge.

In December 1999, aiming to improve the safety of workers who are exposed to explosive environments, the European directive 1999/92/CE (also known as ATEX 137) was released. According to article 3 of this regulation the employer is obligated to take technical and/or organisational measures appropriate to the nature of operation, in order of priority and in accordance with the following basic principles:

- the prevention of the formation of explosive atmospheres, or where the nature of the activity does not allow that,
- the avoidance of the ignition of explosive atmospheres, and
- the mitigation of the detrimental effects of an explosion so as to ensure the health and safety of workers.

These measures shall, where necessary, be combined and/or supplemented with measures against the propagation of explosions and shall be reviewed *regularly* and, in any event, whenever *significant changes* occur [1]. A quantitative description of “regularly” and “significant changes” is not provided in ATEX 137 and should be manifested in the national legislations of EU member states. ATEX 137 is addressed to the EU member states, which are thus bound to implement (at the minimum) the requirements defined by this directive in their national legislation.

In Germany, this directive has been implemented into the Federal law through the Hazardous Substances Ordinance (GefStoffV) and the Ordinance on Industrial Safety and Health (BetrSichV).

According to § 6, Section 9 of the Hazardous Substances Ordinance, the employer (industries where combustible materials are handled) is obligated to conduct an explosion risk assessment and document a protection concept against explosion hazards in the form of a so-called explosion protection document. In order to ensure that the explosion protection document is up to date and that the protection measures are functional and reliable, the Ordinance on Industrial Safety and Health (in its Annex 2, Section 3) obligates the employer to carryout recurring inspections.

According to the Hazardous Substances Ordinance, a comprehensive explosion protection document must include measures with respect to primary (preventing the existence of an explosive atmosphere), secondary (inhibiting the occurrence of an ignition source) and/or tertiary (limiting the consequences of an explosion) explosion protection. These measures are designed on the basis of a system of

characteristic data, which describe the explosion sensitivity and explosion severity of the material under consideration. One of these characteristic parameters is the explosion limiting concentration of the combustible material, referred to as minimum explosible concentration (MEC) for particulate materials and lower explosion limit (LEL) in case the combustible material is a gas/vapour or a mixture of dust and gas/vapour, also known as a hybrid mixture.

When designing an explosion protection concept, the highest priority is given to the primary explosion protection, which essentially means to either replace the combustible material with a non-combustible one (which is almost always not feasible due to material specific processes) or limit the concentration of the flammable material in non-explosible range. The latter can only be achieved if reliable values of MEC or LEL are known. The MEC or LEL of an explosible material (like other safety parameters) is not, as a rule, constant of nature but a value, which is determined under fixed boundary conditions. This leads to the use of standardized measuring apparatuses. Currently employed methods of testing MEC of a dust cloud are based on arbitrary assumptions and possess technical limitations that often lead to values of MEC which are unrealistically low or poorly reproducible. Protection measures designed on the basis of ultraconservative and poorly reproducible values are, on one hand, expensive to be implemented and, on the hand, due to their inherent underlying uncertainties, prone to failure.

For the experimental determination of LEL of hybrid mixtures, no standard device or protocol has been defined so far. While evaluating hybrid mixture explosion hazard, the current state of the art (VDI 2263 part 5) states that if the concentration of the gas in a hybrid mixture is above 20% of its LEL, occurrence of a hybrid mixture should be considered [2, 3]. However, the decrease in the concentration of the dust with respect to the added concentration of the gas/vapor has not been addressed in any of the current regulations e. g. Technical Rules for Hazardous Substances (TRGS) and/or Standards. Furthermore, there exists no specific guideline on how to assess, prevent and mitigate the risk associated with the handling of the explosible hybrid mixtures.

This research work presents the results of the experimental as well as theoretical investigations aimed at improving the understanding of the explosion behaviour of the hybrid mixtures, where the individual concentration of each component is below their respective MEC/LEL.

In what follows, a brief summary of the relevant literature and the current understanding of hybrid mixture explosion behaviour are treated in Chapter 2. Chapter 3 is dedicated to the experimental approach, including the design of the new experimental apparatus and the description of the material properties. Chapter 4 explains a series of the preliminary experiments to check the reliability of measured concentration values, followed by the presentation of the experimentally measured values of the MEC of dusts and the LEL of hybrid mixtures. Chapter 5 describes the theoretical evaluation of the LEL of hybrid mixtures, including

derivation of a new model and a discussion on the comparison of the theoretically calculated LEL values with the experimental ones. Finally, the ignition and combustion propagation behaviour in the hybrid mixtures is explained in Chapter 6, followed by the conclusions and outlook in Chapter 7.

# 2 HYBRID MIXTURES

DIN EN 1127 – 1 defines hybrid mixtures as mixtures of air with flammable materials in different states of aggregates; mixtures of flammable gas with combustible dust, mist or spray [4]. Hybrid mixtures are encountered in several process industries including mining (coal dust and methane) [5], paint factories (pigments and solvents) [6], pharmaceutical industry (solid active principles or excipients and volatile organic vapour) [7] and textile manufacturing [8]. Hybrid mixtures could also be formed from the gases generated from overheated smouldering products, for example in fluidized bed installations, which in many cases are used to process flammable or decomposition prone products [9].

It is not clear from the literature who was the first researcher to investigate the change in the ignition sensitivity and explosion severity of a dust cloud by the introduction of a small amount of flammable gas. The first published research on the topic is of Engler who more than a century ago observed that mixing a non-explosible amount of coal dust (i.e. below its minimum explosible concentration) with methane at a concentration lower than its lower explosion limit could produce an unexpected hazardous environment that has the potential to explode with enormous release of energy, if an ignition source is present in the surrounding [10, 11]. Since then, several investigations have been carried out to understand the peculiar behaviour of hybrid mixtures [11-19]. By summarizing the main outcomes of these studies, one could conclude that the ignition sensitivity and explosion severity of a combustible dust strongly increase by the addition of a few percent of flammable gas, even with contents lower than its LEL. Moreover, hybrid mixtures can also be explosible when both the concentrations of the dust and the gas are lower than their respective MEC and LEL [12, 20-22].

This chapter presents a brief review of the literature relevant to the carried-out research work. It has been divided into two parts. The first part explains the contribution of the research community made so far regarding the understanding of the LEL of hybrid mixtures. This includes currently employed methods for the experimental determination as well as the models for theoretical evaluation of LEL of hybrid mixtures. The second part focuses on the current state of the art and the identification of the research gap regarding comprehension of the ignition and combustion propagation behaviour in hybrid mixtures.

## 2.1 Lower Explosion Limits of hybrid mixtures

The risk of hybrid mixture explosion is characterized by the probability of simultaneous occurrence of an explosible atmosphere and an effective ignition source and the consequences of such an explosion. Generally, to assess the probability of occurrence of an explosible hybrid atmosphere and an effective ignition source, knowledge of the lowest concentration of the hybrid mixture that

would enable a self-supporting flame propagation and the minimum energy of a spark discharge or the minimum temperature of hot surface, which would ignite the hybrid mixture, is required. The former is known as the lean flammability limit or lower explosion limit (LEL) of the hybrid mixture.

LEL of a combustible material is the lowest concentration of the combustible material, which upon combustion provides sufficient energy to activate the adjacent batch of molecules to react. The values of LEL of combustible materials used for designing the explosion protection measures are measured experimentally and are dependent on the initial and boundary conditions of these experiments. In order to have globally harmonized testing procedures and provide a basis for the comparison of results, these initial and boundary conditions have been fixed in the form of standardized measurement apparatuses and procedures. This is, however, only true for fuel components with a single state of aggregate mixed with air, for example, dust, gas or solvent vapours. For the measurement of LEL of hybrid mixtures, no standard device or procedure has been defined so far, which, on one hand, leads to the use of the standard apparatus for measurement of MEC of a dust cloud with a vast spectrum of inhouse modifications and, on the other hand, promotes the use of empirical relationships to estimate the LEL of a hybrid mixtures from the lean flammability limits of the individual components comprising the hybrid mixture.

In the next sections a brief review of the currently employed experimental and theoretical approaches for estimation of LEL of hybrid mixtures is presented.

### 2.1.1 Experimental determination of LEL of hybrid mixtures

As mentioned in the previous section, there exists no standard apparatus or procedure for the experimental measurement of LEL of hybrid mixtures. Almost all of the research work done so far on the subject made use of the standard apparatuses for the measurement of MEC of a dust cloud. EN 14034-3, ASTM E1515 and ISO 6184-1 describe the 1 $m^3$ chamber, which was introduced by Bartknecht [19], as the standard apparatus for the measurement of MEC of a dust cloud [23, 24]. In order to achieve cheaper and faster tests, Siwek [25] developed the 20-l sphere, which was later accepted by the ASTM E1515 and EN 14034-3 as an alternative test equipment.

Both the 20-l sphere and 1$m^3$ chamber consist of a hollow stainless-steel sphere of 20 $dm^3$ and 1 $m^3$ respectively, a dust dispersion system comprising of a dust chamber, a quick-acting valve for dust transportation and a dispersion ring, an exhaust valve, a data acquisition unit and a pressure measurement system. Both apparatuses use pyrotechnical igniters installed at the center of the sphere as the ignition source. According to DIN EN 14034-3 two pyrotechnical igniters of each 5 kJ and 1 kJ should be used for 1 $m^3$ and 20-l sphere respectively [24]. Schematic diagrams of both devices are presented in Figure 2.1.

Standard experimental procedure for both systems includes deposition of a known mass of the dust in the dust chamber followed by the evacuation of the sphere to create underpressure in the sphere. In the next step, an automatic experimental sequence is started, which pressurizes the dust chamber to an overpressure of 20 bar and consequently disperses the dust in the sphere by opening the injection valve. After a certain delay time the ignition source is activated and overpressure values (as a result of the ignition) are recorded. Ignition criteria is a certain overpressure value depending on the device and the standard being followed. The process is repeated by gradually decreasing the concentration of the dust until the point is reached, where no explosion occurs for three consecutive test trials. The maximum concentration of the dust cloud where no ignition was recorded is considered to be the MEC of the dust. The test procedure for measuring the LEL of hybrid mixtures includes the insertion of the flammable gas as the only additional step. This is mostly done with the help of the partial pressure method, prior to the dust dispersion and after the evacuation of the chamber.

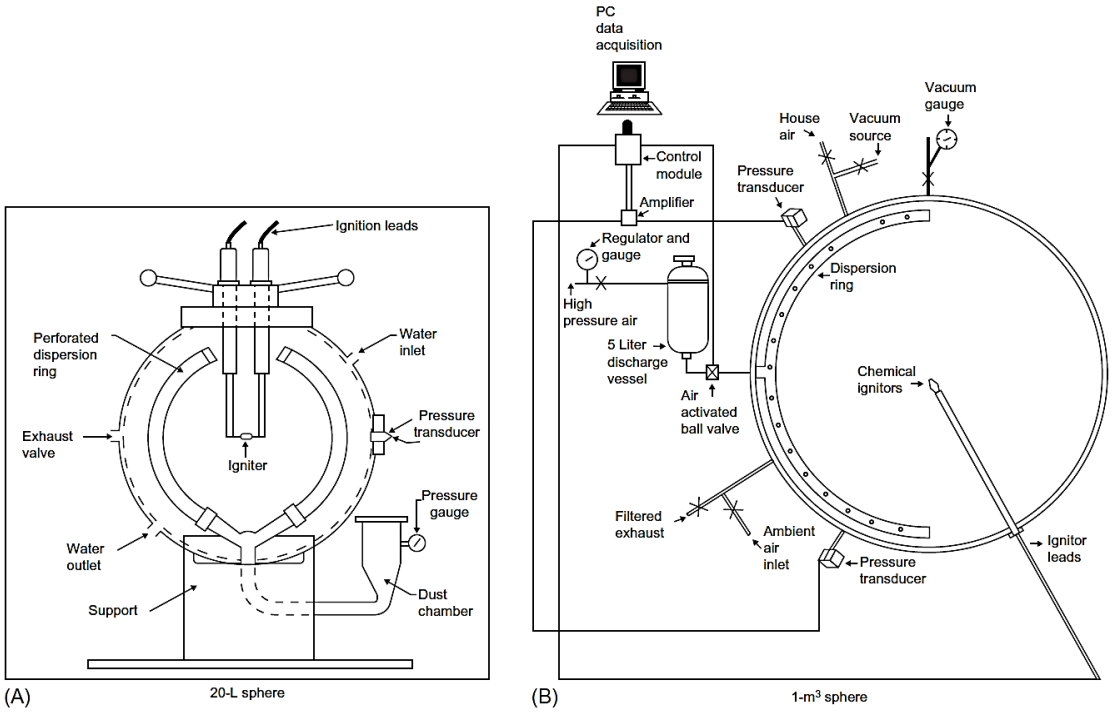


*Figure 2.1: schematic diagrams of 20-l (A) [26] and 1 $m^3$ (B) [17] spherical tests vessels*

Over past few decades, the use of the 20-l sphere has gained more popularity than the 1 $m^3$ vessel because of its cost effectiveness and relatively easier and quicker operation. However, the wide use of the 20-l sphere is accompanied by a number of sources of uncertainties related to the device configurations, experimental procedure and data treatment protocol, which often lead to values of MEC or LEL that are either unrealistically low or poorly reproducible [26]. A classic example in this regard is the MEC of corn starch in air, with the reported values ranging from 8 g/$m^3$ to 400 g/$m^3$, all measured using the standard 20-l sphere [11, 26, 27].

Results reported in literature for the LEL of hybrid mixtures also possess inconsistencies [28]. Hybrid mixture of starch and methane is one of the most commonly tested hybrid mixtures. Figure 2.2 provides a comparison of the decrease in starch concentration in the hybrid mixture with the addition of small amounts of methane, measured experimentally at three laboratories. Herein, the filled markers represent the ignition points, whereas the hollow markers represent the no-ignition points. Although the difference in the median particle size ($d_{50}$) of all three starch samples lied in a narrow range of ± 6 µm, conflicting conclusions were deduced. Jiang et al. claimed that the amount of the dust required to render the hybrid mixture of starch and methane explosible is higher than the one predicted by the Le Chatelier's mixing rule for flammable limits or the Bartknecht's curve [29]. Khalili et al., on the other hand, highlighted that the explosible concentration of the dust in a hybrid system is less, in comparison to the theoretically calculated value using Le Chatelier's rule, however, more than the concentration of dust predicted by Bartknecht's curve [30]. In contrast to the findings of Jiang et al. and Khalili et al., Addai et al. concluded in their research that the hybrid mixture of starch and methane is explosible in the concentration ranges even below the Bartknecht's curve [21].

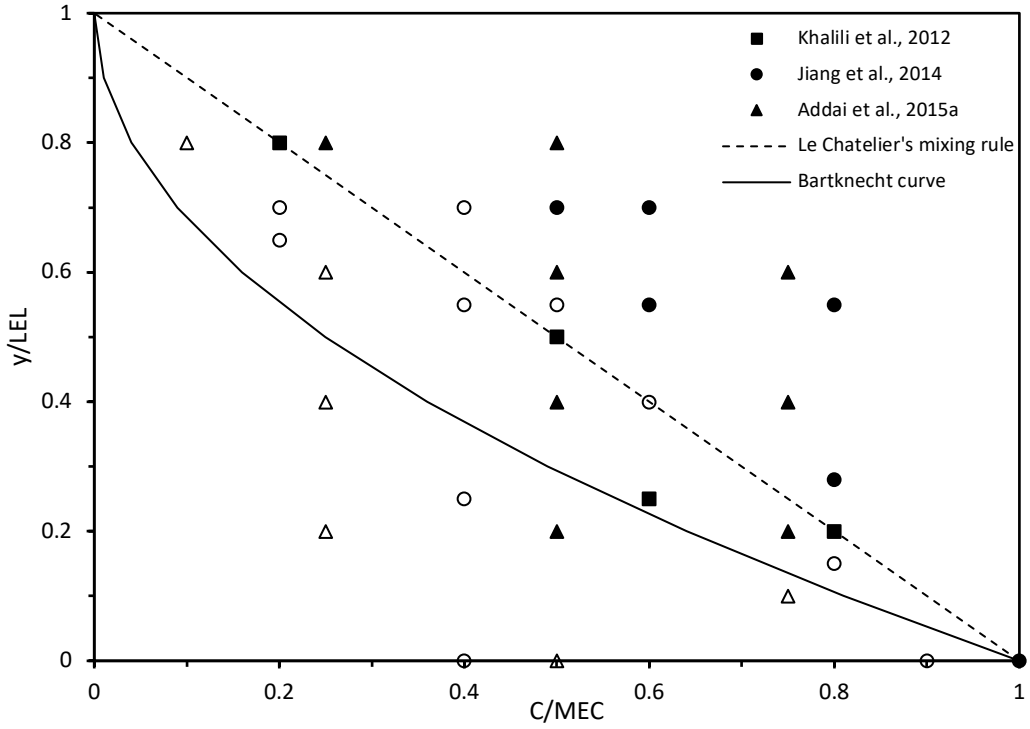


*Figure 2.2: LEL of hybrid mixture of starch and methane (reproduced using data from [21, 29, 30])*

The reasons behind these contradictory findings are the inherent sources of uncertainties or errors that make the results of these experiments stochastic in nature and consequently lead to a poor reproducibility. In what follows, some of the major sources of uncertainties associated with the use of the 20-l sphere according to the standard test protocol (DIN EN 14034-1) will be highlighted.

One of the fundamental flaws in the design of the 20-l sphere test procedure is the use of pyrotechnical igniters. DIN EN 14034-1 recommends using two chemical igniters each having an energy of 1 kJ, whereas ASTM E1515 advises measuring the MEC at 2.5 and 5 kJ. The composition and reactions of the pyrotechnical igniters have been described in detail by Hertzberg et al. and Taveau et al [31, 32]. LEL/MEC, by definition, is the lowest concentration at which a "*self-sustained flame propagation"* could be achieved. The activation of pyrotechnical igniters, irrespective of their energy content, creates a fireball of burning particles that is way bigger than the size of the sphere and practically covers the whole available space (see Figure 4.4) [32] . A self-sustained combustion propagation through a dust or a hybrid mixture cannot be achieved under these conditions and, as a consequence, each test is rather an igniter induced flame propagation. The overdriving effect of pyrotechnical igniters due to volumetric and/or multipoint ignition effects has been investigated by several authors. Further discussion on the topic could be found in [11, 32-39] and in section 4.2.1.

As part of the standard reporting protocol, particle size distribution of the tested dust shall be measured before the commencement of experiments and shall be included in the test report. It is a known fact that the reactivity of the dust particles increases with an increase in their specific surface area, which itself increases with decreasing the particle diameter. Several studies have been performed to investigate the impact of the high-pressure air blast dispersion (during the explosion experiments) on the particle integrity. The work of Bagaria et al., Du et al. and Kalejaiye et al. is of prime importance in this regard [43-45]. Kalejaiye et al. investigated the effect of dust dispersion system on particle breakage in the 20-l sphere by measuring the particle size distribution before and after dispersion. They performed a total of 540 tests at different nominal concentrations of three dusts, namely Gilsonite, purple K and Pittsburgh coal using the rebound and perforated annular dispersion nozzles and reported that the particle size after dispersion was about 50%, 80% and 40% of the original size for Gilsonite, purple K and Pittsburgh coal dust respectively. They attributed the particle size reduction to the unique design of the outlet (dispersion) valve and dispersion nozzle, which impose a strong shearing effect on the dust particles as they flow through. The effect of dust concentration on the extent of particle size reduction was found to be negligible. Bagaria et al. and Du et al. reported similar data in terms of particle size reduction during dispersion, however, contrary to the findings of Kalejaiye et al., they observed that there was a decrease in the particle breakage with increasing dust concentration, owing to the decreased probability of impact per particle. This suggests a maximum particle breakage at the concentrations near the MEC of the dust.

The experimentally determined MEC of a dust cloud decreases by decreasing the particle size. Since the specimen tested in the 20-l sphere has a notably smaller diameter distribution than the original specimen (due to particle breakage), the concentration of the dust that would otherwise not ignite shows an ignition

(pressure rise criteria) in the 20-l sphere because of increased surface area of the particle, which consequently results in overly conservative values of MEC.

DIN EN 14034-1 defines MEC/LEL of an explosible material as the lowest concentration of the material in mixture with air at which an explosion will occur. The same standard in Annex C.4 states that the highest concentration of a combustible dust at which no explosion occurs in three consecutive tests shall be taken as the MEC/LEL. Moreover, the test procedure is designed in a way that the highest non-explosible concentration is always 50% of the lowest explosible concentration. This means that if, for a given dust, there was an explosion recorded at 250 g/m$^3$ and a no-explosion at 125 g/m$^3$ (i.e. 50% of the preceding concentration) in three consecutive tests, according to the standard protocol the reported LEL/MEC would be 125 g/m$^3$. A decrease in the dust concentration with a 50% step is ultraconservative and could induce uncertainties of up to 30% of the reported MEC value, which does not agree with the information included in the test report stating that the results might deviate up to 10% [46].

Standard MEC/LEL apparatuses operate under high turbulence created by a 20 bar air blast, which serves to “homogenously” disperse the powder in the sphere. Since the position and dispersion of particles as well as turbulence levels in the test apparatus are all time dependent, the so-called ignition delay time, which refers to the time between the opening of the dispersion valve and activation of the ignition source, was introduced in the test procedure. DIN EN 14034-1 defines an ignition delay time of 600 ms for the 1 m$^3$ chamber and 60 ms for the 20-l sphere. This definition is based on the claim that the turbulence level and dust homogeneity in the 20-l sphere after 60 ms of opening of the dispersion valve equals the ones at 600 ms in the 1 m$^3$ sphere. The fundament of this claim are the experiments of Bartknecht [19] and Siwek [25], who measured equal $K_{st}$ -values in the 20-l sphere and the 1 m$^3$ vessel using aforementioned ignition delay times. Apart from giving rise to the notion that equal turbulence levels exist in both test vessels at the prescribed ignition delay times of 60 and 600 ms, their research also inspired the widespread belief that a formal cube-root relation exists between dust explosion severities measured in the two test vessels. In addition to that, their research stimulated the use of the cube-root relation $\left(\left({dp}/{dt}\right)_{max}.V^{1/3} = K_{st}\right)$ as a predictive tool, which enables engineers to assess the severity of an industrial dust explosion on the basis of dust explosion severities measured in laboratory test vessels. Several authors have investigated the turbulence fluctuations in the 20-l sphere and 1m$^3$ vessel. These include, among others, Van der Wel et al. [47], Pu et al. [48] and Dahoe et al. [49], who measured turbulence levels in both apparatuses. They concluded that the turbulence levels in the two test vessels at the prescribed ignition delay times are significantly different and could majorly influence the values of the safety characteristics. Apart from this, the use of cube-root relation in the practice of scaling laboratory test results into what might happen

during accidental industrial dust explosions has been regarded as fundamentally wrong by several authors. A detailed discussion can be found in [11, 49-51].

Other sources of unreliability of the reported MEC values of dusts or LEL of hybrid mixtures include the differences in the definition of an explosion or ignition (differences in pressure rise criteria), dust cloud non-uniformity and the consideration of nominal concentration, which are discussed in section 4.2.1.

### 2.1.2 Models for theoretical calculation of LEL of hybrid mixtures

The need to design explosion protection concepts for systems handling or processing hybrid mixtures combined with the lack of standardized testing methods as well as reliable data of explosion characteristics of hybrid mixtures has led to the development of models that, as a quick solution, would (in best case) calculate the LEL of hybrid mixtures based on the single component data. Four competing models for the calculation of LEL of hybrid mixtures could be found in the literature.

#### *Le Chatelier's mixing rule*

In 1891 Le Chatelier [52] first proposed an empirical mixing rule for prediction of LEL of homogenous fuel mixtures. Le Chatelier's mixing rule assumes a constant flame temperature and allows to calculate the LEL of multifuel mixtures provided that the LEL of individual gases comprising the mixture and the composition of the mixture are known.

$$\sum_i \frac{y_i}{LEL_i} = \frac{1}{LEL_{mix}} \qquad (2.1)$$

where $y_i$ is the mole fraction of the $i$th component in the mixture of combustibles (without air) and $LEL_i$ is the LEL of the $i$th component in mol.%.

For a multifuel mixture at its LEL, Le Chatelier's mixing rule can also be presented as following [53, 54]:

$$\sum_i \frac{c_i}{LEL_i} = 1 \qquad (2.2)$$

where $c_i$ is the mole fraction of the component $i$ (in kmol of flammable gas per kmol of flammable gas + air) in a complex mixture of limit composition and $LEL_i$ is the LEL of the component $i$ in kmol of flammable gas per kmol of flammable gas + air.

Over the time several researchers have applied Le Chatelier's mixing rule to the multiphase hybrid mixtures. The first use of equation (2.2) for multiphase hybrid mixtures appears to be by Singer et al., who demonstrated that coal-dust and methane limit mixtures for horizontal propagation in a flame ducting system with vertical and horizontal ducting showed good agreement with theoretical values calculated using Le Chatelier's equation [55]. Cashdollar et al. applied Le Chatelier's equation to the hybrid mixtures of bituminous coal and methane and

found a good agreement between the theoretically calculated and the experimentally determined values of LEL of hybrid mixtures, measured in the 20-l sphere and large scale mine tests [56]. Several other authors have compared their experimental results with the Le Chatelier's equation. Details can be found in [12, 30, 54, 57-59].

Le Chatelier's equation, when applied to hybrid mixtures, gives a linear relationship between LEL of the gas and the MEC of the dust with the weighing factor for gas being its fractional content in the mixture with air and for dust its concentration in grams per $m^3$ of the air as presented in equation (2.3).

$$\frac{c}{MEC} + \frac{y}{LEL} = 1 \qquad (2.3)$$

where c is the concentration of the combustible dust in hybrid mixture ($g/m^3$); MEC is the minimum explosible concentration of the dust ($g/m^3$); y is the mole fraction of the flammable gas in mixture with air (mol/mol); LEL is the lower explosion limit of the gas (mol/mol).

***Bartknecht's curve***

Bartknecht measured LEL of hybrid mixtures of PVC dust with methane and propane in the 1 $m^3$ vessel and discovered that the decrease in concentration of dust by added amount of gas in the hybrid mixtures was more than linear and therefore could not be explained with Le Chatelier's equation [19]. Since it was best fitting to his experimental results, he assumed a parabolic relationship (instead of the linear) and modified Le Chatelier's equation by introducing a quadratic term in the following way:

$$\frac{c}{MEC} = \left(-\frac{y}{LEL} + 1\right) \qquad (2.4)$$

$$c = MEC\left(-\frac{y}{LEL} + 1\right)^2 = MEC\left(\frac{y}{LEL} - 1\right)^2 \qquad (2.5)$$

Equation (2.5) is known as Bartknecht's curve and has been used extensively in the literature for comparison with the experimentally determined values of LEL of hybrid mixtures.

***Pellmont's equation***

Pellmont [15], while testing the LEL of hybrid mixtures of PVC with propane and methane, discovered that the experimental results of PVC with propane perfectly matched the theoretical values of LEL calculated using Bartknecht's formula. He used the standard 1 $m^3$ vessel with 10 kJ chemical igniters for his experiments. However, for the hybrid mixture of methane with PVC he recorded some ignition points in the non-explosible region of Barknechts curve. Therefore, following the same approach as Bartknecht, he assumed a hyperbolic relationship between the decrease in the dust concentration and the increase in gas concentration in a

hybrid mixture at its LEL and derived another empirical equation (equation (2.6)). Detailed derivation is available in [15].

$$c = LEL\left(\frac{1}{\frac{LEL-y}{MEC+LEL}+\frac{y}{LEL}}-1\right) \qquad (2.6)$$

Using equation (2.6), Pellmont presented a good agreement of his experimental values with the theoretically calculated values of LEL of hybrid mixtures.

***Jiang 's model***

Jiang et al. [29] measured the LEL of several hybrid mixtures in a 36-l sphere, which according to Castellanos et al. [60], was calibrated and gave same values of safety characteristics as the 20-l sphere and the 1 $m^3$ vessel. While comparing their experimental findings with the existing models, Jiang et al. found that the values of LEL of hybrid mixtures predicted by Le Chatelier's mixing rule and Bartknecht's equation were unrealistically conservative. Consequently, they developed a model by correlating LEL of hybrid mixtures to $K_{st}$ and $K_G$, which would fit their experimental data. They proposed the following equation for the calculation of LEL of hybrid mixtures.

$$c = MEC\left(1-\frac{y}{LEL}\right)^{(1.12\pm0.03)\frac{K_{st}}{K_G}} \qquad (2.7)$$

The only condition defined by Jiang et al. for the application of their model was that the $K_{st}$ and $K_G$ should be measured under the same turbulence condition.

Figure 2.3 shows the application of the four presented models on the LEL of hybrid mixture of starch and methane. For the calculation of Jiang et al.'s curve the $K_{st}$ and $K_G$ values were taken from their published work [29]. Each of the curves claims to differentiate between the explosible (area above the respective curve in Figure 2.3) and non-explosible concentrations (area below the respective curve in Figure 2.3) of a hybrid mixture. Logically, the safest approach would be to follow Pellmont's formula since it presents the most conservative values of LEL of hybrid mixtures. However, it must be kept in mind that the safety measures designed on the basis of ultra conservative values could be expensive and, in some cases, not practically feasible. A fundamental flaw that was found common in all of the above models is that they were derived empirically by extrapolating a specific set of experimental data. A plausibility check on the basis of fundamental principles of physics is missing for almost all of the above-mentioned models.

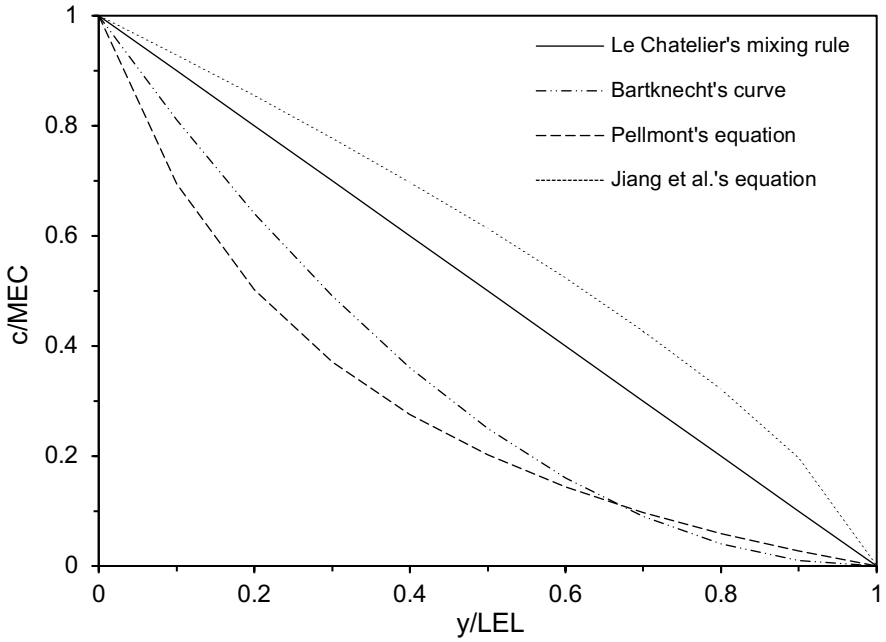


*Figure 2.3: Comparison of models for the theoretical calculation of LEL of hybrid mixture of starch and methane*

Moreover, all of the discussed models attempt to calculate the LEL of a hybrid mixture using experimentally determined MEC and LEL of the individual components of the hybrid mixture. Since experimentally determined values of MEC/LEL are not constants of nature or fixed material properties and are incorporated with a number of uncertainties, it is not surprising that the experimental data obtained by one researcher does not fit the modelled values of the other. This means that these models might hold true for the data that they were based on, but could not be generalized to all the hybrid mixtures.

A more reasonable approach would be to derive an equation based on the conservation equations of mass and energy, which would use basic thermodynamic properties of the individual fuel components as the input data for the calculation of LEL of hybrid mixtures. Such an approach was utilized in this research work to develop a model for the prediction of LEL of hybrid mixtures. Detailed derivation and discussion regarding comparison of the theoretical results with the experimental ones could be found in chapter 5.

## 2.2 Ignition and combustion propagation in hybrid mixtures

Almost all of the research done so far on hybrid mixtures focuses on the measurement of classical explosion characteristics like the lower flammability limit, the minimum ignition energy, the minimum ignition temperature, the maximum explosion pressure and the rate of pressure rise. Only a handful of the research work that does mention the term combustion (or flame) propagation in hybrid mixtures deals exclusively with the measurement of the flame speed and/or laminar burning velocity and therefore concentrates on the fuel rich concentrations of the hybrid mixtures. Research regarding measurement of the turbulent flame speed

and/or laminar burning velocities of hybrid mixtures include the work of Bradley et al. [61, 62], Liu et al. [63], Chen et al. [64], Jiang et al. [65], Yu et al. [66], Kim et al. [67], Pang et al. [68], Cuervo et al. [69], Di Benedetto et al. [70] and Garcia-Agregeda et al. [71].

It must be mentioned at this point that the term “flame”, in a stricter sense, cannot be used for dusts and hybrid mixture. A flame per definition is a gas phase reaction, whereas during the combustion of dust air mixtures or hybrid mixtures it is not only the gas phase (flammable gas and/or volatiles) that burns during an explosion but also the non-volatile particulate matter. Therefore, in case of dust air mixtures and hybrid mixtures the term combustion propagation will be used instead of flame propagation throughout this thesis. Term reaction zone or combustion zone will be used instead of flame for dusts and hybrid mixtures and flame temperature will be replaced by combustion temperature.

There has been no research work done so far to investigate the immediate process of ignition and the early combustion propagation in hybrid mixtures, in which the concentration of flammable gas as well as dust is below their respective LEL or MEC. The focus of this work is to investigate the process of ignition and early development of the reaction zone in lean hybrid mixtures. Moreover, the present work aims to provide new insight into the structure of the combustion zone and the process of combustion propagation in hybrid mixtures at concentrations close their LEL. Further details on the topic along with the presentation of the new findings could be found in Chapter 6.

# 3 EXPERIMENTAL APPROACH AND MATERIALS

This chapter provides a comprehensive detail of the experimental strategies employed in this work. A complete description of the experimental setup is given, followed by the material characteristics. Finally, the employed experimental procedure is explained in detail.

## 3.1 Experimental setup

For experimental purposes of this research work, a special setup has been designed and constructed, enabling a reliable measurement of MEC/LEL of dust and hybrid mixtures in a non-turbulent environment. The conceptual design of the experimental device is based on an open-tube apparatus, first introduced by Krause et al., in 1996 to investigate the influence of flow field intensity and turbulence on combustion propagation through dust-air mixtures [72, 73].

The setup consists of a vertically mounted combustion tube, an ignition system, a concentration measurement unit, a gas delivery unit, a high-speed camera and a digitally operated control and data acquisition unit (Figure 3.1).

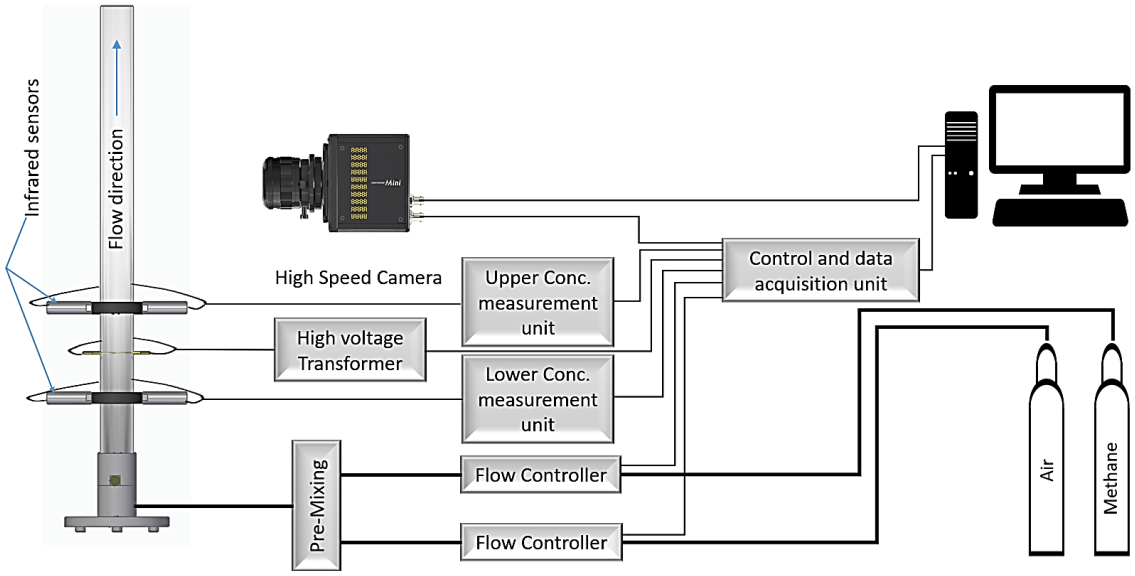


*Figure 3.1: Schematic diagram of the experimental setup*

### 3.1.1 The combustion chamber

The combustion chamber comprises of a vertically mounted acrylic glass tube of 1000 mm length, with an internal diameter of 60 mm and a wall thickness of 5 mm. The upper end of the tube was designed to remain open to allow for venting of gaseous combustion products and to ensure constant pressure conditions during the reaction. The bottom end of the tube is resting on an airtight stainless-steel stand. One of the highlights of this device is the design of the bottom stand, which includes a filter paper (approx. 15 µm pore size), a sintered glass filter (diameter

70 mm, thickness 5.5 mm and 40-100 µm pore size) and a bed of steel wool (Figure 3.2).

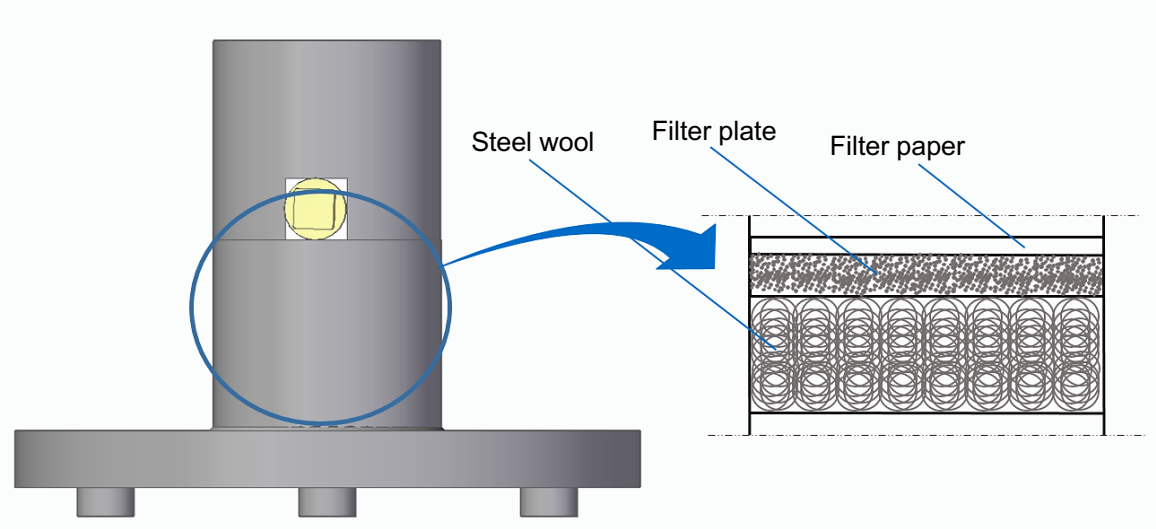


*Figure 3.2: Design of the stainless-steel stand*

The filter disc together with the steel wool act as a flow rectifier, facilitating a uniform profile of the flow velocity.

### 3.1.2 Ignition system

The ignition system constitutes of a high-voltage transformer (Resinblock-2000-compact by Neon Transformers®) connected to two brass electrodes (with a gap of 5±1mm), installed at a height of 330 mm from the bottom end of the tube. According to the product specification sheet, the transformer is designed to produce a maximum output voltage of 10 kV and a short circuit current of 22.5 mA. The theoretical amount of supplied energy over a specific spark duration was calculated using following equation.

$$E = UI\Delta t \tag{3.1}$$

Equation (3.1) yields a maximum theoretical spark energy of 11.25 J for a duration of 50 ms. Since the actual output voltage is dependent on the input load and can be equal to or less than the maximum value provided by the manufacturer, a number of calorimetric tests (at several spark durations) were performed in collaboration with the Federal Institute for Materials Research and Testing (BAM) Berlin to measure the net energy provided by the spark. A newly designed adiabatic brass calorimeter was employed for this purpose. The calorimeter is made of brass cylinder with an inner and outer diameter of 20 mm and 65 mm respectively and a total height of 70 mm. It was isolated by foamed polystyrene with a thickness of at least 90 mm. The temperature increase of the calorimeter was measured with a high precision semiconductor thermistor (TS-NTC-203 by Hygrosens Instruments GmbH) and a self-designed circuit board transferring the changing resistance into the changing voltage. The recorded voltage signal is

proportional to the temperature increase and thus to the released energy. Further details about the measurement procedure and its validation can be found in [74].

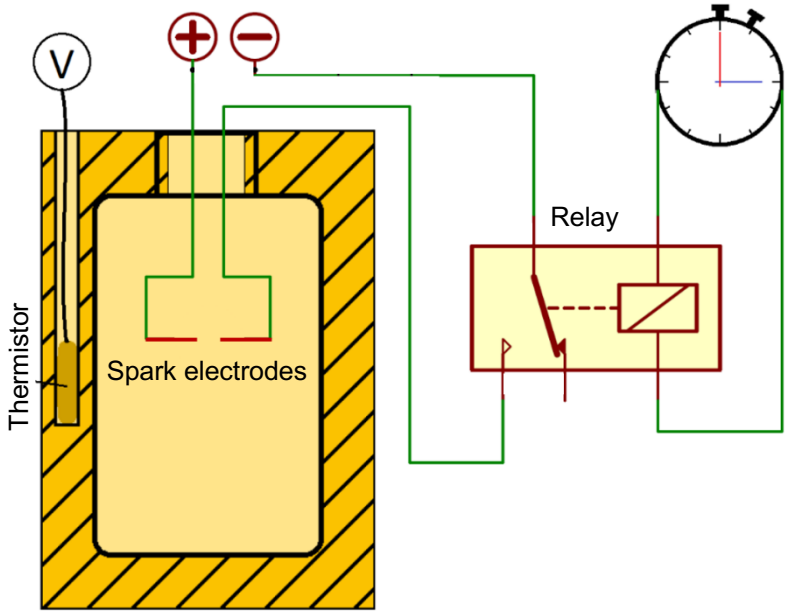


*Figure 3.3: Schematic diagram of the adiabatic calorimeter [73]*

The measured energy was approx. 10 times smaller than the theoretically calculated one. A maximum of 1.5 J, 3.0 J and 4.5 J was measured for a spark duration of 50 ms, 100 ms and 150 ms respectively. These ignition energies seem to be very small in comparison to the 2 kJ recommended by the DIN EN 14034-3 [46], however the results of the experiments investigating the influence of ignition energy on MEC of dust clouds and LEL of hybrid mixtures revealed that an ignition could be obtained even with these small spark energies, provided that a truly homogeneous suspension of dust is achievable. This topic will be discussed in detail in section 4.2.

### 3.1.3 Concentration measurement unit

The concentration measurement unit (SKG 5) comprises of two infrared sensors (installed a few centimetres above and below the spark electrodes) that measure the concentration of the dust and a control unit that processes and displays the signals from these sensors. Each sensor consists of a transmitter diode (wavelength 950 nm), a photodiode, which acts as receiver at the receiving end, and two lenses. Details about the technical specification of SKG 5 are given in Table A.1 in Appendix A.

The measurement procedure of SKG 5 is based on the principle of light extinction, which implies that the energy or intensity of waves (infrared light in this case) is dissipated through suspended particles or a powder bed because of the wave absorption or scattering.

During its operation, the transmitter emits the light with an intensity $I_o$ which, after being partly absorbed by the dust particles, is detected by the photodiode with an

(reduced) intensity $I$ (Figure 3.4). The decrease in the light intensity, when passing through a powder suspension, is described by the following equation:

$$I = I_o e^{-\varepsilon l c} \tag{3.2}$$

where $c$ is the dust concentration, $l$ is the measurement distance and $\varepsilon$ is the extinction coefficient. Equation 3.2 implies that the intensity of the light beam decreases exponentially with the thickness of the layer. This is known as the Lambert–Beer law.

The ratio of measured and emitted light intensity $I/I_o$ is called transmittance. Extinction $E$ is the negative logarithm of the transmittance, described as following:

$$E = -\ln\left(\frac{I}{I_o}\right) = \varepsilon l c \tag{3.3}$$

The extinction coefficient $\varepsilon$ is a material property and is determined through calibration experiments.

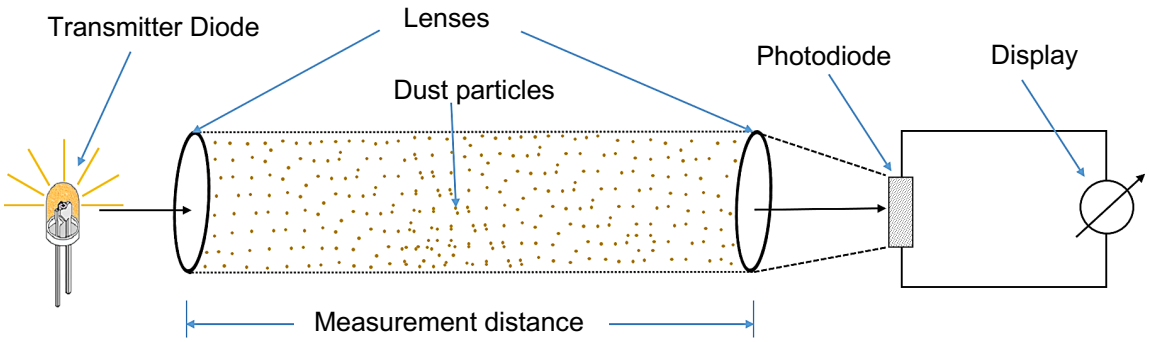


*Figure 3.4: Measurement principle of concentration measurement unit*

During the calibration experiments a known mass of dust is stepwise added to a known volume of an appropriate liquid (e.g. methanol or ethanol) in a cup with same diameter as the diameter of the experimental tube. The mixture is continuously elutriated with the help of a magnetic stirrer and the decrease in the light intensity is recorded for each step. Once appropriate number of data points achieved, a calibration curve is plotted on a concentration $(c)$ vs percentage decrease in the light intensity $\left(I/I_o * 100\right)$ chart. The extinction coefficient $\varepsilon$ for the dust material under consideration is determined by applying equation (3.3) to the data of calibration experiments.

During the explosion experiments, the dust concentration is calculated using following equation:

$$c = -\frac{\ln\left(\frac{I}{I_o} * 100\right)}{\varepsilon l} \tag{3.4}$$

Calibration data of the dusts used in this work can be found in section A.2 in Appendix A.

### 3.1.4 Gas delivery unit

In the gas delivery unit, two thermal mass flow controllers together with a premixing chamber (0.1 l) are integrated on a metallic panel to precisely control the flowrate and concentration of the flammable gas air mixture in the combustion tube (Figure 3.5). Technical details of the flow controllers are mentioned in Table A.2 in Appendix A. The system is controlled digitally through a software module developed inhouse using LabVIEW.

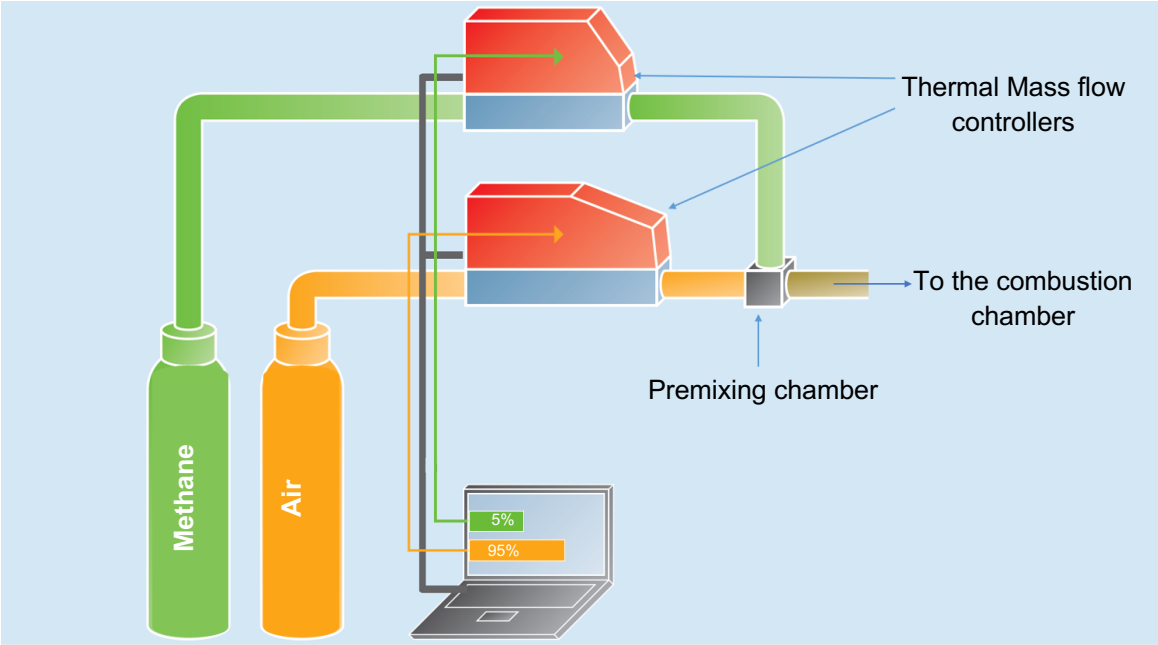


*Figure 3.5:Gas delivery unit*

### 3.1.5 High speed camera

In order to investigate the contribution of dust and gas on the course of combustion propagation, a high-speed camera (FASTCAM Mini UX 50/100), with a maximum frame rate of 100000 frames per second, has been integrated in the setup.

### 3.1.6 Control and data acquisition unit

The control and data acquisition unit consist of a multifunction DAQ device (USB-6000) from NI (National Instruments), a 2-channel relay module and a software module developed in LabVIEW. The DAQ device functions to control the whole experimental loop by giving on/off signals to the relays (which in turn control the spark and the high-speed camera) and also reads the signals coming from the two concentration measurement units. Figure 3.6 shows the schematic diagram of the control and data acquisition unit.

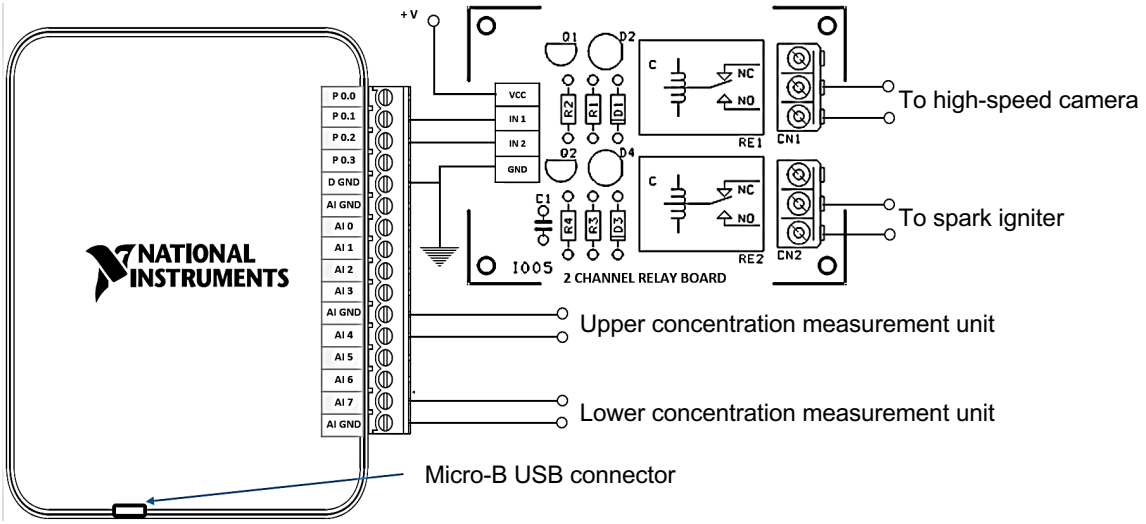


*Figure 3.6: Schematic diagram of control and data acquisition unit*

## 3.2 Combustible materials

The objective of this research work was to investigate the dust-gas hybrid mixtures of organic dusts with high volatile content and metallic dusts with no volatile content. As a representative of organic and metallic dusts, lycopodium and titanium were selected respectively.

Before the commencement of experiments, dust samples were tested to define their moisture and volatile content, particle density and particle shape and size distribution. A brief overview of these tests along with the standard test protocol is provided in the following.

Moisture and volatile content were determined using a thermogravimetric moisture analyser (Sartorius® MA100) in compliance with ISO 5071:1996. According to EN 14034-3, the moisture content of all the dust materials should be below 5% (wt./wt.) to ensure reliable results. In the present scenario, the moisture content of both powders was below 3%. A controlled workstation has been used to regulate the storage conditions of the samples during the complete course of experiments.

For the determination of particle density pycnometer method by fluid displacement, in accordance with ISO 17892-3:2015, was employed.

Results of all these tests are presented in Table 3.1.

*Table 3.1: Properties of dust materials*

| Dust sample | Moisture content (%wt.) | Volatile content (%wt.) | Particle Density (kg/m$^3$) |
|---|---|---|---|
| Lycopodium | 2.5 | 92 | 428 |
| Titanium | 0.4 | - | 3500 |

According to ASTM and European standards, particle size distribution of the dust material must be determined before the commencement of explosion experiments.

This was measured by using a multi-wavelength laser diffraction particle size analyser (Beckman Coulter LS 13320 CAMSIZER®) according to ISO 13319:2007.

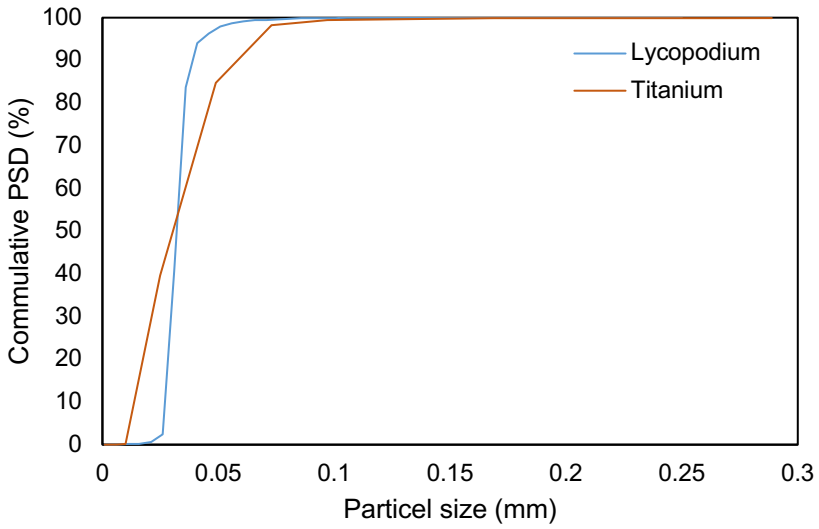


*Figure 3.7: Particle size distribution of dust materials*

The samples were characterized by the $d_{32}$, $d_{50}$ and $d_{90}$ quantiles of the volumetric distribution as indicated in Table 3.2.

*Table 3.2: Particle size distribution*

| Dust material | d32 (µm) | d50 (µm) | d90 (µm) |
|---|---|---|---|
| Lycopodium | 30.3 | 31.7 | 37.9 |
| Titanium | 17.5 | 25.0 | 55.1 |

Dust particles were also examined under scanning electron microscope (SEM), to reveal their surface structure (Figure 3.8).

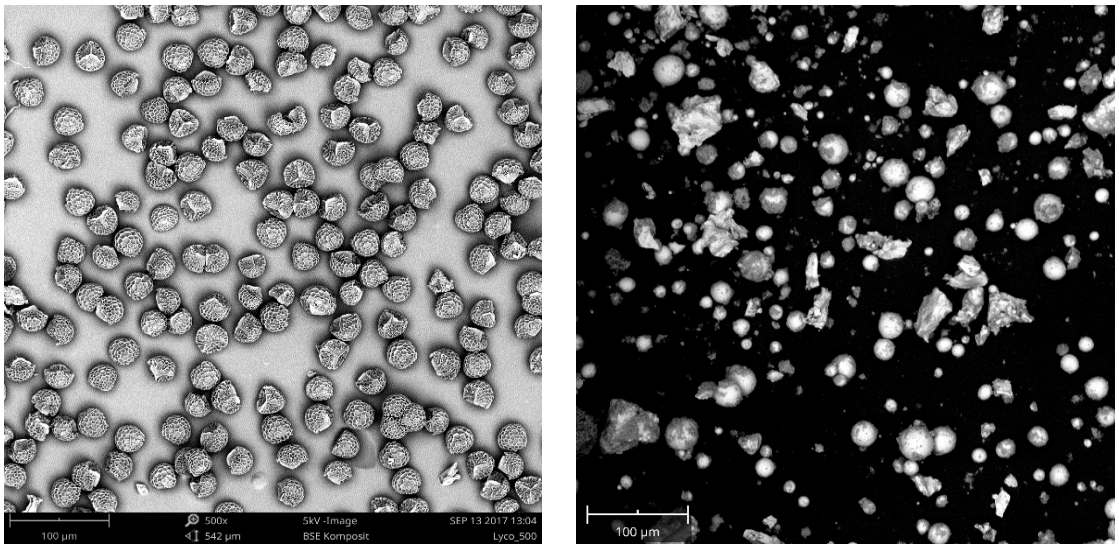


*Figure 3.8: SEM images of lycopodium (left) and titanium (right)*

Properties of gases were mainly taken from [75] and [76] and are given in the following table.

*Table 3.3: Properties of gases*

| Gases | M.wt (g/mol) | Density ($g/m^3$) | Heat Capacity (J/mol.K) | Heat of combustion (kJ/mol) |
|---|---|---|---|---|
| Methane | 16 | 675.2 | 35.69 | 891.2 |
| Propane | 44.1 | 1900 | 73.60 | 2220 |

## 3.3 Experimental procedure

In order to ensure good reproducibility of results, a precise protocol was followed throughout the experiments. At the beginning of each experiment, a known mass of dust material was layered on the filter paper at the bottom of the tube. In the next step boundary conditions for each experiment were defined in the software module of the data acquisition unit. These included flow time, flammable gas concentration, spark duration, delay time and the flowrate of flammable gas-air mixture. Next, an automatic test sequence was started. A constant and steady stream of flammable gas-air mixture (for the measurement of MEC of dust only air) was inserted from the bottom of the tube for the predefined time (flow time), depending on the flow velocity, until the flow front reached the top of the tube. Flow front in this regard refers to particles bed (or plug) moving upward due to the gas flow from the bottom of the tube. At this point, the tube was filled with a homogenous non-turbulent column of the hybrid mixture, the gas flow was stopped and the high-speed camera as well as the spark were initiated with a specific delay time, corresponding to the moment when the dust particles were in a quasi-static state, after decelerating under the action of the gravitational force. This delay time will be referred to as particle deceleration time in the further discussion.

The particle deceleration time was calculated for different flow velocities assuming that all the particles in the cloud move upwards with a constant velocity equivalent to flow front velocity (see section 3.3.1). At the end of the experiment, dust concentration values were displayed in the computer in the form of light intensity detected by the photodiode at the time the spark was activated ($I$ in equation (3.4)). Since $I_o$(intensity of the light beam in the absence of dust particles) was recorded before the start of the experiments and the value of $\varepsilon$ was known from calibration experiments, the dust concentration was calculated using equation (3.4).

Spark energy was controlled by regulating the duration of the spark, keeping the voltage and current at a constant value. An electrode gap of 5 mm was used through the complete course of experiments. Visual flame detachment from the electrodes, as defined by DIN 51649-1, was used as the ignition criteria. In case of an ignition, the dust concentration was decreased by decreasing the inserted mass and the process was repeated until no ignition was possible for at least three test trials, with dust concentrations in the range of max. 10 $g/m^3$ of the lowest concentration where an ignition was observed. Upon fulfilment of this criterion, the lowest concentration of dust where the ignition occurred, was recorded as the MEC of dust in the hybrid mixture.

### 3.3.1 Particle deceleration time

The vertical movement of the dust cloud (in the open tube apparatus) is mainly governed by the balance between the gravity, which acts downwards and the drag force, which acts upwards. The net force in such a system is responsible for the direction and magnitude of particle motion. Drag force acts in opposite direction of the relative motion of particles with respect to the surrounding fluid and is dependent on the relative velocity of particle (slip velocity) with respect to the fluid.

In a particle cloud moving upward (under the action of upwards moving gas) gravity is dominated by the drag force and the net force enables particles to move in upward direction. As soon as the flow of air (or mixture of air and flammable gas) from the bottom of the tube is stopped, a decay in the drag force starts. This decay lasts for a certain time (particle deceleration time) until the gravity equals the drag force and the net force on the particle becomes zero. At this moment, the particles get suspended in a quasi-static condition. This research work was aimed at igniting the dust particles in a quasi-static state in order to minimize the influences related to the motion of particles.

The particle deceleration time can be calculated by writing a force balance equation as following:

$$F_g - F_D = F_{net} \tag{3.5}$$

where $F_g$, $F_D$ and $F_{net}$ are the gravity, drag and net force respectively. For a perfect sphere these forces are given as following:

$$F_g = mg = {}^{\pi}/_{6}\, d_p^3 \rho_p g \tag{3.6}$$

$$F_D = {}^{1}/_{2}\, C_D \rho_g u_s^2 A_p = {}^{1}/_{8}\, \pi\, d_p^2 C_D \rho_g u_s^2 \tag{3.7}$$

$$F_{net} = m\frac{\Delta u}{\Delta t} = {}^{\pi}/_{6}\, d_p^3 \rho_p \frac{\Delta u}{\Delta t} \tag{3.8}$$

where $\rho_g$ and $\rho_p$ are the densities of gas and particle and $d_p, u_s, C_D$ are particle diameter, slip velocity and the drag coefficient respectively. By incorporating equations (3.6) – (3.8) in equation (3.5):

$${}^{\pi}/_{6}\, d_p^3 \rho_p g - {}^{1}/_{8}\, \pi\, d_p^2 C_D \rho_g u_s^2 = {}^{\pi}/_{6}\, d_p^3 \rho_p \frac{\Delta u}{\Delta t} \tag{3.9}$$

$$g - {}^{3}/_{4}\, C_D \frac{\rho_g u_s^2}{\rho_p d_p} = \frac{\Delta u}{\Delta t} \tag{3.10}$$

In equation (3.10), $\Delta u$ is the decay in velocity of the particles under the action of gravity and is given by $\Delta u = u_2 - u_p$, where $u_2$ refers to the aforementioned quasi-static state $(u_2 = 0)$. $u_p$ is the particle velocity at time $t = 0$, (when the gas flow from the bottom of the tube is terminated) and is considered to be equal to the flow front velocity. Flow front velocity in this regard refers to the vertical velocity of the

powder bed (or plug) moving upwards when the gas flow from the bottom of the tube is initiated.

$$t = t_{pd} = \frac{-u_p}{g - {}^{3}/_{4}\, C_D \frac{\rho_g u_s^2}{\rho_p d_p}} \tag{3.11}$$

Equation (3.11) allows us to calculate the particle deceleration time $t_{pd}$ as a function of flow front velocity.

Drag coefficient is calculated using stokes equation [77]:

$$C_D = \frac{24}{Re} \tag{3.12}$$

Equation (3.12) is only valid in a small region where $Re < 0.4$. Knowing the slip velocity $u_s$, $Re$ can be calculated as following:

$$Re = \frac{\rho_g u_s d_p}{\mu_g} \tag{3.13}$$

Slip velocity is the velocity of the particle relative to the gas velocity and is given by $u_s = u_p - u_g$, where $u_p$ is the velocity of the particle (which is assumed to be equal to the flow front velocity) and $u_g$ is the undisturbed velocity of the fluid at the same location and is calculated from the volumetric flowrate of the gas ($V^o$) and cross-sectional area of the tube ($A_t$) as following:

$$u_g = \frac{V^o}{A_t} \tag{3.14}$$

The particle deceleration time was calculated using equations (3.12) – (3.14) for all the flow velocities tested in this research work (Table 3.4).

*Table 3.4: Particle deceleration time*

| $u_p$ $(m/s)$ | $V^o$ $(m^3/s)$ | $u_g$ $(m/s)$ | $u_s$ $(m/s)$ | $\rho_p$ $(kg/m^3)$ | $d_p$ $(\mu m)$ | $Re$ | $C_D$ | $t_{pd}$ $(ms)$ |
|---|---|---|---|---|---|---|---|---|
| **Lycopodium** | | | | | | | | |
| 0.048 | 1.95x10$^{-4}$ | 0.069 | 0.021 | 428 | 31.7 | 0.04 | 600 | 5.9 |
| 0.071 | 2.8x10$^{-4}$ | 0.098 | 0.026 | 428 | 31.7 | 0.05 | 480 | 5.8 |
| 0.095 | 3.6x10$^{-4}$ | 0.127 | 0.032 | 428 | 31.7 | 0.06 | 400 | 5.3 |
| 0.13 | 4.44x10$^{-4}$ | 0.157 | 0.027 | 428 | 31.7 | 0.05 | 480 | 9.3 |
| **Titanium** | | | | | | | | |
| 0.16 | 5.5x10$^{-4}$ | 0.198 | 0.038 | 3500 | 25 | 0.06 | 400 | 42.8 |
| 0.2 | 6.9x10$^{-4}$ | 0.244 | 0.044 | 3500 | 25 | 0.07 | 343 | 70.7 |

For all the flow front velocities tested in this work, $Re \ll 1$, therefore the flow regime is characterized as perfectly laminar.

# 4 EXPERIMENTAL RESULTS OF LEL OF HYBRID MIXTURES

This chapter presents detailed results of the conducted experiments. The results of a large number of preliminary experiments to test the accuracy of the dust and flammable gas concentration in the open tube apparatus are presented, followed by the experimental determination of MEC of pure dust and LEL of flammable gas. In the last section of the chapter the results of the experimental determination of LEL of hybrid mixtures at different flow velocities and ignition energies are explained.

## 4.1 Accuracy of concentration data

Before starting with the measurement of MEC/LEL of dust, gas and hybrid mixtures, a number of experiments were performed to test the accuracy of the dust and gas concentration in the combustion tube.

The reliability of the dust concentration was investigated by comparing two sets of dust concentration data. The first one namely digitally determined concentration values refers to the dust concentration values recorded and processed by the DAQ unit and displayed in the software module at the end of each experiment. The second set of data was obtained by video recording the decrease in voltage values (light intensity, which is a measure of the dust concentration, see section 3.1.3) displayed on the control unit of the dust concentration meter. Since these voltage values were constantly changing as the powder was suspended in the tube, values at the spark initiation time were obtained by post analyses of the videos. This set of concentration data will be referred to as the manual values of dust concentration in the further discussion.

In order to check the accuracy of the gas concentration in the tube, concentration values defined in the software before the start of the experiments were compared with values measured by a gas analyser. Details of these experiments along with the results are explained in the following sections.

### 4.1.1 Accuracy of dust concentration

A total of 560 experiments were performed to quantify the difference between the manual and digital values of dust concentration. During these experiments a known mass of lycopodium was dispersed in the tube at four flow front velocities and at the time the flow front reached the top of the tube, the gas flow from the bottom of the tube was terminated and concentration values in the upper and lower sensors were registered. For each flow velocity the starting mass of lycopodium was chosen to be 1.5 g, which was then stepwise decreased by 0.1 g. At each mass 10 experiments were performed and the concentration values at each of these experiments were subsequently recorded. All the concentration values, where the difference between the readings of two sensors was less than 15% of the average

value, were considered valid. Detailed results of all the experiments, along with the conversion formulae, are given in Appendix B (section B.1). A summary is presented in Figure 4.1.

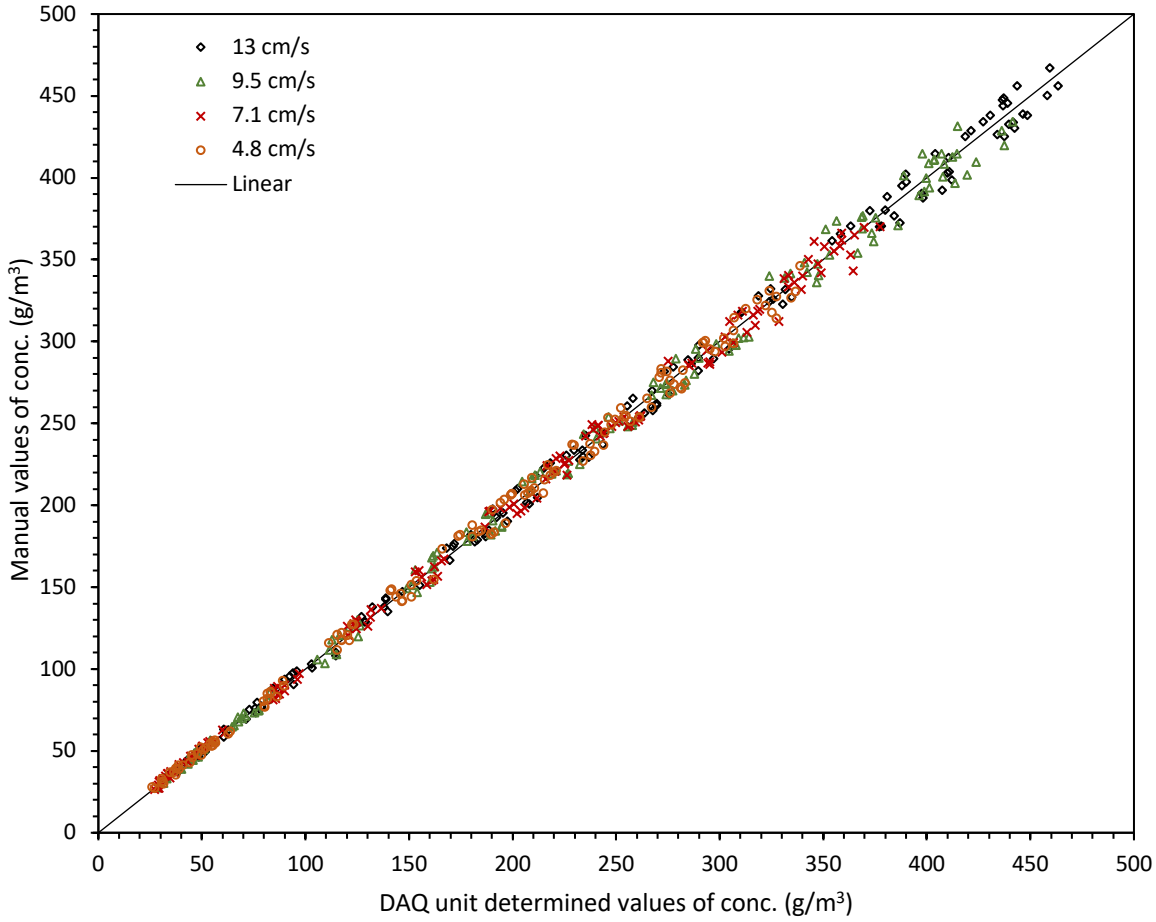


*Figure 4.1: Accuracy of dust concentration data*

By analysing the results, it was found that for most of the experiments, the digital values did not match with the manually determined values of concentration. For a total of 560 trials, 412 tests were such, where the digital values were either greater or smaller than the manually recorded values of concentration. This means a likeliness of approx. 73% that the dust concentration values were contaminated with the intolerable uncertainties. An intolerable uncertainty in this sense refers to an uncertainty value greater than 0.00% of the measured concentration value. The magnitude of these intolerable uncertainties was found to be different for the upper and lower concentration meters and varied between 0.25% and 8% of the measured value (digital) for upper sensor and 1.42 % and 7 % for the lower sensor. Frequencies of occurrence of individual uncertainties for each sensor along with their respective number of occurrences are presented in Table 4.1.

Average uncertainties of 2.6% and 2.3% were calculated for the upper and lower sensors respectively. These were consequently added to all the dust concentration

values measured during the experimental determination of the MEC of the dust and LEL of hybrid mixtures.

*Table 4.1: Frequency of occurrence of individual uncertainties*

| Uncertainty | Number of occurrences | | Frequency (%) | |
|---|---|---|---|---|
| | Upper sensor | Lower sensor | Upper sensor | Lower sensor |
| ≤ 2% | 192 | 246 | 34.3 | 44 |
| 2.01% - 3% | 109 | 124 | 19.5 | 22.1 |
| 3.01% - 4% | 118 | 102 | 21.1 | 18.2 |
| 4.01% - 5% | 74 | 56 | 13.2 | 10 |
| > 5% | 67 | 32 | 11.9 | 5.7 |

It must be mentioned here that the source of these uncertainties in concentration values could not be clearly identified in this investigation. Most probable reason could be the inherent analogue input uncertainty (± 26 mV) associated DAQ unit. This can be eliminated by replacing NI USB-6000 module by a high end and more expensive multifunction I/O device (e.g. NI USB 6363).

### 4.1.2 Accuracy of gas concentration

As mentioned in section 3.3, the flowrate of the flammable gas-air mixture and the concentration of gas in the tube was defined in the software module before the commencement of each experiment, which in turn calculated the individual flowrates of flammable gas and air (with respect to the defined concentration) and assigned it to the respective thermal mass flow controller. This concentration will be referred to as the software defined concentration in the further discussion. Since experiments were performed in an open top tube (without purging), the possibility of having a different gas concentration in the tube than what was originally defined in the software could not be completely overruled. Moreover, the inherent uncertainties associated with the flow controllers could also affect the gas concentration in the tube.

In order to quantify these effects, a series of experiments was conducted, where the concentration in the tube (at a given flowrate) was measured with the help of a gas analyser (Siemens ULTRAMAT 23) by inserting a hose in the tube at the location of the electrodes and the values were compared with the software defined concentration values (Figure 4.2).

All the flowrates mentioned in Table 3.4 (which were used for hybrid mixture LEL testing, section 4.4) were investigated for this purpose. At each flowrate, experiments were performed by defining a gas concentration in the software module starting with 6 vol.-%. This was then stepwise reduced to 1 vol.-%, with each step being 1 vol.-%. Each concentration value was tested 3 times and the respective values measured with the gas analyser were recorded. Detailed data of all these experiments is given in Appendix B (section B.2.4). It is important to mention here that the flow time (the time required by the powder bed to reach the top end of the tube at a given flow front velocity) was not the same as used for the

hybrid mixture LEL experiments. This was modified by adding an extra 11.7 sec (see section B.2.2 for detailed calculation), which is the time that the gas mixture requires to flow from the tube to the gas analyser (under the action of a suction pump integrated in the gas analyser).

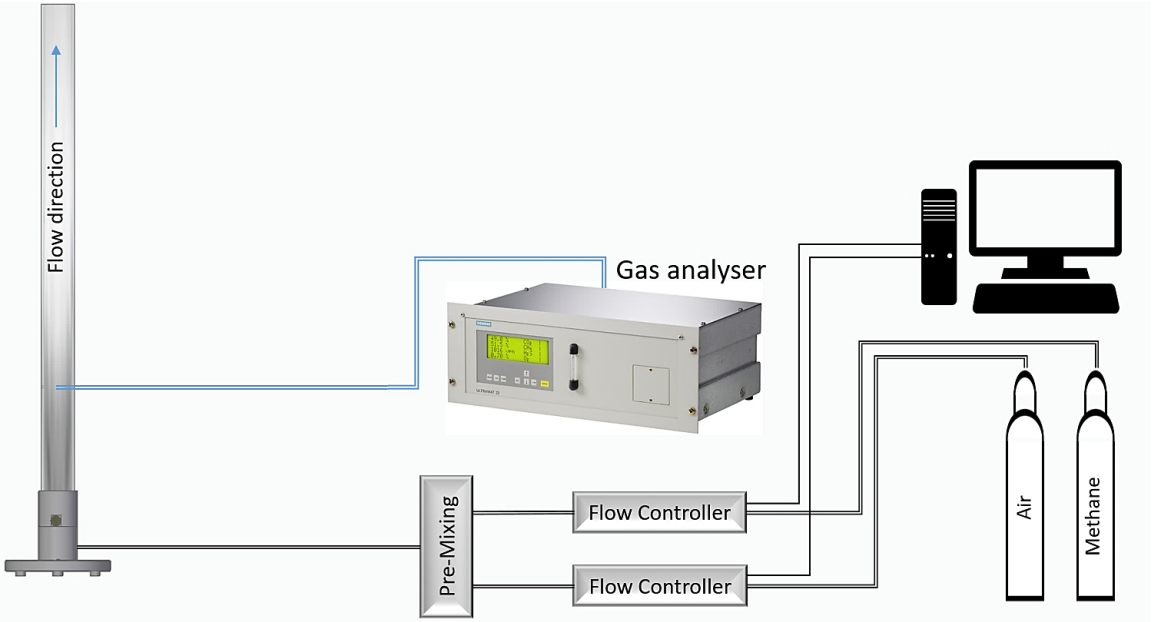


*Figure 4.2: Schematic diagram of experimental setup*

Figure 4.3 shows a graphical representation of the concentration data (section B.2.4), where the straight line shows the ideal situation when the software defined concentration values are precisely equal to the gas analyser values. The dotted lines represent the inherent uncertainty (± 0.1 vol.-%) associated with the gas analyser values.

A statistical analysis of the data presented in Figure 4.3 and section B.2.4 revealed that out of a total of 108 experiments, 81 were such where the difference between gas analyser and software defined concentration values was within the inherent uncertainty of the gas analyser. This makes about 75% of all the tests. For the rest 25% (27 tests), the maximum calculated uncertainty was 0.2 vol.-% (occurrence 2 times out of 108 tests). This means an extra 0.1 vol.-% uncertainty if the inherent uncertainty (± 0.1 vol.-%) of the gas analyser is considered. The inherent uncertainty calculated for flow controllers (Section B.2.3) accounts to be in the range of 0.03 Vol.% – 0.12 Vol.%. Considering above discussion, one could conclude that the difference in the gas analyser and software defined concentration values is due to systematic (inherent) uncertainties associated with both systems and that the influence of “no purging” of the tube on the gas concentration in the tube could be considered inconsequential.

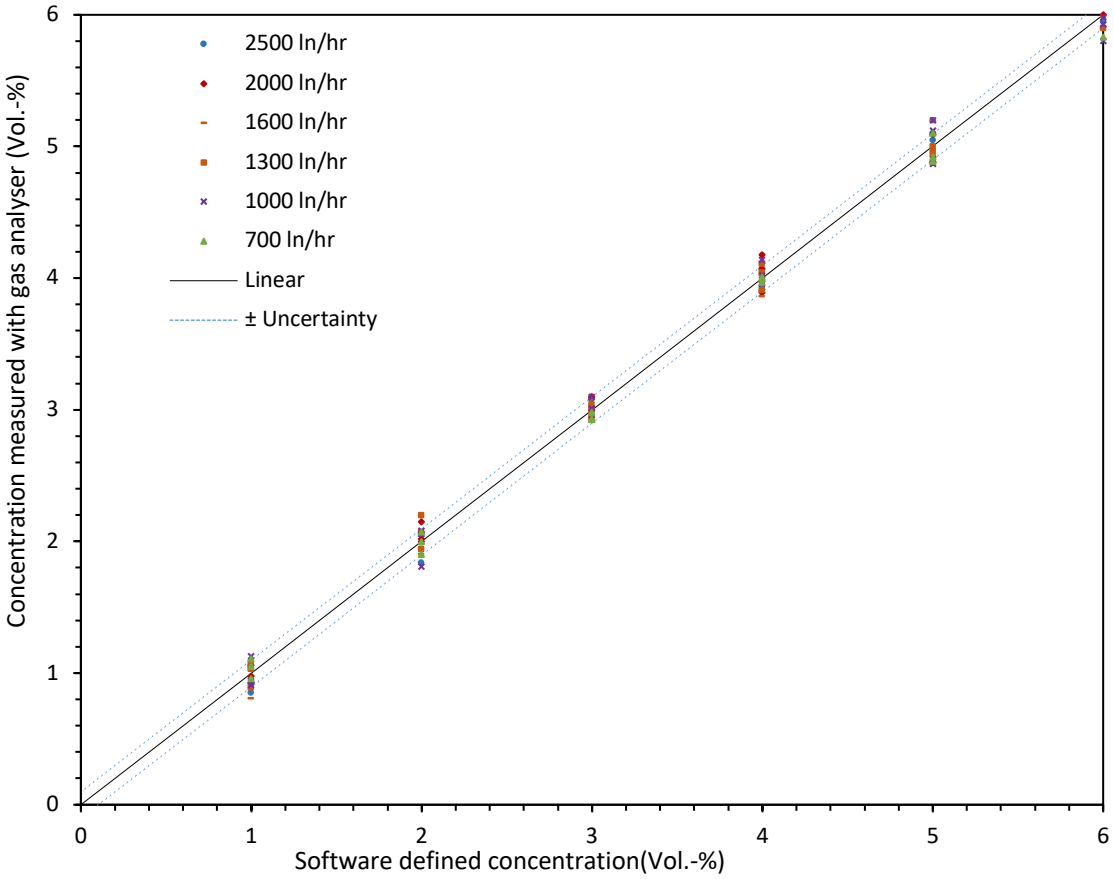


*Figure 4.3: Accuracy of gas concentration*

## 4.2 MEC of dusts

This section presents the results of a series of experiments aimed at investigating the influence of flow front velocity and ignition energy at the MEC of a dust cloud. For this purpose, MEC of lycopodium and titanium was measured at different flow front velocities and ignition energies. The flow velocity was changed by changing the flow rate of air being introduced from the bottom of the tube and the ignition energy was changed by changing the spark duration. For lycopodium dust, MEC was measured at four flow front velocities, whereas for titanium two flow front velocities were employed. Owing to the density difference of the two powders, it was not possible to measure the MEC of both at the same flow front velocities. At lower flow velocities, titanium particles being relatively heavier than the lycopodium could not be suspended in the combustion tube in a concentration that would allow a self-supporting propagation of the reaction zone. On the other hand, lycopodium particles at higher flow velocities (16 and 20 cm/s) moved upwards in the form of a dense plug, leading to concentration inhomogeneities. For each of the tested flow velocity, three ignition energies were tested corresponding to a spark duration of 50ms, 100ms and 150ms (ignition energies of 1.5 J, 3.0 J and 4.5 J).

Results of these experiments along with associated uncertainties are shown in Table 4.2, wherein the reported concentrations are the average of upper and lower

sensor and the uncertainty refers to difference between the values of upper and lower sensor as well as the average uncertainty (±2.6% and ±2.3% for the upper and lower sensor respectively) calculated through reliability experiments.

Considering the uncertainty associated with each of the value in Table 4.2, it could be stated that the MEC of both dusts did not significantly change by changing the flow velocity or the ignition energy. Generally, this statement might not be true, however holds valid for the flow velocities and ignition energies tested in this work. The reasons behind these occurrences are discussed in detail in section 4.4.

*Table 4.2: MEC of lycopodium and titanium*

| Flow front velocity (cm/s) | MEC of lycopodium (g/m$^3$) ±Uncertainty (g/m$^3$) | | | MEC of titanium (g/m$^3$) ±Uncertainty (g/m$^3$) | | |
|---|---|---|---|---|---|---|
| | 1.5 J | 3.0 J | 4.5 J | 1.5 J | 3.0 J | 4.5 J |
| 20 | --- | --- | --- | 105 ±6 | 108 ±7 | 106 ±9 |
| 16 | --- | --- | --- | 106 ±6 | 104 ±8 | 102 ±8 |
| 13 | 50 ±5 | 51 ±5 | 49 ±6 | --- | --- | --- |
| 9.5 | 52 ±4 | 50 ±5 | 49 ±5 | --- | --- | --- |
| 7.14 | 46 ±3 | 49 ±6 | 46 ±4 | --- | --- | --- |
| 4.8 | 48 ±5 | 46 ±5 | 50 ±4 | --- | --- | --- |

Detailed results of all the MEC experiments are presented in Appendix B Section B.3 (Figures B.1 - B.6). A closer look at these data revealed a narrow concentration range, where the ignition and no ignition points overlapped. Above the upper limit of this concentration range an ignition frequency of 100% was recorded and below the lower limit, 0%. This concentration range was found to be 45-55 g/m$^3$ for lycopodium and 100-110 g/m$^3$ for titanium. The percentage of successful ignitions (within these concentration ranges) was calculated for different ignition energies. The results are presented in Table 4.3.

*Table 4.3: Ignition frequency with respect to different ignition energies*

| | Lycopodium (45-55 g/m$^3$) | | | Titanium (100-110 g/m$^3$) | | |
|---|---|---|---|---|---|---|
| | 1.5 J | 3.0 J | 4.5 J | 1.5 J | 3.0 J | 4.5 J |
| **No of trials with ignitions** | 27 | 23 | 25 | 10 | 12 | 13 |
| **No of trials with no-ignitions** | 35 | 25 | 21 | 13 | 9 | 7 |
| **Frequency of ignition** | 44% | 48% | 54% | 43% | 57% | 65% |
| **Overall Frequency** | | 47.3% | | | 55.6% | |

Although increasing the ignition energy did not decrease the MEC of lycopodium and titanium, an increase in ignition frequency was identified. An explanation of this increase was found by analysing the high-speed videos. It was observed that the ignition of the dust cloud began with the combustion of a certain limiting number of particles being simultaneously trapped in spark. This limiting number of particles refers to minimum mass of particulate material, which upon combustion would release enough energy to ignite the next set of particles. At concentrations close

to MEC, the occurrence of an event, where the number of particles trapped in the spark would be equal to or exceed this limiting number seemed to be stochastic, which means that even if the dust concentration was in the explosible range (45-55 g/m$^3$ for lycopodium and 100-110 g/m$^3$ for titanium), not always did it occur that this limiting number of particles simultaneously got trapped in the spark and led to a successful ignition of the cloud. In the current experimental system, the increase in the ignition energy was accompanied by an increase in the spark duration, which implies that at higher ignition energies dust particles had longer time to get trapped in the spark. Since the gas flow from bottom of the tube was stopped before the initiation of the spark, during the spark duration dust particles were continuously moving downward under the action of gravity. Thus, longer spark durations resulted in higher probability that the number of particles trapped in the spark will exceed the limiting value and consequently lead to a successful ignition of the dust cloud.

### 4.2.1 Comparison and validation

Experimental MEC data measured in this work (Table 4.2) do not indicate a discrete concentration value that could be quoted as the MEC, but rather a concentration range, where the probability of a successful ignition (upon coexistence of an active ignition source) is greater than 0% but less than 100%. However, for the purpose of comparison with other data sources, MEC values with smallest uncertainty will be used. These are 46 g/m$^3$ and 105 g/m$^3$ for lycopodium and titanium respectively.

Table 4.4 shows a comparison of the MEC of lycopodium along with the measurement apparatus, median particle size and strength and type of ignition source. A substantial disagreement can be seen in the reported MEC values (ranging from 8 g/m$^3$ – 125 g/m$^3$) of samples of nearly same median particle size.

A number of reasons can be assigned to such a wide scattering of the MEC, all narrowing down to the differences in measurement apparatus and interpretation of data. The MEC value measured with the open tube apparatus seems to be more conservative than the ones measured in the 20-l sphere (using permanent spark), the Nordtest apparatus and GG furnace, however, higher than ones measured following standard protocol [46] in the 20-l or 1 m$^3$ sphere, which uses high energy chemical (pyrotechnical) igniters. Plausibility of the MEC values lower than the ones measured in this research work is questionable due to several reasons.

First one of these is the use of high energy pyrotechnical igniter. The MEC of a dust cloud, by definition, is the lowest concentration of dust at which a self-sustained combustion propagation is achieved. The activation of pyrotechnical igniters, irrespective of their energy content, creates a fireball of burning chunks that is way bigger than the size of the sphere and practically covers the whole available space (Figure 4.4). A self-sustained propagation of the combustion zone through the dust air mixture cannot be achieved under these conditions and, as a consequence, each test is rather an igniter induced combustion propagation. Apart

from this, the ignition criteria in such systems (according to the European standard [46]) is an arbitrarily selected pressure rise of 0.3 bar in case of the 1m$^3$ and 0.5 bar in case of the 20-l sphere [26]. Since, the burning particle clusters from the activation of pyrotechnical igniters practically cover the whole available space in the apparatus, often it occurs that the concentrations that would otherwise not ignite, are forcefully combusted and lead to a small pressure rise, which consequently is counted as an ignition.

*Table 4.4: Comparison of MEC values of lycopodium*

| Source | Median particle size (µm) | Ignition source | Apparatus | MEC (g/m$^3$) |
|---|---|---|---|---|
| Addai [12, 22] | 32 | 10 J permanent spark | 20-l sphere | 125 |
| | | Hot surface at 420 °C | GG furnace | 108 |
| Addo [78] | 31 | 10 kJ chem. igniter | 1m$^3$ sphere | 40 |
| | | 2.5 kJ chem. igniter | 20-l sphere | 40 |
| Dastidar [79] | 31 | 10 kJ chem. Igniter | 1m$^3$ sphere | 34 |
| | | 2.5 kJ chem. Igniter | 20-l sphere | 38 |
| Abrahamsen [80] | 30 | 20 J permanent spark | 15-l Nordtest apparatus | 54 |
| | | 10 kJ chem. igniter | 20-l sphere | 8 |
| Sanchirico [81] | 32 | 10 J permanent spark | 20-l sphere | 125 |
| GESTIS-DUST-EX [82] | 30 | 2 kJ/10 kJ chem. igniter | 20-l/1-m$^3$ sphere | <15 |
| Present work | 31.7 | 1.5/ 3.0/4.5 J permanent spark | Open tube apparatus | 46 |

Apart from this, the concentration values reported in Table 4.4 (except the ones measured in this work) are not measured, rather calculated nominally by assuming a homogenous distribution of dust particles in the whole volume of the apparatus. This means that concentration value reported as the MEC practically refers to the mass of dust equally distributed through the whole volume of the vessel. The problem of non-homogeneity of dust distribution is controlled and (supposedly) eliminated by selection of an appropriate ignition delay time, corresponding to the moment when the dust is equally distributed in the sphere. DIN EN 14034-3, 2011 quotes a constant ignition delay time of 60 ms (20-l sphere), regardless of the size and density of the dust being tested. However, particles with higher density and/or larger particle size (e.g. iron, zirconium) would tend to settle faster than the ones with lower density and/or smaller particle size (e.g. lycopodium, polyethylene).

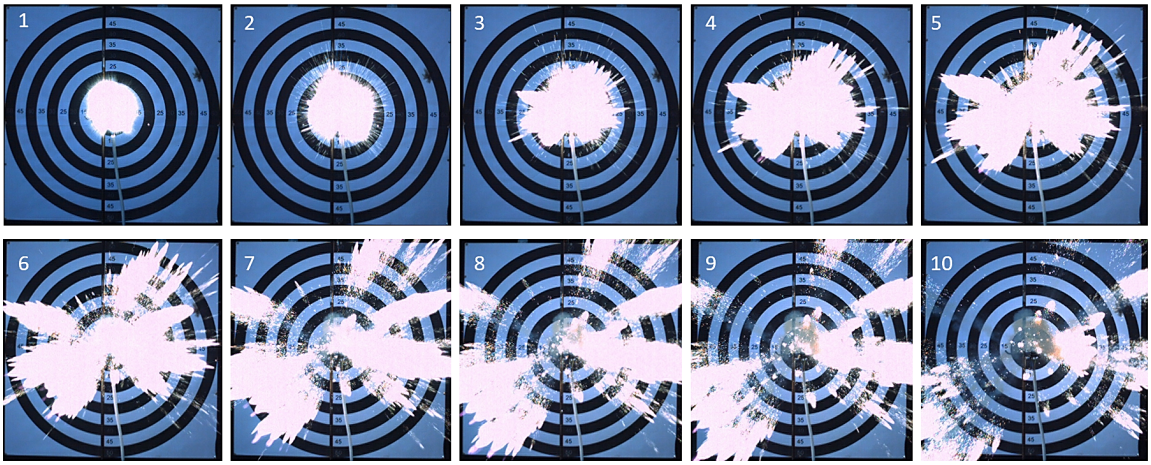


*Figure 4.4: Activation of pyrotechnical igniters [83]*

Two of the data sources listed in Table 4.4, namely Abrahamsen [80] and GESTIS-DUST-EX database [82] report exceptionally low MEC values (8 g/m$^3$ and <15 g/m$^3$ respectively) for lycopodium, although the median particle size is almost the same as all the other data sources. Considering that there are only two organic vapors with MEC values below 30 g/m$^3$,namely acetylene (26.6 g/m$^3$) and propyne (28.8 g/m$^3$), it is physically implausible that dust clouds would be more prone to ignition than vapors [26]. Combustion of dust clouds has all of the types of heat losses that occur as with the burning of vapour clouds, but has additional sources of heat losses, e.g. particulate radiation and endothermic pyrolysis.

Table 4.5 lists MEC values of titanium from different data sources. Considering the relation between the particle size and MEC, the value published in GESTIS-DUST-EX [82] should be higher than the ones recorded by Cashdollar [84] and Boilard [85] (≤ 45 µm) and the ones measured in this work. As reported by Wolanski [86] and quoted in [26] by Babrauskas, a MEC value of 30 g/m$^3$ for any material would mean an adiabatic flame temperature of ca. 600 K at the lean limit. This is physically implausible and obviously not consistent with the concept of a self-sustained flame propagation [26].

Most of reasons that advocate for the validity of MEC values of lycopodium measured in this work also argument for the plausibility of the MEC values of titanium. One of the most important arguments in this regard is that none of the values reported in the literature (Table 4.5) is truly measured MEC of titanium. As previously explained, all these concentration values are rather calculated nominally by assuming a homogenous distribution of a certain mass of dust in the whole volume of the sphere. The values determined in this work, however, are measured by the help of infrared sensors installed in the direct vicinity of the ignition source and therefore demonstrate higher accuracy.

*Table 4.5: Comparison of MEC values of titanium*

| Source | Particle size (µm) | Ignition source | Apparatus | MEC ($g/m^3$) |
|---|---|---|---|---|
| Boilard [85] | ≤ 20<br>≤ 45<br>≤ 150 | 2.5 kJ chem. igniter | 20-l sphere | 50<br>60<br>60 |
| Jacobson [87] | 10-104 | --------- | ------- | 45 |
| Cashdollar [84] | 25 (Median particle size) | 2.5 kJ chem. igniter<br>10 kJ chem. Igniter | 20-l sphere | 60<br>70 |
| GESTIS-DUST-EX [82] | 56 (Median particle size) | 2 kJ/10 kJ chem. igniter | 20-l/1-$m^3$ sphere | 30 |
| Present work | 25 (Median particle size) | 1.5/ 3.0/4.5 J permanent spark | Open tube apparatus | 105 |

## 4.3 LEL of flammable gas

LEL of methane was measured in the tube apparatus at different flow rates. The experimental procedure was similar to the one explained in section 4.1.2 (reliability of gas concentration) except the addition of an ignition source and removal of the gas analyser. Spark energy of 1.5 J (spark duration 50 ms) was used as the ignition source and visual flame detachment from the electrodes, as defined by DIN 51649-1, was used as the ignition criteria.

Independent of the flowrate, the LEL of methane was measured to be 5 vol.-%. Chemsafe database [61] reports a value of 4.4 vol.-% for the LEL of methane at atmospheric pressure and room temperature. The difference in these values could be attributed to the fact that methane flame at its lean flammability limit is very weak and nearly impossible to visualize under normal light conditions. Therefore, no flame could be observed in the tube apparatus at concentrations below 5 vol.-% and consequently a higher value of LEL was recorded. It must be mentioned here that also at 5 vol.-% methane concentration, no visual observation of the flame was possible, and ignition was detected by the deposition of a thin layer of steam on the tube wall, which was generated as a result of the combustion reaction.

## 4.4 LEL of hybrid mixtures

Based on the values of explosion limiting concentrations of individual components, LELs of hybrid mixtures were determined at different flow front velocities and ignition energies. For hybrid mixtures of lycopodium and methane, four flow front velocities, whereas for titanium and methane two flow front velocities were selected. Similar to the experiments with solitary dust, three ignition energies were tested for each of the flow velocity. Mixture compositions were selected as such that the concentration of dust and gas was below its MEC and LEL respectively. A summary of the results is presented in Figure 4.5 and Figure 4.6. The inserts in Figure 4.5 and Figure 4.6 represent the average of all the experiments compared with the linear line between MEC of the dust and LEL of the gas. The values plotted

therein present the lowest dust concentrations at which, in the presence of (a given concentration of) methane, a selfsustained combustion propagation was recorded. Detailed results are presented in Appendix B, sections B.5.1 and B.5.3. It must be mentioned here that the experimental results shown in Appendix B constitute only the results where the uncertainty was in the tolerable range. The tolerable range in this regard refers to the difference between the dust concentration values measured with the upper and lower sensor not exceeding 10 g/m$^3$ value. The data presented in Appendix B, sections B.5.1 and B.5.3 account for approx. less than half of the total experiments performed. The reason behind is simply the stochastic nature of these experiments. During these experiments, it was possible to produce a homogeneous dust cloud (the difference between upper and lower concentration meter negligible), however, not at all the test trials. Uncertainties associated with the measured dust concentrations were individually calculated for each value on the basis of the average uncertainty of 2.6% and 2.3% for the upper and lower sensors (see section 4.1.1) respectively as well as the difference between the values of upper and lower sensor. The values are listed in Table B.1 and Table B.2 in Appendix B.

Considering the uncertainty associated with the experimental values, it can be deduced that the LEL of hybrid mixtures (of lycopodium and methane and titanium and methane) does not significantly change by changing the flow velocity. An explanation to this behaviour could be the design of the experimental scheme, which aims at igniting the dust particles in a quasi-static state by changing the particle deceleration time with respect to the flow front velocity. Moreover, all the flow velocities tested in this work correspond to the laminar flow conditions and therefore do not substantially influence the process of combustion propagation.

It is generally claimed that MEC of dust cloud or LEL of a hybrid mixture decreases by increasing the ignition energy. The decrease in the MEC or LEL might be true for the high energy pyrotechnical igniters used in the 20-l sphere (overdriving effect of pyrotechnical igniters), however, in the present work, no significant change in the LEL of hybrid mixtures was observed by increasing the ignition energy. This is plausible, considering that MIEs of lycopodium, titanium and methane are <5mJ [82], 7mJ (measured inhouse) and 0.29 mJ [61] respectively. Ignition energies used in this research work are three orders of magnitude higher than the highest MIE (i.e. 7mJ).

Basic requirement, as highlighted by Buksowicz & Wolanski is that “ignition energy must be strong enough to ignite the mixture, but it should not affect the ensuing process of flame propagation. This is especially important at concentration limits, where too strong ignition source can support a flame which otherwise would have been extinguished. Furthermore, ignition must be activated at a proper time to match local concentration fluctuations” [88]. This prerequisite is achieved in the open tube apparatus by the application of 1.5 J ignition energy, which is sufficient to ignite the fuel mixture at its LEL without impeding flame propagation. Therefore,

higher energy values of 3.0 J and 4.5 J did not decrease the LEL of hybrid mixtures. Summarizing above discussion, one could affirm that the requirement of high energy pyrotechnical igniter could be relinquished, provided that a truly homogeneous and non-turbulent suspension of dust particles is achievable.

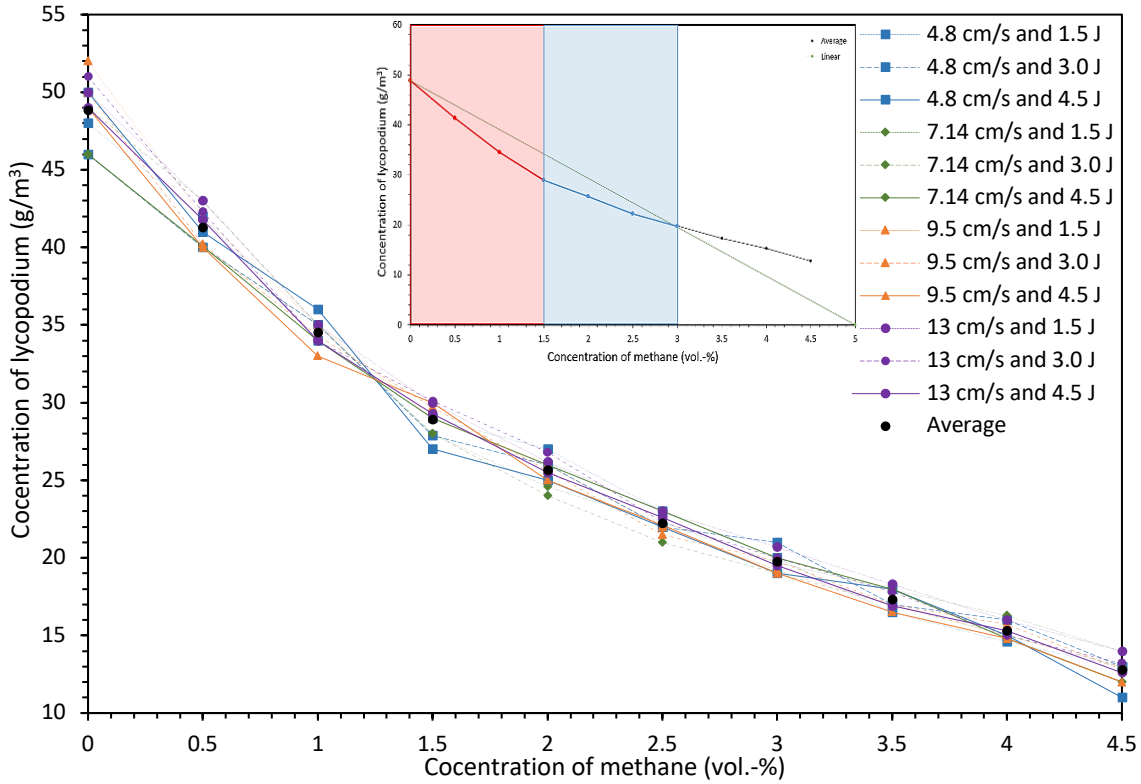


*Figure 4.5: LEL of hybrid mixtures of lycopodium and methane at different flow velocities and ignition energies*

It is a known fact that the dust concentration in a hybrid mixture at its LEL decreases with increasing flammable gas concentration in the mixture. The magnitude of this decrease in dust concentration is one of the major points of disagreement in the research community. Three competing views can be found in the literature. According to these viewpoints, the decrease in the dust concentration in a hybrid mixture at its LEL is

1. more than linear with increasing concentration of flammable gas [29],
2. linear with increasing concentration of flammable gas [30],
3. less than linear with increasing concentration of flammable gas [12].

Investigations carried out within the scope of this work revealed that the decrease in the dust concentration in a hybrid mixture at its LEL cannot be generalized and may follow more than one of the above-mentioned behaviour, depending on the relative concentration of the flammable gas in the mixture. This was especially evident in the case of lycopodium, where more than linear decrease in the dust concentration was observed upon addition of a small amount of methane i.e. 0-25% of its LEL (red section in Figure 4.5 insert). Beyond 25% of the LEL of methane, the decrease in the dust concentration shifted towards the linear line and

intersected it at 60% of the LEL of methane (blue section in Figure 4.5 insert). For methane concentration above 60%, the decrease in the dust concentration became very small (less than linear). Acknowledging the uncertainty associated with the measured dust concentration, no significant decrease in the dust concentration, above 60% of methane LEL, can be claimed with certainty.

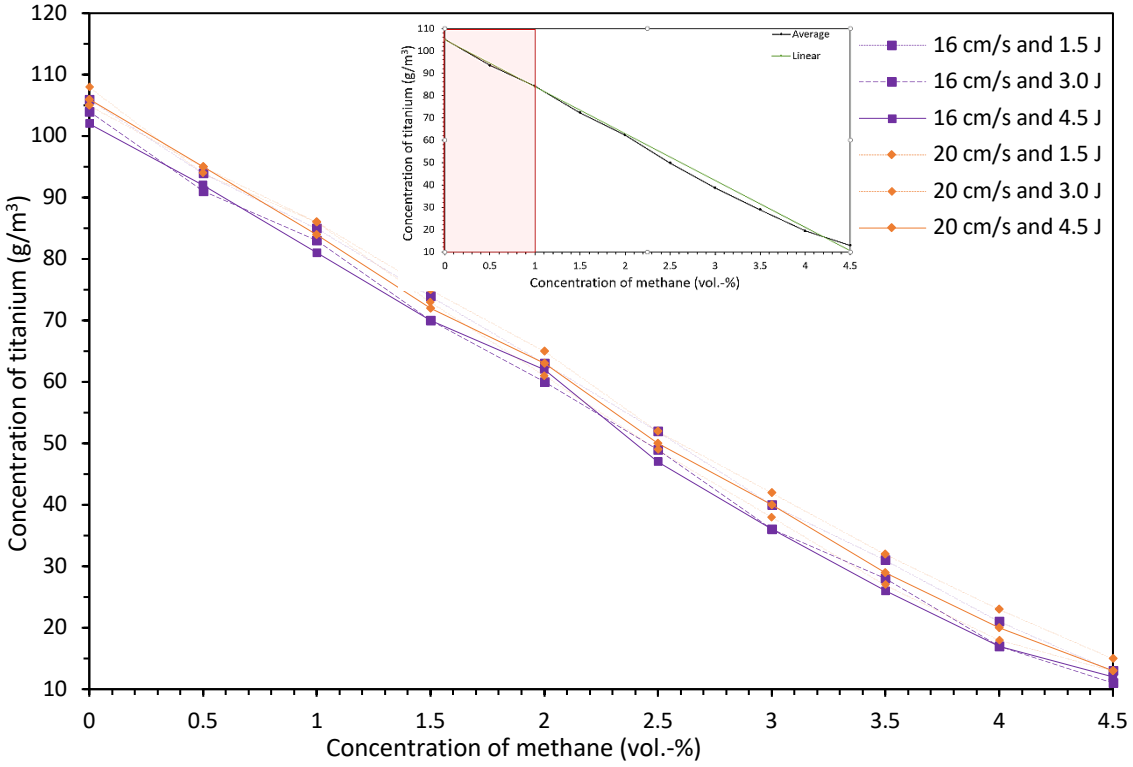


*Figure 4.6: LEL of hybrid mixtures of titanium and methane at different flow velocities and ignition energies*

For the hybrid mixtures of non-volatile dusts (titanium), the decrease in the dust concentration in a hybrid mixture at its LEL was found to be linear (Figure 4.6 insert). An important finding that was recorded for both (high volatile content and non-volatile) dusts is that no ignition was obtained at a concentration below 12 g/m$^3$ for any methane concentration below 5 vol.-%. This means that adding a small amount of dust does not lower the concentration of methane in hybrid mixture at its LEL.

German guideline VDI 2263 part 5 defines an explosible hybrid mixtures as a mixture of combustible dust and flammable gas or solvent, where the concentration of the gas phase is above 20% of its LEL [2, 3]. This means that addition of up to 20% of flammable gas or solvent does not have any effect on the explosibilty of the dust. This claim needs to be reconsidered based on the findings of this research work, where a maximum decrease in the dust concentration (for the case of lycopodium) was recorded in the concentration range 0-20% of the LEL of flammable gas. However, on the other hand, addition of up to 12 g/m$^3$ of combustible dust in a flammable gas at its LEL did not seem to have any effect on the LEL of the gas and therefore could be considered as negligible.

# 5 THEORETICAL EVALUATION OF LEL OF HYBRID MIXTURES

Hybrid mixture explosion is a complex phenomenon that may include a number of dynamic (time dependent) processes like laminar and turbulent fluid flow, heat transfer from an ignition source to the dusts suspended in air and to the gas-air mixtures, multiphase turbulent combustion, and combustion acceleration by mechanisms that are poorly understood even for gas-air mixtures alone. Given the intricacy of these processes, a multitude of parameters (related to the combustible dusts and flammable gases, turbulent effects, combustion dynamics, ignition source and to the enclosure) are required to describe the physics of the hybrid mixture explosions. Baker [41] reported over 40 parameters to characterise such explosions.

Since most of the research on hybrid mixtures is experimental and the interaction between dust and gas is not fully understood so far, there exist different opinions in the research community about the transformation of explosion behaviour of combustible dusts by the addition of the flammable gases. Two of the most important differences of opinion in this regard are the definition of the worst-case scenario and the evolution of LEL of hybrid mixture by increasing gas concentration in the mixture. One school of thought suggests that the explosion severity decreases with the dust addition along the lines of constant mixed stoichiometric ratios and the worst-case condition is pure gas near its stoichiometric concentration [14, 89]. In contrast, several other studies advocate that the worst-case scenario occurs at different concentrations of dust and gas in the hybrid mixture [12, 90-92].

The second bone of contention deals with two competing models, namely Le Chatelier's mixing rule and Bartknecht's relation, for the theoretical evaluation of lower explosion limits of hybrid mixtures. A detailed review of these models is presented in Chapter 2. The empirical nature of these models together with the lack of a physical and/or thermodynamic explanation makes the results of these models unreliable. This means that these models might hold true in certain cases for a first-order approximation of the LEL of hybrid mixtures, however, in some cases these represent overly conservative values and in others not conservative enough, which essentially implies that there is a non-zero probability of occurrence of an explosible mixture in the non-explosible concentration ranges defined by these relations. Thus, a more sophisticated and general correlation, able to define the LEL of a hybrid mixture as function of basic thermodynamic properties of the individual fuel components, is required.

This chapter provides the derivation of a mathematical model for the evolution of LEL of hybrid fuel mixtures with increasing gas concentration in the fuel mixture, utilizing conservation equations of mass and energy as its origin. The derived model will then be applied to different hybrid mixtures to calculate their LEL. The

theoretical results are then to be compared with and validated through experimentally determined LEL values.

## 5.1 Model derivation

LEL of any combustible material is the concentration below which, in spite of the triggering of a sufficiently strong ignition source, self-supporting flame propagation is no longer possible. In other words, it is the lowest amount of fuel per unit volume of the fuel oxidant mixture, which upon complete combustion produces enough energy to raise the temperature of the next unit volume of reaction mixture from ambient to the flame temperature.

This definition of LEL/MEC of a dust or gas is not new. Burgess and Wheeler [93] in 1911 first utilized this approach to define the LEL of flammable gases in terms of heat balance [53, 94, 95]. Later, in 1958, Zabetakis, Lambiris and Scott [96] applied this rule to many combustible gas air mixtures [95]. According to Burgess and Wheeler, when a source of energy, such as an electric spark, is introduced into a mixture of a combustible gas and air, flame propagation will not occur until two conditions are simultaneously fulfilled. The first of these is that the initial source of heat is of a volume, intensity, and duration sufficient to raise the temperature of the layer of gases in its immediate vicinity to a temperature higher than, or as high as, the ignition (flame) temperature of the mixture. The second condition implies that the heat contained in the products of combustion of this first layer is sufficient to raise the adjacent layer to its ignition-temperature. The LEL of a flammable gas in this regard refers to the smallest concentration of the gas that would allow the second condition to be fulfilled.

An energy balance based definition of the MEC of a dust cloud is also not new, in fact, the first attempt to predict the MEC of a dust cloud was presented by Jaeckel following the same concept [11, 12, 97, 98]. Jaeckel considered a space of constant volume as such that on one side of this space a hot plane surface was assumed. One dimensional heat transfer from a plane flame front to the adjacent layer of the dust was considered. The explosion of the dust cloud was proposed to start by heating and ignition of the dust particles in the layer parallel with and adjacent to the hot surface. The energy released by this combustion in turn heated and ignited the next dust/air layers, and in this manner, explosion propagated through the dust cloud. Jaeckel considered that in a lower limit mixture there are just

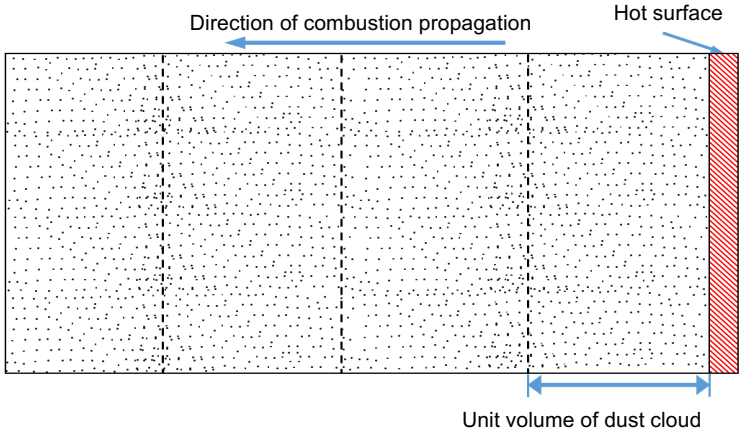


*Figure 5.1: Jaeckel's space of constant volume [96]*

enough particles in each parallel layer to produce the heat (of combustion) required to bring the adjacent layer to the combustion temperature and to take care of the heat losses by radiation and conduction to the surrounding.

Jaeckel was the first one, however not the only one relating the MEC of a dust cloud to the heat of combustion and the combustion temperature. Several other authors have employed the same energy balance concept, however with slight modifications, for the determination of the MEC of a dust cloud. Zehr modified Jaeckel's theory by replacing the assumption of an ignition temperature of finite value by the assumption that the dust clouds near the MEC have a combustion temperature of 1000 °C [98]. Other authors utilizing same approach (with certain modifications) include Schönewald, Schevchuk, Buksowics and Wolanski [11, 12, 88, 98]. Details regarding these models can be found in [11, 12, 98].

Khalili [30] employed an enthalpy balance approach (similar to Jaeckel's theory) to calculate LEL of hybrid mixtures, however it did not bring any added advantage to Le Chatelier's model. One of the major drawbacks in Khalili's approach was to introduce the experimentally determined LEL/MEC values of individual components in his equation, which itself is incorporated with inherent uncertainties and sources of errors and cannot be taken as an absolute value.

The fundamentals of modelling explosion limiting concentration of a hybrid mixture are based on the mass balance of the combustible component content and the enthalpy balance of the whole system. For a stationary flame in one dimensional model, these balances are given as follows:

$$-\dot{m}\frac{dx_F}{dy} + D_{F,m}\rho_m\frac{d^2x}{dy^2} + \nu_F M_m r = 0 \qquad (5.1)$$

$$-\dot{m}C_{p,m}\frac{dT}{dy} + \lambda_m\frac{d^2T}{dy^2} + (-\Delta h_R)r = 0 \qquad (5.2)$$

Where, $\dot{m}$ is the superficial mass velocity, $\nu_F$ is the stoichiometric coefficient and $M_m$ is the molecular weight. Subscripts $F$ and $m$ represent the fuel and the mixture of fuel and oxidant (air in this case) respectively.

The mass and energy transfer equations, (equations (5.1) and (5.2)) may be simplified to equations (5.3) and (5.4), accordingly, by considering only convective parts, neglecting the conductive terms:

$$-\dot{m}\frac{dx_F}{dy} + \nu_F M_m r = 0 \qquad (5.3)$$

$$-\dot{m}C_{p,m}\frac{dT}{dy} + (-\Delta h_R)r = 0 \qquad (5.4)$$

Solving these equations for the rate of reaction, r, yields:

$$r = -\frac{\dot{m}}{\nu_F M_m} \cdot \frac{dx_F}{dy} = -\frac{\dot{m} C_{p,m}}{(-\Delta h_R)} \cdot \frac{dT}{dy} \quad (5.5)$$

$$\frac{dx_F}{dy} = \frac{\nu_F \overline{C}_{p,m}}{(-\Delta h_R)} \cdot \frac{dT}{dy} \quad (5.6)$$

where $M_m \cdot C_{p,m} = \overline{C}_{p,m}$ is the molar heat capacity of the reaction mixture. Equation (5.6) may also be written as:

$$\int_{x_{F,i}}^{0} dx_F = \frac{\nu_F \overline{C}_{p,m}}{(-\Delta h_R)} \cdot \int_{T_i}^{T_f} dT \quad (5.7)$$

Figure 5.2 represents the temperature and concentration gradients in a one-dimensional stationary flame without heat loss. At $y = 0$, the limiting component $F$ is completely oxidized or combusted, where the temperature is equal to the combustion (or flame) temperature, $T_f$. The initial concentration and temperature of hybrid fuel mixture are given by $x_{F,i}$ and $T_i$ respectively.

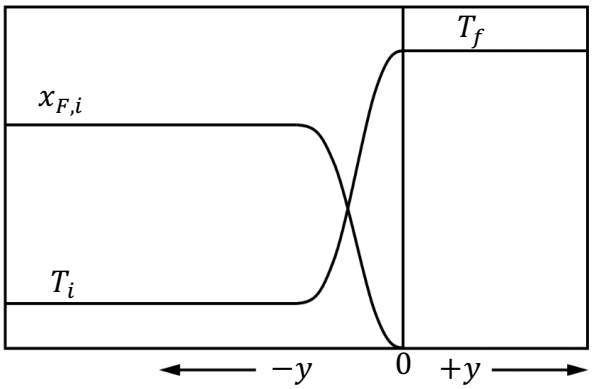


*Figure 5.2: Temperature and concentration gradients in a one-dimensional stationary flame*

The boundary conditions for equation (5.7) are:

$y = -\infty \qquad x_F = x_{F,i} \qquad T = T_i$

$y = 0 \qquad x_F = 0 \qquad T = T_f$

An integration of equation (5.7) gives:

$$-x_{F,i} = \frac{\nu_F \overline{C}_{p,m}}{(-\Delta h_R)} \cdot (T_f - T_i) \quad (5.8)$$

Since $(-\Delta h_R)$ is based on one kmol of combustible fuel mixture, $\nu_F = -1$. Moreover, $\overline{C}_{p,m}$ is the mean molar heat capacity of the reaction mixture and is given by:

$$\overline{C}_{p,m} = x_F \overline{C}_{p,F} + x_A \overline{C}_{p,A} = x_F \overline{C}_{p,F} - x_F \overline{C}_{p,A} + \overline{C}_{p,A} \quad (5.9)$$

Thus, by incorporating equation (5.9) in equation (5.8), the following equation can be derived:

$$x_{F,i} = x_F = \frac{\left(x_F \overline{C}_{p,F} - x_F \overline{C}_{p,A} + \overline{C}_{p,A}\right)}{(-\Delta h_R)} \cdot \Delta T \qquad (5.10)$$

where $\Delta T = \left(T_f - T_i\right)$ represents the rise in temperature from ambient or initial to the combustion temperature.

By applying all the simplifications, Equation (5.10) could be rewritten as:

$$x_F = \frac{\overline{C}_{p,A} \Delta T}{(-\Delta h_R) - \overline{C}_{p,F}\, \Delta T + \overline{C}_{p,A}\, \Delta T} \qquad (5.11)$$

where $\overline{C}_{p,F}$ and $(-\Delta h_R)$ correspond to the mean molar heat capacity and the heat of combustion of the fuel mixture. Since in case of hybrid mixtures of combustible dust and flammable gas, fuel constitutes the total amount of dust and flammable gas in the system, $\overline{C}_{p,F}$ and $(-\Delta h_R)$ are given as:

$$\overline{C}_{p,F} = x_d \overline{C}_{p,d} + x_g \overline{C}_{p,g} \qquad (5.12)$$

$$(-\Delta h_R) = x_d\left(-\Delta h_{R,d}\right) + x_g\left(-\Delta h_{R,g}\right) \qquad (5.13)$$

These relations assume that the net heat of combustion and the mean molar heat capacity are deduced from the heat of combustion and molar specific heat of the individual species. This postulates that the presence of reactants or products in the reaction of the dust does not affect the reaction stoichiometry of the flammable gas and vice versa. Hence, merging these values in Equation (5.11) yields:

$$x_F = \frac{\overline{C}_{p,A} \Delta T}{x_d\left(\left(-\Delta h_{R,d}\right) - \overline{C}_{p,d}\, \Delta T\right) + x_g\left(\left(-\Delta h_{R,g}\right) - \overline{C}_{p,g}\, \Delta T\right) + \overline{C}_{p,A}\, \Delta T} \qquad (5.14)$$

In equation (5.14), $x_d$ and $x_g$ account for the relative amount of dust and gas in the hybrid fuel mixture. $x_F$ is the ratio of number of moles of fuel mixture and the total number of moles in the system (fuel and air). In other words, it represents the minimum amount of explosible fuel mixture, which, upon complete combustion, would release sufficient energy to raise the temperature of the whole reaction mixture from ambient to the combustion temperature. This amount is referred to as the LEL of the hybrid fuel mixture.

$$LEL_H = \frac{\overline{C}_{p,A} \Delta T}{x_d\left(\left(-\Delta h_{R,d}\right) - \overline{C}_{p,d}\, \Delta T\right) + x_g\left(\left(-\Delta h_{R,g}\right) - \overline{C}_{p,g}\, \Delta T\right) + \overline{C}_{p,A}\, \Delta T} \cdot 100 \qquad (5.15)$$

Equation (5.15) calculates the LEL of hybrid mixture (in mol.-%) as a function of mole fractions of its individual constituents (fuel only basis) and their basic thermodynamic properties. It can also be used to calculate the MEC of pure dust or LEL of pure gas by defining the combustible fraction of the reaction mixture as 100% dust or gas respectively.

Assumptions required to arrive at this equation include:

- Complete combustion of the total fuel present in the system.
- No radiation heat losses occur from the system.
- Combustion kinetics of the pure species are independent and unchanged by the presence of other combustible species.
- The combustion temperature at the LEL is the same for all the species.
- Dust particles are sufficiently small so that the influence of particle size distribution may be neglected, and the dust cloud may be treated as a premixed gas.

## 5.2 Material Characterization for model parameters

In order to calculate LEL of hybrid mixtures using Equation (5.15), a number of input parameters were required. Parameters related to gases (e.g. heat capacity, heat of combustion, density) are listed in Table 3.3. A discussion on the employed values of parameters related to dusts and hybrid mixtures, along with their validity, is presented in the following sections.

### 5.2.1 Combustion temperature

***Hybrid mixtures of organic dusts***

For the calculation of the theoretical values of LEL, a constant temperature rise (ΔT) of 1000 K ($T_f \approx 1300\ \mathrm{K}$) was selected as an ignition criterion for all the hybrid mixtures of organic dusts. This value of temperature rise ties well with the previous studies of Zehr [11, 98].

Considering that the combustion (or flame) temperature is one of the main parameters determining the application of the presented model, assuming a constant value of the combustion temperature for different materials and their mixtures might seem to be an unrealistic approach. However, it should be underlined that the actual temperature of the combustion zone is often greatly different from adiabatic one, which is widely quoted in literature and is considered to be a material property. For example, in case of methane and starch mixtures, Khalili [30] calculated the adiabatic flame temperatures (using the software CEA) of 2595K and 1705K (for starch and methane, respectively) being greatly different than the actually obtained maximum value of 1400K at stoichiometric concentration.

Several other authors have also investigated the combustion temperature of dust clouds [99-103]. Figure 5.3 presents a summary of experimentally measured combustion temperatures of lycopodium, wherein the reported values vary

between 952 K (measured by Proust for a concentration of 39 g/m$^3$) and 1473 K (measured by Han for a concentration of 52 g/m$^3$). Furthermore, Zabetakis [96] carried out an extensive investigation on the flame temperatures of limit mixtures for a number of hydrocarbon gases and reported values in the range of 1500 K (for methane) to 1660 K (for n-Butane). Klemens and Wolanski [104] measured the combustion temperature of hybrid mixtures of lignite and methane (4.2 vol.-% methane and 19 g/m$^3$ lignite) in an open tube apparatus and reported values between 1100 K to 1500 K for different locations in the tube.

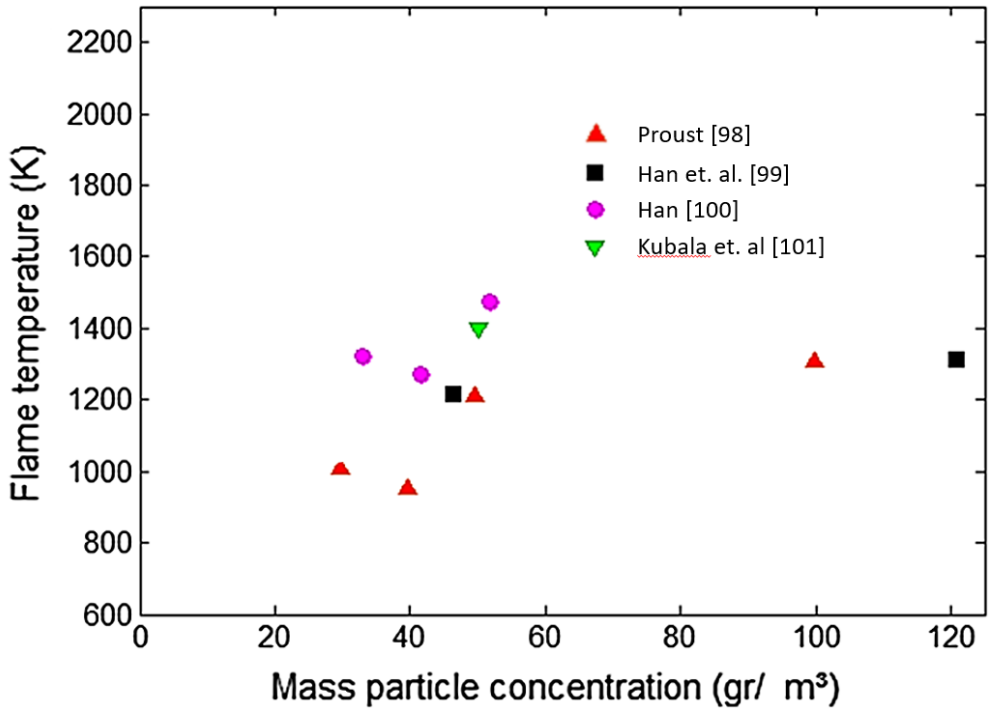


*Figure 5.3: Combustion temperature of lycopodium as a function of its concentration (according to [103])*

It must be added at this point that the "flame" temperature for a dust cloud - in a strict sense - does not exist. A flame is a gas phase reaction and the measured temperature (for example in Figure 5.3) is the reaction temperature of the volatiles being combusted. The temperature at which the heterogeneous reaction of the dust particles takes place could in principle also be measured, but appropriate measurement techniques for fast moving particles do not exist. All the "flame" temperature data reported in the the literature are lumped temperatures with questionable theoretical backing. Moreover, any temperature measurement has a response time. In thermocouple measurements applied to fast moving flames the thermal inertia could lead to large errors.

Summarizing above discussion, it can be concluded that considering a combustion temperature value of 1300 K is a plausible approximation for the calculation of LEL of hybrid mixtures of hydrocarbon dusts and gases, taking into account the large scatter in the experimental data and the shortcomings of the existing measurement methods.

### *Hybrid mixtures of titanium*

It has been quoted by several authors that the metal powders combust at considerably higher temperature values than the hydrocarbon gases [11, 85]. Considering that this temperature is several hundred Kelvins higher than the flammable gas temperature, using a single value of temperature for the calculation of LEL of hybrid mixtures with different proportions of dust and gas would be unrealistic. To overcome this problem, an average temperature of the mixture, which would change by changing the mixture composition, could be calculated utilizing the heat balance in the combustion zone.

Consider a hybrid mixture combustion zone consisting of a given number of particles of mass ($m_p$) and a flammable gas of mass ($m_g$), combusting at their respective temperatures. The heat balance equation for this system can be formulated as following:

$$H = C\bar{T} = m_g C_{p,g} T_g + m_d C_{p,d} T_d \qquad (5.16)$$

where C and $\bar{T}$ are the overall heat capacity and the average combustion temperature of the fuel mixture, respectively, and are given by:

$$C = m_g C_{p,g} + m_d C_{p,d} \qquad (5.17)$$

$$\bar{T} = \frac{m_g C_{p,g} T_g + m_d C_{p,d} T_d}{C} \qquad (5.18)$$

$C_{p,d}$ and $C_{p,g}$ are the specific heat capacities and $T_g$ and $T_d$ are the combustion temperatures of the titanium and methane respectively. Following the argumentation as for the hybrid mixtures of lycopodium and methane, the flame temperature of methane $T_g$ was considered to be 1300 K. The values of $C_{p,d}$, $C_{p,g}$ and $T_d$ were taken from literature and are listed below.

$C_{p,d}\ at\ 2000\ K = 0.787\ J/g.K$ [105]
$C_{p,g}\ at\ 1300\ K = 6.67\ J/g.K$ [75]
$T_d = 2050\ K$ [106]

$m_g$ and $m_d$ are the mass of methane and titanium particles in the combustion zone and can be calculated from the high-speed images of the reaction zone, if the volume of the reaction zone and concentration of dust and gas in the system is known. Figure 5.4 shows a high-speed image of the reaction zone of a hybrid mixture of titanium and methane with concentrations of 29 g/m$^3$ ($C_d$) and 3.5 vol.-% ($C_g$), respectively.

For this system, $m_g$ and $m_d$ are given as:

$$m_d = C_d \cdot V_f \qquad (5.19)$$

$$m_g = \left({}^{C_g}/_{100}\right) \cdot \rho_g \cdot V_f \qquad (5.20)$$

where $\rho_g$ is the density of methane and $V_f$ is the volume of the reaction zone, which is calculated by dividing the reaction zone into a hemisphere and a cylinder. The sum of the volume of the hemisphere and the cylinder is equal to the volume of the reaction zone.

$$V_f = \left(\frac{2}{3}\pi r^3\right) + (\pi r^2 h) \qquad (5.21)$$

where

$r = radius = 20\,mm$
$h = height = 13\,mm$

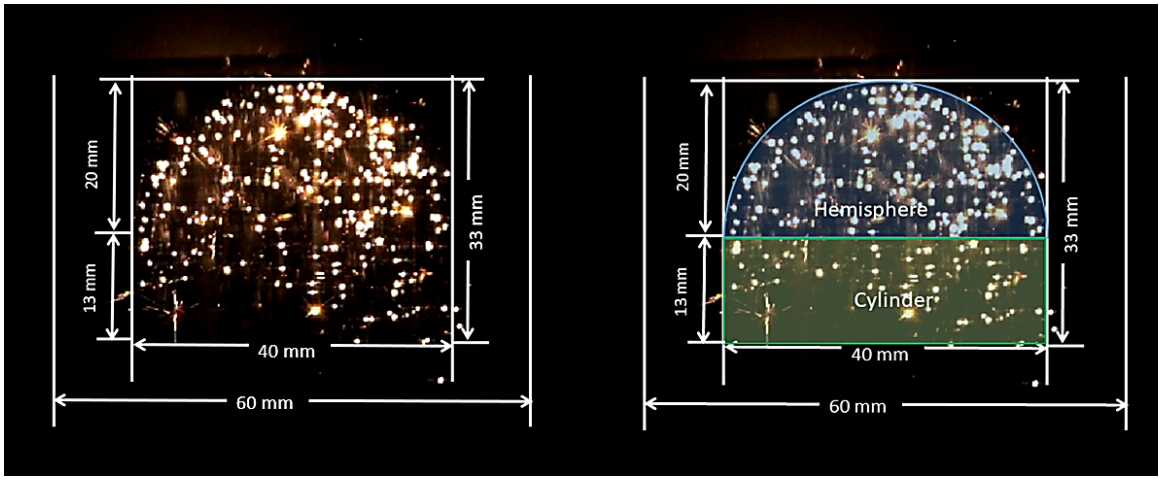


*Figure 5.4: Combustion zone of hybrid mixture of titanium and methane*

Following this procedure, the average combustion temperature for hybrid mixtures of titanium and methane was calculated with respect to different mixture compositions. Results are presented in Table 5.1.

*Table 5.1: Average combustion temperatures of hybrid mixtures of titanium and methane*

| $C_d\ (g/m^3)$ | $C_g\ (vol.\%)$ | $\overline{T}\ (K)$ |
|---|---|---|
| 105 | 0 | 2050 |
| 94 | 0.5 | 1783 |
| 84 | 1 | 1635 |
| 72 | 1.5 | 1537 |
| 62 | 2 | 1472 |
| 50 | 2.5 | 1421 |
| 39 | 3 | 1383 |
| 29 | 3.5 | 1355 |
| 19 | 4 | 1333 |
| 13 | 4.5 | 1320 |
| 0 | 5 | 1300 |

### 5.2.2 Heat of combustion and molar heat capacity

The heat of combustion or calorific values of all the dusts were measured experimentally by employing a combustion calorimeter (IKA®, C 200). The measured values were validated according to DIN 51900.

The values of molar heat capacities of dusts were taken from the literature and are listed in Table 5.2.

*Table 5.2: Heat of combustion and molar heat capacities of dust materials*

| Dust Sample | Heat of combustion (MJ/mol) | Molar heat capacity (J/(mol*K)) |
|---|---|---|
| Lycopodium | 2.3 | 107 [107] |
| Corn Starch | 2.73 | 264 [108, 109] |
| Niacin | 2.7 | 152,5 [71, 108] |
| Titanium | 1.05 | 24,9 [105] |

### 5.2.3 Elemental analysis

In order to define the LEL of a hybrid mixture in molar units, the average molecular weight of dusts was required. This was calculated by utilizing the quantitative elemental analysis data, collected inhouse by using CS230 (LECO®) for sulphur and CHN628 (LECO®) for carbon, hydrogen, oxygen and nitrogen, in accordance with ISO 29541 and ISO 19579:2002, respectively. Results are listed in Table 5.3. An example of the molecular weight calculation using elemental analysis data is presented in Appendix A.4.

*Table 5.3: Average molecular weight of dust materials*

| Dust sample | Elemental analysis (wt. -%) | | | | | Average M.wt (g/mol) |
|---|---|---|---|---|---|---|
| | C | H | O | S | N | |
| Lycopodium | 68.4 | 9.6 | 20.7 | 0.3 | 1 | 76 |
| Corn Starch | 43.7 | 7.3 | 48.8 | 0.2 | 0 | 162 |
| Niacin | 58.6 | 4.4 | 26 | 0 | 11 | 123 |
| Titanium | -- | -- | -- | -- | -- | 47.8 |

## 5.3 Comparison and validation with experimental results

The impact of relative amounts of the mixture constituents (dust and gas) on its LEL was predicted for a number of hybrid mixtures, using the proposed model. For the sake of comparison and validation of modelled results, two series of experiments were performed using different apparatuses, namely the 20-l sphere and the open tube apparatus. Details about these experiments are presented in the following sections.

### 5.3.1 20-l sphere

The experimental protocol was the same as defined by EN 14034-3 [46] for the measurement of MEC of dust cloud, however, with two modifications. These included the employment of a permanent electrical spark instead of the pyrotechnical igniters as the ignition source and the introduction of a flammable

gas through partial pressure method. Further details about the experimental setup and procedure can be found in [12, 13].

Based on quantifiable errors in the experimental system, an uncertainty of ±12% was considered and consequently added to all the values of dust concentration where an explosion was recorded. A detailed calculation of the experimental uncertainty of this system is presented in [12].

Results are presented in Figure 5.5 - Figure 5.7, wherein the proposed model is plotted along with Le Chatelier's law and Bartknecht's model and compared with the current and previous experimental findings of Addai et. al., [21], who used the same experimental system to investigate LEL of hybrid mixtures. In addition to the classical representation of LEL of hybrid mixtures, where dust concentration is presented in mass per unit volume and gas concentration in vol.-%, the results are plotted in molar units, where relative amount of dust and gas in the mixture is presented in mole fractions of the fuel mixture and LEL of hybrid mixture is presented in mol.-% of the total reaction mixture. For this purpose the experimental values reported by Addai [21] were converted into molar units. Conversion formulas are given in Appendix B.6**.**

In order to demonstrate the dependency of theoretically calculated LEL of a hybrid mixture using equation (5.15) on the combustion temperature, two additional lines with respect to the combustion temperatures of 1000 K and 1600 K were plotted (Figure 5.5 - Figure 5.7). In the following discussion, theoretically calculated LEL or the values calculated by the model refer to the values of LEL of hybrid mixtures, calculated using equation (5.15) and a combustion temperature of 1300 K ($\Delta T$=1000 K). These are presented in Figure 5.5 - Figure 5.7 by a solid black line.

A comparison of experimental values with the models revealed that for the hybrid mixtures of niacin, the experimental values were closest to the Le Chatelier's line. For lycopodium and starch hybrid mixtures, the values lied in between Le Chatelier's line and Bartknecht's curve, except one outlier. Addai et. al., [21] recorded a clear explosion at 50% of MEC of starch (102 g/m$^3$) and 20% of LEL of methane (0.92 vol.-%), thus registering an explosion in the non-explosible area defined by Bartknecht's curve (Figure 5.7 A and B).

The reasons why certain hybrid mixtures deviate from the above-mentioned models are twofold and closely connected. Both of these models calculate the change in the LEL of a hybrid mixture, with respect to change in its composition, based on the individual explosion limits of solitary dust and gas, which are experimentally measured. It has been discussed in detail in sections 2.1.1 and 4.2.1, that the MEC/LEL values measured in the 20-l sphere are unreliable and possess large uncertainties. Therefore, it is natural that the models of Bartknecht and Le Chatelier do not always correspond to the experimental values.

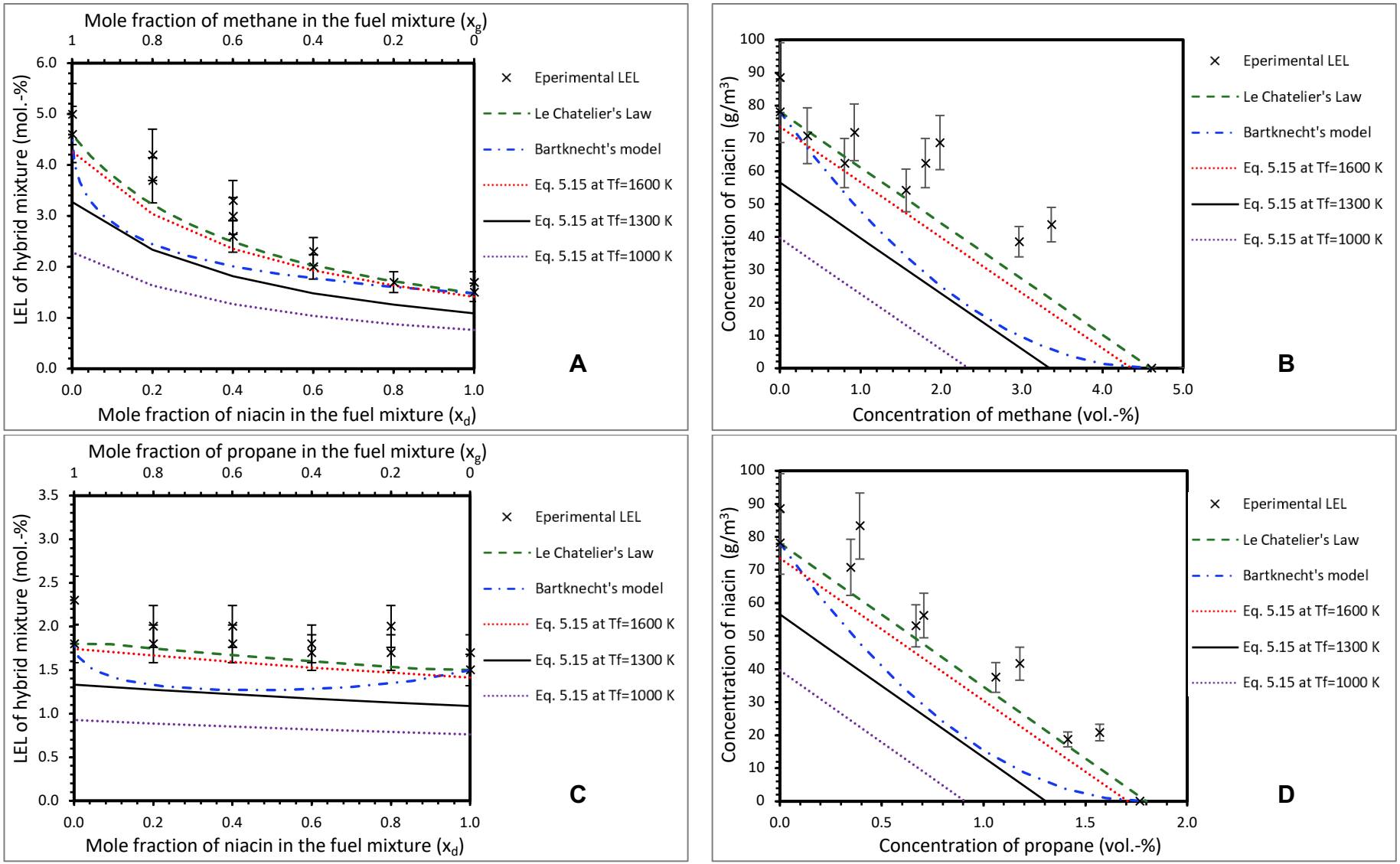


*Figure 5.5: LEL of hybrid mixtures of Niacin with methane and propane*

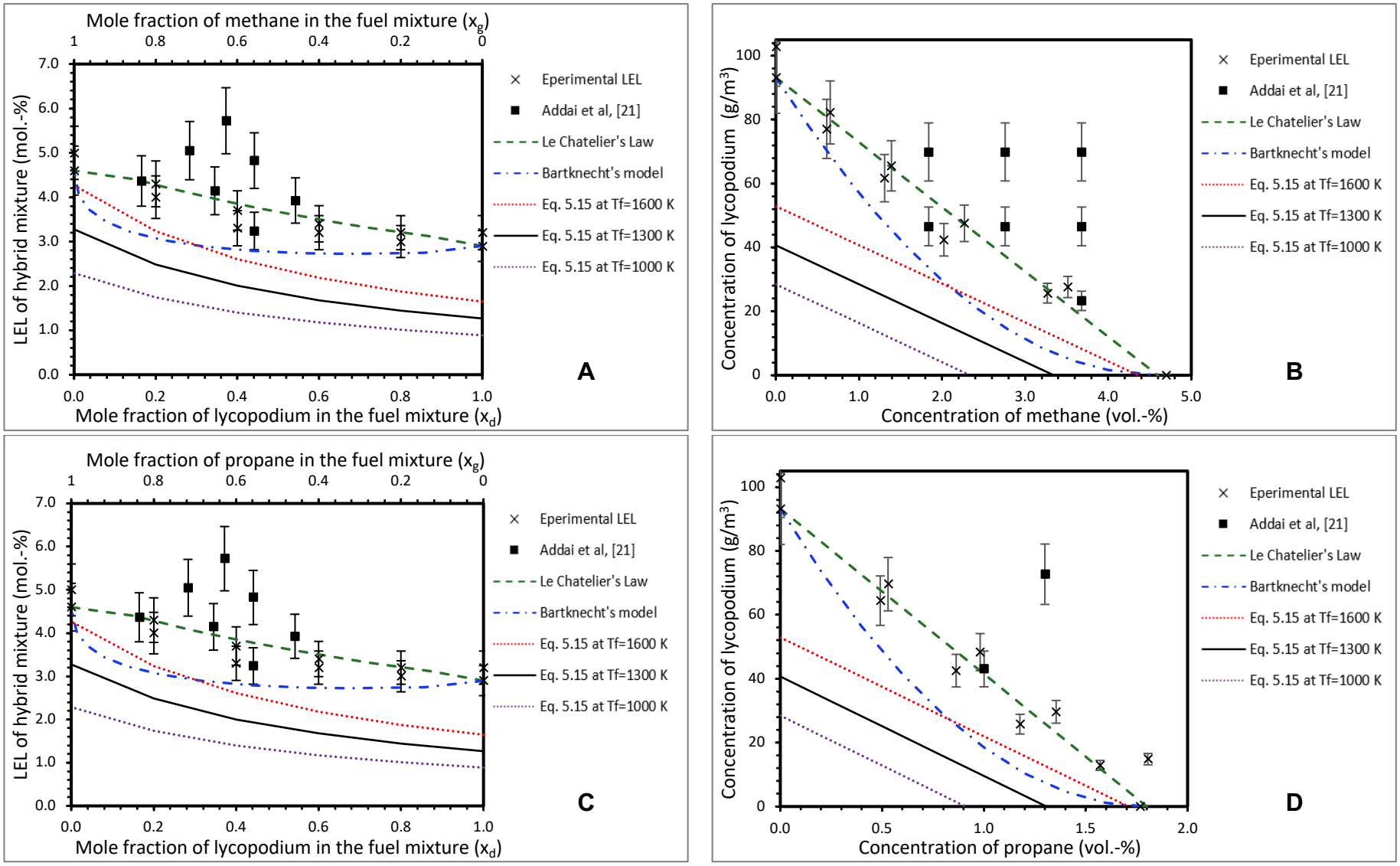


*Figure 5.6: LEL of hybrid mixtures of lycopodium with methane and propane*

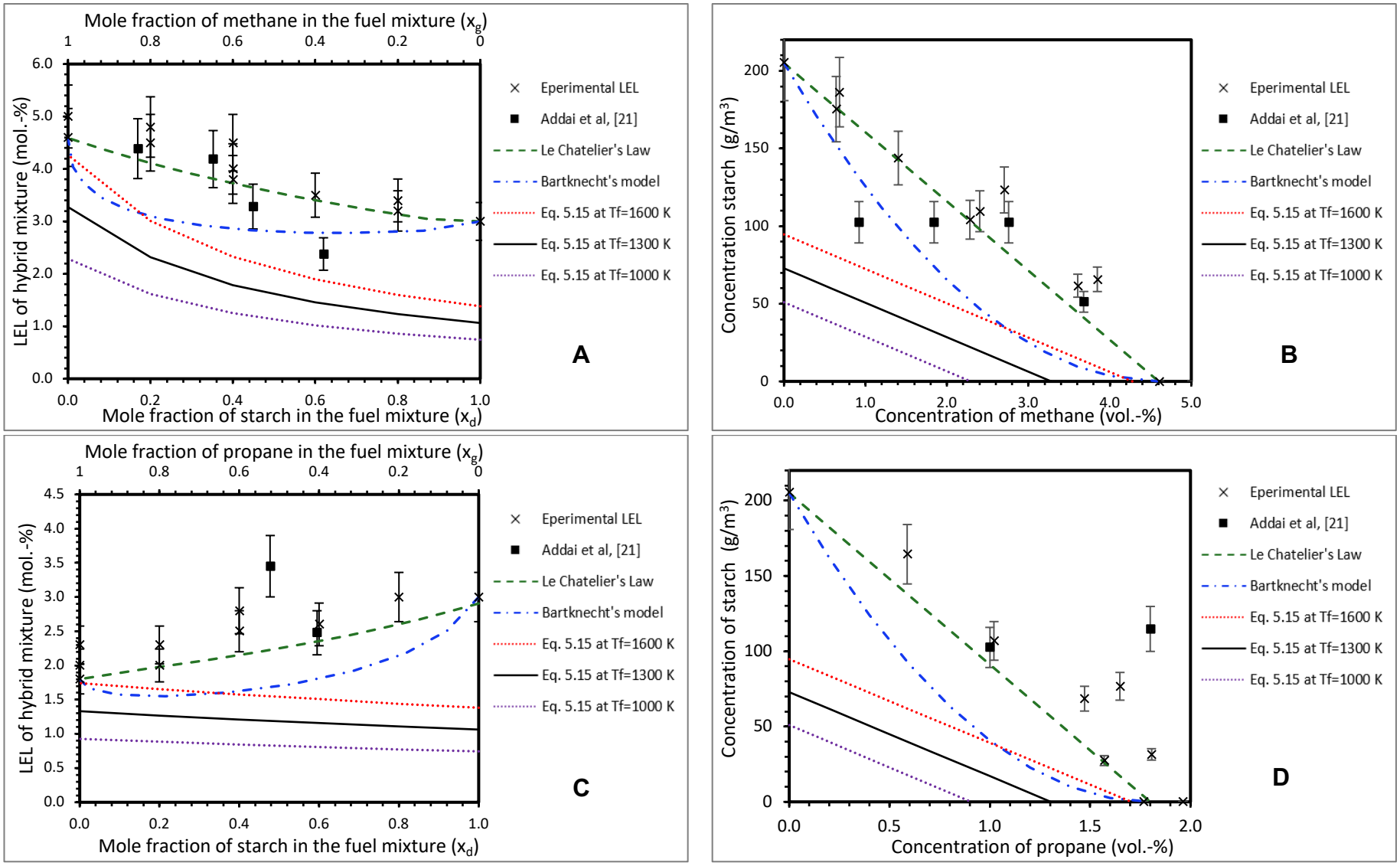


*Figure 5.7: LEL of hybrid mixtures of starch with methane and propane*

On the other hand, the experimentally determined values of LEL of hybrid mixtures (for the comparison with theoretical values) using the 20-l sphere (because of its unreliability) can also not be taken as a final word. Even if the models were correct, it is inconclusive to evaluate them based on the experimental results, which themselves cannot be described as accurate. An approach, where unreliable and biased experimental results are employed to validate the results of empirical equations that were developed using the same erratic experimental data, is indecisive. A better approach can be, as proposed in this research work, developing models that are independent of experimental data and calculate the LEL of hybrid mixtures based on fundamental thermodynamic data of the individual materials and consequently validating the results of these models by employing experimental methods, which are free of bias and unrealistic assumptions.

Irrespective of the inaccuracies induced through discrepancies in the experimentally determined MEC/LEL of dust or gas, Bartknecht's model, when analysed in an energy balance perspective, leads to implausible results. This is especially evident for hybrid mixtures, where the MEC and LEL of solitary dust and gas, respectively, lie in a close proximity of each other, when presented in the same unit system. To demonstrate this with the help of an example, let us consider Figure 5.8, where change in the LEL of hybrid mixture of niacin and methane, with respect to changing mixture composition, is presented in molar units. For this hybrid mixture, niacin (with 1.5 mol.-%) has a lower value of lean flammability limit in comparison to propane (1.8 mol.-%).

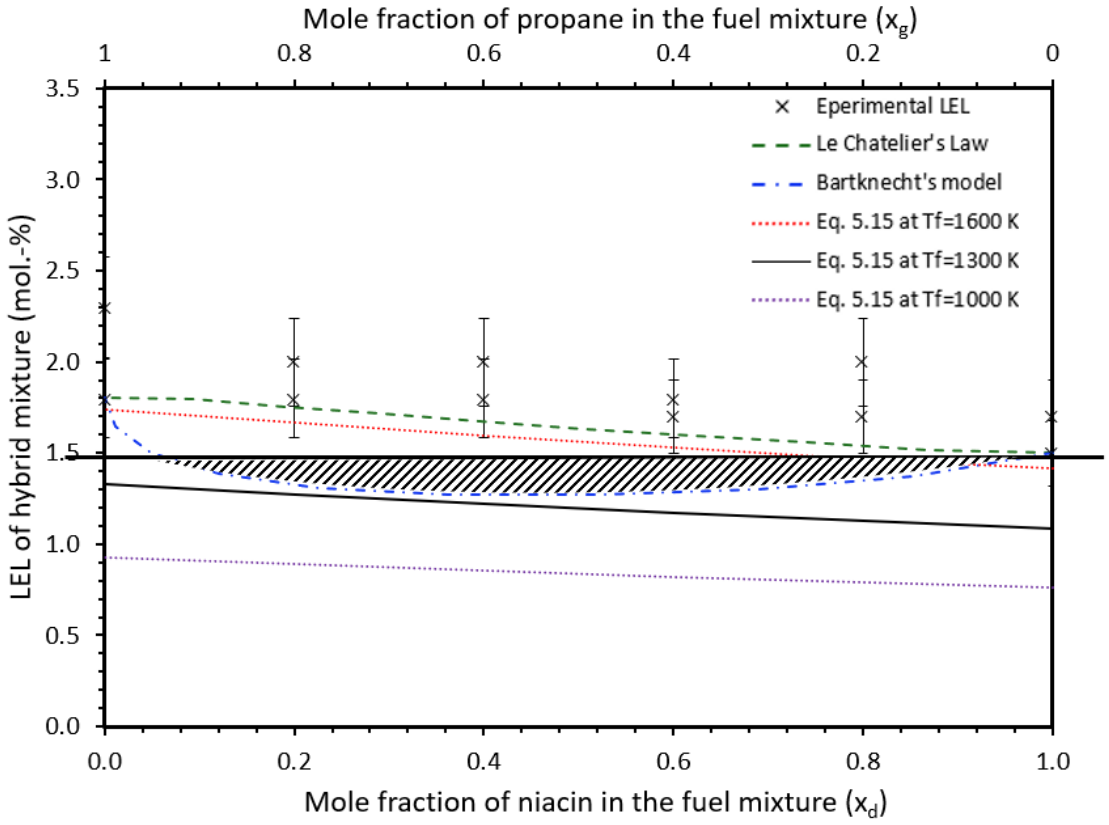


*Figure 5.8: LEL of hybrid mixture of niacin and propane*

Plotting a horizontal line, starting from the MEC of niacin, reveals a region of Bartknecht's curve, where for certain mixture compositions, the LEL of hybrid mixture can be lower than the MEC of niacin. From a heat balance perspective, this suggests that burning a certain amount of niacin and propane together would liberate more heat per unit mass then the sum of the heat that would be released, when they are being combusted alone. This is physically inconceivable and can only be justified in the case when propane and niacin, before reacting with the oxygen, react with each other and create new species that are able to release more energy per unit mass than both niacin and propane. However, in this case, the reaction of niacin and propane unquestionably needs to be highly endothermic. Since an endothermic reaction would require external energy input, which of course is not present in this case, Bartknecht's formula can be regarded as far-fetched and unexplainable according to the laws of physics.

In contrast to Bartknecht's formula, the model proposed in this work attempts to describe the hybrid mixture explosion (where concentration of dust and gas is below their respective MEC/LEL) by the consideration of energy contribution by each individual species upon combustion that would contribute to the total heat generation in the system, resulting in an overall increase in temperature. When this total energy produced equals the energy required to heat the system to the reaction temperature, the mixture is considered to be at its LEL. The LEL in this context concerns the total fuel content of the system. For the example shown in Figure 5.8, the overall effect of heat generation (as a result of combustion) and heat absorption (resulting in temperature rise) for propane and niacin is in comparable range. Reducing the amount of propane below its explosible concentration, by changing the composition of the mixture, results in an energy deficient system, which lacks a certain amount of energy to enable the combustion reaction to prevail through whole system. This energy is provided by approximately the same amount (molar units) of niacin (since the heat of combustion is roughly the same), thus keeping the overall amount of fuel more or less constant.

### 5.3.2 Open tube apparatus

As mentioned in section 4.4, for the LEL measurements in open tube apparatus, hybrid mixtures of two dusts, namely lycopodium and titanium with methane were selected. Experimental values of LEL of hybrid mixtures being presented in this section are the average of the values measured at different flow front velocities and ignition energies (see section 4.4). For the values measured in the open tube apparatus, an average uncertainty of ±5 g/m$^3$ and ±8 g/m$^3$ was considered for the lycopodium and titanium concentration, respectively, which in molar units corresponds to 0.2 mol.-% and 0.3 mol.-%, respectively.

For the theoretically calculated values of LEL of hybrid mixtures of lycopodium and methane, the same combustion temperature criterion as explained in the previous section was used, while for the titanium methane mixtures, variable values of

combustion temperature calculated in section 5.2.1, listed in Table 5.1, were employed. Results are shown in Figure 5.9.

For the hybrid mixtures of both dust (lycopodium and titanium) with methane, a comparison of the theoretically calculated LEL values with the experimentally determined ones yielded plausible results. The theoretically calculated values of LEL were at all concentrations lower than the experimentally measured ones.

For the hybrid mixtures of lycopodium and methane, LEL values measured with the open tube apparatus were more conservative than the ones measured with the 20-l sphere. A possible reason behind this deviation could be that the open tube apparatus measures the LEL of hybrid mixtures under quasi-static conditions, whereas the 20-l sphere operates under high turbulence. As it will be explained in Chapter 6 in detail, hybrid mixture flames near their lean flammability limits are weak and dependent on the local heat buildup around the ignition source. In the 20-l sphere the turbulence is so high that the local heat buildup may not make it to form an ignition kernel that would grow into a local combustion zone and consequently ignite the rest of the fuel. The high turbulence in the 20-l sphere may quench the combustion reaction at a very early stage of its development. In the presence of high energy pyrotechnical igniters that covers the whole volume of the 20-l sphere, the quenching effect due to high turbulence becomes irrelevant. Since in the present work only a point ignition source was used, the high turbulence might have had affected the growth of the combustion zone negatively. In rich mixtures the heat and mass transfer are enhanced by the turbulence and the combustion propagation velocity would increase due to better mixing. However, in hybrid mixtures close to their flammability limits, this might result in quenching of the combustion and therefore no explosion.

An important finding that could be pointed out by analyzing Figures 5.5 - 5.9 is that when plotting the explosion limits of hybrid mixtures in molar units, the individual LEL/MEC of the respective components define the limiting values within which the LEL of the hybrid mixtures would lie. However, how the LEL of the hybrid mixture would change within these limits with respect to the variations in the mixture composition depends on the overall effect of heat generation capacity (as a result of combustion) and heat absorption potential (resulting in the temperature rise) of the individual components. Starting with the LEL of the component with higher value the decrease in the LEL of the hybrid could be either linear or more or less than linear depending on the combustion temperature, heat capacity and calorific values of individual components of the hybrid mixture.

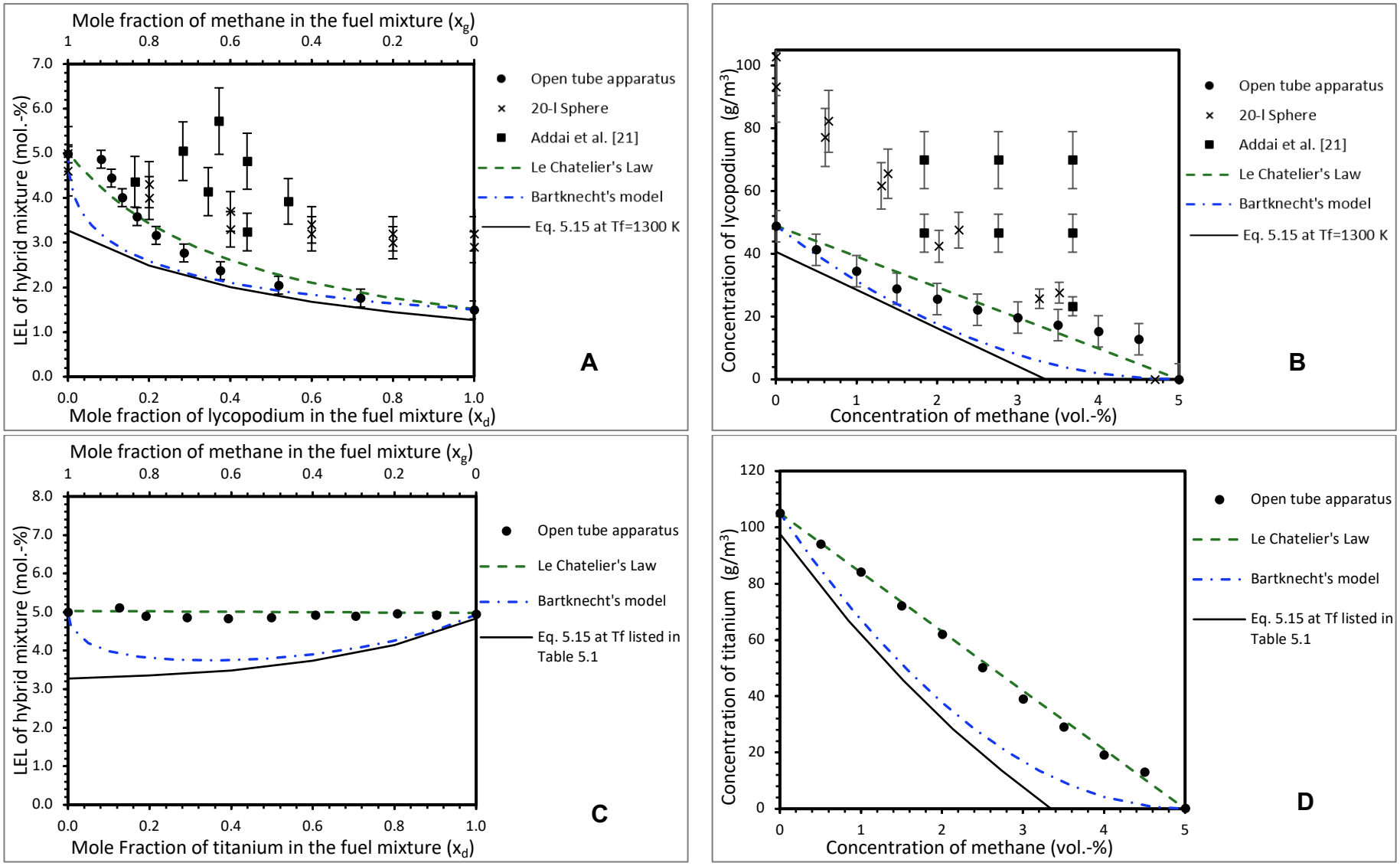


*Figure 5.9: LEL of hybrid mixtures of lycopodium (A&B) and titanium (C&D) with methane*

# 6 IGNITION AND COMBUSTION PROPAGATION IN HYBRID MIXTURES NEAR LEAN FLAMMABILITY LIMITS

Hybrid mixture combustion is a complex phenomenon, where individual constituents of a hybrid mixture (e.g. dust and gas) get oxidized at their own finite rate. In hybrid mixtures, where the concentration of each component is below their respective explosion limit, burning of only one component cannot support an autonomous combustion propagation. Since for hybrid mixtures of dust and gas the combustion of former is the slowest process, it seems reasonable to deduce that the propagation of combustion wave in a hybrid mixture (with concentration close to its LEL) could be mainly controlled by the dynamics of dust combustion.

The behaviour of dust combustion depends on a number of successive steps of the oxidation process of the combustible fraction. For the volatile dusts (dusts that release volatile components up on heating) these include devolatilization of the volatile content of the solid fuel, mixing of the volatiles with oxygen in the gas phase, combustion of the volatiles and combustion of the remaining solid fraction (mostly char). Alternatively, for non-volatile dusts (e.g. metal powders) combustion occurs on solid surface, where a gaseous reactant (usually oxygen) diffuses to the surface of the particle, adsorbs onto the surface of the fuel particle, reacts with the solid to form a product, which desorbs from the surface and diffuses back into the free stream environment. In both cases, it is sometimes not clear which of the above-mentioned steps determines the rate of the combustion reaction. However, it is evident that the combustion of dust particles is mainly influenced by the conditions of mass transfer in the vicinity of the combustion zone [73].

In the following sections, experimental findings regarding the ignition and the combustion propagation in hybrid mixtures of volatile and non-volatile dusts, with a focus on experimental observations, will be presented utilizing the high-speed videos. For all the experiments presented in this chapter, a spark duration of 50 milliseconds was used. The experimental setup and procedure have been explained in detail in Chapter 3**.**

## 6.1 Hybrid mixtures of organic dusts with high volatile content

Hybrid mixtures of lycopodium and methane were selected as representative of hybrid mixtures of organic dusts with high volatile content. In order to have a comprehensive investigation and to be able to differentiate between the dust and the hybrid mixture explosion behaviour, ignition and propagation of the combustion wave in lycopodium-air mixtures (in the absence of methane) was first examined.

### 6.1.1 Ignition and combustion propagation in dust air mixture

Experiments were performed at four flow front velocities with the lycopodium concentration corresponding to the MEC value at each flow velocity. Following observations were made:

- The ignition started with the local combustion of powder particles getting trapped in the spark, creating a spherical shaped ignition kernel directly above the spark igniters. The ignition kernel continued to grow upwards into a more prominent combustion zone for the first 35 to 50 ms of the activation of the ignition source. For example, at the flow velocity of 4.8cm/s this growth lasted for 37 ms. (frame # 1 to frame # 7 in Figure 6.1). During its growth phase, the combustion zone spread for approximately 50 to 70 mm upwards from the ignition source.

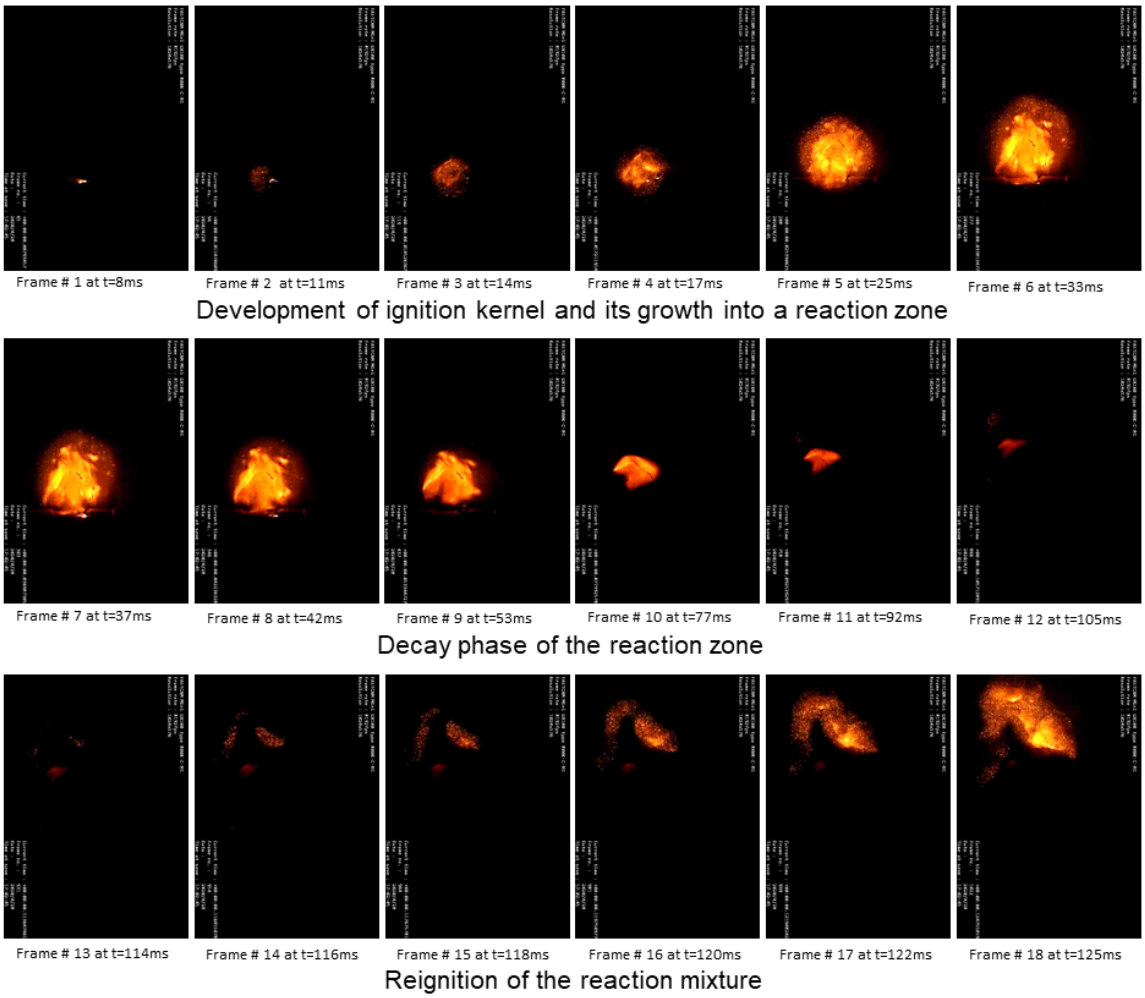


*Figure 6.1: Combustion propagation in lycopodium dust air mixture (flow velocity = 4.8 cm/s, dust concentration = 48 g/m$^3$)*

After the growth phase, the decay of the combustion zone started, which lasted for about 40 to 80 ms (frame #7 to frame # 12 in Figure 6.1). After a partial or complete decay, the reaction mixture got reignited, travelled for approximately 200 to 300 mm vertically and eventually got quenched.

- Combustion propagation speed was measured at four flow front velocities with a dust concentration corresponding to the MEC at each flow velocity. Although the measured dust concentration at all the flow velocities was in a narrow range (46 to 52 g/m$^3$), a *"random"* distribution of combustion propagation speed values was observed. The word *"random"* has been deliberately used here because the change in the combustion propagation velocity could not be attributed to the variations in the flow velocity or the dust concentration.

*Table 6.1: Average combustion propagation speed of lycopodium-air mixtures*

| Flow velocity (cm/s) | Dust concentration (g/m$^3$) | Combustion propagation speed (m/s) |
|---|---|---|
| 4.8 | 48 ±5 | 0.98 |
| 7.14 | 46 ±3 | 0.79 |
| 9.5 | 52 ±4 | 1.29 |
| 13 | 50 ±5 | 0.86 |

A probable explanation to the "random" change in the combustion propagation speed might lie in the measurement procedure. The combustion propagation speed was measured by recording the time required for the reaction zone to travel a vertical distance of 12 cm above the spark igniters. The starting point in this regard was the initiation of the spark igniters. The initiation of the spark, however, did not always result in the immediate development and growth of an ignition kernel. At the flow velocity of 7.14 cm/s, an active and growing ignition kernel could only be observed after approximately 60 ms of the activation of the spark (Figure 6.2). Whereas, at the flow velocity of 9.5 cm/s, the ignition kernel was observable immediately after the activation of the spark igniters. The delay of 60 ms for the former case was not considered in the calculation of the combustion propagation speed.

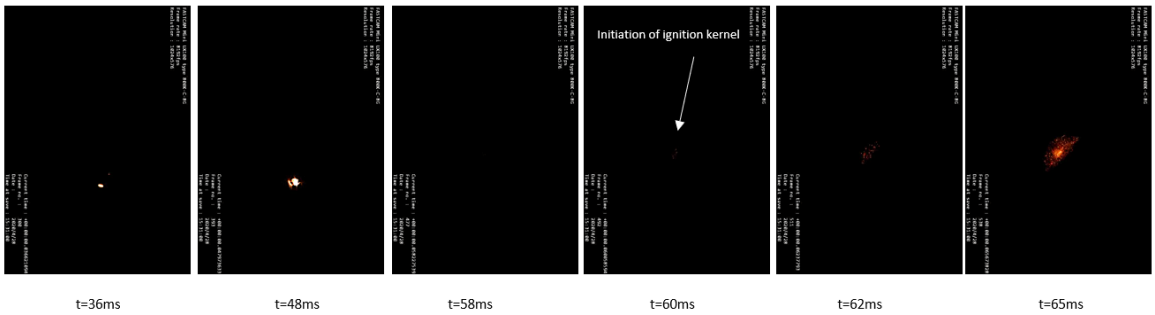


*Figure 6.2: Delayed ignition at flow velocity of 7.14 cm/s*

- Based on the light intensity, the combustion zone in lycopodium dust could be divided into two parts: a central mostly irregular shaped highly luminous zone and a (relatively) spherical shaped low intensity zone that formed an envelope around the luminous zone (Figure 6.3). The luminous zone could either be due to formation of the heated soot particles, which are formed by the decomposition or cracking of the hydrocarbons present in the volatile matter that is released

from the particles as a result of pyrolysis, or due to the generation of carbon monoxide owing to the partial combustion of the non-volatile matter (mostly char) at the centre of the reaction zone, since most of the oxygen is consumed by the outer (gaseous) flame and the leftover non-volatile matter is starved of oxygen. The outer low intensity part of the reaction zone was considered to be the gas phase combustion zone.

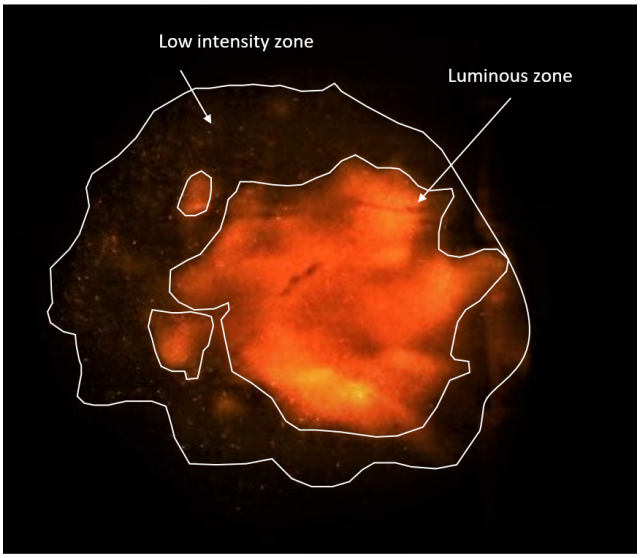


*Figure 6.3: Structure of lycopodium combustion zone close to its MEC*

- In all the experiments, the ignition started with the creation of the low intensity gas flame, which, while growing upwards, developed into the high intensity reaction zone at its centre or the lower part.
- During the decay phase of the combustion zone, the gaseous (or low intensity) flame disappeared within the first 10 to 15 ms. The luminous part on the other hand either travelled upwards or got stretched upwards or laterally under the effect of buoyancy.
- For all the experiments in which the concentration of lycopodium was close to its MEC, a combustion propagation was observed only in the upward direction. A backward propagation of the combustion wave was observed only in the rich mixtures.
- In dust air mixtures, where the concentration of dust was reasonably above the MEC, activation of the ignition source created an ignition kernel that immediately expanded through the whole tube, swallowing almost all of the unburnt fuel-air mixture. Contrary to this, in dust-air mixtures where the concentration of the dust was close to its MEC, the ignition kernel did not expand through the whole unburnt fuel-air mixture. In such mixtures, the combustion zone rather exhibited an intermittent state and got completely or partially extinguished, and then reignited once or several times while travelling through the unburnt fuel-air mixture.

### 6.1.2 Ignition and combustion propagation in hybrid mixtures

Following the experiments on the pure dust-air mixtures, hybrid mixtures of lycopodium and methane were tested. Starting with the addition of 0.5 vol.% of methane, the ignition and combustion propagation mechanism were investigated at the minimum dust concentration at which an ignition was registered. Next, the flammable gas concentration was gradually increased with a step of 0.5 vol.% and for each step the ignition and combustion propagation at the minimum concentration of dust, which would allow a successful ignition, was studied. The maximum gas concentration tested was 4.5 vol.%. Similar to the dust air mixtures, four flow front velocities were tested.

The results of the hybrid mixtures experiments showed similarities and differences compared to the observations made in the pure dust experiments. In all of the hybrid mixtures experiments, the ignition started with the development of an ignition kernel upon activation of the ignition source.

Regarding combustion propagation, two distinct mechanisms were observed.

#### 6.1.2.1 Intermittent combustion propagation

Intermittent combustion propagation refers to the type of combustion propagation in which the combustion zone does not exhibit a continuous growth through the whole unburnt fuel oxidant mixture but rather evinces an intermittent state and, while travelling through the unburnt fuel oxidant mixture, partially or globally extinguishes. After a time span of a few milliseconds, the fuel oxidant mixture reignites and an upward moving combustion wave is re-established.

As mentioned previously, combustion propagation in lean hybrid mixtures was investigated at four flow front velocities, namely 4.8 cm/s, 7.14 cm/s, 9.5 cm/s and 13 cm/s. All the experiments conducted at the flow velocity of 4.8 cm/s showed an intermittent combustion propagation. At the flow velocities of 7.14 and 9.5 cm/s, the combustion propagation was predominantly continuous (see section 6.1.2.2) with seldom random cases of intermittent combustion propagation. There was no intermittent combustion propagation observed at the flow velocity of 13 cm/s.

In all the experiments where an intermittent combustion propagation was observed, it was rather seldom that the combustion wave would propagate through the whole tube. Approximately 20 % of the experiments were such, where the combustion wave got extinguished and reignited more than once. For the rest of the 80%, the combustion wave only reappeared once and got quenched after travelling a distance of 80 to 100 mm from the spark igniters. However, since the ignition criterion defined in this work was visible detachment of the combustion zone from the ignition source, these were registered as successful ignitions.

By analysing the intermittent combustion propagation recorded in this work, it was observed that in all of the experiments the ignition kernel did not grow into a combustion wave that would detach from the ignition source and travel vertically for a few centimetres, as was observed for the case of pure lycopodium, but rather

it was confined to the close vicinity of the ignition source and got quenched immediately after the spark was deactivated. The very few cases in which the ignition kernel physically detached from the igniters were during the decay phase of it, after the spark was deactivated. Figure 6.4 shows an example of such a case, where the central luminous part of the ignition kernel could be seen detaching from the ignition source and moving upwards under the effect of buoyancy.

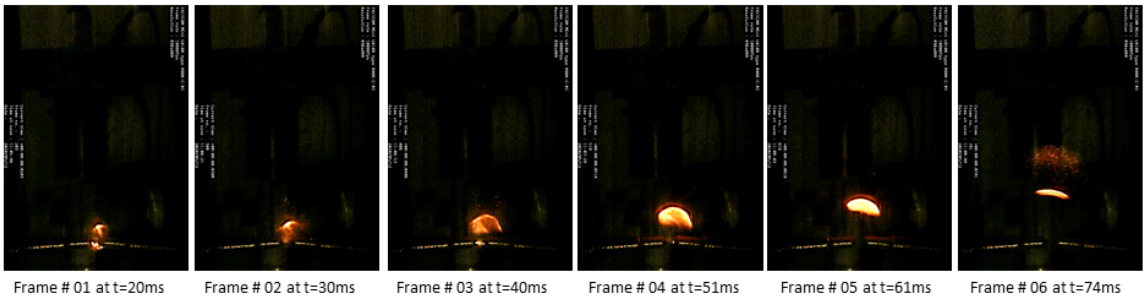


*Figure 6.4: Ignition kernel in hybrid mixture of lycopodium (30 g/m$^3$) and methane (1.5 vol.%) at flow velocity of 4.8 cm/s*

Figure 6.5 presents an example of the intermittent combustion propagation in hybrid mixtures of lycopodium and methane. Contrary to the dust air mixtures, where the development of the ignition kernel was mostly delayed, a fully-grown ignition kernel can be seen within the first 15 ms of the activation of the spark (frame # 06). Interestingly, instead of growing further in size, the ignition kernel started decaying between 19 and 44 ms (frame # 07 – frame # 11) even though a permanent spark was constantly present. After almost a complete decay of the ignition kernel, the fuel got reignited at 45 ms. This contributed to the further growth of the ignition kernel before it got completely quenched after 60 ms of the activation of the spark. Following a short pause of approx. 7 ms, a combustion zone emerged at a location a few centimetres above the spark igniters, which followed a growth phase of 20 ms (frame # 17 to frame # 21) and a decay phase of another 15 ms (frame # 21 to frame # 24). At 102 ms (shortly after frame # 24), the combustion zone got completely extinguished and there was no combustion propagation observed for the next 82 ms. This time, in which there was no visual detection of the combustion zone possible, will be referred to as deadtime in the further discussion. An upward propagation of the combustion zone was re-established at 184 ms (frame # 25) at a location slightly above the spot, where the combustion zone got quenched.

A probable reason behind the intermittent combustion propagation could be that the development of the ignition kernel generated a wave, which pushed the particles around the kernel away for a short distance. This created a partially empty zone, where the concentration of the hybrid mixture was so low that the growth of the ignition kernel into a self-supporting combustion zone could not be achieved, and a fuel rich zone directly above the empty zone, where the upward moving particle came in contact with the downward moving particles. When reaching the

empty zone, the growth of the combustion zone stopped due to lack of unburnt fuel, and the combustion zone started decaying. The hot combustion gases however continued to move upwards, eventually encountering the fuel rich zone.

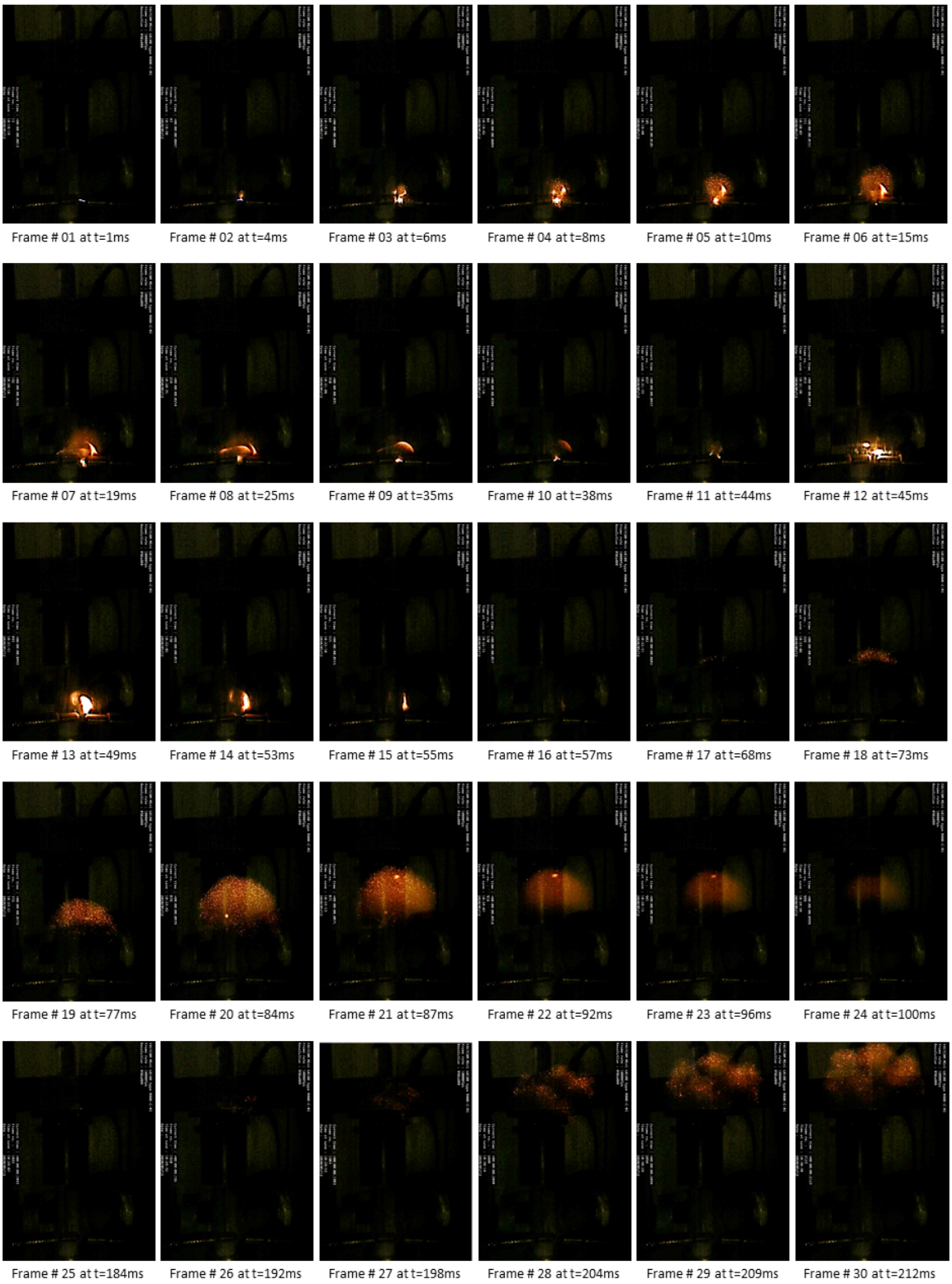


*Figure 6.5: Combustion propagation in hybrid mixture of methane (2 vol.%) and lycopodium (30 g/m$^3$) at flow front velocity of 4.8 cm/s*

In most of the experiments two successive combustion zones were detached from each other in space and time. Therefore, the outset of the second combustion zone could not be explained with absolute certainty. A most probable and logical explanation could be that the hot gases released from the combustion of the first combustion zone pyrolyzed the dust particles in the fuel rich zone, releasing hot pyrolysis gases. Due to the presence of hot combustion gases in the immediate surrounding, the local temperature of the pyrolysis gases surpassed their auto-ignition temperature resulting in the reignition of the fuel mixture.

#### 6.1.2.2 Continuous propagation of the combustion zone

Continuous combustion propagation refers to the type of combustion propagation where the combustion zone does not get extinguished while travelling through the unburnt fuel air mixture, but rather exhibits a continuous growth without a decay phase or a deadtime.

It is of prime importance to differentiate between the continuous combustion propagation that is generally observed in rich fuel-air mixtures and what was observed in hybrid mixtures at concentrations close to their LEL. The combustion propagation in rich hybrid mixtures recorded in this study was accompanied by an initiation of the ignition kernel within the first 3 to 8 ms (depending on the fuel concentration), followed by the rapid growth of the kernel into a combustion zone that spread through the whole available space in the tube. Figure 6.6 shows the combustion propagation in a hybrid mixture of lycopodium and methane with a respective concentration of 41 g/m$^3$ and 2.5 vol.%. The lowest dust concentration allowing a successful ignition for this particular hybrid mixture (2.5 vol.% methane) was 22 g/m$^3$.

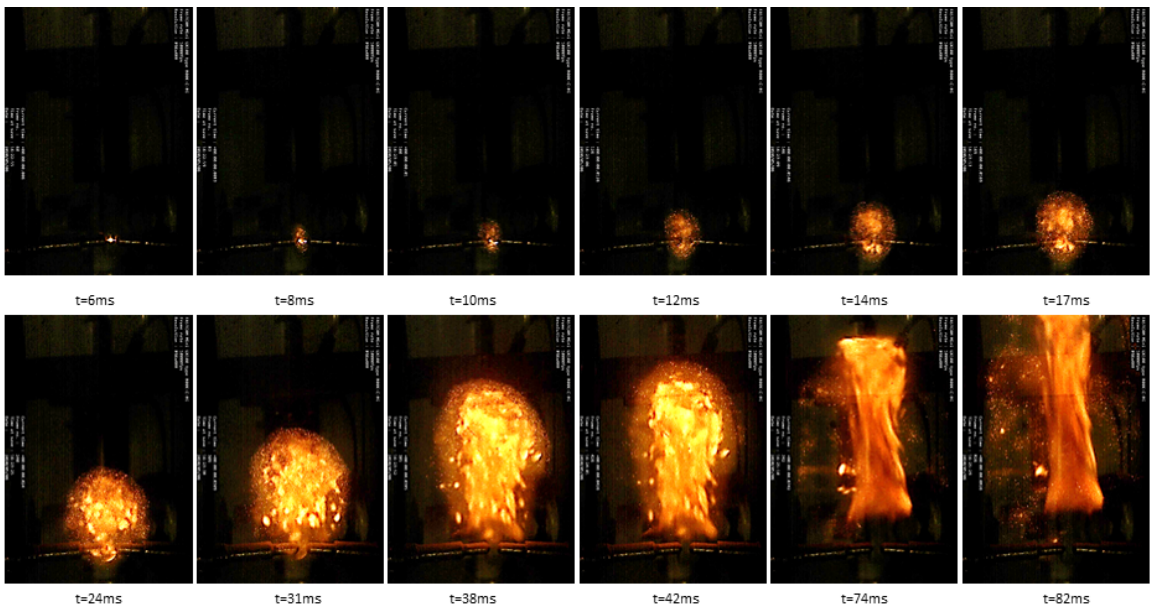


*Figure 6.6: Combustion propagation in hybrid mixture of lycopodium (41g/m$^3$) and methane (2.5 vol.%)*

The continuous combustion propagation in hybrid mixtures at their LEL was substantially different than that of the rich mixtures (Figure 6.7). The first prominent difference observed was the initiation time, shape and size of the ignition kernel. Due to a low fuel concentration, as expected, the growth of the ignition kernel was relatively slower and mostly did not end up in a spherical shaped ignition kernel, but rather in an irregular shaped highly luminous local zone, partly surrounded by a low intensity burning gas cloud. As it was seen in the case of intermittent combustion propagation, here as well the ignition kernel did not grow into a combustion zone, but rather dissipated immediately after the spark was deactivated. Contrary to intermittent combustion propagation, in continuous combustion propagation the ignition kernel, during its decay phase, gave rise to one or several local combustion zones (frame # 07 in Figure 6.7).

Careful observation of the high-speed videos revealed that these local combustion zones (in the early stage of combustion propagation) were independent particle clusters burning at their individual finite burning rates, contributing to the heat release in their immediate surrounding. Each of these burning particle clusters was comprised of a central, highly luminous part bordered by a relatively narrow, low intensity part, which was interpreted as the gaseous flame (similar to Figure 6.3). The heat released from these local combustion zones pyrolyzed the dust particles in their immediate surrounding, which contributed to the increased flammable gas concentration (due to pyrolysis of the neighbouring dust particles). After a few milliseconds, the appearance of an upward moving continuous gaseous flame front could be observed, which, while moving upwards, turned into a parabolic laminar flame front. In contrast to the fuel rich mixtures, the combustion zone in limit hybrid mixtures was of smaller volume and contained randomly occurring, highly luminous spots. Moreover, the combustion propagation was only limited to the central part of the combustion tube, covering approximately half to two thirds of the tube's diameter.

Contrary to the intermittent combustion propagation, in which most of the time the combustion zone only travelled a vertical distance of a maximum of 100 mm from the ignition source, in continuous mode a combustion propagation from the ignition source till the top end of the tube was observed. Furthermore, a continuous combustion propagation in hybrid mixtures at their LEL only occurred in upwards direction. A backward combustion propagation as was seen in fuel rich hybrid mixtures was not observed.

It must be mentioned here that it was not always possible to point out a clear gaseous flame front in the experiments categorised as continuous combustion propagation. Approximately half of the high-speed videos were such, where only local combustion zones (burning particles clusters) could be seen appearing and disappearing in an irregular manner. Figure 6.8 presents an example of such a case.

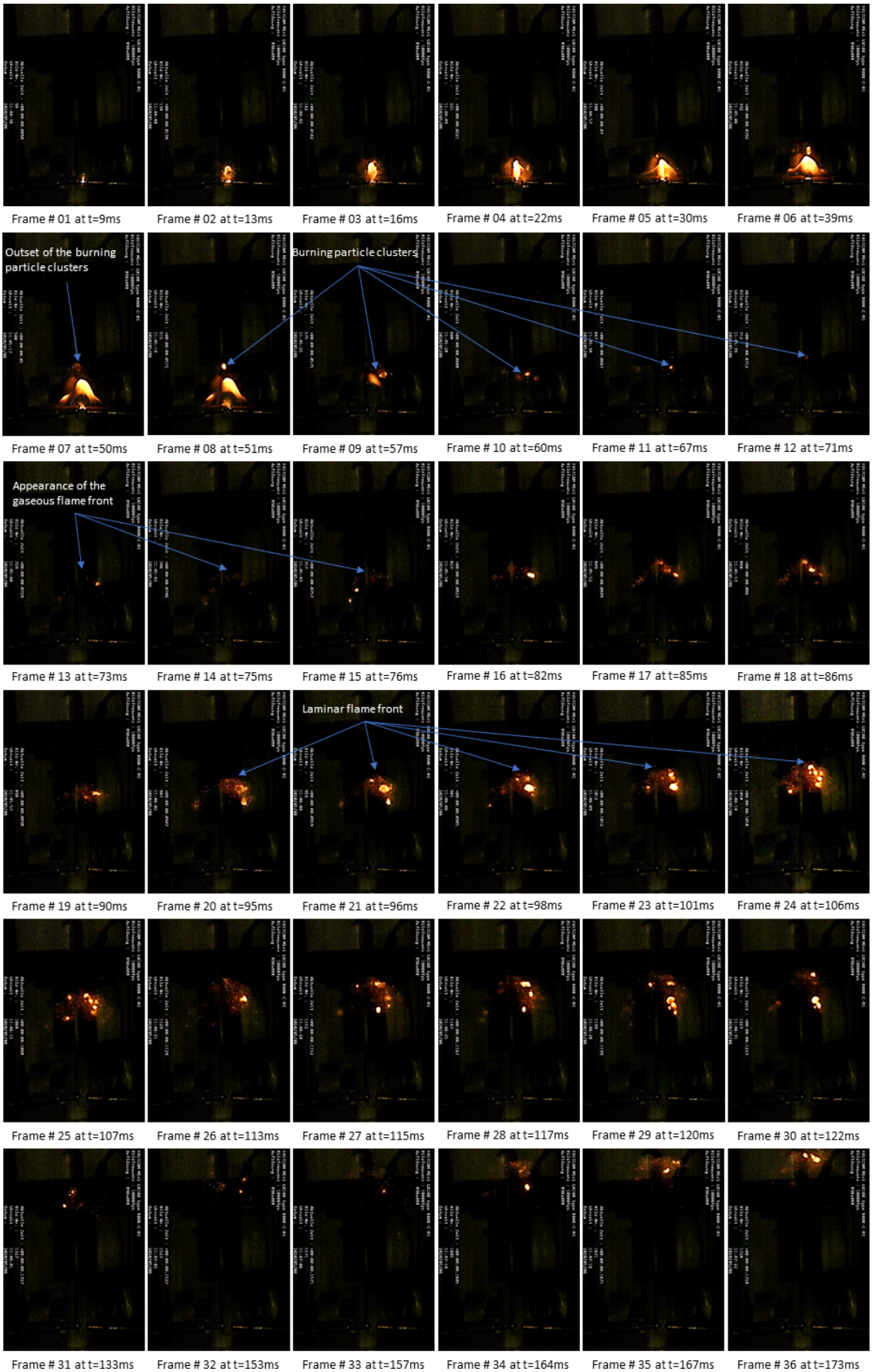


*Figure 6.7: Continuous combustion propagation hybrid mixture of lycopodium (29 g/m$^3$) and methane (1.5 vol.%) at flow velocity of 9.5 cm/s*

Strictly seen, such a combustion propagation could not be categorised as continuous since a continuously growing combustion zone was not visible. However, since the local burning particles clusters with a relatively short life time of 1 to 3 ms (frame # 06 and frame # 07 in Figure 6.8) were continuously popping up and dying out, and there was practically no deadtime, where combustion would come to a halt, it was assumed that there existed a continuous heat and mass transfer communication between these local burning particles clusters. Moreover, it could not be overruled that there might have existed an invisible gaseous flame envelop around these local burning particle clusters, which, under the employed experimental conditions, was not visually perceivable.

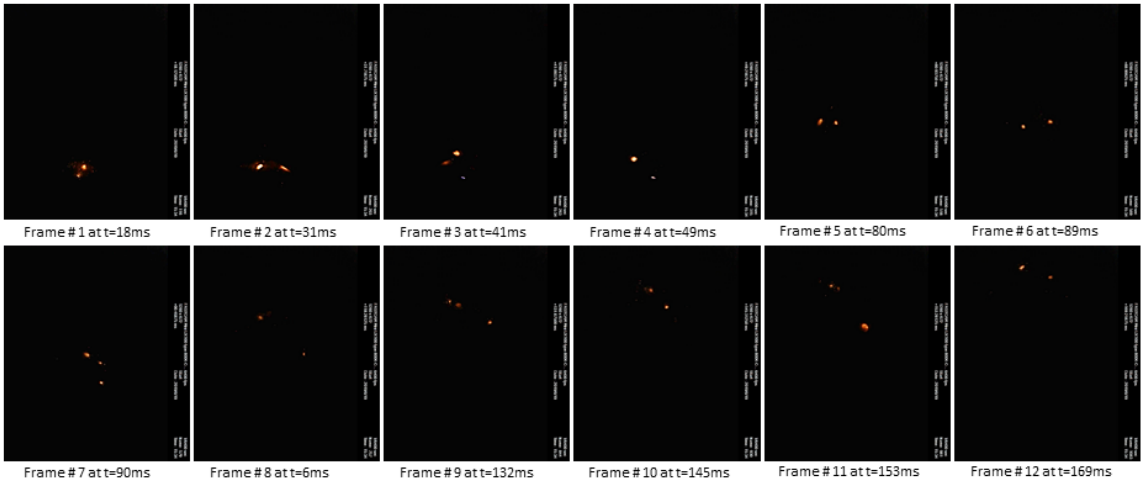


*Figure 6.8: Local burning particles clusters in continuous combustion propagation in hybrid mixture of lycopodium (17 g/m$^3$) and methane (3.5 vol.%) at flow velocity of 9.5 cm/s*

### 6.1.3 Combustion propagation speed in hybrid mixtures

It is a general perception that the combustion propagation speed in hybrid mixtures increases with increasing flammable gas concentration in the hybrid mixture. This concept holds true for fuel rich hybrid mixtures, which has been the focus of all the investigations so far concerning measurement of combustion propagation speed in hybrid mixtures. For hybrid mixtures, where the concentration of each component is below their respective MEC/LEL and the mixture concentration is close to its LEL, a successful ignition and subsequent combustion propagation cannot be supported by the combustion of a single component and therefore requires a two-way interaction between dust and gas during the combustion. In such a system, an increase in the gas concentration implies a decrease in the dust concentration to keep the mixture concentration at its LEL, therefore it is not per se that the combustion propagation velocity should increase by increasing the gas concentration in the system.

In order to examine the change in the combustion propagation speed with respect to the changing dust and gas concentration in a hybrid mixture at its LEL high-speed videos were evaluated. It must be mentioned at this point that in the case of

continuous combustion propagation a clear front of the combustion zone could not be pointed out for approximately half of the experiments (see section 6.1.2.2), especially for the mixtures with relatively higher gas concentrations (> 2.5 vol.%), which essentially implied that the scope of the investigation of change in the combustion propagation speed with respect to changing mixture composition had to be narrowed down to the intermittent combustion propagation only (flow velocity 4.8 cm/s).

As explained in section 6.1.2.1, during the intermittent combustion propagation, the combustion zone underwent several (mostly two) growth phases in which the volume of the combustion zone and its vertical speed increased, and decay phases in which the combustion zone shrank and decelerated. Therefore, the combustion propagation speed in the following discussion refers to the average combustion propagation speed calculated by dividing the distance travelled by the combustion zone over the time required (starting with the activation of the spark) to cover this distance. For the measurement of the distance, a calibrated line was used as a reference. For the case of the intermittent combustion propagation, it was rather seldom that the combustion zone would travel up to the calibrated line, hence the maximum distance travelled before the beginning of the final decay phase (in which the combustion zone got quenched permanently) was taken as a fixed criterion.

Figure 6.9 shows the results of the combustion propagation velocity measurement with respect to different dust and gas concentrations in hybrid mixtures of lycopodium and methane at their LEL. Herein the red horizontal line represents the maximum distance travelled by the combustion wave before it got quenched permanently. The results showed a random distribution of combustion propagation speed, which could not be related to the apparent change in the mixture composition. The lowest combustion propagation speed was recorded for the hybrid mixtures with the highest methane concentrations: 0.56 m/s for 4 vol% and 0.58 m/s for 4.5 vol.%. The reason behind this occurrence was that, during its propagation, the combustion zone got quenched and reignited twice (an example is shown in Figure 6.5), whereas for all the other mixtures presented in Figure 6.9 this happened only once. This accounted for an additional deadtime (the time between quenching and reignition of the combustion zone) of approximately 25 ms for the hybrid mixture with 4.5 vol.% methane and 36 ms for the hybrid mixture with 4 vol.% methane, which eventually resulted in a lower average combustion propagation speed.

For pure lycopodium at the same initial and boundary conditions, a combustion propagation speed of 0.98 m/s was measured, which is more than all of the hybrid mixtures shown in Figure 6.9. Comparing the high-speed videos of pure dust and hybrid mixture, a major difference that could be pointed out was the magnitude of the deadtime. For pure lycopodium the reignition (preceded by the decay phase) of the combustion zone occurred after a partial extinguishment of the combustion zone, which essentially means that there was practically no deadtime to be

considered for the calculation of the combustion speed. This occurrence could be related to the reduced dust concentration in case of hybrid mixtures, which resulted in dust particles being further apart from each other. The increased distance between the dust particles might have affected the underlying heat and mass transfer processes adversely. A build-up of an ignitable gas cloud, as a result of pyrolysis in this case, would logically take longer than it would when particles are closer to each other. According to this logic, a decrease in the dust concentration should have had resulted in a general decrease in the combustion propagation speed while comparing only hybrid mixtures at their LEL. However, since the decrease in the dust concentration was accompanied by a gradual increase in the flammable gas concentration in the system, the adverse effect of decreasing dust concentration on the combustion propagation speed was to some extent compensated by the increased presence of flammable gas, leading to a random distribution of combustion propagation speed values.

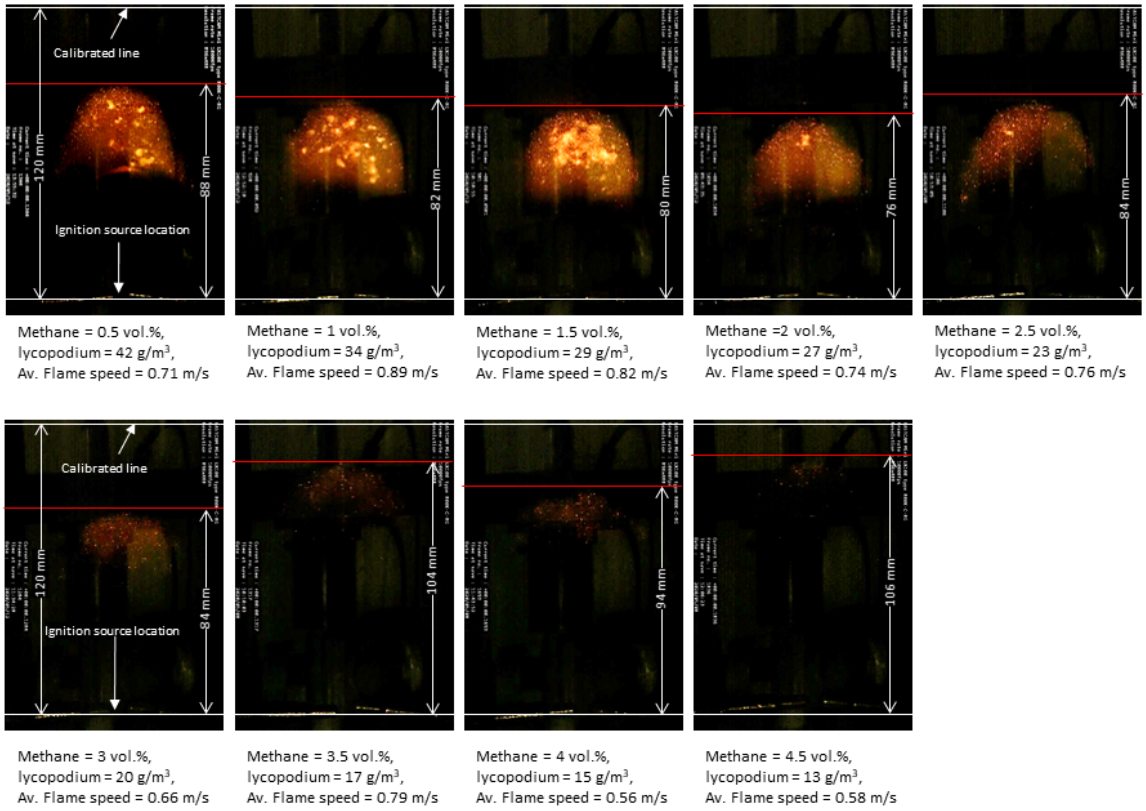


*Figure 6.9: Evolution of average combustion propagation speed with respect to changing mixture composition in hybrid mixtures of lycopodium and methane at flow velocity of 4.8 cm/s*

Apart from the speed, Figure 6.9 also highlights the change in the structure of the combustion zone with the changing mixture composition. For hybrid mixtures at concentrations close to their LEL, the volume of the combustion zone decreased by increasing the relative amount of flammable gas in the system, which consequently implies a decrease in the dust concentration. Moreover, the luminosity of the combustion zone also decreased by increasing the gas

concentration in the mixture. This observation was consistent with the observation of flames in pure gas-air and dust-air mixtures. As it was mentioned in section 4.3, a methane flame close to its LEL was not visible under normal light conditions. In the experiments, wherein the LEL of pure gas was measured, a successful ignition and flame propagation was merely detected by the deposition of a thin steam layer on the tube wall.

Figure 6.10 and Figure 6.11 present a comparison of the average combustion propagation speed measured at four flow front velocities and the flammable gas concentrations of 1.5 and 1 vol.% respectively. For the hybrid mixtures shown in Figure 6.10, the combustion propagation at the flow front velocity of 4.8 cm/s exhibited an intermittent behaviour, whereas for the case of Figure 6.11, an intermittent combustion propagation was observed at the flow front velocities of 4.8 and 7.14 cm/s. For all the other hybrid mixtures in both cases, a continuous combustion propagation was recorded.

Analysing the results, a specific pattern, which would indicate the dependency of the combustion propagation speed on the flow front velocity, could not be identified. This finding goes in line with the intended outcome, considering that the design of the experimental set-up as well as the procedure was aimed at minimizing the influence of the flow regime on the LEL and the combustion propagation speed.

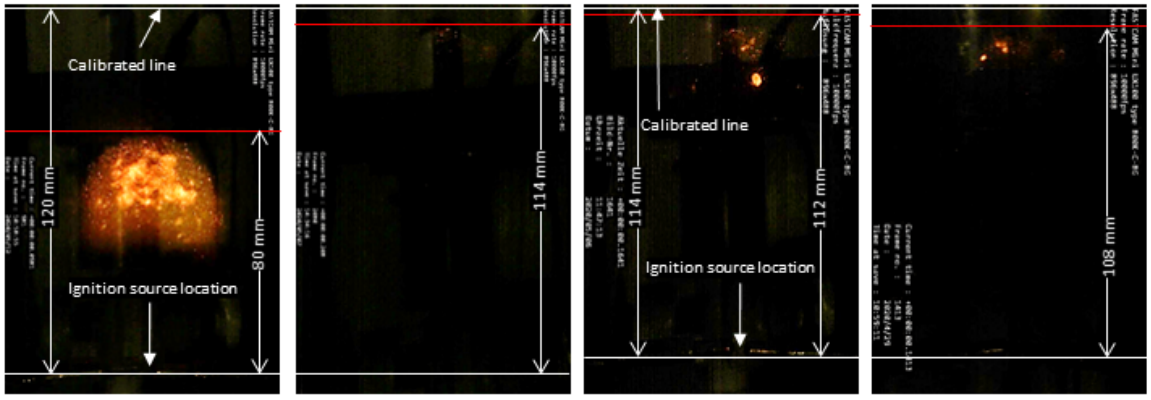


*Figure 6.10: Change in the average combustion propagation speed with respect to changing flow front velocity for hybrid mixtures of lycopodium and methane (1.5 vol.%)*

In addition to the flow front velocity, it was also examined if the fluctuations in the combustion propagation speed could be attributed to the type of combustion propagation mechanism. Logically, it would have had been plausible, if the continuous combustion propagation had shown slightly higher combustion propagation speed than the intermittent combustion propagation, since for the former the combustion propagated continuously through the unburnt fuel air mixture, and there was no lost time because of the decay phase of the combustion

zone or the deadtime. The results shown in Figure 6.10 exhibit exactly the opposite of this expectation by suggesting the highest combustion propagation speed for the case of intermittent combustion propagation. A look at the values of combustion propagation speed presented in Figure 6.11, however, quickly invalidates any dependency of the combustion propagation speed on the type of combustion propagation mechanism.

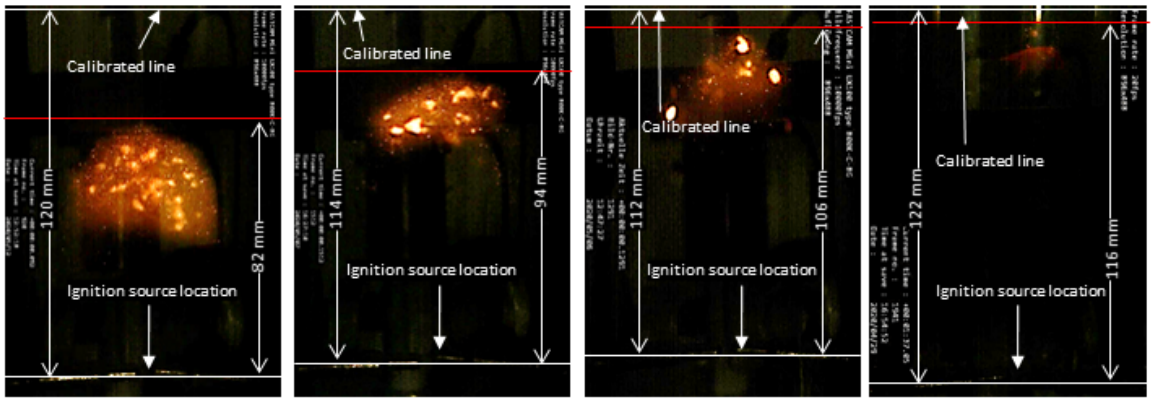


Flow velocity = 4.8 cm/s
Methane = 1.0 vol.%,
lycopodium = 34 g/m$^3$,
Flame propagation type = Intermittent,
Av. Flame speed = 0.82 m/s

Flow velocity = 7.14 cm/s
Methane = 1.0 vol.%,
lycopodium = 35 g/m$^3$,
Flame propagation type = Intermittent,
Av. Flame speed = 0.62 m/s

Flow velocity = 9.5 cm/s
Methane = 1.0 vol.%,
lycopodium = 35 g/m$^3$,
Flame propagation type = continuous,
Av. Flame speed = 0.82 m/s

Flow velocity = 13 cm/s
Methane = 1.0 vol.%,
lycopodium = 35 g/m$^3$,
Flame propagation type = continuous,
Av. Flame speed = 0.60 m/s

*Figure 6.11: Change in the average combustion propagation speed with respect to changing flow front velocity for hybrid mixtures of lycopodium and methane (1.0 vol.%)*

Taken together the discussion on the ignition and combustion propagation in hybrid mixtures of dusts with high volatile content and flammable gas, the following conclusions could be extracted:

- Hybrid mixtures at their LEL exhibit two types of combustion propagation mechanisms, namely intermittent combustion propagation and continuous combustion propagation. A dependency of the combustion propagation mechanism on the experimental conditions investigated within the scope of this research work (flow front velocity and the composition of the hybrid mixture) could not be established.
- The combustion propagation in hybrid mixtures was found to be slower than in pure dust air mixtures, irrespective of the relative amount of dust and gas in the system, provided that the concentration of dust in the hybrid mixture is less than its MEC and the hybrid mixture is at its LEL.
- For a hybrid mixture at its LEL, the change in the average combustion propagation speed by changing the mixture composition did not exhibit a specific pattern which could be associated with an increase in the relative amount of dust or flammable gas in the system.
- Regarding the variations in the combustion propagation speed with respect to change in the flow front velocity, no evidence could be found which would

suggest an influence of the flow front velocity on the combustion propagation speed.

## 6.2 Hybrid mixtures of non-volatile metal dusts

This section presents a discussion on the experimental findings regarding the ignition and combustion propagation in hybrid mixtures of light metals and flammable gas at their LEL. As representative of such systems, hybrid mixtures of titanium and methane were selected.

### 6.2.1 Ignition and combustion propagation in dust air mixture

Similar to the experimental series of lycopodium and methane, as a starting point the experiments were conducted to examine the ignition and propagation of the combustion wave in titanium air mixtures (in the absence of methane). Two flow front velocities, namely 16 and 20 cm/s, were employed. The focus of these experiments was to study the ignition and combustion propagation mechanism, as well as combustion propagation speed in titanium air mixtures, with titanium concentration being close to its MEC. Following observations were made:

- The ignition of titanium dust started with the particles getting into an excited state upon contact with the spark, which was accompanied by a rapid transformation of the particles into glowing embers. In case of the flow velocity of 16 cm/s, the activation of spark within the first 4 ms, resulted in a group of particles getting simultaneously in the excited state, forming a cluster of burning particles directly next to spark (frame # 1a and 2a in Figure 6.12). This burning particle cluster grew in size and visually detached from the igniters, approx. 60 ms after the activation of the spark (frame # 4a in Figure 6.12). On the other hand, for the flow velocity of 20 cm/s, the formation of the burning particle cluster was delayed by approximately 34 ms. In this case, the activation of the spark immediately caused a deflection of the glowing particles away from the spark in upward, downward and lateral directions, due to which an accumulation of a simultaneously burning particle chunk was hindered (frame # 1b in Figure 6.12). At approximately 34 ms after the spark activation, another set of particles got caught in the spark leading to a successful accumulation of the combusting particle cluster, which, following the same pattern as observed in case of 16 cm/s grew in size and got detached from the ignition source at approximately 74 ms after the activation of the spark (frame # 2b, 3b and 4b in Figure 6.12).
- Analysing the high-speed videos of successful ignition and comparing them with failed ignition (no ignition), it was observed that a successful ignition not only required the concentration of dust being in the explosible range, but also the occurrence of an event in which a certain limiting number of particles would simultaneously get trapped in the spark or get diverted in the same direction and accumulate themselves in the close adjacency of each other.

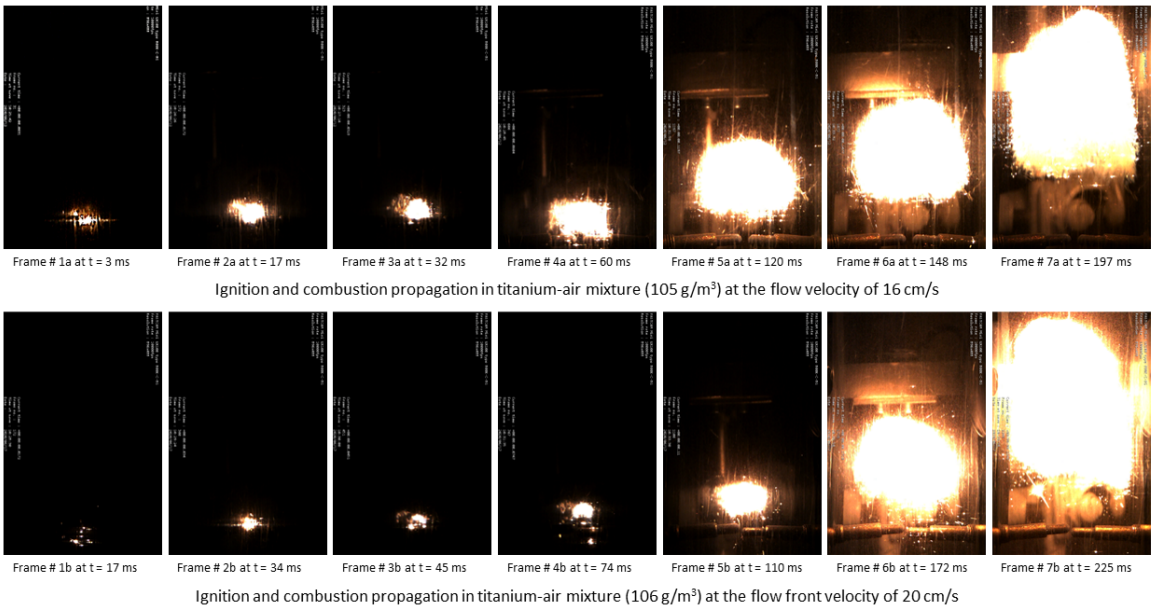


*Figure 6.12: Ignition and combustion propagation in titanium-air mixture at its MEC*

- The propagation of the combustion wave in titanium-air mixtures was accompanied by the growth and upward movement of the above-mentioned burning particle cluster. Owing to relatively long particle burning time, the volume of the combustion zone was larger in comparison to lycopodium air mixtures. In order to have a basis of comparison with hybrid mixtures and to inspect the influence of flow front velocity on the combustion propagation, the average speed of combustion wave was measured at both flow front velocities. Same measurement procedure as for the case of lycopodium air mixtures was employed. Results are given in Table 6.2. At a first glance the values presented in Table 6.2 suggest an adverse effect of the increase in the flow front velocity on the speed of the combustion wave. However, considering that for the case of 20 cm/s the ignition and formation of a burning particle cluster was delayed by approximately 34 ms (combustion propagation velocity of 0.53 m/s considering this delay), it could be deduced that under the employed experimental conditions, the flow front velocity had a negligible effect on the combustion speed.

*Table 6.2: Average speed of combustion wave propagation in titanium air mixtures*

| **Flow velocity (cm/s)** | **Dust concentration ($g/m^3$)** | **Combustion wave speed (m/s)** |
|---|---|---|
| 16 | 105 ±6 | 0.55 |
| 20 | 106 ±3 | 0.41 |

- An examination of the single particle combustion was not included in the scope of this study, however, some important observations regarding the titanium particle combustion are worth describing at this point. Figure 6.13 shows successive steps in the combustion of a single titanium particle. The frames were extracted from the high-speed video of the combustion of titanium-air

mixture at its MEC (106 g/m$^3$) at the flow front velocity of 20 cm/s. The combustion of a single titanium particle began with it getting heated and glowing after absorbing energy from the ignition source or from the neighbouring burning particles. The increase in the glow intensity of the particles was accompanied by an increase in the particle size, presumably due to swelling of the particle, which was assumed to be because of the penetration of the gas phase to the particle core through the thin oxide layer. As reported by Glotov [107], titanium powder at room temperature gets covered by a natural protective layer of $TiO_2$, when exposed to air. Owing to this film of around 1 to 10 nm thickness, titanium is resistant to corrosion at temperatures of up to 773-823 K. Generally, it took a few milliseconds (approximately 1 to 5 ms depending on the size of the particle) for the particle to reach the largest size and the brightest state during its combustion (frame # 1 to # 5 in Figure 6.13). The combustion of the titanium particle was terminated with the particle explosion and ejection of fragments, which were most probably caused by the release of gas in the particle interior as a result of changes in its phase composition.

For most of the cases, the complete combustion (frame # 1 to frame # 18) of a titanium particle took approximately 5 to 20 ms. There were, however, a handful of exceptional cases, where it took up to 50 ms for a complete disappearance of the particle fragments after the explosion (Figure 6.13).

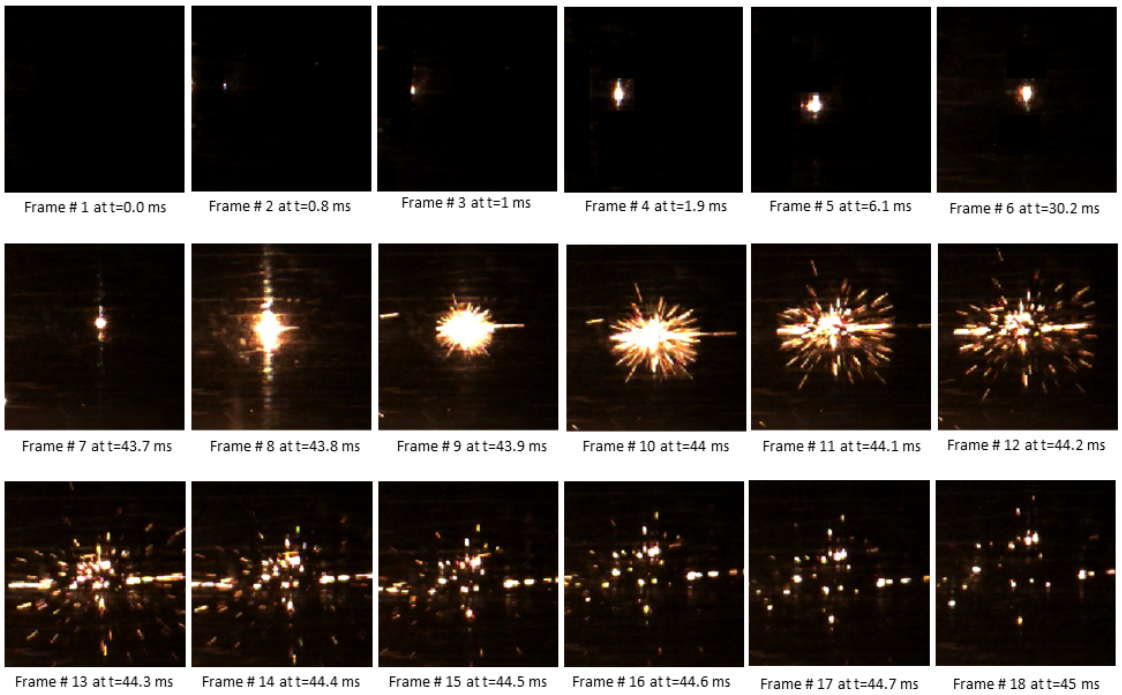


*Figure 6.13: Combustion evolution of a single titanium particle*

Following the experiments on pure dust-air mixtures, hybrid mixtures of titanium and methane were tested. Except the introduction of methane in the gas stream, all the other initial and boundary conditions of the experiments were the same as

for pure titanium-air mixtures. Methane was introduced in the system following the same protocol as for the lycopodium methane hybrid mixtures (see section 6.1).

### 6.2.2 Ignition and combustion propagation in hybrid mixtures

In hybrid mixtures of titanium and methane, the ignition always started with the titanium particle getting in a physical contact with the spark. The result of this contact was, however, not always the same and can be sorted out into two categories, namely particle explosions and particle divergence upon contact with the spark. A clear association of either of these mechanisms with the dust or gas concentration in the system or the flow front velocity could not be established.

#### 6.2.2.1 Particle explosion upon contact with the spark:

This type of mechanism was predominantly (however, not only) observed in pure titanium-air mixtures and in hybrid mixtures of titanium and methane with relatively higher fraction of titanium powder (methane concentration < 3.0 vol.%). A characteristic feature of this type of ignition was the immediate explosion of titanium particles upon contact with the spark. The explosion of the titanium particles released hot flying debris, which hit the particles in their immediate surrounding and together with the high radiation emission (acting as a heat source), led to the birth of a burning particle cluster directly above the ignition source (frame # 1a & b to # 6a & b in Figure 6.14). The burning particle cluster visually detached itself form the ignition source in the next few milliseconds and began an upward movement through the unburnt fuel air mixture.

Comparing the ignition by particle explosion in titanium-methane hybrid mixtures at their LEL with a higher relative amount of dust (and smaller methane concentration) with the ones in which the fraction of methane was higher than that of titanium, it was observed that the creation of an upward moving burning particle cluster took much longer in the latter case. For the examples shown in Figure 6.14, this took roughly twice as much time for the hybrid mixture with 4.5 vol.% methane (frame # 9b) as for the hybrid mixture with 1 vol. % methane (frame # 9a). Considering that the gases burn faster than the dusts, one would expect the opposite of this finding. Focusing only on the dust concentration, the delay in the latter case could be explained by the occurrence of an increased interparticle distance, which logically slowed down the heat transfer between the particles. The role of methane in the process of ignition in such systems could not be explained with the help of current results. Carrying out a similar investigation with the help of high-speed infrared camera could be of great benefit in this regard.

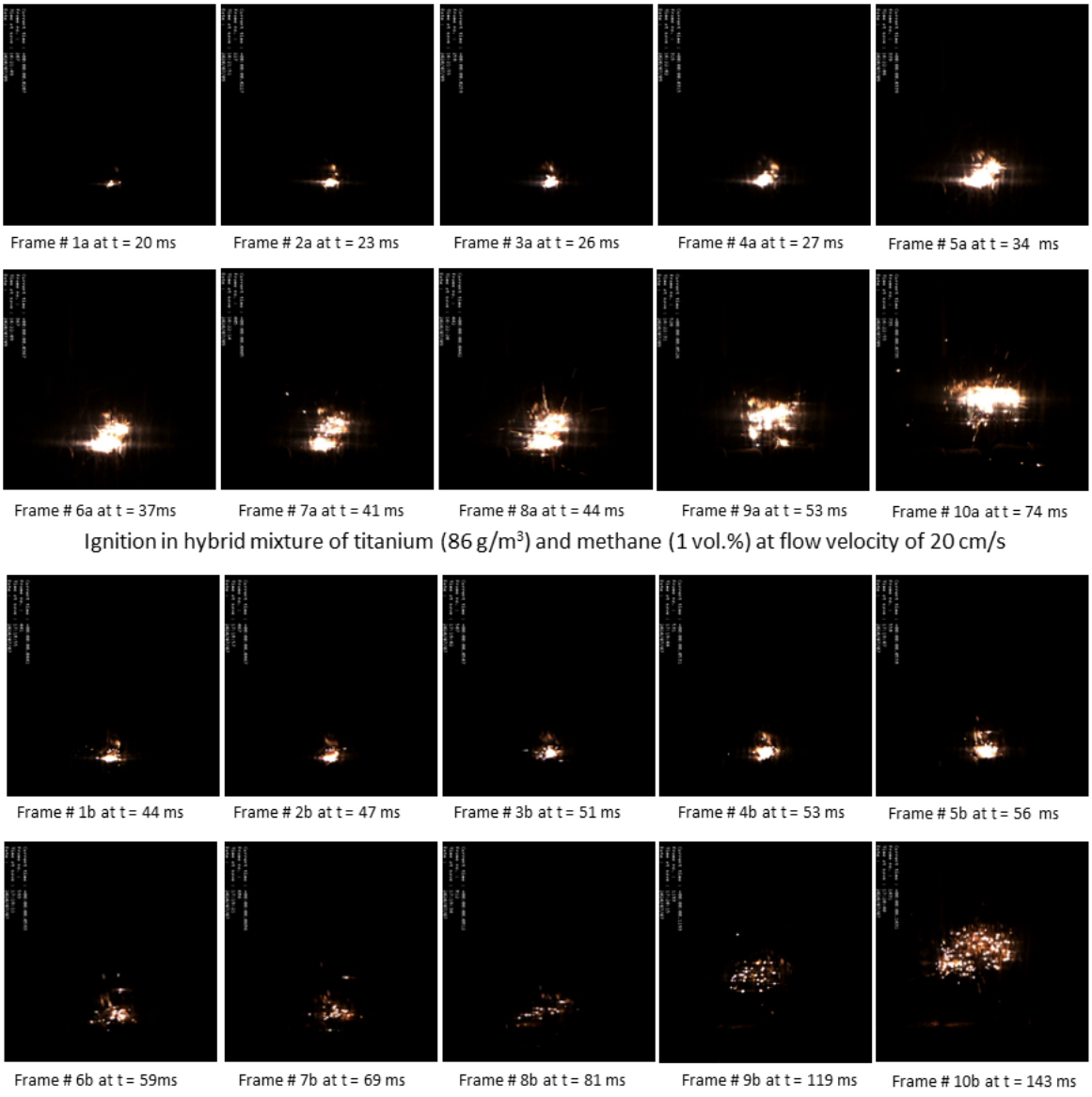


*Figure 6.14: Ignition by particle explosion upon contact with the spark*

### 6.2.2.2 Particle divergence upon contact with the spark:

In this type of ignition mechanism, the titanium particles, after getting in contact with the electric arc got pushed away in arbitrary directions. For all the experiments in which a successful ignition preceded by the particle divergence was recorded, an accumulation of the particles in the close vicinity of each other, after being redirected by the electric arc, was found common. This seems plausible considering that a smaller interparticle distance would enhance the heat transfer between the particles. An increased heat transfer between the particles would consequently lead to the build-up of a burning particles zone in which the rate of heat generation (due to combustion) would surpass the rate of heat loss (due to heating up of neighbouring particles as well as the heat loss to the surrounding), thus giving rise to a self-sustained propagation of the combustion wave.

The direction of the particle flight upon contact with the electrical arc was found to be dependent on the shape of the arc. Generally, the shape of the electrical arc resembled a straight line joining the centres of the tips of two igniters. Upon contact with the particles, the shape of the spark arc changed (even several times during one experiment), stochastically. An evidence of what might have caused the shift in the arc shape could not be established. Figure 6.15 shows different shapes of the electrical arc and their influence on the direction of the particle flight.

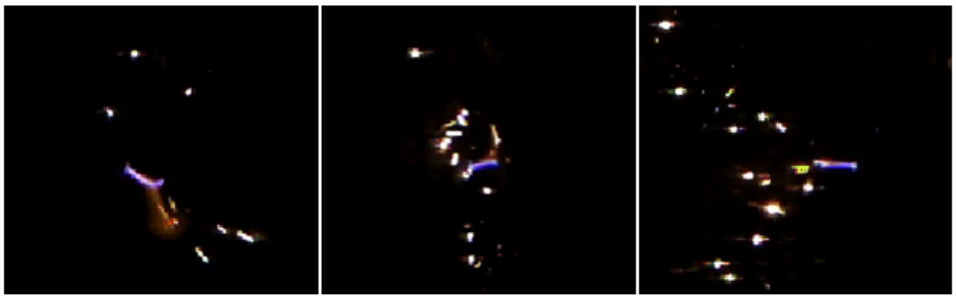


*Figure 6.15: Effect of the electrical arc shape on the particle divergence direction*

Figure 6.16 presents the screenshots of an ignition process in which the particle divergence upon contact with the spark was observed. Starting at approximately 9 ms (frame # 2), a sideways divergence of titanium particles was observed for the first 25 ms of the spark activation (frame # 15). For the rest of the spark duration (50 ms) no further particle flight under the action of the spark was observed. The number of simultaneously ignited particles started to decrease gradually until its minimum at approximately 56 ms. By this time, enough energy (as a result of particle combustion) had been stored in the system, that a self-sustained growth and upward propagation of the combustion zone could be supported, which led to an increase in the number of simultaneously burning particles and a formation of the combustion wave that propagated upwards through the unburnt fuel air mixture.

It is important to mention here that the occurrence of the two ignition mechanisms explained above were not mutually exclusive events. A substantial number of hybrid mixture experiments were such, where the particle divergence without a successful ignition was observed for the first 25 to 40 ms, followed by the particle explosion upon contact with the spark, which eventually led to a successful ignition.

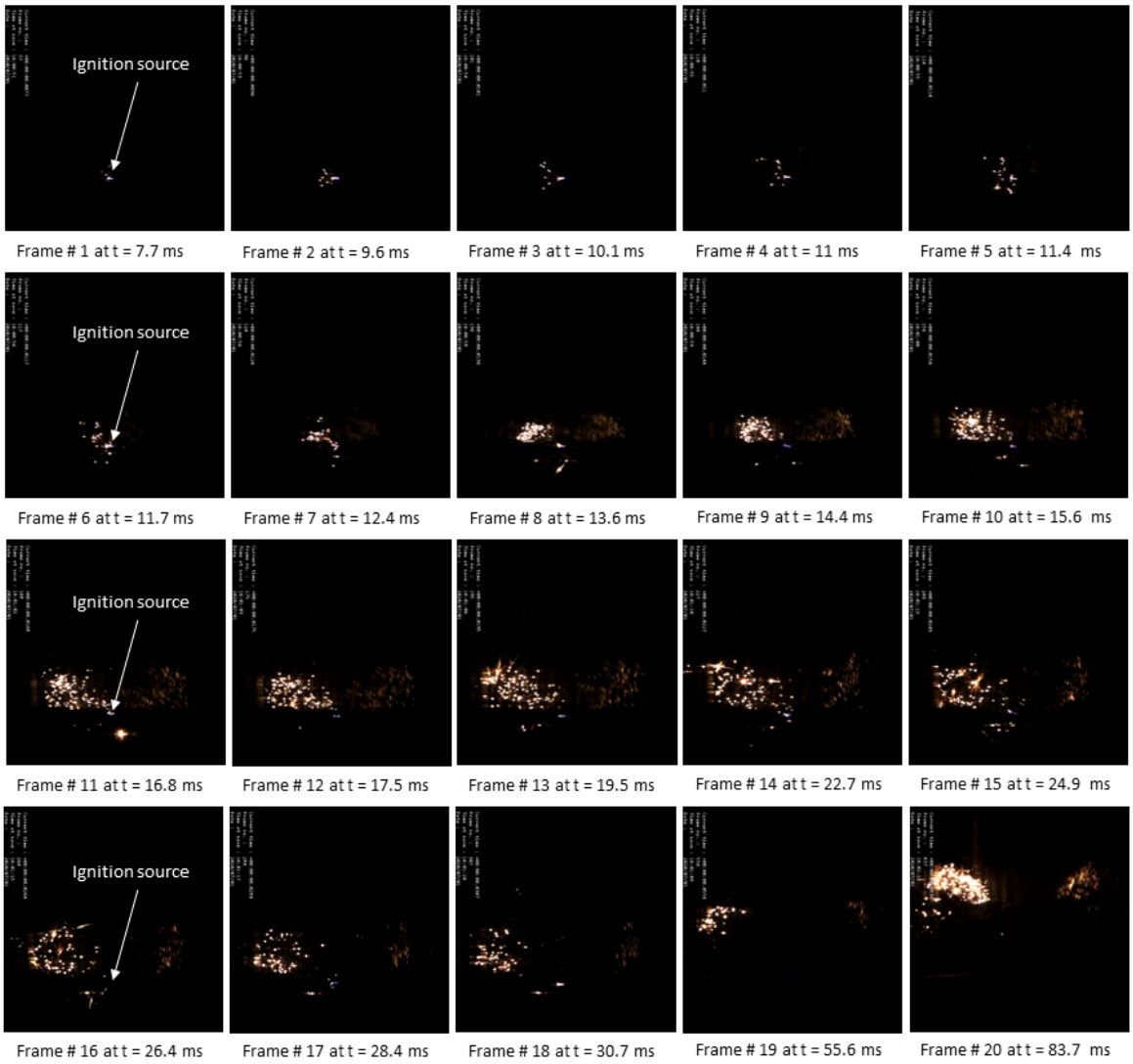


*Figure 6.16: Ignition by particle divergence in hybrid mixture of titanium (32 g/m$^3$) and methane (3.5 vol.%) at the flow front velocity of 16 cm/s*

Figure 6.17 shows the change in the structure of the combustion wave in hybrid mixtures of titanium and methane with respect to the changing mixture composition. Following key observations were made regarding the structure and propagation of the combustion wave:

- In most of the cases, especially at higher gas concentrations, the leading edge of the combustion wave had the shape of the laminar flame front, as observed in the case of lycopodium-methane hybrid mixtures.
- In most of the experiments, the combustion wave was limited to the central part of the tube and did not expand through the whole diameter of the tube.
- An addition of a few percent of methane led to a successful ignition of titanium concentrations that in its absence did not ignite. This highlights the fact that even though the concentration of methane in the system was below its LEL, it combusted and consequently released energy, which contributed to the total heat accumulation in the system enabling a smooth propagation of the

combustion wave. The combustion mechanism of methane in such hybrid mixtures could not be explained and argued with evidence on the basis of the results of this study.

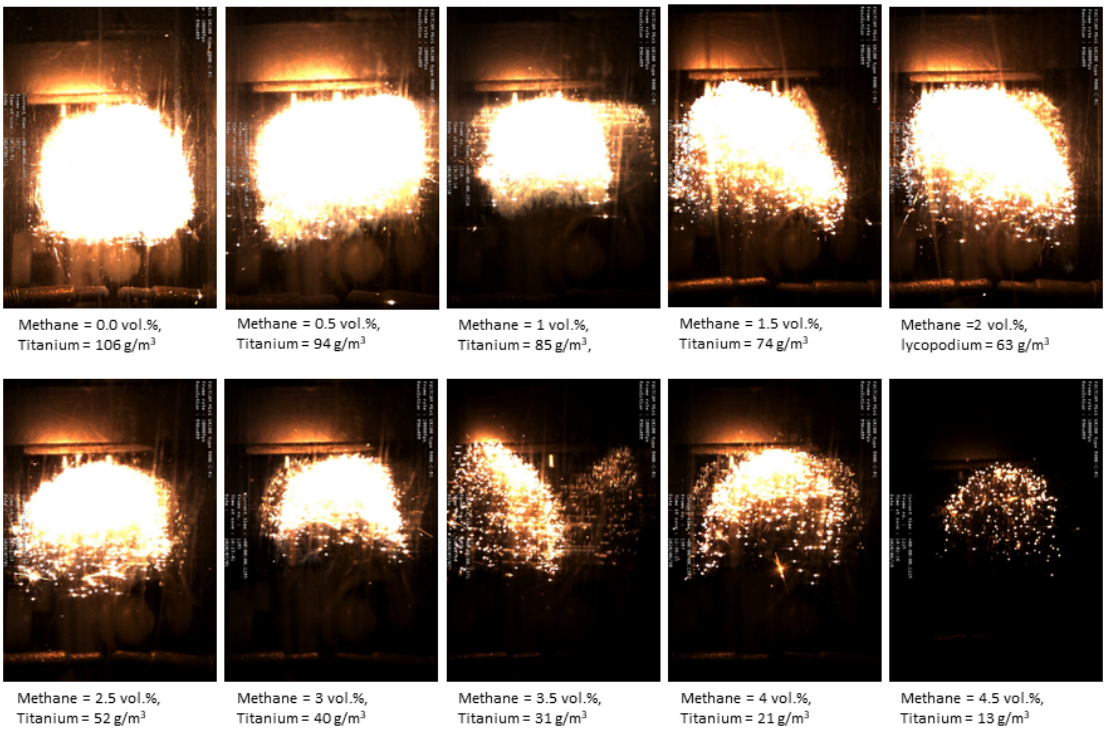


Structure of the combustion wave in hybrid mixtures of titanium and methane at flow velocity of 16 cm/s

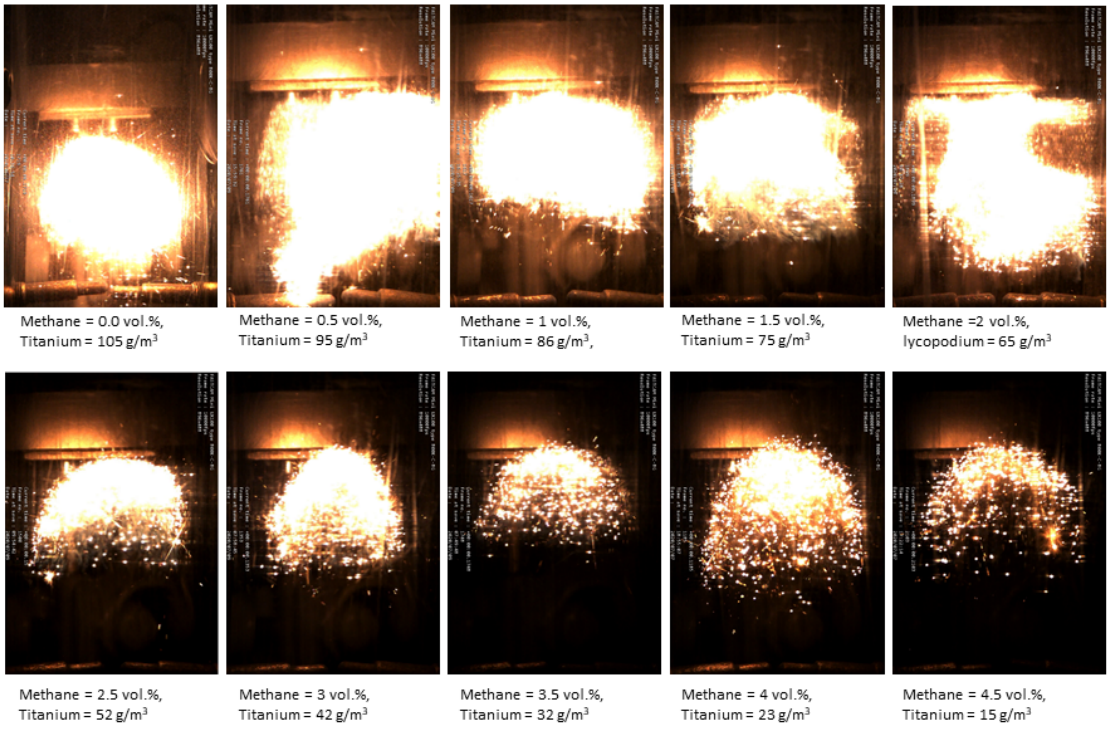


Structure of the combustion wave in hybrid mixtures of titanium and methane at flow velocity of 20 cm/s

*Figure 6.17: Structure of the combustion wave in hybrid mixtures of titanium and methane*

### 6.2.3 Combustion propagation speed in hybrid mixtures

In order to investigate the change in the speed of the combustion wave with respect to the changing dust and gas concentration in a hybrid mixture at its LEL, the average speed of the combustion wave was determined by evaluating the high-speed videos. The measurement procedure was the same as for the lycopodium-methane hybrid mixtures, with one difference. For hybrid mixtures of lycopodium and methane, due to the occurrence of intermittent combustion propagation and quenching of the combustion zone before reaching the calibrated line, the maximum distance travelled by the combustion wave before the beginning of the final decay phase (when the combustion wave got quenched permanently) was divided by the time required to travel this distance. For hybrid mixtures of titanium and methane the combustion wave mostly travelled until the top end of the tube, therefore a distance of 100 mm was marked as fixed criterion and the time required to travel this distance was extracted from the high-speed videos. The results are shown in Table 6.3, wherein for each methane concentration in the hybrid mixture the measured titanium concentration (along with the absolute uncertainty) and combustion propagation speed have been listed.

For the flow front velocity of 16 cm/s, the combustion propagation speed varied within a narrow range of 0.54 to 0.65 m/s by changing the relative amount of dust and flammable gas in the hybrid mixtures at their LEL, whereas, at the flow front velocity of 20 cm/s, this variation was mostly within the range of 0.48 to 0.59 m/s, with two exceptions. These were 0.7 m/s and 0.84 m/s at the methane concentrations of 3.0 vol.% and 4.0 vol.%, respectively. A specific trend that would justify the dependence of the combustion propagation velocity on the mixture composition could not be identified.

*Table 6.3: Combustion propagation speed with respect to changing flow front velocity and mixture composition in hybrid mixtures of titanium and methane*

| **Methane** | **Flow velocity 16 cm/s** | | **Flow velocity 20 cm/s** | |
|---|---|---|---|---|
| **(Vol.%)** | **Titanium ($g/m^3$)** | **Comb. propagation speed (m/s)** | **Titanium ($g/m^3$)** | **Comb. propagation speed (m/s)** |
| 0 | 106 ± 6 | 0.55 | 105 ± 6 | 0.41 |
| 0.5 | 94 ± 6 | 0.61 | 95 ± 9 | 0.51 |
| 1.0 | 85 ± 8 | 0.57 | 86 ± 5 | 0.56 |
| 1.5 | 74 ± 6 | 0.54 | 75 ± 8 | 0.51 |
| 2.0 | 63 ± 8 | 0.57 | 65 ± 8 | 0.49 |
| 2.5 | 52 ± 5 | 0.63 | 52 ± 7 | 0.59 |
| 3.0 | 40 ± 5 | 0.67 | 42 ± 6 | 0.70 |
| 3.5 | 31 ± 6 | 0.68 | 32 ± 6 | 0.54 |
| 4.0 | 21 ± 7 | 0.65 | 23 ± 5 | 0.84 |
| 4.5 | 13 ± 2 | 0.65 | 15 ± 6 | 0.48 |

Generally, the values of the combustion propagation speed determined at the flow velocity of 16 cm/s were slightly higher than the ones at 20 cm/s, except for the aforementioned two exceptions. Logically, an increase in the flow front velocity should have had resulted in an increase in the combustion propagation speed. Since the results listed in Table 6.3 suggest the opposite of it, it could be deduced that the variations in the combustion propagation speed are not related to the change in the flow front velocity.

A critical observation of the high-speed videos revealed some interesting occurrences, which could, to some extent, explain the random changes in the combustion propagation speed values presented in Table 6.3. In hybrid mixtures of titanium and methane at their LEL, it was rather rare that the activation of the spark would immediately lead to a successful ignition, which was characterised by the birth of a burning particle cluster that would detach from the ignition source. In most of the experiments, the birth of the burning particle cluster was preceded by a delay, which would be termed as the ignition delay time in the further discussion. The ignition delay time in this sense refers to the time between the activation of the spark and the birth of the burning particle cluster. The magnitude of the ignition delay time was randomly different for each experiment and mostly varied between 20 and 55 ms. For example, for the case of the hybrid mixture of 15 g/m$^3$ titanium powder and 4.5 vol.% methane at flow front velocity of 20 cm/s, an autonomous growth in the number of simultaneously burning titanium particles could only be observed approximately 53 ms after the activation of the spark. For the calculation of the combustion propagation speed, the recorded time required to travel a distance of 100 mm started with the activation of the spark and not with the birth of the burning particle cluster, which consequently resulted in a smaller combustion propagation speed value for the experiments with a longer ignition delay time.

Figure 6.18 shows a comparison of the ignition delay times and their effect on the subsequent growth duration of the combustion propagation. On the left-hand side, the frames of the fastest combustion wave (4 vol.% methane and 23 g/m$^3$ titanium) are presented and on the right-hand side, the frames of the slowest (4.5 vol.% methane and 15 g/m$^3$ titanium). In both cases the ignition occurred by particle explosion upon contact with the spark. From the point of view of the concentration, both of the hybrid mixtures were in explosible range, however, for the case of the hybrid mixture with 4.5 vol.% methane, it took substantially longer for an autonomously growing burning particle cluster to come into existence (frames 1 b and 2 b in Figure 6.18). This consequently slowed down the whole process of the growth and propagation of the combustion wave. As a result, for the hybrid mixture with 4.5 vol.% methane, it took more than twice the time for the combustion wave of roughly the same size to cover approximately the same distance as for the hybrid mixture with 4 vol.% methane.


Hybrid mixture of titanium (23 g/m³) and methane (4 vol.%) at flow front velocity of 20 m/s. Calculated combustion propagation speed: 0.84 m/s

Left: Birth of the burning particle cluster at 15 ms after the spark initiation.
Right: Mature autonomously propagating combustion wave at 50 ms after the spark initiation

Hybrid mixture of titanium (15 g/m³) and methane (4.5 vol.%) at flow front velocity of 20 m/s. Calculated combustion propagation speed: 0.48 m/s

Left: Birth of the burning particle cluster at 53 ms after the spark initiation.
Right: Mature autonomously propagating combustion wave at 139 ms after the spark initiation

*Figure 6.18: Comparison of ignition delay time and its effect on the combustion propagation speed in hybrid mixtures of titanium and methane*

Another stochastic event that might have had a substantial influence on the combustion propagation velocity, especially in case of the hybrid mixtures in which an ignition by particle divergence was observed, was the phenomenon of divergence itself. As explained in section 6.2.2.2, during the process of ignition by particle divergence, the titanium particles were redirected in random directions (depending on the shape of the electrical arc, see Figure 6.15) after coming in contact with the spark, a successful ignition was only recorded for the experiments in which a certain minimum number of simultaneously burning particles were accumulated in the close vicinity of each other. Due to the stochastic nature of the process, the point where the particle accumulation after divergence occurred, was different in space and time for each experiment. The result of this random occurrence coupled with the fixed criterion for the measurement of combustion propagation speed (time required to travel a fixed vertical distance of 100 mm) was that the experiments in which the particles accumulated upwards from the ignition source generally yielded a higher value of the combustion propagation speed in comparison to the ones in which the particles were diverted and accumulated below or lateral to the spark (close to the tube walls).

Summarizing the discussion on the ignition and combustion propagation in hybrid mixtures of non-volatile dusts (light metals) and flammable gas, following main conclusions could be drawn:

- Hybrid mixtures at their LEL exhibit two types of ignition mechanisms, namely particle explosions and particle divergence upon contact with the spark. Based on the results of this research work, the occurrence of either of these mechanisms was independent of the dust or flammable gas concentration in the system or the flow front velocity.

- Generally, the combustion propagation speed in hybrid mixtures of titanium and methane at their LEL was slightly higher than in case of titanium-air mixtures (in the absence of methane).
- For a hybrid mixture at its LEL, the variations in the combustion propagation speed with respect to the changing mixture composition, as well as the flow front velocity, were mostly limited within a rather narrow range. The results of this investigation indicate that the combustion propagation velocity in hybrid mixtures at their LEL is not influenced by changes in the flow front velocity or the relative amount of dust or flammable gas in the system.

# 7 CONCLUSIONS AND OUTLOOK

The aim of this research work was to study the explosion behaviour of hybrid mixtures under non-turbulent conditions. The experimental part of this investigation included the measurement of the LEL of hybrid mixtures, followed by the evaluation of the progression of the LEL of hybrid mixtures with respect to changing flow conditions as well as ignition energies. Furthermore, the ignition and combustion propagation mechanisms were explored with the objective of getting new insights into the birth and growth of a combustion wave in hybrid mixtures at concentrations close to their LEL. The theoretical part of this study included the development of a model for the calculation of the LEL of hybrid mixtures utilizing conservation equations of mass and energy as its origin.

The main outcome of this study is the design of an innovative method (namely open tube apparatus) for the experimental determination of MEC of a dust cloud and/or LEL of a hybrid mixture, which in the long run could lead to a new standard. The open tube apparatus is equipped with the possibility of creating a non-turbulent quasi-static dust cloud at the time of the ignition, and an in-situ measurement of the dust concentration, using two infrared sensors installed a few centimetres above and below the ignition source. The execution of the experiments is controlled using a software module developed inhouse using LabVIEW in combination with a control and data acquisition (DAQ) unit that serves to control the whole experimental loop and process the dust concentration values, which are displayed in the software interface at the end of the experiments.

A large set of experiments was performed to quantify the uncertainties associated with the dust concentration values that were transmitted by the DAQ unit and shown in the software interface. Average uncertainties of 2.6% and 2.3 % were determined for the upper and lower sensors, respectively, which were consequently added to all the concentration values measured during the experimental determination of the MEC of a dust cloud and the LEL of a hybrid mixture. Moreover, the effect of ‘no purging’ on the gas concentration at the time of ignition was examined and found to be insignificant.

Following the dust and gas concentration reliability experiments, the MEC of lycopodium and titanium were measured at four and two different flow front velocities, respectively, and three ignition energies. Taking into account the uncertainties associated with the measured concentration values, the changes in the MEC of both dusts with respect to changing the flow front velocity and ignition energy were considered inconsequential. This finding was in line with the objective of the apparatus design, which aimed at igniting the dust particles in a quasi-static state, thus to minimise the influence of flow field on the lean flammability limits of dusts and hybrid mixtures. An interesting finding of these experiments was the

revelation of a narrow concentration range, where the ignition and no ignition points overlapped. Above the upper limit of this range, an ignition frequency of 100% was observed, and below the lower limit, 0%. For both lycopodium and titanium, a gradual increase in the ignition frequency was observed when the ignition energies were increased. The MEC values measured in this work have been compared with the ones reported in the literature, which show a wide range of MEC values (lycopodium: 8 – 125 g/m$^3$, titanium: 30 – 70 g/m$^3$) depending on the initial and boundary conditions of the experiments. The arguments that favour a higher accuracy of the results of this study include: in-situ measurement of dust concentration vs. consideration of nominal concentration and homogenous distribution of dust, quasi-static state of dust particles vs. highly turbulent environment at the time of ignition and the use of point ignition source vs. massively oversized pyrotechnical igniters.

Following the experiments on pure dusts, the dependence of the LEL of hybrid mixtures on flow front velocity as well as ignition energy was experimentally investigated. The results revealed that the LEL of hybrid mixtures in the tube apparatus did not significantly change with respect to changing the flow front velocity or the ignition energy. It is an established fact that an increase in the flammable gas concentration in a hybrid mixture at its LEL leads to a decrease in the concentration of dust in the mixture. Regarding the magnitude of this decrease, three competing point of views could be found in the research community, namely linear, more than linear and less than linear. The results of this contribution suggest that in case of hybrid mixtures of volatile organic powders with hydrocarbon gases, this decrease in the dust concentration may follow more than one pattern depending on the mixture composition. For the hybrid mixtures of lycopodium and methane, a more than linear decrease in the dust concentration was observed in the concentration range of 0 - 25% of the LEL of the gas. For the concentration ranges of 25 - 60% and 60 - 90% of the LEL of the gas, a linear and more than linear decrease in the dust concentration was, respectively, recorded.

The German guideline VDI 2263 part 5 quotes that in case of hybrid mixtures of dust and gas, a hybrid behaviour is only to be expected when the concentration of the gas in the system is equal to or greater than 20 % of its LEL. It is recommended to reconsider this rule of thumb in the light of the results of this work, which suggest a maximum decrease in the dust concentration by addition of a flammable gas in the concentration range of 0 - 20% of its LEL. On the other hand, the addition of a dust concentration of up to 10% of its MEC does not have a notable influence on the explosion properties of hybrid mixtures and could be considered negligible.

The experimentally determined values of LEL of hybrid mixtures were compared with the theoretical ones, calculated using Le Chatelier's mixing rule, Bartknecht's equation and a new model developed within the scope of this research work. Generally, Le Chatelier's mixing rule overestimated the LEL values of hybrid mixtures, whereas the values calculated utilizing Bartknecht's equation and the

model developed in this work tied well with the experimental data. A prime advantage of the model presented in this study over Bartknecht's equation is that the former uses basic thermodynamic properties of the individual components of a hybrid mixture as the input parameters. Whereas, the later calculates the LEL of a hybrid mixture using experimentally determined MEC/LEL of individual components of the hybrid mixture. Depending on the quality of this data, this could lead to implausible results that are either ultra conservative or not conservative enough. Moreover, Bartknecht's equation, when analysed in an energy balance perspective, led to conclusions which are not explainable according to basic laws of physics. Therefore, it is recommended to use the model presented in this work for the prediction of the LEL of hybrid mixtures, when no precise experimental data is available.

Apart from the theoretical as well as experimental investigation of the LEL of hybrid mixtures, ignition and combustion propagation mechanisms in hybrid mixtures with concentrations close to their LEL were studied with the help of high-speed videos. Hybrid mixtures of lycopodium and titanium with methane were selected as representatives of hybrid mixtures of organic (high volatile content) and metallic (non-volatile) dusts, respectively. For hybrid mixtures of lycopodium and methane, the ignition started with the birth of the ignition kernel as a result of dust particles being combusted upon contact with the spark and getting converted into highly luminous soot spot, which flash pyrolyzed the dust particles in its surrounding, resulting in a gaseous flame envelop around the highly luminous spot. In almost all the experiments it was observed that the ignition kernel did not develop into a self-sustaining combustion wave, but rather died as soon as the spark was deactivated. Regarding the combustion propagation, two types of mechanisms were observed, namely intermittent combustion propagation and continuous combustion propagation. During the intermittent combustion propagation, a few milliseconds after the disappearance of the ignition kernel, an autonomously growing combustion zone appeared, which instead of propagating through the whole unburnt fuel air mixture got quenched after travelling a few centimeters. After a pause of several milliseconds, the fuel oxidant mixture got reignited and an upward moving combustion wave was reestablished. In continuous combustion propagation, the ignition kernel, during its decay phase, gave rise to one or several discrete local combustion zones. These local combustion zones repeatedly appeared at locations which were mostly random, but indicated an upward motion of the combustion wave. For roughly half of the experiments categorized as continuous combustion propagation, after a few milliseconds of appearance and disappearance of the local combustion zones, a gaseous flame enveloping these local zones could be observed, which eventually took the shape of a smooth laminar flame front. For the other half, the combustion wave propagated until the top end of the tube in the form of randomly appearing local combustion zones. A dependency of the combustion propagation mechanism on the experimental

conditions investigated within the scope of this research work (the flow front velocity and the composition of the hybrid mixture) could not be established.

Hybrid mixtures of titanium and methane at their LEL exhibited two types of ignition mechanisms, namely particle explosions and particle divergence upon contact with the spark. In the former case the titanium particles exploded upon contact with the spark, resulting in the release of energy and particle debris that contributed to the formation of a burning particle cluster. Contrary to this, in the second case, the titanium particles got redirected upon contact with the spark and gathered themselves in the close proximity of each other, resulting in a chunk of simultaneously burning particles. The direction of the particle divergence was found to be related to the shape of the electrical arc. In both cases, the burning particle cluster eventually developed into an upward moving combustion wave. The occurrence of either of these mechanisms was considered stochastic and could not be associated with the dust or flammable gas concentration in the system or the flow front velocity.

The combustion propagation speed in hybrid mixtures of titanium and methane was generally higher than the pure titanium dust. In contrast, the combustion propagation in hybrid mixtures of lycopodium and methane was found to be slower than in pure dust air mixtures. The combustion propagation speed in hybrid mixtures at their LEL varied randomly within a relatively narrow range with respect to changing the relative amount of dust and gas in the system, as well as the flow front velocity. The results indicate the combustion propagation speed is independent of the hybrid mixture composition or the flow front velocity. The general understanding that the combustion propagation speed in a hybrid mixture increases with an increasing gas concentration in the system does not hold true for the hybrid mixtures at their LEL.

The main shortcoming of this work was the limitations of the experimental setup to visualize or locate gaseous flame. In future, it could be useful to use an optical schlieren system to get new insights into the role of the flammable gas during the combustion propagation in limit hybrid mixtures (specially for non-volatile dusts). Furthermore, an integration of a high-speed infrared camera in the setup could help in extracting information regarding temperature profiles during ignition and combustion propagation in hybrid mixtures, which might support in resolving a never-ending bone of contention between the research community, namely ‘whether or not considering a constant flame temperature for a multi fuel system is plausible?’. Moreover, this information could be very useful for the finetuning of mathematical as well as simulation models for prediction of explosion characteristics of hybrid mixtures. An integration of the capacitor discharge unit into the tube apparatus could allow the measurement of MIE of dusts and hybrid mixtures under non-turbulent conditions.

## References


1. *Directive 1999/92/EC of the European Parliament and of the COUNCIL of 16 December 1999 on minimum requirements for improving the safety and health protection of workers potentially at risk from explosive atmospheres (15th individual Directive within the meaning of Article 16 (1) of Directive 89/391/EEC).* Official Journal of the European Communities, 1999: p. 57-64.
2. VDI, *Richtlinie 2263 Blatt 5, „Staubbrände und Staubexplosionen Gefahren-BeurteilungSchutzmaßnahmen Explosionsschutz bei Wirbelschichttrocknern,“*. 2005.
3. Hesener, U. and M. Beck, *Forschungsbericht, "Sicherheitstechnische Kenngrößen von hybriden Gemischen", DEKRA Exam*. 2016.
4. Norm, D., *EN 1127-1 Explosionsfähige Atmosphären-Explosionsschutz-Teil 1: Grundlagen und Methodik*. 2019.
5. Amyotte, P.R., K.J. Mintz, M.J. Pegg and Y.H. Sun, *The ignitability of coal dust-air and methane-coal dust-air mixtures.* Fuel, 1993. 72(5): p. 671-679.
6. Amyotte, P.R. and R.K. Eckhoff, *Dust explosion causation, prevention and mitigation: An overview.* Journal of Chemical Health & Safety, 2010. 17(1): p. 15-28.
7. Hossaina, M.N., P.R. Amyottea and F.I. Khanb, *Influence of solvent admixture on explosibility of a pharmaceutical powder at laboratory-and industrial-scale.* Hazards, 2014. 25(160): p. 1-12.
8. Marmo, L., R. Sanchirico, A. Di Benedetto, V. Di Sarli, D. Riccio and E. Danzi, *Study of the explosible properties of textile dusts.* Journal of Loss Prevention in the Process Industries, 2018. 54: p. 110-122.
9. VDI, *Guideline 2263 Part 6, Dust fires and dust explosions,Hazards – assessment – protective measures,Dust fires and explosion protection in dust extracting installations.* 2017.
10. Engler, K.O.V., *Beiträge zur Kenntniss der Staubexplosionen*. 1885: J. Springer.
11. Eckhoff, R.K., *Dust explosions in the process industries: identification, assessment and control of dust hazards*. 2003: elsevier.
12. Addai, E.K., *Investigation of explosion characteristics of multiphase fuel mixtures with air*. 2016: Western Engineering, Inc.
13. Abbas, Z., R. Zinke, D. Gabel, E.K. Addai, A.F. Darbanan and U. Krause, *Theoretical evaluation of lower explosion limit of hybrid mixtures.* Journal of Loss Prevention in the Process Industries, 2019. 60: p. 296-302.
14. Garcia-Agreda, A., A. Di Benedetto, P. Russo, E. Salzano and R. Sanchirico, *Dust/gas mixtures explosion regimes.* Powder Technology, 2011. 205(1-3): p. 81-86.
15. Pellmont, G., *Explosions-und Zündverhalten von hybriden Gemischen aus brennbaren Stäuben und Brenngasen*. 1979, ETH Zurich.

16. Cashdollar, K.L. and M. Hertzberg, *20-l explosibility test chamber for dusts and gases.* Review of Scientific Instruments, 1985. 56(4): p. 596-602.

17. Chatrathi, K., *Dust and hybrid explosibility in a 1 m3 spherical chamber.* Process safety progress, 1994. 13(4): p. 183-189.

18. Pilao, R., E. Ramalho and C. Pinho, *Explosibility of cork dust in methane/air mixtures.* Journal of loss prevention in the process industries, 2006. 19(1): p. 17-23.

19. Bartknecht, W. and H. Brauer, *Explosionen: Ablauf und schutzmassnahmen*. 1980: Springer Berlin.

20. Amyotte, P., M. Lindsay, R. Domaratzki, N. Marchand, A. Di Benedetto and P. Russo, *Prevention and mitigation of dust and hybrid mixture explosions.* Process Safety Progress, 2010. 29(1): p. 17-21.

21. Addai, E.K., D. Gabel and U. Krause, *Lower explosion limit of hybrid mixtures of burnable gas and dust.* Journal of loss prevention in the process industries, 2015. 36: p. 497-504.

22. Addai, E.K., D. Gabel and U. Krause, *Lower explosion limit/minimum explosible concentration testing for hybrid mixtures in the Godbert-Greenwald furnace.* Process Safety Progress, 2017. 36(1): p. 81-94.

23. ASTM, E., *1515-14.* Standard Test Method for Minimum Explosible Concentration of Combustible Dusts, 2014.

24. EN, *14034-3,"* in *Determination of explosion characteristics of dust clouds-Part*. 2006.

25. Siwek, R., *20-L Laborapparatur für die Bestimmung der Explosionskenngrößen brennbarer Stäube.* Diploma Dissert, 1977.

26. Babrauskas, V. and L.G. Britton, *Errors in the compilations of minimum explosion concentration values for dust clouds.* Fire technology, 2018. 54(1): p. 37-55.

27. Makris, A., *Lean flammability limits of dust-air mixtures.* 1988.

28. Abbas, Z., D. Gabel, A. Krietsch and U. Krause, *Quasi-static dispersion of dusts for the determination of lower explosion limits of hybrid mixtures.* Journal of Loss Prevention in the Process Industries, 2022. 74: p. 104640.

29. Jiang, J., Y. Liu and M.S. Mannan, *A correlation of the lower flammability limit for hybrid mixtures.* Journal of loss prevention in the process industries, 2014. 32: p. 120-126.

30. Khalili, I., O. Dufaud, M. Poupeau, N. Cuervo-Rodriguez and L. Perrin, *Ignition sensitivity of gas–vapor/dust hybrid mixtures.* Powder technology, 2012. 217: p. 199-206.

31. Hertzberg, M., K.L. Cashdollar and I.A. Zlochower. *Flammability limit measurements for dusts and gases: ignition energy requirements and pressure dependences*. in *Symposium (international) on combustion*. 1988. Elsevier.

32. Taveau, J., J. Going, S. Hochgreb, S. Lemkowitz and D. Roekaerts, *Igniter-induced hybrids in the 20-l sphere.* Journal of Loss Prevention in the Process Industries, 2017. 49: p. 348-356.

33. Going, J.E., K. Chatrathi and K.L. Cashdollar, *Flammability limit measurements for dusts in 20-L and 1-m3 vessels.* Journal of Loss Prevention in the Process Industries, 2000. 13(3-5): p. 209-219.

34. Proust, C., A. Accorsi and L. Dupont, *Measuring the violence of dust explosions with the "20 l sphere" and with the standard "ISO 1 m3 vessel": Systematic comparison and analysis of the discrepancies.* Journal of Loss Prevention in the Process Industries, 2007. 20(4-6): p. 599-606.

35. Thomas, J.K., D.C. Kirby and J.E. Going, *Explosibility of a urea dust sample.* Process Safety Progress, 2013. 32(2): p. 189-192.

36. Zhen, G. and W. Leuckel, *Effects of ignitors and turbulence on dust explosions.* Journal of Loss Prevention in the Process Industries, 1997. 10(5-6): p. 317-324.

37. Mintz, K., *Problems in experimental measurements of dust explosions.* Journal of hazardous materials, 1995. 42(2): p. 177-186.

38. Gao, W., S. Zhong, N. Miao and H. Liu, *Effect of ignition on the explosion behavior of 1-Octadecanol/air mixtures.* Powder technology, 2013. 241: p. 105-114.

39. Ajrash, M.J., J. Zanganeh and B. Moghtaderi, *Effects of ignition energy on fire and explosion characteristics of dilute hybrid fuel in ventilation air methane.* Journal of Loss Prevention in the Process Industries, 2016. 40: p. 207-216.

40. Ogle, R.A., *Dust explosion dynamics*. 2016: Butterworth-Heinemann.

41. BAKER, W. and M. TANG, *Gas, Dust and Hybrid Explosions*. 1991.

42. Dufaud, O., I. Khalili, N. Cuervo, R. Olcese, A. Dufour, L. Perrin and A. Laurent, *Highlighting the importance of the pyrolysis step on dust explosions.* Chemical Engineering Transactions, 2012. 26: p. 369-374.

43. Kalejaiye, O., P.R. Amyotte, M.J. Pegg and K.L. Cashdollar, *Effectiveness of dust dispersion in the 20-L Siwek chamber.* Journal of loss prevention in the process industries, 2010. 23(1): p. 46-59.

44. Bagaria, P., J. Zhang and C. Mashuga, *Effect of dust dispersion on particle breakage and size distribution in the minimum ignition energy apparatus.* Journal of Loss Prevention in the Process Industries, 2018. 56: p. 518-523.

45. Du, B., W. Huang, L. Liu, T. Zhang, H. Li, Y. Ren and H. Wang, *Visualization and analysis of dispersion process of combustible dust in a transparent Siwek 20-L chamber.* Journal of Loss Prevention in the Process Industries, 2015. 33: p. 213-221.

46. DIN EN 14034-3, *Bestimmung der Explosionskenngrößen von Staub/Luft-Gemischen –* in *Teil 3: Bestimmung der unteren Explosionsgrenze UEG von Staub/Luft-Gemischen;*. 2011, Beuth Verlag GmbH: Berlin.

47. Van der Wel, P.G.J., *Ignition and propagation of dust explosions.* 1993.

48. Pu, Y., J. Jarosinski, V. Johnson and C. Kauffman. *Turbulence effects on dust explosions in the 20-liter spherical vessel*. in *Symposium (International) on Combustion*. 1991. Elsevier.

49. Dahoe, A., R. Cant, M. Pegg and B. Scarlett, *On the transient flow in the 20-liter explosion sphere.* Journal of Loss Prevention in the Process Industries, 2001. 14(6): p. 475-487.

50. D. Bradley, Z.C.a.J.R.S. *Burning rates in turbulent dust–air explosions*. in *2nd Symposium (International) on Combustion, The Combusion Institute, Pittsburgh (1988),*. 1988.

51. Dahoe, A., J. Zevenbergen, S. Lemkowitz and B. Scarlett, *Dust explosions in spherical vessels: the role of flame thickness in the validity of the 'cube-root law'.* Journal of Loss Prevention in the Process Industries, 1996. 9(1): p. 33-44.

52. Le Chatelier, H. and O. Boudouard, *Limits of flammability of gaseous mixtures.* Bulletin de la Société Chimique de France (Paris), 1898. 19: p. 483-488.

53. Rennhack, R. and A. Thiel-Boehm, *Die Simulation der Expolosiosgrenzen brennfähiger Gasgemische für sicherheitstechnische Analysen.* Chemieingenieurtechnik, 1991. 63(11): p. 1154-1155.

54. Cardillo, P. and A. EJ, *The flammability limits of hybrid gas and dust systems.* 1978.

55. Singer, J.M., E.B. Cook and J. Grumer, *Equivalences and lower ignition limits of coal dust and methane mixtures*. Vol. 6931. 1967: US Department of the Interior, Bureau of Mines.

56. Cashdollar, K.L., M. Hertzberg, M. Sapko and E. Weiss, *Laboratory and mine dust explosion research at the Bureau of Mines*. 1987: ASTM International.

57. Nagy, J. and W.M. Portman, *Explosibility of coal dust in an atmosphere containing a low percentage of methane*. Vol. 5815. 1961: US Department of the Interior, Bureau of Mines.

58. Russo, P., A. Di Benedetto and R. Sanchirico, *Theoretical evaluation of the explosion regimes of hybrid mixtures.* CHEMICAL ENGINEERING, 2012. 26.

59. Jiang, J., *Study of Dust-Gas Hybrid Mixture Explosions*. 2015.

60. Castellanos, D., V.H. Carreto-Vazquez, C.V. Mashuga, R. Trottier, A.F. Mejia and M.S. Mannan, *The effect of particle size polydispersity on the explosibility characteristics of aluminum dust.* Powder technology, 2014. 254: p. 331-337.

61. Bradley, D., S.E.-D. Habik and J. Swithenbank. *Laminar burning velocities of CH4—air-graphite mixtures and coal dusts*. in *Symposium (International) on Combustion*. 1988. Elsevier.

62. Bradley, D., G. Dixon-Lewis and S.E.-D. Habik, *Lean flammability limits and laminar burning velocities of CH4-air-graphite mixtures and fine coal dusts.* Combustion and flame, 1989. 77(1): p. 41-50.

63. Liu, Y., J. Sun and D. Chen, *Flame propagation in hybrid mixture of coal dust and methane.* Journal of Loss Prevention in the Process Industries, 2007. 20(4-6): p. 691-697.

64. Chen, D., J. Sun, Q. Wang and Y. Liu, *Combustion behaviors and flame structure of methane/coal dust hybrid in a vertical rectangle chamber.* Combustion science and technology, 2008. 180(8): p. 1518-1528.

65. Jiang, H., M. Bi, Z. Gao, Z. Zhang and W. Gao, *Effect of turbulence intensity on flame propagation and extinction limits of methane/coal dust explosions.* Energy, 2022. 239: p. 122246.

66. Yu, X., J. Yu, C. Wang, X. Lv, Y. Wang, Y. Hou and X. Yan, *Experimental study on the overpressure and flame propagation of hybrid hydrogen/aluminum dust explosions in a square closed vessel.* Fuel, 2021. 285: p. 119222.

67. Kim, W., S. Anraku, T. Endo and K. Choi, *Flammability and flame propagation of propane/L-leucine powder hybrid mixtures.* Powder Technology, 2020. 372: p. 694-702.

68. Pang, L., J. Cao, Y. Zhao, C. Yuan, K. Yang and Z. Zhang, *Flame propagation behaviours and overpressure characteristics of LDPE dust/ethylene hybrid mixture explosions.* Combustion Science and Technology, 2021: p. 1-30.

69. Cuervo, N., O. Dufaud and L. Perrin, *Determination of the burning velocity of gas/dust hybrid mixtures.* Process Safety and Environmental Protection, 2017. 109: p. 704-715.

70. Di Benedetto, A., A. Garcia-Agreda, O. Dufaud, I. Khalili, R. Sanchirico, N. Cuervo, L. Perrin and P. Russo. *Flame propagation of dust and gas-air mixtures in a tube*. in *Proceedings of the 7th Mediterranean Combustion Symposium*. 2011. Chia Laguna Cagliari, Sardinia, Italy.

71. Garcia-Agreda, A., *Study of hybrid mixture explosions*. 2010, PhD thesis, Universita degli Studi di Napoli Federico II, Naples, Italy.

72. Krause, U., T. Kasch and B. Gebauer, *Velocity and concentration effects on the laminar burning velocity of dust-air mixtures.* Archivum Combustionis, 1996. 16: p. 159-176.

73. Krause, U. and T. Kasch, *The influence of flow and turbulence on flame propagation through dust-air mixtures.* Journal of Loss Prevention in the Process Industries, 2000. 13(3-5): p. 291-298.

74. Spitzer, S., E. Askar, A. Krietsch and V. Schröder, *Comparative study on standardized ignition sources used for explosion testing*, in *13th International Symposium on Hazards, Prevention, and Mitigation of Industrial Explosions*. 2020: Braunschweig, GERMANY.

75. Gurvich, L.V. and I. Veyts, *Thermodynamic Properties of Individual Substances: Elements and Compounds*. Vol. 2. 1990: CRC press.

76. Chao, J., R.C. Wilhoit and B.J. Zwolinski, *Ideal gas thermodynamic properties of ethane and propane.* Journal of Physical and Chemical Reference Data, 1973. 2(2): p. 427-438.

77. Stokes, G.G., *On the effect of the internal friction of fluids on the motion of pendulums.* 1851.

78. Addo, A., A.G. Dastidar, J.R. Taveau, L.S. Morrison, F.I. Khan and P.R. Amyotte, *Niacin, lycopodium and polyethylene powder explosibility in 20-L and 1-m3 test chambers.* Journal of Loss Prevention in the Process Industries, 2019. 62: p. 103937.

79. Amyotte, P.R. and F. Khan, *Methods in Chemical Process Safety*. Vol. volume 3. 2017: Academic Press.

80. Abrahamsen, A.R., *The UK approach to dust explosibility assessment and its relevance to explosion prevention and protection*, in *Industrial Dust Explosions*. 1987, ASTM International.

81. Sanchirico, R., P. Russo, V. Di Sarli and A. Di Benedetto, *On the explosion and flammability behavior of mixtures of combustible dusts.* Process Safety and Environmental Protection, 2015. 94: p. 410-419.

82. GESTIS-DUST-EX, I., *Database Combustion and explosion characteristics of dusts*.

83. Spitzer, S., *Influence of the ignition source on the Safety Characteristics of hybrid dust-gas mixtures*. 2023.

84. Cashdollar, K.L., *Flammability of metals and other elemental dust clouds.* Process Safety Progress, 1994. 13(3): p. 139-145.

85. Boilard, S.P., P.R. Amyotte, F.I. Khan, A.G. Dastidar and R.K. Eckhoff, *Explosibility of micron-and nano-size titanium powders.* Journal of Loss Prevention in the Process Industries, 2013. 26(6): p. 1646-1654.

86. Wolański, P., *Dust explosions.* KONA Powder and Particle Journal, 1996. 14: p. 144-152.

87. Jacobson, M., A.R. Cooper and J. Nagy, *Explosibility of metal powders*. Vol. 6516. 1964: US Department of the Interior, Bureau of Mines.

88. Buksowicz, W. and P. Wolanski, *Flame propagation in dust-air mixtures at minimum explosive concentration.* Prog Astronaut and Aeronaut, 1983. 87: p. 414-425.

89. Sanchirico, R., A. Di Benedetto, A. Garcia-Agreda and P. Russo, *Study of the severity of hybrid mixture explosions and comparison to pure dust–air and vapour–air explosions.* Journal of loss prevention in the process industries, 2011. 24(5): p. 648-655.

90. Dufaud, O., L. Perrin, M. Traore, S. Chazelet and D. Thomas, *Explosions of vapour/dust hybrid mixtures: a particular class.* Powder Technology, 2009. 190(1-2): p. 269-273.

91. Denkevits, A., *Explosibility of hydrogen–graphite dust hybrid mixtures.* Journal of loss prevention in the process industries, 2007. 20(4-6): p. 698-707.

92. Denkevits, A. and B. Hoess, *Hybrid H2/Al dust explosions in Siwek sphere.* Journal of Loss Prevention in the Process Industries, 2015. 36: p. 509-521.

93. Burgess, M.J. and R.V. Wheeler, *CCXXVIII.—The lower limit of inflammation of mixtures of the paraffin hydrocarbons with air.* Journal of the Chemical Society, Transactions, 1911. 99: p. 2013-2030.

94. Gasse, A.S., *Experimentelle Bestimmung und Simulation von Explosionsgrenzen, untersucht an wasserstoffhaltigen Brenngasgemischen*. 1992: Shaker.

95. Gündüz, G., J. Stickling and R. Rennhack, *Experimental determination and simulation of explosion limits of benzene-inert gas-air mixtures.* Chemical Engineering & Technology: Industrial Chemistry-Plant Equipment-Process Engineering-Biotechnology, 1995. 18(6): p. 403-408.

96. Zabetakis, M., S. Lambiris and G. Scott. *Flame temperatures of limit mixtures*. in *Symposium (International) on Combustion*. 1958. Elsevier.

97. Jaeckel, G., *Die staubexplosionen.* Zeitschrift für technische Physik, 1924. 5: p. 67-68.

98. Mittal, M., *Models for minimum explosible concentration of organic dust clouds handled in industries.* Chemical Engineering & Technology: Industrial Chemistry-Plant Equipment-Process Engineering-Biotechnology, 1997. 20(7): p. 502-509.

99. Proust, C., *Flame propagation and combustion in some dust-air mixtures.* Journal of Loss Prevention in the Process Industries, 2006. 19(1): p. 89-100.

100. Han, O.-S., M. Yashima, T. Matsuda, H. Matsui, A. Miyake and T. Ogawa, *Behavior of flames propagating through lycopodium dust clouds in a vertical duct.* Journal of Loss Prevention in the Process Industries, 2000. 13(6): p. 449-457.

101. Han, O., *Flame Propagation Characteristics Through Suspended Combustible Particles in a Full-Scaled Duct.* Korean Chemical Engineering Research, 2009. 47(5): p. 572-579.

102. Kubala, T.A., F.J. Perzak and E.L. Litchfield, *Electric ignition of lycopodium powder in a modified Hartmann apparatus*. Vol. 8600. 1981: US Dept. of the Interior, Bureau of Mines.

103. Bidabadi, M., H.B. Dizaji, F.F. Dizaji and S.A. Mostafavi, *A parametric study of lycopodium dust flame.* Journal of Engineering Mathematics, 2015. 92(1): p. 147-165.

104. Klemens, R. and P. Wolanski, *Flame structure in dust-air and hybrid-air mixtures near the leanflammability limit.* Dynamics of Reactive Systems Part II: Modeling and Heterogeneous Combustion, 1986: p. 169.

105. Thurnay, K., *Thermal properties of transition metals*. 1998, Forschungszentrum Karlsruhe GmbH Technik und Umwelt (Germany). Inst. fuer ….

106. Molodetsky, I., E. Vicenzi, E. Dreizin and C. Law, *Phases of titanium combustion in air.* Combustion and Flame, 1998. 112(4): p. 522-532.

107. Han, O., I. Han and Y. Choi, *Prediction of flame propagation velocity based on the behavior of dust particles.* Korean Chemical Engineering Research, 2009. 47(6): p. 705-709.

108. Copelli, S., M. Barozzi, M.S. Scotton, A. Fumagalli, M. Derudi and R. Rota, *A predictive model for the estimation of the deflagration index of organic dusts.* Process safety and environmental protection, 2019. 126: p. 329-338.

109. Hwang, C., D. Heldman, R. Chao and T. Taylor, *Changes in specific heat of corn starch due to gelatinization.* Journal of food science, 1999. 64(1): p. 141-144.

110. Glotov, O.G., *Ignition and combustion of titanium particles: experimental methods and results.* Physics-Uspekhi, 2019. 62(2): p. 131.

# Appendix A EXPERIMENTAL EQUIPMENT AND CALIBRATION

*Appendix A consists of a description of the experimental equipment and calibration data of the dust concentration meters for all the dusts.*

## A.1 Technical data of the concentration measurement unit

SKG 5 developed by Research Centre for Applied System Safety and Industrial Medicine (FSA).

*Table A.1: Technical data SKG 5*

| | |
|---|---|
| Supply voltage | 220 V ~ ± 10%, 48-60 Hz |
| Power consumption | Approx. 30 VA |
| Device fuse | 0.2 A, slow acting |
| Sensor fuse | 80 mA, fast acting |
| Temperature range | 2 to 48 °C for the device, -20 to 75 °C for the sensor; <10 ms 2000 °C |
| Humidity range | 0-90 % |
| Display | 0 to 1999 mV, Resolution 1 mV |
| Analog outputs | Direct output with filtering<br>Average output over 1 to 10 sec<br>Both outputs 0-2 V; with max. 3000 Ω |
| Sample frequencies | 2,4,8,16 kHz internally switchable<br>Default at 8 kHz |
| Filter frequencies (low pass filter) | 250, 500, 1000, 2000 Hz internally switchable<br>Default setting at 1000 Hz |
| Temperature drift | Approx. -7.5 mV/°C for the sensor<br><1 mV over temperature range 2-48 °C for the control unit |

## A.2 Concentration measurement unit calibration

### A.2.1 Calibration data for lycopodium

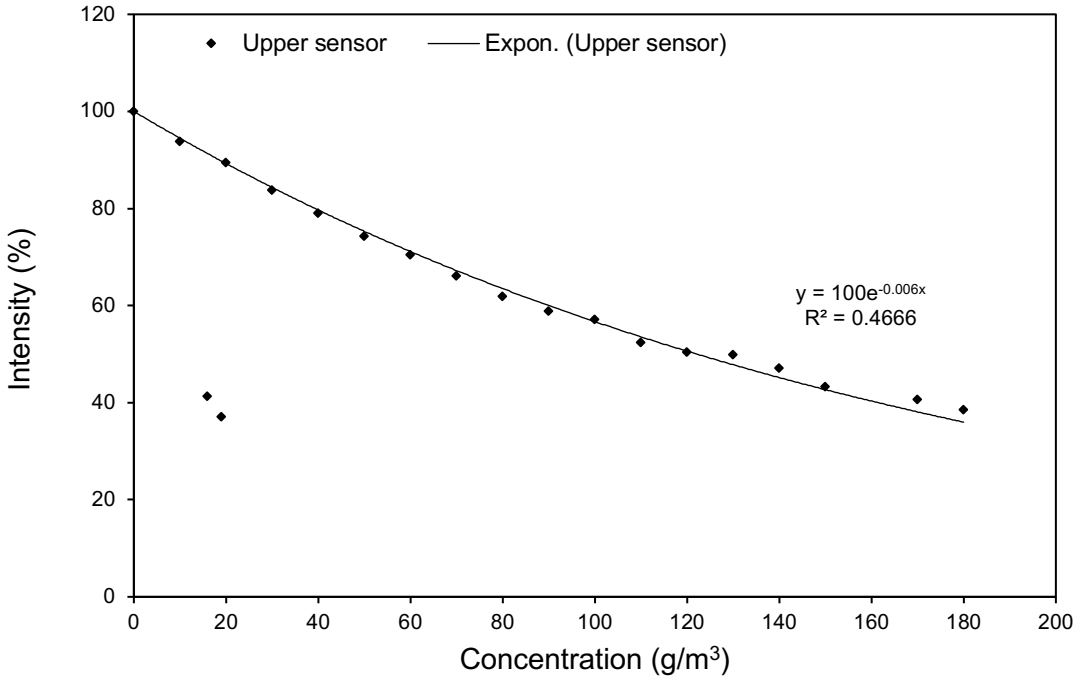


*Figure A.1: Calibration data for lycopodium (upper sensor)*

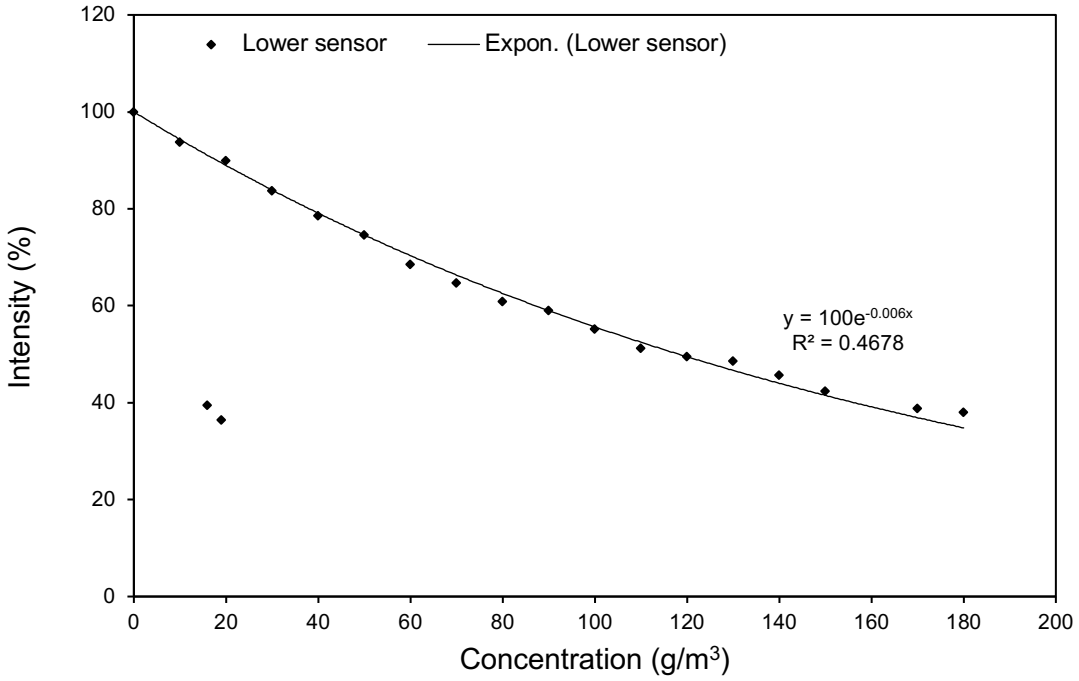


*Figure A.2: Calibration data for lycopodium (lower sensor)*

### A.2.2 Calibration data for titanium

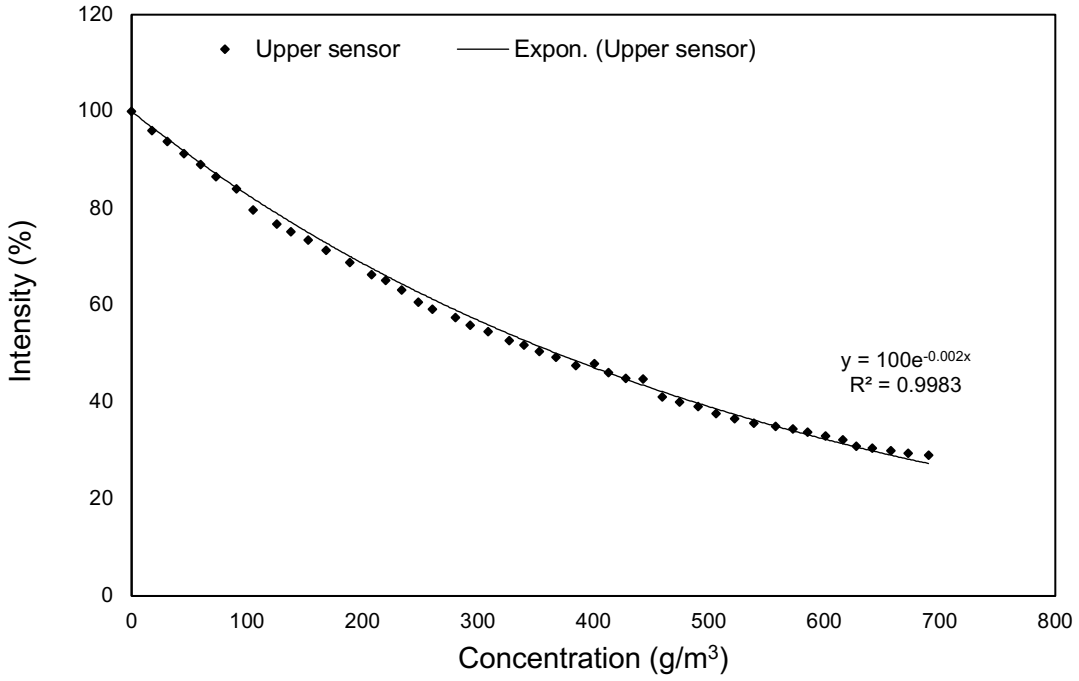


*Figure A.3: Calibration data for titanium (upper Sensor)*

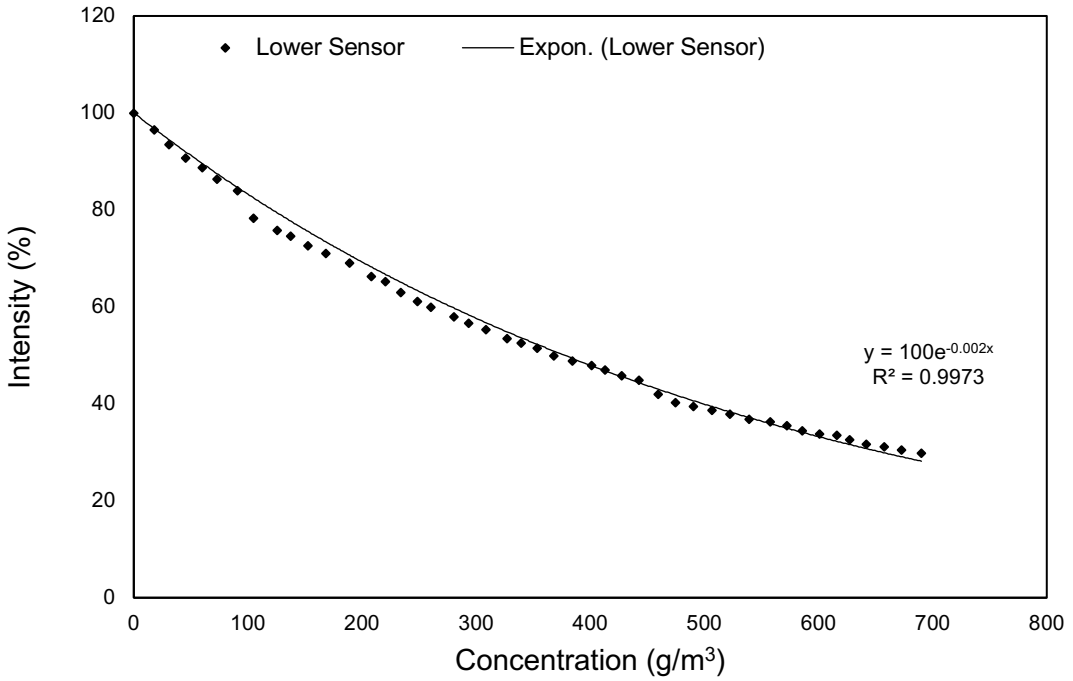


*Figure A.4: Calibration data for titanium (lower sensor)*

## A.3 Gas Delivery system

*Table A.2: Technical details of the thermal mass flow controllers*

| | |
|---|---|
| Medium | Methane (real gas calibrated) |
| Measuring range | 2 – 200ln/h<br>Ref. Cond. 1013mbar / 0°C |
| Accuracy | ± 0.3% of full scale<br>Plus ± 0.5% of the measured value |
| Reproducibility | ± 0.2% of full scale |
| Temperature | +20°C |
| Upstream Pressure | 5…6 bar gauge |
| Downstream Pressure | 0…3.5 bar gauge |
| Connection | G 1/4" female thread |
| Housing material | Aluminum |
| gaskets | FKM |
| Protection class | IP 50 |
| Power supply | +18...+30 Vdc (max. 250 mA) |
| Set point | RS485 (Modbus RTU) & 4...20 mA |
| Output | RS485 (Modbus RTU) & 4...20 mA |
| Control valve | 0.5 mm (24.6%) |
| Leakage rate | < 1x10-6 mbar l/s He |

## A.4 Calculation of Molecular weight from Elemental analysis

For the calculation of molecular weight from elemental analysis will be demonstrated with the example of lycopodium.

Values from the elemental analysis:

C=68.4%, H=9.6%, O=20.7%

Considering 100g of lycopodium as basis:

C = 68.4 g = 5.7 mol

H = 9.6 g = 9.6 mol

O = 20.7 g = 1.29 mol

Dividing number of moles of all the elements by 1.29

C = 4,4 mol, H = 7.44 mol, O = 1 mol

Average molecular weight can be calculated by

M. wt of lycopodium = 4.4x12+7.44+16= 76.24 g/mol

# Appendix B EXPERIMENTAL RESULTS

## B.1 Dust concentration reliability data

In this section complete data of dust concentration reliability experiments is presented (sections B.1.1 - B.1.4). An explanation of the symbols used in Tables along with the conversion formulae is given in the following Table. The average uncertainties of upper and lower sensors were calculated as an average of all the uncertainties values of the respective sensor.

| Symbol | Parameter | Conversion formulae |
|---|---|---|
| $M_d$ | Mass of dust | |
| $I_{U,M}$ | Light intensity, upper sensor manually measured | |
| $I_{U,D}$ | Light intensity, upper sensor digitally measured | |
| $I_{o,U}$ | Initial light intensity, upper sensor before dust dispersion | |
| $C_{U,M}$ | Concentration, upper sensor manually measured | $=-\ln(I_{U,M} / I_{o,U})/0.005$ |
| $C_{U,D}$ | Concentration, upper sensor digitally measured | $=-\ln(I_{U,D} / I_{o,U})/0.005$ |
| $I_{L,M}$ | Light intensity, lower sensor manually measured | |
| $I_{L,D}$ | Light intensity, lower sensor digitally measured | |
| $I_{o,U}$ | Initial light intensity, lower sensor before the dispersion | |
| $C_{L,M}$ | Concentration, lower sensor measured manually | $=-\ln(I_{L,M} / I_{o,L})/0.005$ |
| $C_{L,D}$ | Concentration, lower sensor measured digitally | $=-\ln(I_{L,D} / I_{o,L})/0.005$ |
| $C_{Av.M}$ | Average concentration, measured manually | $=\text{Average}(C_{U,M}, C_{L,M})$ |
| $C_{Av.D}$ | Average concentration, measured digitally | $=\text{Average}(C_{U,D}, C_{L,D})$ |
| $U_U$ | Uncertainty, upper sensor | $=(\text{Abs}(C_{U,M} - C_{U,D})/C_{U,D})*100$ |
| $U_L$ | Uncertainty, lower sensor | $=(\text{Abs}(C_{L,M} - C_{L,D})/C_{L,D})*100$ |

### B.1.1 Dust concentration reliability data at a flow velocity of 13 cm/s

| $m_d$ (g) | $I_{U,M}$ (mV) | $I_{U,D}$ (mV) | $I_{o,U}$ (mV) | $C_{U,M}$ (g/m$^3$) | $C_{U,D}$ (g/m$^3$) | $I_{L,M}$ (mV) | $I_{L,D}$ (mV) | $I_{o,U}$ (mV) | $C_{L,M}$ (g/m$^3$) | $C_{L,D}$ (g/m$^3$) | $C_{Av.M}$ (g/m$^3$) | $C_{Av.D}$ (g/m$^3$) | $U_U$ (%) | $U_L$ (%) |
|---|---|---|---|---|---|---|---|---|---|---|---|---|---|---|
| 1.5 | 169 | 185 | 1600 | 449.6 | 431.5 | 97 | 101 | 1556 | 462.5 | 455.8 | 456.0 | 443.6 | 4.19 | 1.48 |
| 1.5 | 114 | 119 | 1305 | 487.6 | 479.0 | 115 | 120 | 1676 | 446.5 | 439.4 | 467.0 | 459.2 | 1.79 | 1.61 |
| 1.5 | 111 | 115 | 1000 | 439.6 | 432.6 | 109 | 113 | 1633 | 451.1 | 445.1 | 445.4 | 438.8 | 1.64 | 1.35 |
| 1.5 | 118 | 110 | 1025 | 432.4 | 446.4 | 121 | 116 | 1730 | 443.3 | 450.4 | 437.9 | 448.4 | 3.15 | 1.56 |
| 1.5 | 113 | 108 | 1037 | 443.3 | 452.4 | 97 | 93 | 1503 | 456.8 | 463.8 | 450.0 | 458.1 | 2.00 | 1.51 |
| 1.5 | 173 | 166 | 1638 | 449.6 | 457.8 | 101 | 97 | 1615 | 462.0 | 468.7 | 455.8 | 463.3 | 1.80 | 1.44 |
| 1.5 | 150 | 156 | 1300 | 431.9 | 424.1 | 102 | 106 | 1461 | 443.7 | 437.2 | 437.8 | 430.6 | 1.85 | 1.47 |
| 1.5 | 110 | 119 | 1000 | 441.5 | 425.7 | 107 | 111 | 1622 | 453.1 | 447.0 | 447.3 | 436.4 | 3.69 | 1.37 |
| 1.5 | 172 | 179 | 1534 | 437.6 | 429.6 | 104 | 108 | 1550 | 450.3 | 444.0 | 443.9 | 436.8 | 1.86 | 1.42 |
| 1.5 | 140 | 152 | 1278 | 442.3 | 425.8 | 103 | 107 | 1575 | 454.5 | 448.2 | 448.4 | 437.0 | 3.86 | 1.42 |
| 1.4 | 211 | 219 | 1720 | 419.6 | 412.2 | 109 | 113 | 1445 | 430.8 | 424.7 | 425.2 | 418.5 | 1.81 | 1.41 |
| 1.4 | 163 | 156 | 1389 | 428.5 | 437.3 | 117 | 112 | 1630 | 439.0 | 446.3 | 433.8 | 441.8 | 2.01 | 1.63 |
| 1.4 | 167 | 160 | 1487 | 437.3 | 445.9 | 106 | 102 | 1490 | 440.5 | 446.9 | 438.9 | 446.4 | 1.92 | 1.43 |
| 1.4 | 141 | 129 | 1167 | 422.7 | 440.5 | 126 | 121 | 1640 | 427.7 | 434.4 | 425.2 | 437.5 | 4.04 | 1.55 |
| 1.4 | 182 | 175 | 1562 | 429.9 | 437.8 | 126 | 121 | 1711 | 434.8 | 441.5 | 432.4 | 439.6 | 1.79 | 1.53 |
| 1.4 | 162 | 168 | 1378 | 428.2 | 420.9 | 120 | 125 | 1684 | 440.2 | 433.4 | 434.2 | 427.2 | 1.73 | 1.57 |
| 1.4 | 177 | 190 | 1220 | 386.1 | 371.9 | 118 | 123 | 1686 | 443.2 | 436.3 | 414.7 | 404.1 | 3.81 | 1.59 |
| 1.4 | 177 | 184 | 1546 | 433.5 | 425.7 | 138 | 144 | 1756 | 423.9 | 416.8 | 428.7 | 421.3 | 1.82 | 1.70 |
| 1.4 | 148 | 135 | 1298 | 434.3 | 452.7 | 131 | 126 | 1686 | 425.8 | 432.3 | 430.0 | 442.5 | 4.06 | 1.50 |
| 1.4 | 159 | 153 | 1374 | 431.3 | 439.0 | 140 | 134 | 1755 | 421.4 | 428.7 | 426.4 | 433.9 | 1.75 | 1.70 |
| 1.3 | 207 | 193 | 1452 | 389.6 | 403.6 | 168 | 161 | 1696 | 385.3 | 392.4 | 387.5 | 398.0 | 3.47 | 1.81 |
| 1.3 | 191 | 170 | 1376 | 394.9 | 418.2 | 167 | 160 | 1728 | 389.5 | 396.6 | 392.2 | 407.4 | 5.57 | 1.80 |
| 1.3 | 135 | 140 | 985 | 397.5 | 390.2 | 176 | 183 | 1854 | 392.4 | 385.9 | 395.0 | 388.1 | 1.86 | 1.68 |
| 1.3 | 186 | 193 | 1376 | 400.2 | 392.8 | 163 | 170 | 1737 | 394.4 | 387.4 | 397.3 | 390.1 | 1.88 | 1.81 |

| $m_d$ (g) | $I_{U,M}$ (mV) | $I_{U,D}$ (mV) | $I_{o,U}$ (mV) | $C_{U,M}$ (g/m$^3$) | $C_{U,D}$ (g/m$^3$) | $I_{L,M}$ (mV) | $I_{L,D}$ (mV) | $I_{o,U}$ (mV) | $C_{L,M}$ (g/m$^3$) | $C_{L,D}$ (g/m$^3$) | $C_{Av.M}$ (g/m$^3$) | $C_{Av.D}$ (g/m$^3$) | $U_U$ (%) | $U_L$ (%) |
|---|---|---|---|---|---|---|---|---|---|---|---|---|---|---|
| 1.3 | 195 | 214 | 1476 | 404.8 | 386.2 | 160 | 166 | 1759 | 399.6 | 393.4 | 402.2 | 389.8 | 4.81 | 1.56 |
| 1.3 | 163 | 160 | 1376 | 426.6 | 430.4 | 165 | 172 | 1795 | 397.8 | 390.9 | 412.2 | 410.6 | 0.86 | 1.77 |
| 1.3 | 149 | 143 | 985 | 377.7 | 386.0 | 156 | 150 | 1746 | 402.5 | 409.1 | 390.1 | 397.5 | 2.13 | 1.60 |
| 1.3 | 186 | 179 | 1376 | 400.2 | 407.9 | 151 | 145 | 1718 | 405.3 | 412.0 | 402.8 | 410.0 | 1.88 | 1.64 |
| 1.3 | 199 | 191 | 1476 | 400.8 | 409.0 | 160 | 154 | 1835 | 406.6 | 413.0 | 403.7 | 411.0 | 2.01 | 1.54 |
| 1.3 | 255 | 230 | 1845 | 395.8 | 416.4 | 153 | 147 | 1699 | 401.2 | 407.9 | 398.5 | 412.2 | 4.96 | 1.63 |
| 1.2 | 211 | 219 | 1389 | 376.9 | 369.5 | 169 | 176 | 1676 | 382.4 | 375.6 | 379.6 | 372.5 | 2.01 | 1.80 |
| 1.2 | 212 | 220 | 1300 | 362.7 | 355.3 | 189 | 197 | 1722 | 368.2 | 361.3 | 365.5 | 358.3 | 2.09 | 1.91 |
| 1.2 | 203 | 195 | 1278 | 368.0 | 376.0 | 174 | 167 | 1631 | 373.0 | 379.8 | 370.5 | 377.9 | 2.14 | 1.80 |
| 1.2 | 242 | 232 | 1567 | 373.6 | 382.0 | 164 | 157 | 1597 | 379.3 | 386.6 | 376.5 | 384.3 | 2.21 | 1.88 |
| 1.2 | 191 | 199 | 1356 | 392.0 | 383.8 | 176 | 183 | 1765 | 384.2 | 377.7 | 388.1 | 380.8 | 2.14 | 1.72 |
| 1.2 | 259 | 269 | 1600 | 364.2 | 356.6 | 103 | 107 | 884 | 358.3 | 351.9 | 361.2 | 354.3 | 2.12 | 1.80 |
| 1.2 | 208 | 216 | 1305 | 367.3 | 359.7 | 96 | 100 | 903 | 373.6 | 366.8 | 370.4 | 363.2 | 2.10 | 1.86 |
| 1.2 | 160 | 154 | 1000 | 366.5 | 374.2 | 100 | 96 | 939 | 373.3 | 380.1 | 369.9 | 377.1 | 2.04 | 1.79 |
| 1.2 | 162 | 145 | 1025 | 369.0 | 391.1 | 95 | 91 | 906 | 375.9 | 383.0 | 372.4 | 387.1 | 5.67 | 1.87 |
| 1.2 | 158 | 158 | 1037 | 376.3 | 376.3 | 90 | 90 | 899 | 383.6 | 383.6 | 379.9 | 379.9 | 0.00 | 0.00 |
| 1.1 | 326 | 326 | 1638 | 322.9 | 322.9 | 154 | 154 | 1108 | 328.9 | 328.9 | 325.9 | 325.9 | 0.00 | 0.00 |
| 1.1 | 252 | 252 | 1300 | 328.1 | 328.1 | 119 | 119 | 889 | 335.2 | 335.2 | 331.7 | 331.7 | 0.00 | 0.00 |
| 1.1 | 264 | 275 | 1000 | 266.4 | 258.2 | 114 | 119 | 819 | 328.6 | 321.5 | 297.5 | 289.8 | 3.16 | 2.23 |
| 1.1 | 289 | 300 | 1534 | 333.8 | 326.4 | 114 | 119 | 825 | 329.9 | 322.7 | 331.9 | 324.5 | 2.29 | 2.22 |
| 1.1 | 245 | 259 | 1278 | 330.4 | 319.2 | 130 | 135 | 912 | 324.7 | 318.4 | 327.5 | 318.8 | 3.48 | 1.98 |
| 1.1 | 190 | 182 | 985 | 329.1 | 337.7 | 143 | 137 | 1003 | 324.7 | 331.8 | 326.9 | 334.8 | 2.55 | 2.15 |
| 1.1 | 271 | 260 | 1376 | 325.0 | 333.3 | 114 | 109 | 779 | 320.3 | 327.8 | 322.6 | 330.5 | 2.49 | 2.28 |
| 1.1 | 298 | 310 | 1476 | 320.0 | 312.1 | 151 | 157 | 1004 | 315.7 | 309.3 | 317.9 | 310.7 | 2.53 | 2.10 |
| 1.1 | 263 | 274 | 1300 | 319.6 | 311.4 | 136 | 141 | 903 | 315.5 | 309.5 | 317.6 | 310.4 | 2.63 | 1.94 |
| 1.1 | 196 | 196 | 1000 | 325.9 | 325.9 | 117 | 117 | 808 | 322.1 | 322.1 | 324.0 | 324.0 | 0.00 | 0.00 |

| $m_d$ (g) | $I_{U,M}$ (mV) | $I_{U,D}$ (mV) | $I_{o,U}$ (mV) | $C_{U,M}$ (g/m$^3$) | $C_{U,D}$ (g/m$^3$) | $I_{L,M}$ (mV) | $I_{L,D}$ (mV) | $I_{o,U}$ (mV) | $C_{L,M}$ (g/m$^3$) | $C_{L,D}$ (g/m$^3$) | $C_{Av.M}$ (g/m$^3$) | $C_{Av.D}$ (g/m$^3$) | $U_U$ (%) | $U_L$ (%) |
|---|---|---|---|---|---|---|---|---|---|---|---|---|---|---|
| 1 | 356 | 356 | 1534 | 292.1 | 292.1 | 155 | 155 | 869 | 287.3 | 287.3 | 289.7 | 289.7 | 0.00 | 0.00 |
| 1 | 309 | 309 | 1278 | 283.9 | 283.9 | 157 | 157 | 885 | 288.2 | 288.2 | 286.1 | 286.1 | 0.00 | 0.00 |
| 1 | 424 | 407 | 1720 | 280.1 | 288.3 | 148 | 142 | 813 | 283.9 | 290.8 | 282.0 | 289.5 | 2.84 | 2.37 |
| 1 | 453 | 425 | 1389 | 224.1 | 236.9 | 141 | 135 | 808 | 291.0 | 298.2 | 257.5 | 267.5 | 5.39 | 2.43 |
| 1 | 344 | 325 | 1487 | 292.8 | 304.1 | 140 | 134 | 835 | 297.6 | 304.9 | 295.2 | 304.5 | 3.74 | 2.39 |
| 1 | 308 | 335 | 1248 | 279.8 | 263.0 | 218 | 218 | 1195 | 283.6 | 283.6 | 281.7 | 273.3 | 6.39 | 0.00 |
| 1 | 424 | 455 | 1745 | 283.0 | 268.8 | 199 | 199 | 1107 | 286.0 | 286.0 | 284.5 | 277.4 | 5.25 | 0.00 |
| 1 | 347 | 355 | 1189 | 246.3 | 241.8 | 179 | 179 | 1040 | 293.3 | 293.3 | 269.8 | 267.5 | 1.89 | 0.00 |
| 1 | 327 | 340 | 1374 | 287.1 | 279.3 | 196 | 196 | 1116 | 289.9 | 289.9 | 288.5 | 284.6 | 2.79 | 0.00 |
| 1 | 344 | 330 | 1452 | 288.0 | 296.3 | 197 | 189 | 1129 | 291.0 | 297.9 | 289.5 | 297.1 | 2.80 | 2.32 |
| 0.9 | 390 | 374 | 1376 | 252.2 | 260.5 | 230 | 221 | 1061 | 254.8 | 261.5 | 253.5 | 261.0 | 3.22 | 2.54 |
| 0.9 | 351 | 337 | 985 | 206.4 | 214.5 | 240 | 230 | 1090 | 252.2 | 259.3 | 229.3 | 236.9 | 3.79 | 2.74 |
| 0.9 | 385 | 371 | 1376 | 254.7 | 262.1 | 215 | 206 | 1010 | 257.8 | 265.0 | 256.3 | 263.6 | 2.83 | 2.69 |
| 0.9 | 404 | 395 | 1476 | 259.1 | 263.6 | 232 | 219 | 1113 | 261.3 | 271.0 | 260.2 | 267.3 | 1.71 | 3.55 |
| 0.9 | 488 | 469 | 1845 | 266.0 | 273.9 | 237 | 226 | 1189 | 268.8 | 276.7 | 267.4 | 275.3 | 2.90 | 2.86 |
| 0.9 | 371 | 386 | 1389 | 264.0 | 256.1 | 235 | 244 | 1161 | 266.2 | 260.0 | 265.1 | 258.0 | 3.10 | 2.41 |
| 0.9 | 356 | 363 | 1300 | 259.0 | 255.1 | 211 | 219 | 1013 | 261.5 | 255.3 | 260.3 | 255.2 | 1.53 | 2.43 |
| 0.9 | 426 | 443 | 1278 | 219.7 | 211.9 | 214 | 223 | 1052 | 265.4 | 258.5 | 242.6 | 235.2 | 3.69 | 2.66 |
| 0.9 | 425 | 408 | 1567 | 261.0 | 269.1 | 268 | 257 | 1300 | 263.2 | 270.2 | 262.1 | 269.7 | 3.03 | 2.59 |
| 0.9 | 370 | 352 | 1356 | 259.8 | 269.7 | 265 | 254 | 1278 | 262.2 | 269.3 | 261.0 | 269.5 | 3.70 | 2.62 |
| 0.8 | 529 | 512 | 1720 | 235.8 | 242.4 | 376 | 361 | 1567 | 237.9 | 244.7 | 236.9 | 243.5 | 2.70 | 2.77 |
| 0.8 | 433 | 441 | 1389 | 233.1 | 229.5 | 365 | 375 | 1487 | 234.1 | 229.6 | 233.6 | 229.5 | 1.60 | 1.96 |
| 0.8 | 478 | 466 | 1487 | 227.0 | 232.1 | 318 | 309 | 1248 | 227.9 | 232.7 | 227.4 | 232.4 | 2.19 | 2.06 |
| 0.8 | 397 | 380 | 1248 | 229.1 | 237.8 | 339 | 339 | 1350 | 230.3 | 230.3 | 229.7 | 234.1 | 3.68 | 0.00 |
| 0.8 | 567 | 590 | 1745 | 224.8 | 216.9 | 300 | 312 | 1165 | 226.1 | 219.6 | 225.5 | 218.2 | 3.67 | 2.98 |
| 0.8 | 431 | 448 | 1189 | 203.0 | 195.2 | 308 | 320 | 1247 | 233.1 | 226.7 | 218.0 | 211.0 | 3.96 | 2.81 |

| $m_d$ (g) | $I_{U,M}$ (mV) | $I_{U,D}$ (mV) | $I_{o,U}$ (mV) | $C_{U,M}$ (g/m$^3$) | $C_{U,D}$ (g/m$^3$) | $I_{L,M}$ (mV) | $I_{L,D}$ (mV) | $I_{o,U}$ (mV) | $C_{L,M}$ (g/m$^3$) | $C_{L,D}$ (g/m$^3$) | $C_{Av.M}$ (g/m$^3$) | $C_{Av.D}$ (g/m$^3$) | $U_U$ (%) | $U_L$ (%) |
|---|---|---|---|---|---|---|---|---|---|---|---|---|---|---|
| 0.8 | 435 | 442 | 1374 | 230.0 | 226.8 | 306 | 317 | 1223 | 230.9 | 225.0 | 230.5 | 225.9 | 1.41 | 2.62 |
| 0.8 | 479 | 498 | 1452 | 221.8 | 214.0 | 340 | 354 | 1297 | 223.1 | 216.4 | 222.5 | 215.2 | 3.64 | 3.11 |
| 0.8 | 429 | 429 | 1376 | 233.1 | 233.1 | 304 | 304 | 1239 | 234.2 | 234.2 | 233.6 | 233.6 | 0.00 | 0.00 |
| 0.8 | 379 | 379 | 1389 | 259.8 | 259.8 | 363 | 363 | 1426 | 228.0 | 228.0 | 243.9 | 243.9 | 0.00 | 0.00 |
| 0.7 | 481 | 468 | 1300 | 198.9 | 204.3 | 378 | 366 | 1285 | 203.9 | 209.3 | 201.4 | 206.8 | 2.68 | 2.57 |
| 0.7 | 475 | 456 | 1278 | 197.9 | 206.1 | 419 | 402 | 1417 | 203.1 | 210.0 | 200.5 | 208.0 | 3.96 | 3.29 |
| 0.7 | 557 | 535 | 1567 | 206.9 | 214.9 | 398 | 382 | 1341 | 202.5 | 209.3 | 204.7 | 212.1 | 3.75 | 3.27 |
| 0.7 | 460 | 478 | 1320 | 210.8 | 203.2 | 425 | 442 | 1467 | 206.5 | 199.9 | 208.7 | 201.5 | 3.78 | 3.27 |
| 0.7 | 466 | 485 | 1345 | 212.0 | 204.0 | 393 | 409 | 1366 | 207.6 | 201.0 | 209.8 | 202.5 | 3.92 | 3.31 |
| 0.7 | 400 | 416 | 1086 | 199.8 | 191.9 | 406 | 422 | 1312 | 195.5 | 189.1 | 197.6 | 190.5 | 4.09 | 3.41 |
| 0.7 | 404 | 404 | 1093 | 199.1 | 199.1 | 393 | 393 | 1239 | 191.4 | 191.4 | 195.2 | 195.2 | 0.00 | 0.00 |
| 0.7 | 613 | 613 | 1634 | 196.1 | 196.1 | 395 | 395 | 1225 | 188.6 | 188.6 | 192.4 | 192.4 | 0.00 | 0.00 |
| 0.7 | 555 | 533 | 1419 | 187.7 | 195.8 | 409 | 393 | 1299 | 192.6 | 199.3 | 190.2 | 197.5 | 4.13 | 3.34 |
| 0.7 | 679 | 661 | 1566 | 167.1 | 172.5 | 439 | 421 | 1410 | 194.5 | 201.5 | 180.8 | 187.0 | 3.11 | 3.46 |
| 0.6 | 560 | 551 | 1310 | 170.0 | 173.2 | 440 | 431 | 1166 | 162.4 | 165.9 | 166.2 | 169.5 | 1.87 | 2.08 |
| 0.6 | 515 | 529 | 1267 | 180.0 | 174.7 | 475 | 485 | 1337 | 172.5 | 169.0 | 176.3 | 171.8 | 3.07 | 2.05 |
| 0.6 | 476 | 483 | 1114 | 170.1 | 167.1 | 362 | 371 | 1063 | 179.5 | 175.4 | 174.8 | 171.3 | 1.75 | 2.33 |
| 0.6 | 455 | 456 | 1103 | 177.1 | 176.7 | 337 | 344 | 1032 | 186.5 | 183.1 | 181.8 | 179.9 | 0.25 | 1.87 |
| 0.6 | 524 | 542 | 1219 | 168.9 | 162.1 | 454 | 465 | 1324 | 178.4 | 174.4 | 173.6 | 168.2 | 4.17 | 2.29 |
| 0.6 | 457 | 439 | 1113 | 178.0 | 186.1 | 392 | 392 | 1207 | 187.4 | 187.4 | 182.7 | 186.8 | 4.32 | 0.00 |
| 0.6 | 483 | 464 | 1189 | 180.2 | 188.2 | 361 | 361 | 1123 | 189.1 | 189.1 | 184.7 | 188.7 | 4.26 | 0.00 |
| 0.6 | 489 | 469 | 1161 | 172.9 | 181.3 | 399 | 399 | 1192 | 182.4 | 182.4 | 177.7 | 181.8 | 4.61 | 0.00 |
| 0.6 | 414 | 397 | 1013 | 179.0 | 187.3 | 423 | 423 | 1234 | 178.4 | 178.4 | 178.7 | 182.9 | 4.48 | 0.00 |
| 0.6 | 562 | 540 | 1052 | 125.4 | 133.4 | 596 | 596 | 1720 | 176.6 | 176.6 | 151.0 | 155.0 | 5.99 | 0.00 |
| 0.5 | 575 | 575 | 1096 | 129.0 | 129.0 | 746 | 746 | 1614 | 128.6 | 128.6 | 128.8 | 128.8 | 0.00 | 0.00 |
| 0.5 | 588 | 588 | 1226 | 147.0 | 147.0 | 686 | 686 | 1655 | 146.8 | 146.8 | 146.9 | 146.9 | 0.00 | 0.00 |

| $m_d$ (g) | $I_{U,M}$ (mV) | $I_{U,D}$ (mV) | $I_{o,U}$ (mV) | $C_{U,M}$ (g/m$^3$) | $C_{U,D}$ (g/m$^3$) | $I_{L,M}$ (mV) | $I_{L,D}$ (mV) | $I_{o,U}$ (mV) | $C_{L,M}$ (g/m$^3$) | $C_{L,D}$ (g/m$^3$) | $C_{Av.M}$ (g/m$^3$) | $C_{Av.D}$ (g/m$^3$) | $U_U$ (%) | $U_L$ (%) |
|---|---|---|---|---|---|---|---|---|---|---|---|---|---|---|
| 0.5 | 747 | 728 | 1467 | 135.0 | 140.1 | 651 | 633 | 1462 | 134.8 | 139.5 | 134.9 | 139.8 | 3.68 | 3.35 |
| 0.5 | 641 | 660 | 1247 | 133.1 | 127.3 | 705 | 720 | 1540 | 130.2 | 126.7 | 131.7 | 127.0 | 4.59 | 2.77 |
| 0.5 | 973 | 988 | 1776 | 120.3 | 117.3 | 718 | 730 | 1634 | 137.1 | 134.3 | 128.7 | 125.8 | 2.61 | 2.06 |
| 0.5 | 868 | 884 | 1783 | 144.0 | 140.3 | 609 | 622 | 1419 | 141.0 | 137.5 | 142.5 | 138.9 | 2.60 | 2.56 |
| 0.5 | 862 | 891 | 1728 | 139.1 | 132.5 | 692 | 709 | 1566 | 136.1 | 132.1 | 137.6 | 132.3 | 5.00 | 3.06 |
| 0.5 | 779 | 801 | 1703 | 156.4 | 150.9 | 600 | 613 | 1310 | 130.1 | 126.6 | 143.3 | 138.7 | 3.69 | 2.82 |
| 0.5 | 895 | 895 | 1715 | 130.1 | 130.1 | 636 | 636 | 1365 | 127.3 | 127.3 | 128.7 | 128.7 | 0.00 | 0.00 |
| 0.5 | 766 | 766 | 1542 | 139.9 | 139.9 | 563 | 563 | 1270 | 135.6 | 135.6 | 137.8 | 137.8 | 0.00 | 0.00 |
| 0.4 | 883 | 883 | 1570 | 115.1 | 115.1 | 621 | 621 | 1072 | 91.0 | 91.0 | 103.0 | 103.0 | 0.00 | 0.00 |
| 0.4 | 847 | 830 | 1572 | 123.7 | 127.7 | 619 | 599 | 1100 | 95.8 | 101.3 | 109.8 | 114.5 | 3.17 | 5.40 |
| 0.4 | 899 | 863 | 1519 | 104.9 | 113.1 | 550 | 534 | 1072 | 111.2 | 116.1 | 108.1 | 114.6 | 7.23 | 4.24 |
| 0.4 | 991 | 978 | 1642 | 101.0 | 103.6 | 767 | 755 | 1397 | 99.9 | 102.6 | 100.5 | 103.1 | 2.55 | 2.56 |
| 0.4 | 1060 | 1039 | 1696 | 94.0 | 98.0 | 770 | 751 | 1294 | 86.5 | 90.7 | 90.3 | 94.3 | 4.08 | 4.59 |
| 0.4 | 1023 | 1039 | 1613 | 91.1 | 88.0 | 754 | 773 | 1340 | 95.8 | 91.7 | 93.5 | 89.8 | 3.53 | 4.52 |
| 0.4 | 1013 | 1026 | 1645 | 97.0 | 94.4 | 759 | 777 | 1334 | 94.0 | 90.1 | 95.5 | 92.2 | 2.70 | 4.34 |
| 0.4 | 949 | 961 | 1564 | 99.9 | 97.4 | 851 | 866 | 1522 | 96.9 | 94.0 | 98.4 | 95.7 | 2.58 | 3.10 |
| 0.4 | 1023 | 1039 | 1678 | 99.0 | 95.9 | 976 | 999 | 1735 | 95.9 | 92.0 | 97.4 | 93.9 | 3.24 | 4.22 |
| 0.4 | 1043 | 1070 | 1627 | 88.9 | 83.8 | 1039 | 1055 | 1753 | 87.2 | 84.6 | 88.1 | 84.2 | 6.10 | 3.01 |
| 0.3 | 1149 | 1149 | 1688 | 76.9 | 76.9 | 1065 | 1065 | 1667 | 74.7 | 74.7 | 75.8 | 75.8 | 0.00 | 0.00 |
| 0.3 | 1247 | 1247 | 1534 | 41.4 | 41.4 | 1106 | 1106 | 1623 | 63.9 | 63.9 | 52.7 | 52.7 | 0.00 | 0.00 |
| 0.3 | 1164 | 1164 | 1619 | 66.0 | 66.0 | 1147 | 1147 | 1638 | 59.4 | 59.4 | 62.7 | 62.7 | 0.00 | 0.00 |
| 0.3 | 1039 | 1024 | 1633 | 90.4 | 93.3 | 741 | 730 | 1075 | 62.0 | 64.5 | 76.2 | 78.9 | 3.12 | 3.86 |
| 0.3 | 1154 | 1143 | 1730 | 81.0 | 82.9 | 695 | 687 | 1076 | 72.8 | 74.8 | 76.9 | 78.8 | 2.31 | 2.58 |
| 0.3 | 1023 | 1009 | 1503 | 76.9 | 79.7 | 683 | 671 | 1035 | 69.3 | 72.2 | 73.1 | 76.0 | 3.46 | 4.09 |
| 0.3 | 1144 | 1128 | 1615 | 69.0 | 71.8 | 645 | 639 | 977 | 69.2 | 70.8 | 69.1 | 71.3 | 3.92 | 2.20 |
| 0.3 | 984 | 999 | 1461 | 79.1 | 76.0 | 566 | 573 | 912 | 79.5 | 77.5 | 79.3 | 76.7 | 3.98 | 2.64 |

| $m_d$ (g) | $I_{U,M}$ (mV) | $I_{U,D}$ (mV) | $I_{o,U}$ (mV) | $C_{U,M}$ (g/m$^3$) | $C_{U,D}$ (g/m$^3$) | $I_{L,M}$ (mV) | $I_{L,D}$ (mV) | $I_{o,U}$ (mV) | $C_{L,M}$ (g/m$^3$) | $C_{L,D}$ (g/m$^3$) | $C_{Av.M}$ (g/m$^3$) | $C_{Av.D}$ (g/m$^3$) | $U_U$ (%) | $U_L$ (%) |
|---|---|---|---|---|---|---|---|---|---|---|---|---|---|---|
| 0.3 | 1115 | 1129 | 1622 | 75.0 | 72.5 | 897 | 908 | 1410 | 75.4 | 73.4 | 75.2 | 72.9 | 3.44 | 2.77 |
| 0.3 | 1131 | 1145 | 1550 | 63.0 | 60.6 | 798 | 810 | 1166 | 63.2 | 60.7 | 63.1 | 60.6 | 4.06 | 4.10 |
| 0.2 | 1227 | 1239 | 1575 | 49.9 | 48.0 | 989 | 1000 | 1337 | 50.2 | 48.4 | 50.1 | 48.2 | 4.06 | 3.81 |
| 0.2 | 1024 | 1009 | 1445 | 68.9 | 71.8 | 800 | 790 | 1063 | 47.4 | 49.5 | 58.1 | 60.6 | 4.11 | 4.24 |
| 0.2 | 1263 | 1277 | 1630 | 51.0 | 48.8 | 1206 | 1216 | 1642 | 51.4 | 50.1 | 51.2 | 49.4 | 4.52 | 2.75 |
| 0.2 | 1184 | 1167 | 1490 | 46.0 | 48.9 | 1284 | 1271 | 1696 | 46.4 | 48.1 | 46.2 | 48.5 | 5.92 | 3.53 |
| 0.2 | 1284 | 1263 | 1640 | 48.9 | 52.2 | 1199 | 1189 | 1613 | 49.4 | 50.8 | 49.2 | 51.5 | 6.31 | 2.75 |
| 0.2 | 1333 | 1333 | 1711 | 49.9 | 49.9 | 1215 | 1215 | 1645 | 50.5 | 50.5 | 50.2 | 50.2 | 0.00 | 0.00 |
| 0.2 | 1400 | 1389 | 1684 | 36.9 | 38.5 | 1250 | 1238 | 1564 | 37.4 | 39.0 | 37.1 | 38.7 | 4.10 | 4.13 |
| 0.2 | 1387 | 1387 | 1686 | 39.0 | 39.0 | 1325 | 1325 | 1678 | 39.4 | 39.4 | 39.2 | 39.2 | 0.00 | 0.00 |
| 0.2 | 1489 | 1501 | 1756 | 33.0 | 31.4 | 1303 | 1314 | 1627 | 37.0 | 35.6 | 35.0 | 33.5 | 5.12 | 3.93 |
| 0.2 | 1219 | 1226 | 1519 | 44.0 | 42.9 | 1024 | 1033 | 1337 | 44.5 | 43.0 | 44.2 | 42.9 | 2.67 | 3.39 |

### B.1.2 Dust concentration reliability data at a flow velocity of 9.5 cm/s

| $m_d$ (g) | $I_{U,M}$ (mV) | $I_{U,D}$ (mV) | $I_{o,U}$ (mV) | $C_{U,M}$ (g/m$^3$) | $C_{U,D}$ (g/m$^3$) | $I_{L,M}$ (mV) | $I_{L,D}$ (mV) | $I_{o,U}$ (mV) | $C_{L,M}$ (g/m$^3$) | $C_{L,D}$ (g/m$^3$) | $C_{Av.M}$ (g/m$^3$) | $C_{Av.D}$ (g/m$^3$) | $U_U$ (%) | $U_L$ (%) |
|---|---|---|---|---|---|---|---|---|---|---|---|---|---|---|
| 1.5 | 197 | 218 | 1600 | 418.9 | 398.7 | 145 | 157 | 1701 | 410.4 | 397.1 | 414.6 | 397.9 | 5.08 | 3.34 |
| 1.5 | 148 | 161 | 1305 | 435.3 | 418.5 | 110 | 121 | 1428 | 427.3 | 411.4 | 431.3 | 414.9 | 4.02 | 3.86 |
| 1.5 | 146 | 152 | 1000 | 384.8 | 376.8 | 113 | 118 | 1511 | 432.2 | 425.0 | 408.5 | 400.9 | 2.14 | 1.70 |
| 1.5 | 156 | 145 | 1025 | 376.5 | 391.1 | 125 | 125 | 1597 | 424.6 | 424.6 | 400.6 | 407.9 | 3.74 | 0.00 |
| 1.5 | 149 | 149 | 1037 | 388.0 | 388.0 | 110 | 110 | 1514 | 437.0 | 437.0 | 412.5 | 412.5 | 0.00 | 0.00 |
| 1.5 | 197 | 197 | 1638 | 423.6 | 423.6 | 95 | 95 | 1084 | 405.8 | 405.8 | 414.7 | 414.7 | 0.00 | 0.00 |
| 1.5 | 150 | 144 | 1300 | 431.9 | 440.1 | 118 | 113 | 1514 | 425.3 | 432.5 | 428.6 | 436.3 | 1.86 | 1.67 |
| 1.5 | 145 | 138 | 1000 | 386.2 | 396.1 | 85 | 76 | 1141 | 432.8 | 451.5 | 409.5 | 423.8 | 2.50 | 4.13 |
| 1.5 | 172 | 165 | 1534 | 437.6 | 445.9 | 136 | 131 | 1802 | 430.7 | 436.9 | 434.1 | 441.4 | 1.86 | 1.43 |

| $m_d$ (g) | $I_{U,M}$ (mV) | $I_{U,D}$ (mV) | $I_{o,U}$ (mV) | $C_{U,M}$ (g/m$^3$) | $C_{U,D}$ (g/m$^3$) | $I_{L,M}$ (mV) | $I_{L,D}$ (mV) | $I_{o,U}$ (mV) | $C_{L,M}$ (g/m$^3$) | $C_{L,D}$ (g/m$^3$) | $C_{Av.M}$ (g/m$^3$) | $C_{Av.D}$ (g/m$^3$) | $U_U$ (%) | $U_L$ (%) |
|---|---|---|---|---|---|---|---|---|---|---|---|---|---|---|
| 1.5 | 157 | 144 | 1278 | 419.4 | 436.6 | 115 | 103 | 1430 | 420.1 | 438.5 | 419.7 | 437.5 | 3.96 | 4.19 |
| 1.4 | 217 | 226 | 1720 | 414.0 | 405.9 | 95 | 99 | 1100 | 408.2 | 401.3 | 411.1 | 403.6 | 2.00 | 1.71 |
| 1.4 | 200 | 210 | 1389 | 387.6 | 377.8 | 149 | 163 | 1793 | 414.6 | 399.6 | 401.1 | 388.7 | 2.58 | 3.75 |
| 1.4 | 189 | 197 | 1487 | 412.6 | 404.3 | 135 | 140 | 1639 | 416.1 | 410.0 | 414.3 | 407.1 | 2.05 | 1.48 |
| 1.4 | 145 | 151 | 1167 | 417.1 | 409.0 | 160 | 166 | 1804 | 403.8 | 397.6 | 410.4 | 403.3 | 1.98 | 1.54 |
| 1.4 | 205 | 205 | 1562 | 406.1 | 406.1 | 157 | 157 | 1844 | 410.6 | 410.6 | 408.4 | 408.4 | 0.00 | 0.00 |
| 1.4 | 203 | 203 | 1378 | 383.0 | 383.0 | 156 | 156 | 1894 | 416.1 | 416.1 | 399.6 | 399.6 | 0.00 | 0.00 |
| 1.4 | 178 | 159 | 1220 | 385.0 | 407.5 | 146 | 135 | 1794 | 418.1 | 431.2 | 401.5 | 419.3 | 5.54 | 3.03 |
| 1.4 | 223 | 214 | 1546 | 387.3 | 395.5 | 159 | 153 | 1757 | 400.4 | 406.8 | 393.8 | 401.2 | 2.08 | 1.58 |
| 1.4 | 184 | 172 | 1298 | 390.7 | 404.2 | 101 | 89 | 1128 | 402.2 | 423.3 | 396.5 | 413.7 | 3.34 | 4.98 |
| 1.4 | 200 | 192 | 1374 | 385.4 | 393.6 | 105 | 101 | 1141 | 397.6 | 404.1 | 391.5 | 398.8 | 2.07 | 1.60 |
| 1.3 | 248 | 227 | 1452 | 353.5 | 371.1 | 198 | 187 | 1802 | 368.1 | 377.6 | 360.8 | 374.4 | 4.77 | 2.52 |
| 1.3 | 229 | 220 | 1376 | 358.6 | 366.7 | 152 | 146 | 1430 | 373.6 | 380.3 | 366.1 | 373.5 | 2.19 | 1.76 |
| 1.3 | 162 | 162 | 985 | 361.0 | 361.0 | 118 | 118 | 1128 | 376.3 | 376.3 | 368.6 | 368.6 | 0.00 | 0.00 |
| 1.3 | 224 | 208 | 1376 | 363.1 | 377.9 | 118 | 107 | 1141 | 378.2 | 394.5 | 370.6 | 386.2 | 3.92 | 4.13 |
| 1.3 | 234 | 234 | 1476 | 368.4 | 368.4 | 182 | 182 | 1802 | 382.1 | 382.1 | 375.2 | 375.2 | 0.00 | 0.00 |
| 1.3 | 232 | 246 | 1376 | 356.0 | 344.3 | 146 | 167 | 1430 | 380.3 | 357.9 | 368.2 | 351.1 | 3.40 | 6.26 |
| 1.3 | 162 | 177 | 985 | 361.0 | 343.3 | 169 | 186 | 1708 | 385.5 | 369.6 | 373.3 | 356.4 | 5.16 | 4.32 |
| 1.3 | 224 | 233 | 1376 | 363.1 | 355.2 | 184 | 191 | 1890 | 388.2 | 382.0 | 375.6 | 368.6 | 2.22 | 1.63 |
| 1.3 | 239 | 249 | 1476 | 364.1 | 355.9 | 174 | 181 | 1795 | 389.0 | 382.4 | 376.5 | 369.2 | 2.30 | 1.72 |
| 1.3 | 258 | 248 | 1845 | 393.5 | 401.4 | 186 | 179 | 1869 | 384.6 | 391.0 | 389.0 | 396.2 | 1.97 | 1.64 |
| 1.2 | 252 | 237 | 1389 | 341.4 | 353.7 | 205 | 189 | 1844 | 366.1 | 379.7 | 353.7 | 366.7 | 3.47 | 3.57 |
| 1.2 | 252 | 242 | 1300 | 328.1 | 336.2 | 203 | 195 | 1684 | 352.6 | 359.3 | 340.4 | 347.8 | 2.41 | 1.86 |
| 1.2 | 264 | 245 | 1278 | 315.4 | 330.4 | 211 | 203 | 1794 | 356.7 | 363.2 | 336.1 | 346.8 | 4.52 | 1.77 |
| 1.2 | 314 | 314 | 1567 | 321.5 | 321.5 | 199 | 199 | 1757 | 363.0 | 363.0 | 342.3 | 342.3 | 0.00 | 0.00 |
| 1.2 | 265 | 265 | 1356 | 326.5 | 326.5 | 190 | 190 | 1726 | 367.8 | 367.8 | 347.1 | 347.1 | 0.00 | 0.00 |

| $m_d$ (g) | $I_{U,M}$ (mV) | $I_{U,D}$ (mV) | $I_{o,U}$ (mV) | $C_{U,M}$ (g/m$^3$) | $C_{U,D}$ (g/m$^3$) | $I_{L,M}$ (mV) | $I_{L,D}$ (mV) | $I_{o,U}$ (mV) | $C_{L,M}$ (g/m$^3$) | $C_{L,D}$ (g/m$^3$) | $C_{Av.M}$ (g/m$^3$) | $C_{Av.D}$ (g/m$^3$) | $U_U$ (%) | $U_L$ (%) |
|---|---|---|---|---|---|---|---|---|---|---|---|---|---|---|
| 1.2 | 261 | 261 | 1600 | 362.6 | 362.6 | 124 | 124 | 972 | 343.2 | 343.2 | 352.9 | 352.9 | 0.00 | 0.00 |
| 1.2 | 255 | 260 | 1305 | 326.5 | 322.7 | 169 | 200 | 1406 | 353.1 | 325.0 | 339.8 | 323.8 | 1.20 | 8.64 |
| 1.2 | 197 | 205 | 1000 | 324.9 | 316.9 | 131 | 136 | 1084 | 352.2 | 346.0 | 338.6 | 331.5 | 2.51 | 1.80 |
| 1.2 | 199 | 207 | 1025 | 327.8 | 319.9 | 180 | 187 | 1514 | 354.9 | 348.6 | 341.4 | 334.3 | 2.46 | 1.82 |
| 1.2 | 194 | 202 | 1037 | 335.2 | 327.2 | 186 | 193 | 1624 | 361.2 | 355.0 | 348.2 | 341.1 | 2.47 | 1.73 |
| 1.1 | 394 | 383 | 1638 | 285.0 | 290.6 | 213 | 195 | 1373 | 310.6 | 325.3 | 297.8 | 308.0 | 1.95 | 4.52 |
| 1.1 | 306 | 288 | 1300 | 289.3 | 301.4 | 258 | 248 | 1707 | 314.9 | 321.5 | 302.1 | 311.5 | 4.02 | 2.05 |
| 1.1 | 230 | 221 | 1000 | 293.9 | 301.9 | 204 | 196 | 1308 | 309.7 | 316.4 | 301.8 | 309.1 | 2.64 | 2.11 |
| 1.1 | 351 | 331 | 1534 | 295.0 | 306.7 | 235 | 220 | 1511 | 310.2 | 321.1 | 302.6 | 313.9 | 3.83 | 3.42 |
| 1.1 | 298 | 286 | 1278 | 291.2 | 299.4 | 254 | 244 | 1597 | 306.4 | 313.1 | 298.8 | 306.3 | 2.75 | 2.14 |
| 1.1 | 230 | 230 | 985 | 290.9 | 290.9 | 248 | 248 | 1551 | 305.5 | 305.5 | 298.2 | 298.2 | 0.00 | 0.00 |
| 1.1 | 328 | 315 | 1376 | 286.8 | 294.9 | 210 | 195 | 1283 | 301.6 | 314.0 | 294.2 | 304.4 | 2.74 | 3.93 |
| 1.1 | 360 | 360 | 1476 | 282.2 | 282.2 | 247 | 247 | 1471 | 297.4 | 297.4 | 289.8 | 289.8 | 0.00 | 0.00 |
| 1.1 | 317 | 333 | 1300 | 282.2 | 272.4 | 197 | 211 | 1169 | 296.8 | 285.3 | 289.5 | 278.9 | 3.62 | 4.01 |
| 1.1 | 237 | 246 | 1000 | 287.9 | 280.5 | 185 | 192 | 1135 | 302.3 | 296.1 | 295.1 | 288.3 | 2.66 | 2.09 |
| 1 | 381 | 396 | 1534 | 278.6 | 270.8 | 276 | 287 | 1406 | 271.4 | 264.8 | 275.0 | 267.8 | 2.85 | 2.46 |
| 1 | 329 | 329 | 1278 | 271.4 | 271.4 | 372 | 372 | 1892 | 271.1 | 271.1 | 271.2 | 271.2 | 0.00 | 0.00 |
| 1 | 452 | 452 | 1720 | 267.3 | 267.3 | 180 | 180 | 894 | 267.1 | 267.1 | 267.2 | 267.2 | 0.00 | 0.00 |
| 1 | 353 | 353 | 1389 | 274.0 | 274.0 | 172 | 172 | 889 | 273.8 | 273.8 | 273.9 | 273.9 | 0.00 | 0.00 |
| 1 | 367 | 352 | 1487 | 279.8 | 288.2 | 171 | 164 | 919 | 280.3 | 287.2 | 280.1 | 287.7 | 2.90 | 2.43 |
| 1 | 328 | 315 | 1248 | 267.3 | 275.3 | 264 | 256 | 1315 | 267.6 | 272.7 | 267.4 | 274.0 | 2.94 | 1.88 |
| 1 | 452 | 434 | 1745 | 270.2 | 278.3 | 281 | 270 | 1414 | 269.3 | 276.0 | 269.7 | 277.1 | 2.92 | 2.41 |
| 1 | 298 | 286 | 1189 | 276.8 | 285.0 | 298 | 286 | 1559 | 275.8 | 282.6 | 276.3 | 283.8 | 2.88 | 2.42 |
| 1 | 349 | 337 | 1374 | 274.1 | 281.1 | 287 | 266 | 1475 | 272.8 | 285.5 | 273.5 | 283.3 | 2.49 | 4.44 |
| 1 | 367 | 367 | 1452 | 275.1 | 275.1 | 312 | 312 | 1614 | 273.9 | 273.9 | 274.5 | 274.5 | 0.00 | 0.00 |
| 0.9 | 412 | 412 | 1376 | 241.2 | 241.2 | 277 | 277 | 1167 | 239.7 | 239.7 | 240.4 | 240.4 | 0.00 | 0.00 |

| $m_d$ (g) | $I_{U,M}$ (mV) | $I_{U,D}$ (mV) | $I_{o,U}$ (mV) | $C_{U,M}$ (g/m$^3$) | $C_{U,D}$ (g/m$^3$) | $I_{L,M}$ (mV) | $I_{L,D}$ (mV) | $I_{o,U}$ (mV) | $C_{L,M}$ (g/m$^3$) | $C_{L,D}$ (g/m$^3$) | $C_{Av.M}$ (g/m$^3$) | $C_{Av.D}$ (g/m$^3$) | $U_U$ (%) | $U_L$ (%) |
|---|---|---|---|---|---|---|---|---|---|---|---|---|---|---|
| 0.9 | 334 | 334 | 985 | 216.3 | 216.3 | 288 | 288 | 1199 | 237.7 | 237.7 | 227.0 | 227.0 | 0.00 | 0.00 |
| 0.9 | 407 | 423 | 1376 | 243.6 | 235.9 | 259 | 275 | 1111 | 242.7 | 232.7 | 243.2 | 234.3 | 3.27 | 4.29 |
| 0.9 | 428 | 445 | 1476 | 247.6 | 239.8 | 292 | 304 | 1282 | 246.6 | 239.9 | 247.1 | 239.8 | 3.25 | 2.80 |
| 0.9 | 518 | 539 | 1845 | 254.1 | 246.1 | 300 | 312 | 1372 | 253.4 | 246.8 | 253.7 | 246.5 | 3.23 | 2.65 |
| 0.9 | 393 | 393 | 1389 | 252.5 | 252.5 | 299 | 299 | 1345 | 250.6 | 250.6 | 251.6 | 251.6 | 0.00 | 0.00 |
| 0.9 | 377 | 377 | 1300 | 247.6 | 247.6 | 326 | 326 | 1427 | 246.1 | 246.1 | 246.8 | 246.8 | 0.00 | 0.00 |
| 0.9 | 364 | 349 | 1278 | 251.2 | 259.6 | 304 | 292 | 1363 | 250.1 | 256.8 | 250.6 | 258.2 | 3.24 | 2.61 |
| 0.9 | 450 | 429 | 1567 | 249.5 | 259.1 | 354 | 337 | 1569 | 248.1 | 256.4 | 248.8 | 257.7 | 3.69 | 3.20 |
| 0.9 | 391 | 375 | 1356 | 248.7 | 257.1 | 278 | 267 | 1225 | 247.2 | 253.9 | 247.9 | 255.5 | 3.25 | 2.65 |
| 0.8 | 556 | 534 | 1720 | 225.9 | 233.9 | 316 | 303 | 1213 | 224.2 | 231.2 | 225.0 | 232.6 | 3.45 | 3.03 |
| 0.8 | 463 | 480 | 1389 | 219.7 | 212.5 | 357 | 371 | 1341 | 220.6 | 214.2 | 220.1 | 213.3 | 3.39 | 2.99 |
| 0.8 | 501 | 521 | 1487 | 217.6 | 209.8 | 337 | 350 | 1224 | 215.0 | 208.7 | 216.3 | 209.2 | 3.73 | 3.02 |
| 0.8 | 417 | 434 | 1248 | 219.2 | 211.3 | 510 | 530 | 1873 | 216.8 | 210.4 | 218.0 | 210.8 | 3.78 | 3.05 |
| 0.8 | 594 | 634 | 1745 | 215.5 | 202.5 | 467 | 486 | 1677 | 213.1 | 206.4 | 214.3 | 204.5 | 6.44 | 3.22 |
| 0.8 | 391 | 391 | 1189 | 222.4 | 222.4 | 454 | 454 | 1696 | 219.7 | 219.7 | 221.0 | 221.0 | 0.00 | 0.00 |
| 0.8 | 457 | 457 | 1374 | 220.2 | 220.2 | 468 | 468 | 1727 | 217.6 | 217.6 | 218.9 | 218.9 | 0.00 | 0.00 |
| 0.8 | 516 | 516 | 1452 | 206.9 | 206.9 | 490 | 490 | 1729 | 210.1 | 210.1 | 208.5 | 208.5 | 0.00 | 0.00 |
| 0.8 | 465 | 446 | 1376 | 217.0 | 225.3 | 445 | 427 | 1671 | 220.5 | 227.4 | 218.7 | 226.4 | 3.70 | 3.03 |
| 0.8 | 473 | 454 | 1389 | 215.4 | 223.6 | 369 | 354 | 1406 | 223.0 | 229.9 | 219.2 | 226.8 | 3.67 | 3.01 |
| 0.7 | 542 | 520 | 1300 | 175.0 | 183.3 | 521 | 500 | 1724 | 199.4 | 206.3 | 187.2 | 194.8 | 4.52 | 3.32 |
| 0.7 | 535 | 509 | 1278 | 174.2 | 184.1 | 441 | 423 | 1452 | 198.6 | 205.6 | 186.4 | 194.8 | 5.41 | 3.38 |
| 0.7 | 628 | 628 | 1567 | 182.9 | 182.9 | 452 | 452 | 1480 | 197.7 | 197.7 | 190.3 | 190.3 | 0.00 | 0.00 |
| 0.7 | 519 | 540 | 1320 | 186.7 | 178.8 | 356 | 370 | 1195 | 201.8 | 195.4 | 194.3 | 187.1 | 4.44 | 3.29 |
| 0.7 | 526 | 547 | 1345 | 187.8 | 179.9 | 356 | 370 | 1202 | 202.8 | 196.4 | 195.3 | 188.2 | 4.35 | 3.27 |
| 0.7 | 451 | 466 | 1086 | 175.8 | 169.2 | 459 | 472 | 1443 | 190.9 | 186.3 | 183.3 | 177.7 | 3.87 | 2.50 |
| 0.7 | 456 | 456 | 1093 | 174.8 | 174.8 | 444 | 444 | 1363 | 186.9 | 186.9 | 180.9 | 180.9 | 0.00 | 0.00 |

| $m_d$ (g) | $I_{U,M}$ (mV) | $I_{U,D}$ (mV) | $I_{o,U}$ (mV) | $C_{U,M}$ (g/m$^3$) | $C_{U,D}$ (g/m$^3$) | $I_{L,M}$ (mV) | $I_{L,D}$ (mV) | $I_{o,U}$ (mV) | $C_{L,M}$ (g/m$^3$) | $C_{L,D}$ (g/m$^3$) | $C_{Av.M}$ (g/m$^3$) | $C_{Av.D}$ (g/m$^3$) | $U_U$ (%) | $U_L$ (%) |
|---|---|---|---|---|---|---|---|---|---|---|---|---|---|---|
| 0.7 | 691 | 691 | 1634 | 172.1 | 172.1 | 447 | 447 | 1348 | 184.0 | 184.0 | 178.0 | 178.0 | 0.00 | 0.00 |
| 0.7 | 589 | 565 | 1419 | 175.9 | 184.2 | 463 | 444 | 1429 | 187.8 | 194.8 | 181.8 | 189.5 | 4.52 | 3.58 |
| 0.7 | 643 | 617 | 1566 | 178.0 | 186.3 | 496 | 476 | 1551 | 190.0 | 196.9 | 184.0 | 191.6 | 4.43 | 3.48 |
| 0.6 | 629 | 604 | 1310 | 146.7 | 154.8 | 495 | 475 | 1283 | 158.7 | 165.6 | 152.7 | 160.2 | 5.24 | 4.15 |
| 0.6 | 580 | 580 | 1267 | 156.3 | 156.3 | 536 | 536 | 1471 | 168.3 | 168.3 | 162.3 | 162.3 | 0.00 | 0.00 |
| 0.6 | 535 | 535 | 1114 | 146.7 | 146.7 | 408 | 408 | 1169 | 175.4 | 175.4 | 161.1 | 161.1 | 0.00 | 0.00 |
| 0.6 | 512 | 532 | 1103 | 153.5 | 145.8 | 380 | 395 | 1135 | 182.4 | 175.9 | 167.9 | 160.9 | 5.26 | 3.67 |
| 0.6 | 588 | 612 | 1219 | 145.8 | 137.8 | 511 | 531 | 1456 | 174.5 | 168.1 | 160.2 | 153.0 | 5.81 | 3.81 |
| 0.6 | 514 | 535 | 1113 | 154.5 | 146.5 | 494 | 514 | 1485 | 183.4 | 176.8 | 169.0 | 161.7 | 5.47 | 3.74 |
| 0.6 | 544 | 566 | 1189 | 156.4 | 148.5 | 422 | 439 | 1282 | 185.2 | 178.6 | 170.8 | 163.5 | 5.34 | 3.69 |
| 0.6 | 592 | 592 | 1161 | 134.7 | 134.7 | 515 | 515 | 1372 | 163.3 | 163.3 | 149.0 | 149.0 | 0.00 | 0.00 |
| 0.6 | 499 | 499 | 1013 | 141.6 | 141.6 | 513 | 513 | 1345 | 160.6 | 160.6 | 151.1 | 151.1 | 0.00 | 0.00 |
| 0.6 | 538 | 516 | 1052 | 134.1 | 142.5 | 550 | 529 | 1427 | 158.9 | 165.4 | 146.5 | 153.9 | 5.86 | 3.92 |
| 0.5 | 696 | 678 | 1096 | 90.8 | 96.1 | 680 | 653 | 1363 | 115.9 | 122.6 | 103.4 | 109.3 | 5.46 | 5.51 |
| 0.5 | 718 | 701 | 1226 | 107.0 | 111.8 | 710 | 682 | 1569 | 132.2 | 138.9 | 119.6 | 125.3 | 4.29 | 4.83 |
| 0.5 | 907 | 882 | 1467 | 96.2 | 101.8 | 683 | 656 | 1414 | 121.3 | 128.0 | 108.7 | 114.9 | 5.49 | 5.25 |
| 0.5 | 778 | 778 | 1247 | 94.4 | 94.4 | 772 | 772 | 1559 | 117.1 | 117.1 | 105.7 | 105.7 | 0.00 | 0.00 |
| 0.5 | 929 | 929 | 1776 | 129.6 | 129.6 | 704 | 704 | 1475 | 123.3 | 123.3 | 126.4 | 126.4 | 0.00 | 0.00 |
| 0.5 | 916 | 938 | 1783 | 133.2 | 128.5 | 754 | 777 | 1614 | 126.8 | 121.8 | 130.0 | 125.1 | 3.70 | 4.11 |
| 0.5 | 908 | 927 | 1728 | 128.7 | 124.6 | 826 | 850 | 1723 | 122.5 | 117.8 | 125.6 | 121.2 | 3.33 | 4.05 |
| 0.5 | 919 | 933 | 1703 | 123.4 | 120.3 | 901 | 928 | 1821 | 117.3 | 112.4 | 120.3 | 116.3 | 2.51 | 4.38 |
| 0.5 | 938 | 963 | 1715 | 120.7 | 115.4 | 809 | 831 | 1608 | 114.5 | 110.0 | 117.6 | 112.7 | 4.56 | 4.06 |
| 0.5 | 932 | 932 | 1542 | 100.7 | 100.7 | 814 | 814 | 1694 | 122.1 | 122.1 | 111.4 | 111.4 | 0.00 | 0.00 |
| 0.4 | 1178 | 1178 | 1570 | 57.5 | 57.5 | 1100 | 1100 | 1797 | 81.8 | 81.8 | 69.6 | 69.6 | 0.00 | 0.00 |
| 0.4 | 1153 | 1138 | 1572 | 62.0 | 64.6 | 930 | 912 | 1561 | 86.3 | 89.6 | 74.2 | 77.1 | 4.05 | 3.64 |
| 0.4 | 1121 | 1107 | 1519 | 60.8 | 63.3 | 1033 | 1019 | 1723 | 85.3 | 87.5 | 73.0 | 75.4 | 3.97 | 2.60 |

| $m_d$ (g) | $I_{U,M}$ (mV) | $I_{U,D}$ (mV) | $I_{o,U}$ (mV) | $C_{U,M}$ (g/m$^3$) | $C_{U,D}$ (g/m$^3$) | $I_{L,M}$ (mV) | $I_{L,D}$ (mV) | $I_{o,U}$ (mV) | $C_{L,M}$ (g/m$^3$) | $C_{L,D}$ (g/m$^3$) | $C_{Av.M}$ (g/m$^3$) | $C_{Av.D}$ (g/m$^3$) | $U_U$ (%) | $U_L$ (%) |
|---|---|---|---|---|---|---|---|---|---|---|---|---|---|---|
| 0.4 | 1201 | 1188 | 1642 | 62.6 | 64.7 | 855 | 838 | 1441 | 87.0 | 90.3 | 74.8 | 77.5 | 3.36 | 3.70 |
| 0.4 | 1116 | 1116 | 1696 | 83.7 | 83.7 | 934 | 934 | 1502 | 79.2 | 79.2 | 81.4 | 81.4 | 0.00 | 0.00 |
| 0.4 | 1201 | 1201 | 1613 | 59.0 | 59.0 | 847 | 847 | 1397 | 83.4 | 83.4 | 71.2 | 71.2 | 0.00 | 0.00 |
| 0.4 | 1224 | 1243 | 1645 | 59.1 | 56.0 | 722 | 736 | 1179 | 81.7 | 78.5 | 70.4 | 67.3 | 5.50 | 4.08 |
| 0.4 | 1149 | 1166 | 1564 | 61.7 | 58.7 | 730 | 741 | 1210 | 84.2 | 81.7 | 72.9 | 70.2 | 5.00 | 3.05 |
| 0.4 | 1071 | 1089 | 1678 | 89.8 | 86.5 | 715 | 730 | 1179 | 83.4 | 79.9 | 86.6 | 83.2 | 3.86 | 4.33 |
| 0.4 | 1248 | 1248 | 1627 | 53.0 | 53.0 | 975 | 975 | 1537 | 75.9 | 75.9 | 64.4 | 64.4 | 0.00 | 0.00 |
| 0.3 | 1186 | 1186 | 1688 | 70.6 | 70.6 | 964 | 964 | 1423 | 64.9 | 64.9 | 67.7 | 67.7 | 0.00 | 0.00 |
| 0.3 | 1278 | 1267 | 1534 | 36.5 | 38.2 | 1056 | 1039 | 1474 | 55.6 | 58.3 | 46.0 | 48.3 | 4.52 | 4.64 |
| 0.3 | 1379 | 1368 | 1619 | 32.1 | 33.7 | 1076 | 1067 | 1467 | 51.7 | 53.1 | 41.9 | 43.4 | 4.75 | 2.64 |
| 0.3 | 1373 | 1361 | 1633 | 34.7 | 36.4 | 1211 | 1203 | 1674 | 54.0 | 55.1 | 44.3 | 45.8 | 4.82 | 2.01 |
| 0.3 | 1234 | 1234 | 1730 | 67.6 | 67.6 | 1160 | 1160 | 1697 | 63.4 | 63.4 | 65.5 | 65.5 | 0.00 | 0.00 |
| 0.3 | 1220 | 1220 | 1503 | 41.7 | 41.7 | 1237 | 1237 | 1777 | 60.4 | 60.4 | 51.0 | 51.0 | 0.00 | 0.00 |
| 0.3 | 1245 | 1257 | 1615 | 52.0 | 50.1 | 1128 | 1140 | 1607 | 59.0 | 57.2 | 55.5 | 53.7 | 3.83 | 3.08 |
| 0.3 | 1167 | 1181 | 1461 | 44.9 | 42.6 | 1190 | 1204 | 1784 | 67.5 | 65.5 | 56.2 | 54.0 | 5.61 | 2.97 |
| 0.3 | 1234 | 1248 | 1622 | 54.7 | 52.4 | 1323 | 1341 | 1705 | 42.3 | 40.0 | 48.5 | 46.2 | 4.30 | 5.63 |
| 0.3 | 1230 | 1246 | 1550 | 46.2 | 43.7 | 1254 | 1271 | 1733 | 53.9 | 51.7 | 50.1 | 47.7 | 5.92 | 4.34 |
| 0.2 | 1445 | 1438 | 1575 | 17.2 | 18.2 | 1230 | 1217 | 1590 | 42.8 | 44.6 | 30.0 | 31.4 | 5.34 | 3.97 |
| 0.2 | 1343 | 1338 | 1445 | 14.6 | 15.4 | 1321 | 1309 | 1682 | 40.3 | 41.8 | 27.5 | 28.6 | 4.85 | 3.64 |
| 0.2 | 1289 | 1303 | 1630 | 46.9 | 44.8 | 1366 | 1379 | 1775 | 43.7 | 42.1 | 45.3 | 43.4 | 4.82 | 3.75 |
| 0.2 | 1234 | 1226 | 1490 | 37.7 | 39.0 | 1277 | 1265 | 1619 | 39.5 | 41.1 | 38.6 | 40.1 | 3.34 | 3.83 |
| 0.2 | 1456 | 1456 | 1640 | 23.8 | 23.8 | 1250 | 1250 | 1608 | 42.0 | 42.0 | 32.9 | 32.9 | 0.00 | 0.00 |
| 0.2 | 1359 | 1359 | 1711 | 46.1 | 46.1 | 1310 | 1310 | 1694 | 42.8 | 42.8 | 44.5 | 44.5 | 0.00 | 0.00 |
| 0.2 | 1413 | 1421 | 1684 | 35.1 | 34.0 | 1486 | 1501 | 1797 | 31.7 | 30.0 | 33.4 | 32.0 | 3.32 | 5.58 |
| 0.2 | 1423 | 1435 | 1686 | 33.9 | 32.2 | 1599 | 1605 | 1955 | 33.5 | 32.9 | 33.7 | 32.6 | 5.21 | 1.90 |
| 0.2 | 1499 | 1511 | 1756 | 31.6 | 30.1 | 1285 | 1300 | 1605 | 37.1 | 35.1 | 34.4 | 32.6 | 5.31 | 5.51 |

### B.1.3 Dust concentration reliability data at flow velocity of 7.1 cm/s

| $m_d$ (g) | $I_{U,M}$ (mV) | $I_{U,D}$ (mV) | $I_{o,U}$ (mV) | $C_{U,M}$ (g/m$^3$) | $C_{U,D}$ (g/m$^3$) | $I_{L,M}$ (mV) | $I_{L,D}$ (mV) | $I_{o,U}$ (mV) | $C_{L,M}$ (g/m$^3$) | $C_{L,D}$ (g/m$^3$) | $C_{Av.M}$ (g/m$^3$) | $C_{Av.D}$ (g/m$^3$) | $U_U$ (%) | $U_L$ (%) |
|---|---|---|---|---|---|---|---|---|---|---|---|---|---|---|
| 1.5 | 197 | 218 | 1600 | 418.9 | 398.7 | 145 | 157 | 1701 | 410.4 | 397.1 | 414.6 | 397.9 | 5.08 | 3.34 |
| 1.5 | 148 | 161 | 1305 | 435.3 | 418.5 | 110 | 121 | 1428 | 427.3 | 411.4 | 431.3 | 414.9 | 4.02 | 3.86 |
| 1.5 | 146 | 152 | 1000 | 384.8 | 376.8 | 113 | 118 | 1511 | 432.2 | 425.0 | 408.5 | 400.9 | 2.14 | 1.70 |
| 1.5 | 156 | 145 | 1025 | 376.5 | 391.1 | 125 | 125 | 1597 | 424.6 | 424.6 | 400.6 | 407.9 | 3.74 | 0.00 |
| 1.5 | 149 | 149 | 1037 | 388.0 | 388.0 | 110 | 110 | 1514 | 437.0 | 437.0 | 412.5 | 412.5 | 0.00 | 0.00 |
| 1.5 | 197 | 197 | 1638 | 423.6 | 423.6 | 95 | 95 | 1084 | 405.8 | 405.8 | 414.7 | 414.7 | 0.00 | 0.00 |
| 1.5 | 150 | 144 | 1300 | 431.9 | 440.1 | 118 | 113 | 1514 | 425.3 | 432.5 | 428.6 | 436.3 | 1.86 | 1.67 |
| 1.5 | 145 | 138 | 1000 | 386.2 | 396.1 | 85 | 76 | 1141 | 432.8 | 451.5 | 409.5 | 423.8 | 2.50 | 4.13 |
| 1.5 | 172 | 165 | 1534 | 437.6 | 445.9 | 136 | 131 | 1802 | 430.7 | 436.9 | 434.1 | 441.4 | 1.86 | 1.43 |
| 1.5 | 157 | 144 | 1278 | 419.4 | 436.6 | 115 | 103 | 1430 | 420.1 | 438.5 | 419.7 | 437.5 | 3.96 | 4.19 |
| 1.4 | 217 | 226 | 1720 | 414.0 | 405.9 | 95 | 99 | 1100 | 408.2 | 401.3 | 411.1 | 403.6 | 2.00 | 1.71 |
| 1.4 | 200 | 210 | 1389 | 387.6 | 377.8 | 149 | 163 | 1793 | 414.6 | 399.6 | 401.1 | 388.7 | 2.58 | 3.75 |
| 1.4 | 189 | 197 | 1487 | 412.6 | 404.3 | 135 | 140 | 1639 | 416.1 | 410.0 | 414.3 | 407.1 | 2.05 | 1.48 |
| 1.4 | 145 | 151 | 1167 | 417.1 | 409.0 | 160 | 166 | 1804 | 403.8 | 397.6 | 410.4 | 403.3 | 1.98 | 1.54 |
| 1.4 | 205 | 205 | 1562 | 406.1 | 406.1 | 157 | 157 | 1844 | 410.6 | 410.6 | 408.4 | 408.4 | 0.00 | 0.00 |
| 1.4 | 203 | 203 | 1378 | 383.0 | 383.0 | 156 | 156 | 1894 | 416.1 | 416.1 | 399.6 | 399.6 | 0.00 | 0.00 |
| 1.4 | 178 | 159 | 1220 | 385.0 | 407.5 | 146 | 135 | 1794 | 418.1 | 431.2 | 401.5 | 419.3 | 5.54 | 3.03 |
| 1.4 | 223 | 214 | 1546 | 387.3 | 395.5 | 159 | 153 | 1757 | 400.4 | 406.8 | 393.8 | 401.2 | 2.08 | 1.58 |
| 1.4 | 184 | 172 | 1298 | 390.7 | 404.2 | 101 | 89 | 1128 | 402.2 | 423.3 | 396.5 | 413.7 | 3.34 | 4.98 |
| 1.4 | 200 | 192 | 1374 | 385.4 | 393.6 | 105 | 101 | 1141 | 397.6 | 404.1 | 391.5 | 398.8 | 2.07 | 1.60 |
| 1.3 | 248 | 227 | 1452 | 353.5 | 371.1 | 198 | 187 | 1802 | 368.1 | 377.6 | 360.8 | 374.4 | 4.77 | 2.52 |
| 1.3 | 229 | 220 | 1376 | 358.6 | 366.7 | 152 | 146 | 1430 | 373.6 | 380.3 | 366.1 | 373.5 | 2.19 | 1.76 |
| 1.3 | 162 | 162 | 985 | 361.0 | 361.0 | 118 | 118 | 1128 | 376.3 | 376.3 | 368.6 | 368.6 | 0.00 | 0.00 |
| 1.3 | 224 | 208 | 1376 | 363.1 | 377.9 | 118 | 107 | 1141 | 378.2 | 394.5 | 370.6 | 386.2 | 3.92 | 4.13 |

| $m_d$ (g) | $I_{U,M}$ (mV) | $I_{U,D}$ (mV) | $I_{o,U}$ (mV) | $C_{U,M}$ (g/m$^3$) | $C_{U,D}$ (g/m$^3$) | $I_{L,M}$ (mV) | $I_{L,D}$ (mV) | $I_{o,U}$ (mV) | $C_{L,M}$ (g/m$^3$) | $C_{L,D}$ (g/m$^3$) | $C_{Av.M}$ (g/m$^3$) | $C_{Av.D}$ (g/m$^3$) | $U_U$ (%) | $U_L$ (%) |
|---|---|---|---|---|---|---|---|---|---|---|---|---|---|---|
| 1.3 | 234 | 234 | 1476 | 368.4 | 368.4 | 182 | 182 | 1802 | 382.1 | 382.1 | 375.2 | 375.2 | 0.00 | 0.00 |
| 1.3 | 232 | 246 | 1376 | 356.0 | 344.3 | 146 | 167 | 1430 | 380.3 | 357.9 | 368.2 | 351.1 | 3.40 | 6.26 |
| 1.3 | 162 | 177 | 985 | 361.0 | 343.3 | 169 | 186 | 1708 | 385.5 | 369.6 | 373.3 | 356.4 | 5.16 | 4.32 |
| 1.3 | 224 | 233 | 1376 | 363.1 | 355.2 | 184 | 191 | 1890 | 388.2 | 382.0 | 375.6 | 368.6 | 2.22 | 1.63 |
| 1.3 | 239 | 249 | 1476 | 364.1 | 355.9 | 174 | 181 | 1795 | 389.0 | 382.4 | 376.5 | 369.2 | 2.30 | 1.72 |
| 1.3 | 258 | 248 | 1845 | 393.5 | 401.4 | 186 | 179 | 1869 | 384.6 | 391.0 | 389.0 | 396.2 | 1.97 | 1.64 |
| 1.2 | 252 | 237 | 1389 | 341.4 | 353.7 | 205 | 189 | 1844 | 366.1 | 379.7 | 353.7 | 366.7 | 3.47 | 3.57 |
| 1.2 | 252 | 242 | 1300 | 328.1 | 336.2 | 203 | 195 | 1684 | 352.6 | 359.3 | 340.4 | 347.8 | 2.41 | 1.86 |
| 1.2 | 264 | 245 | 1278 | 315.4 | 330.4 | 211 | 203 | 1794 | 356.7 | 363.2 | 336.1 | 346.8 | 4.52 | 1.77 |
| 1.2 | 314 | 314 | 1567 | 321.5 | 321.5 | 199 | 199 | 1757 | 363.0 | 363.0 | 342.3 | 342.3 | 0.00 | 0.00 |
| 1.2 | 265 | 265 | 1356 | 326.5 | 326.5 | 190 | 190 | 1726 | 367.8 | 367.8 | 347.1 | 347.1 | 0.00 | 0.00 |
| 1.2 | 261 | 261 | 1600 | 362.6 | 362.6 | 124 | 124 | 972 | 343.2 | 343.2 | 352.9 | 352.9 | 0.00 | 0.00 |
| 1.2 | 255 | 260 | 1305 | 326.5 | 322.7 | 169 | 200 | 1406 | 353.1 | 325.0 | 339.8 | 323.8 | 1.20 | 8.64 |
| 1.2 | 197 | 205 | 1000 | 324.9 | 316.9 | 131 | 136 | 1084 | 352.2 | 346.0 | 338.6 | 331.5 | 2.51 | 1.80 |
| 1.2 | 199 | 207 | 1025 | 327.8 | 319.9 | 180 | 187 | 1514 | 354.9 | 348.6 | 341.4 | 334.3 | 2.46 | 1.82 |
| 1.2 | 194 | 202 | 1037 | 335.2 | 327.2 | 186 | 193 | 1624 | 361.2 | 355.0 | 348.2 | 341.1 | 2.47 | 1.73 |
| 1.1 | 394 | 383 | 1638 | 285.0 | 290.6 | 213 | 195 | 1373 | 310.6 | 325.3 | 297.8 | 308.0 | 1.95 | 4.52 |
| 1.1 | 306 | 288 | 1300 | 289.3 | 301.4 | 258 | 248 | 1707 | 314.9 | 321.5 | 302.1 | 311.5 | 4.02 | 2.05 |
| 1.1 | 230 | 221 | 1000 | 293.9 | 301.9 | 204 | 196 | 1308 | 309.7 | 316.4 | 301.8 | 309.1 | 2.64 | 2.11 |
| 1.1 | 351 | 331 | 1534 | 295.0 | 306.7 | 235 | 220 | 1511 | 310.2 | 321.1 | 302.6 | 313.9 | 3.83 | 3.42 |
| 1.1 | 298 | 286 | 1278 | 291.2 | 299.4 | 254 | 244 | 1597 | 306.4 | 313.1 | 298.8 | 306.3 | 2.75 | 2.14 |
| 1.1 | 230 | 230 | 985 | 290.9 | 290.9 | 248 | 248 | 1551 | 305.5 | 305.5 | 298.2 | 298.2 | 0.00 | 0.00 |
| 1.1 | 328 | 315 | 1376 | 286.8 | 294.9 | 210 | 195 | 1283 | 301.6 | 314.0 | 294.2 | 304.4 | 2.74 | 3.93 |
| 1.1 | 360 | 360 | 1476 | 282.2 | 282.2 | 247 | 247 | 1471 | 297.4 | 297.4 | 289.8 | 289.8 | 0.00 | 0.00 |
| 1.1 | 317 | 333 | 1300 | 282.2 | 272.4 | 197 | 211 | 1169 | 296.8 | 285.3 | 289.5 | 278.9 | 3.62 | 4.01 |
| 1.1 | 237 | 246 | 1000 | 287.9 | 280.5 | 185 | 192 | 1135 | 302.3 | 296.1 | 295.1 | 288.3 | 2.66 | 2.09 |

| $m_d$ (g) | $I_{U,M}$ (mV) | $I_{U,D}$ (mV) | $I_{o,U}$ (mV) | $C_{U,M}$ (g/m$^3$) | $C_{U,D}$ (g/m$^3$) | $I_{L,M}$ (mV) | $I_{L,D}$ (mV) | $I_{o,U}$ (mV) | $C_{L,M}$ (g/m$^3$) | $C_{L,D}$ (g/m$^3$) | $C_{Av.M}$ (g/m$^3$) | $C_{Av.D}$ (g/m$^3$) | $U_U$ (%) | $U_L$ (%) |
|---|---|---|---|---|---|---|---|---|---|---|---|---|---|---|
| 1 | 381 | 396 | 1534 | 278.6 | 270.8 | 276 | 287 | 1406 | 271.4 | 264.8 | 275.0 | 267.8 | 2.85 | 2.46 |
| 1 | 329 | 329 | 1278 | 271.4 | 271.4 | 372 | 372 | 1892 | 271.1 | 271.1 | 271.2 | 271.2 | 0.00 | 0.00 |
| 1 | 452 | 452 | 1720 | 267.3 | 267.3 | 180 | 180 | 894 | 267.1 | 267.1 | 267.2 | 267.2 | 0.00 | 0.00 |
| 1 | 353 | 353 | 1389 | 274.0 | 274.0 | 172 | 172 | 889 | 273.8 | 273.8 | 273.9 | 273.9 | 0.00 | 0.00 |
| 1 | 367 | 352 | 1487 | 279.8 | 288.2 | 171 | 164 | 919 | 280.3 | 287.2 | 280.1 | 287.7 | 2.90 | 2.43 |
| 1 | 328 | 315 | 1248 | 267.3 | 275.3 | 264 | 256 | 1315 | 267.6 | 272.7 | 267.4 | 274.0 | 2.94 | 1.88 |
| 1 | 452 | 434 | 1745 | 270.2 | 278.3 | 281 | 270 | 1414 | 269.3 | 276.0 | 269.7 | 277.1 | 2.92 | 2.41 |
| 1 | 298 | 286 | 1189 | 276.8 | 285.0 | 298 | 286 | 1559 | 275.8 | 282.6 | 276.3 | 283.8 | 2.88 | 2.42 |
| 1 | 349 | 337 | 1374 | 274.1 | 281.1 | 287 | 266 | 1475 | 272.8 | 285.5 | 273.5 | 283.3 | 2.49 | 4.44 |
| 1 | 367 | 367 | 1452 | 275.1 | 275.1 | 312 | 312 | 1614 | 273.9 | 273.9 | 274.5 | 274.5 | 0.00 | 0.00 |
| 0.9 | 412 | 412 | 1376 | 241.2 | 241.2 | 277 | 277 | 1167 | 239.7 | 239.7 | 240.4 | 240.4 | 0.00 | 0.00 |
| 0.9 | 334 | 334 | 985 | 216.3 | 216.3 | 288 | 288 | 1199 | 237.7 | 237.7 | 227.0 | 227.0 | 0.00 | 0.00 |
| 0.9 | 407 | 423 | 1376 | 243.6 | 235.9 | 259 | 275 | 1111 | 242.7 | 232.7 | 243.2 | 234.3 | 3.27 | 4.29 |
| 0.9 | 428 | 445 | 1476 | 247.6 | 239.8 | 292 | 304 | 1282 | 246.6 | 239.9 | 247.1 | 239.8 | 3.25 | 2.80 |
| 0.9 | 518 | 539 | 1845 | 254.1 | 246.1 | 300 | 312 | 1372 | 253.4 | 246.8 | 253.7 | 246.5 | 3.23 | 2.65 |
| 0.9 | 393 | 393 | 1389 | 252.5 | 252.5 | 299 | 299 | 1345 | 250.6 | 250.6 | 251.6 | 251.6 | 0.00 | 0.00 |
| 0.9 | 377 | 377 | 1300 | 247.6 | 247.6 | 326 | 326 | 1427 | 246.1 | 246.1 | 246.8 | 246.8 | 0.00 | 0.00 |
| 0.9 | 364 | 349 | 1278 | 251.2 | 259.6 | 304 | 292 | 1363 | 250.1 | 256.8 | 250.6 | 258.2 | 3.24 | 2.61 |
| 0.9 | 450 | 429 | 1567 | 249.5 | 259.1 | 354 | 337 | 1569 | 248.1 | 256.4 | 248.8 | 257.7 | 3.69 | 3.20 |
| 0.9 | 391 | 375 | 1356 | 248.7 | 257.1 | 278 | 267 | 1225 | 247.2 | 253.9 | 247.9 | 255.5 | 3.25 | 2.65 |
| 0.8 | 556 | 534 | 1720 | 225.9 | 233.9 | 316 | 303 | 1213 | 224.2 | 231.2 | 225.0 | 232.6 | 3.45 | 3.03 |
| 0.8 | 463 | 480 | 1389 | 219.7 | 212.5 | 357 | 371 | 1341 | 220.6 | 214.2 | 220.1 | 213.3 | 3.39 | 2.99 |
| 0.8 | 501 | 521 | 1487 | 217.6 | 209.8 | 337 | 350 | 1224 | 215.0 | 208.7 | 216.3 | 209.2 | 3.73 | 3.02 |
| 0.8 | 417 | 434 | 1248 | 219.2 | 211.3 | 510 | 530 | 1873 | 216.8 | 210.4 | 218.0 | 210.8 | 3.78 | 3.05 |
| 0.8 | 594 | 634 | 1745 | 215.5 | 202.5 | 467 | 486 | 1677 | 213.1 | 206.4 | 214.3 | 204.5 | 6.44 | 3.22 |
| 0.8 | 391 | 391 | 1189 | 222.4 | 222.4 | 454 | 454 | 1696 | 219.7 | 219.7 | 221.0 | 221.0 | 0.00 | 0.00 |

| $m_d$ (g) | $I_{U,M}$ (mV) | $I_{U,D}$ (mV) | $I_{o,U}$ (mV) | $C_{U,M}$ (g/m$^3$) | $C_{U,D}$ (g/m$^3$) | $I_{L,M}$ (mV) | $I_{L,D}$ (mV) | $I_{o,U}$ (mV) | $C_{L,M}$ (g/m$^3$) | $C_{L,D}$ (g/m$^3$) | $C_{Av.M}$ (g/m$^3$) | $C_{Av.D}$ (g/m$^3$) | $U_U$ (%) | $U_L$ (%) |
|---|---|---|---|---|---|---|---|---|---|---|---|---|---|---|
| 0.8 | 457 | 457 | 1374 | 220.2 | 220.2 | 468 | 468 | 1727 | 217.6 | 217.6 | 218.9 | 218.9 | 0.00 | 0.00 |
| 0.8 | 516 | 516 | 1452 | 206.9 | 206.9 | 490 | 490 | 1729 | 210.1 | 210.1 | 208.5 | 208.5 | 0.00 | 0.00 |
| 0.8 | 465 | 446 | 1376 | 217.0 | 225.3 | 445 | 427 | 1671 | 220.5 | 227.4 | 218.7 | 226.4 | 3.70 | 3.03 |
| 0.8 | 473 | 454 | 1389 | 215.4 | 223.6 | 369 | 354 | 1406 | 223.0 | 229.9 | 219.2 | 226.8 | 3.67 | 3.01 |
| 0.7 | 542 | 520 | 1300 | 175.0 | 183.3 | 521 | 500 | 1724 | 199.4 | 206.3 | 187.2 | 194.8 | 4.52 | 3.32 |
| 0.7 | 535 | 509 | 1278 | 174.2 | 184.1 | 441 | 423 | 1452 | 198.6 | 205.6 | 186.4 | 194.8 | 5.41 | 3.38 |
| 0.7 | 628 | 628 | 1567 | 182.9 | 182.9 | 452 | 452 | 1480 | 197.7 | 197.7 | 190.3 | 190.3 | 0.00 | 0.00 |
| 0.7 | 519 | 540 | 1320 | 186.7 | 178.8 | 356 | 370 | 1195 | 201.8 | 195.4 | 194.3 | 187.1 | 4.44 | 3.29 |
| 0.7 | 526 | 547 | 1345 | 187.8 | 179.9 | 356 | 370 | 1202 | 202.8 | 196.4 | 195.3 | 188.2 | 4.35 | 3.27 |
| 0.7 | 451 | 466 | 1086 | 175.8 | 169.2 | 459 | 472 | 1443 | 190.9 | 186.3 | 183.3 | 177.7 | 3.87 | 2.50 |
| 0.7 | 456 | 456 | 1093 | 174.8 | 174.8 | 444 | 444 | 1363 | 186.9 | 186.9 | 180.9 | 180.9 | 0.00 | 0.00 |
| 0.7 | 691 | 691 | 1634 | 172.1 | 172.1 | 447 | 447 | 1348 | 184.0 | 184.0 | 178.0 | 178.0 | 0.00 | 0.00 |
| 0.7 | 589 | 565 | 1419 | 175.9 | 184.2 | 463 | 444 | 1429 | 187.8 | 194.8 | 181.8 | 189.5 | 4.52 | 3.58 |
| 0.7 | 643 | 617 | 1566 | 178.0 | 186.3 | 496 | 476 | 1551 | 190.0 | 196.9 | 184.0 | 191.6 | 4.43 | 3.48 |
| 0.6 | 629 | 604 | 1310 | 146.7 | 154.8 | 495 | 475 | 1283 | 158.7 | 165.6 | 152.7 | 160.2 | 5.24 | 4.15 |
| 0.6 | 580 | 580 | 1267 | 156.3 | 156.3 | 536 | 536 | 1471 | 168.3 | 168.3 | 162.3 | 162.3 | 0.00 | 0.00 |
| 0.6 | 535 | 535 | 1114 | 146.7 | 146.7 | 408 | 408 | 1169 | 175.4 | 175.4 | 161.1 | 161.1 | 0.00 | 0.00 |
| 0.6 | 512 | 532 | 1103 | 153.5 | 145.8 | 380 | 395 | 1135 | 182.4 | 175.9 | 167.9 | 160.9 | 5.26 | 3.67 |
| 0.6 | 588 | 612 | 1219 | 145.8 | 137.8 | 511 | 531 | 1456 | 174.5 | 168.1 | 160.2 | 153.0 | 5.81 | 3.81 |
| 0.6 | 514 | 535 | 1113 | 154.5 | 146.5 | 494 | 514 | 1485 | 183.4 | 176.8 | 169.0 | 161.7 | 5.47 | 3.74 |
| 0.6 | 544 | 566 | 1189 | 156.4 | 148.5 | 422 | 439 | 1282 | 185.2 | 178.6 | 170.8 | 163.5 | 5.34 | 3.69 |
| 0.6 | 592 | 592 | 1161 | 134.7 | 134.7 | 515 | 515 | 1372 | 163.3 | 163.3 | 149.0 | 149.0 | 0.00 | 0.00 |
| 0.6 | 499 | 499 | 1013 | 141.6 | 141.6 | 513 | 513 | 1345 | 160.6 | 160.6 | 151.1 | 151.1 | 0.00 | 0.00 |
| 0.6 | 538 | 516 | 1052 | 134.1 | 142.5 | 550 | 529 | 1427 | 158.9 | 165.4 | 146.5 | 153.9 | 5.86 | 3.92 |
| 0.5 | 696 | 678 | 1096 | 90.8 | 96.1 | 680 | 653 | 1363 | 115.9 | 122.6 | 103.4 | 109.3 | 5.46 | 5.51 |
| 0.5 | 718 | 701 | 1226 | 107.0 | 111.8 | 710 | 682 | 1569 | 132.2 | 138.9 | 119.6 | 125.3 | 4.29 | 4.83 |

| $m_d$ (g) | $I_{U,M}$ (mV) | $I_{U,D}$ (mV) | $I_{o,U}$ (mV) | $C_{U,M}$ (g/m$^3$) | $C_{U,D}$ (g/m$^3$) | $I_{L,M}$ (mV) | $I_{L,D}$ (mV) | $I_{o,U}$ (mV) | $C_{L,M}$ (g/m$^3$) | $C_{L,D}$ (g/m$^3$) | $C_{Av.M}$ (g/m$^3$) | $C_{Av.D}$ (g/m$^3$) | $U_U$ (%) | $U_L$ (%) |
|---|---|---|---|---|---|---|---|---|---|---|---|---|---|---|
| 0.5 | 907 | 882 | 1467 | 96.2 | 101.8 | 683 | 656 | 1414 | 121.3 | 128.0 | 108.7 | 114.9 | 5.49 | 5.25 |
| 0.5 | 778 | 778 | 1247 | 94.4 | 94.4 | 772 | 772 | 1559 | 117.1 | 117.1 | 105.7 | 105.7 | 0.00 | 0.00 |
| 0.5 | 929 | 929 | 1776 | 129.6 | 129.6 | 704 | 704 | 1475 | 123.3 | 123.3 | 126.4 | 126.4 | 0.00 | 0.00 |
| 0.5 | 916 | 938 | 1783 | 133.2 | 128.5 | 754 | 777 | 1614 | 126.8 | 121.8 | 130.0 | 125.1 | 3.70 | 4.11 |
| 0.5 | 908 | 927 | 1728 | 128.7 | 124.6 | 826 | 850 | 1723 | 122.5 | 117.8 | 125.6 | 121.2 | 3.33 | 4.05 |
| 0.5 | 919 | 933 | 1703 | 123.4 | 120.3 | 901 | 928 | 1821 | 117.3 | 112.4 | 120.3 | 116.3 | 2.51 | 4.38 |
| 0.5 | 938 | 963 | 1715 | 120.7 | 115.4 | 809 | 831 | 1608 | 114.5 | 110.0 | 117.6 | 112.7 | 4.56 | 4.06 |
| 0.5 | 932 | 932 | 1542 | 100.7 | 100.7 | 814 | 814 | 1694 | 122.1 | 122.1 | 111.4 | 111.4 | 0.00 | 0.00 |
| 0.4 | 1178 | 1178 | 1570 | 57.5 | 57.5 | 1100 | 1100 | 1797 | 81.8 | 81.8 | 69.6 | 69.6 | 0.00 | 0.00 |
| 0.4 | 1153 | 1138 | 1572 | 62.0 | 64.6 | 930 | 912 | 1561 | 86.3 | 89.6 | 74.2 | 77.1 | 4.05 | 3.64 |
| 0.4 | 1121 | 1107 | 1519 | 60.8 | 63.3 | 1033 | 1019 | 1723 | 85.3 | 87.5 | 73.0 | 75.4 | 3.97 | 2.60 |
| 0.4 | 1201 | 1188 | 1642 | 62.6 | 64.7 | 855 | 838 | 1441 | 87.0 | 90.3 | 74.8 | 77.5 | 3.36 | 3.70 |
| 0.4 | 1116 | 1116 | 1696 | 83.7 | 83.7 | 934 | 934 | 1502 | 79.2 | 79.2 | 81.4 | 81.4 | 0.00 | 0.00 |
| 0.4 | 1201 | 1201 | 1613 | 59.0 | 59.0 | 847 | 847 | 1397 | 83.4 | 83.4 | 71.2 | 71.2 | 0.00 | 0.00 |
| 0.4 | 1224 | 1243 | 1645 | 59.1 | 56.0 | 722 | 736 | 1179 | 81.7 | 78.5 | 70.4 | 67.3 | 5.50 | 4.08 |
| 0.4 | 1149 | 1166 | 1564 | 61.7 | 58.7 | 730 | 741 | 1210 | 84.2 | 81.7 | 72.9 | 70.2 | 5.00 | 3.05 |
| 0.4 | 1071 | 1089 | 1678 | 89.8 | 86.5 | 715 | 730 | 1179 | 83.4 | 79.9 | 86.6 | 83.2 | 3.86 | 4.33 |
| 0.4 | 1248 | 1248 | 1627 | 53.0 | 53.0 | 975 | 975 | 1537 | 75.9 | 75.9 | 64.4 | 64.4 | 0.00 | 0.00 |
| 0.3 | 1186 | 1186 | 1688 | 70.6 | 70.6 | 964 | 964 | 1423 | 64.9 | 64.9 | 67.7 | 67.7 | 0.00 | 0.00 |
| 0.3 | 1278 | 1267 | 1534 | 36.5 | 38.2 | 1056 | 1039 | 1474 | 55.6 | 58.3 | 46.0 | 48.3 | 4.52 | 4.64 |
| 0.3 | 1379 | 1368 | 1619 | 32.1 | 33.7 | 1076 | 1067 | 1467 | 51.7 | 53.1 | 41.9 | 43.4 | 4.75 | 2.64 |
| 0.3 | 1373 | 1361 | 1633 | 34.7 | 36.4 | 1211 | 1203 | 1674 | 54.0 | 55.1 | 44.3 | 45.8 | 4.82 | 2.01 |
| 0.3 | 1234 | 1234 | 1730 | 67.6 | 67.6 | 1160 | 1160 | 1697 | 63.4 | 63.4 | 65.5 | 65.5 | 0.00 | 0.00 |
| 0.3 | 1220 | 1220 | 1503 | 41.7 | 41.7 | 1237 | 1237 | 1777 | 60.4 | 60.4 | 51.0 | 51.0 | 0.00 | 0.00 |
| 0.3 | 1245 | 1257 | 1615 | 52.0 | 50.1 | 1128 | 1140 | 1607 | 59.0 | 57.2 | 55.5 | 53.7 | 3.83 | 3.08 |
| 0.3 | 1167 | 1181 | 1461 | 44.9 | 42.6 | 1190 | 1204 | 1784 | 67.5 | 65.5 | 56.2 | 54.0 | 5.61 | 2.97 |

| $m_d$ (g) | $I_{U,M}$ (mV) | $I_{U,D}$ (mV) | $I_{o,U}$ (mV) | $C_{U,M}$ (g/m$^3$) | $C_{U,D}$ (g/m$^3$) | $I_{L,M}$ (mV) | $I_{L,D}$ (mV) | $I_{o,U}$ (mV) | $C_{L,M}$ (g/m$^3$) | $C_{L,D}$ (g/m$^3$) | $C_{Av.M}$ (g/m$^3$) | $C_{Av.D}$ (g/m$^3$) | $U_U$ (%) | $U_L$ (%) |
|---|---|---|---|---|---|---|---|---|---|---|---|---|---|---|
| 0.3 | 1234 | 1248 | 1622 | 54.7 | 52.4 | 1323 | 1341 | 1705 | 42.3 | 40.0 | 48.5 | 46.2 | 4.30 | 5.63 |
| 0.3 | 1230 | 1246 | 1550 | 46.2 | 43.7 | 1254 | 1271 | 1733 | 53.9 | 51.7 | 50.1 | 47.7 | 5.92 | 4.34 |
| 0.2 | 1445 | 1438 | 1575 | 17.2 | 18.2 | 1230 | 1217 | 1590 | 42.8 | 44.6 | 30.0 | 31.4 | 5.34 | 3.97 |
| 0.2 | 1343 | 1338 | 1445 | 14.6 | 15.4 | 1321 | 1309 | 1682 | 40.3 | 41.8 | 27.5 | 28.6 | 4.85 | 3.64 |
| 0.2 | 1289 | 1303 | 1630 | 46.9 | 44.8 | 1366 | 1379 | 1775 | 43.7 | 42.1 | 45.3 | 43.4 | 4.82 | 3.75 |
| 0.2 | 1234 | 1226 | 1490 | 37.7 | 39.0 | 1277 | 1265 | 1619 | 39.5 | 41.1 | 38.6 | 40.1 | 3.34 | 3.83 |
| 0.2 | 1456 | 1456 | 1640 | 23.8 | 23.8 | 1250 | 1250 | 1608 | 42.0 | 42.0 | 32.9 | 32.9 | 0.00 | 0.00 |
| 0.2 | 1359 | 1359 | 1711 | 46.1 | 46.1 | 1310 | 1310 | 1694 | 42.8 | 42.8 | 44.5 | 44.5 | 0.00 | 0.00 |
| 0.2 | 1413 | 1421 | 1684 | 35.1 | 34.0 | 1486 | 1501 | 1797 | 31.7 | 30.0 | 33.4 | 32.0 | 3.32 | 5.58 |
| 0.2 | 1423 | 1435 | 1686 | 33.9 | 32.2 | 1599 | 1605 | 1955 | 33.5 | 32.9 | 33.7 | 32.6 | 5.21 | 1.90 |
| 0.2 | 1499 | 1511 | 1756 | 31.6 | 30.1 | 1285 | 1300 | 1605 | 37.1 | 35.1 | 34.4 | 32.6 | 5.31 | 5.51 |
| 0.2 | 1237 | 1237 | 1519 | 41.1 | 41.1 | 1326 | 1326 | 1663 | 37.7 | 37.7 | 39.4 | 39.4 | 0.00 | 0.00 |

### B.1.4 Dust concentration reliability data at flow velocity of 4.8 cm/s

| $m_d$ (g) | $I_{U,M}$ (mV) | $I_{U,D}$ (mV) | $I_{o,U}$ (mV) | $C_{U,M}$ (g/m$^3$) | $C_{U,D}$ (g/m$^3$) | $I_{L,M}$ (mV) | $I_{L,D}$ (mV) | $I_{o,U}$ (mV) | $C_{L,M}$ (g/m$^3$) | $C_{L,D}$ (g/m$^3$) | $C_{Av.M}$ (g/m$^3$) | $C_{Av.D}$ (g/m$^3$) | $U_U$ (%) | $U_L$ (%) |
|---|---|---|---|---|---|---|---|---|---|---|---|---|---|---|
| 1.5 | 197 | 218 | 1600 | 418.9 | 398.7 | 145 | 157 | 1701 | 410.4 | 397.1 | 414.6 | 397.9 | 5.08 | 3.34 |
| 1.5 | 148 | 161 | 1305 | 435.3 | 418.5 | 110 | 121 | 1428 | 427.3 | 411.4 | 431.3 | 414.9 | 4.02 | 3.86 |
| 1.5 | 146 | 152 | 1000 | 384.8 | 376.8 | 113 | 118 | 1511 | 432.2 | 425.0 | 408.5 | 400.9 | 2.14 | 1.70 |
| 1.5 | 156 | 145 | 1025 | 376.5 | 391.1 | 125 | 125 | 1597 | 424.6 | 424.6 | 400.6 | 407.9 | 3.74 | 0.00 |
| 1.5 | 149 | 149 | 1037 | 388.0 | 388.0 | 110 | 110 | 1514 | 437.0 | 437.0 | 412.5 | 412.5 | 0.00 | 0.00 |
| 1.5 | 197 | 197 | 1638 | 423.6 | 423.6 | 95 | 95 | 1084 | 405.8 | 405.8 | 414.7 | 414.7 | 0.00 | 0.00 |
| 1.5 | 150 | 144 | 1300 | 431.9 | 440.1 | 118 | 113 | 1514 | 425.3 | 432.5 | 428.6 | 436.3 | 1.86 | 1.67 |
| 1.5 | 145 | 138 | 1000 | 386.2 | 396.1 | 85 | 76 | 1141 | 432.8 | 451.5 | 409.5 | 423.8 | 2.50 | 4.13 |
| 1.5 | 172 | 165 | 1534 | 437.6 | 445.9 | 136 | 131 | 1802 | 430.7 | 436.9 | 434.1 | 441.4 | 1.86 | 1.43 |

| $m_d$ (g) | $I_{U,M}$ (mV) | $I_{U,D}$ (mV) | $I_{o,U}$ (mV) | $C_{U,M}$ (g/m$^3$) | $C_{U,D}$ (g/m$^3$) | $I_{L,M}$ (mV) | $I_{L,D}$ (mV) | $I_{o,U}$ (mV) | $C_{L,M}$ (g/m$^3$) | $C_{L,D}$ (g/m$^3$) | $C_{Av.M}$ (g/m$^3$) | $C_{Av.D}$ (g/m$^3$) | $U_U$ (%) | $U_L$ (%) |
|---|---|---|---|---|---|---|---|---|---|---|---|---|---|---|
| 1.5 | 157 | 144 | 1278 | 419.4 | 436.6 | 115 | 103 | 1430 | 420.1 | 438.5 | 419.7 | 437.5 | 3.96 | 4.19 |
| 1.4 | 217 | 226 | 1720 | 414.0 | 405.9 | 95 | 99 | 1100 | 408.2 | 401.3 | 411.1 | 403.6 | 2.00 | 1.71 |
| 1.4 | 200 | 210 | 1389 | 387.6 | 377.8 | 149 | 163 | 1793 | 414.6 | 399.6 | 401.1 | 388.7 | 2.58 | 3.75 |
| 1.4 | 189 | 197 | 1487 | 412.6 | 404.3 | 135 | 140 | 1639 | 416.1 | 410.0 | 414.3 | 407.1 | 2.05 | 1.48 |
| 1.4 | 145 | 151 | 1167 | 417.1 | 409.0 | 160 | 166 | 1804 | 403.8 | 397.6 | 410.4 | 403.3 | 1.98 | 1.54 |
| 1.4 | 205 | 205 | 1562 | 406.1 | 406.1 | 157 | 157 | 1844 | 410.6 | 410.6 | 408.4 | 408.4 | 0.00 | 0.00 |
| 1.4 | 203 | 203 | 1378 | 383.0 | 383.0 | 156 | 156 | 1894 | 416.1 | 416.1 | 399.6 | 399.6 | 0.00 | 0.00 |
| 1.4 | 178 | 159 | 1220 | 385.0 | 407.5 | 146 | 135 | 1794 | 418.1 | 431.2 | 401.5 | 419.3 | 5.54 | 3.03 |
| 1.4 | 223 | 214 | 1546 | 387.3 | 395.5 | 159 | 153 | 1757 | 400.4 | 406.8 | 393.8 | 401.2 | 2.08 | 1.58 |
| 1.4 | 184 | 172 | 1298 | 390.7 | 404.2 | 101 | 89 | 1128 | 402.2 | 423.3 | 396.5 | 413.7 | 3.34 | 4.98 |
| 1.4 | 200 | 192 | 1374 | 385.4 | 393.6 | 105 | 101 | 1141 | 397.6 | 404.1 | 391.5 | 398.8 | 2.07 | 1.60 |
| 1.3 | 248 | 227 | 1452 | 353.5 | 371.1 | 198 | 187 | 1802 | 368.1 | 377.6 | 360.8 | 374.4 | 4.77 | 2.52 |
| 1.3 | 229 | 220 | 1376 | 358.6 | 366.7 | 152 | 146 | 1430 | 373.6 | 380.3 | 366.1 | 373.5 | 2.19 | 1.76 |
| 1.3 | 162 | 162 | 985 | 361.0 | 361.0 | 118 | 118 | 1128 | 376.3 | 376.3 | 368.6 | 368.6 | 0.00 | 0.00 |
| 1.3 | 224 | 208 | 1376 | 363.1 | 377.9 | 118 | 107 | 1141 | 378.2 | 394.5 | 370.6 | 386.2 | 3.92 | 4.13 |
| 1.3 | 234 | 234 | 1476 | 368.4 | 368.4 | 182 | 182 | 1802 | 382.1 | 382.1 | 375.2 | 375.2 | 0.00 | 0.00 |
| 1.3 | 232 | 246 | 1376 | 356.0 | 344.3 | 146 | 167 | 1430 | 380.3 | 357.9 | 368.2 | 351.1 | 3.40 | 6.26 |
| 1.3 | 162 | 177 | 985 | 361.0 | 343.3 | 169 | 186 | 1708 | 385.5 | 369.6 | 373.3 | 356.4 | 5.16 | 4.32 |
| 1.3 | 224 | 233 | 1376 | 363.1 | 355.2 | 184 | 191 | 1890 | 388.2 | 382.0 | 375.6 | 368.6 | 2.22 | 1.63 |
| 1.3 | 239 | 249 | 1476 | 364.1 | 355.9 | 174 | 181 | 1795 | 389.0 | 382.4 | 376.5 | 369.2 | 2.30 | 1.72 |
| 1.3 | 258 | 248 | 1845 | 393.5 | 401.4 | 186 | 179 | 1869 | 384.6 | 391.0 | 389.0 | 396.2 | 1.97 | 1.64 |
| 1.2 | 252 | 237 | 1389 | 341.4 | 353.7 | 205 | 189 | 1844 | 366.1 | 379.7 | 353.7 | 366.7 | 3.47 | 3.57 |
| 1.2 | 252 | 242 | 1300 | 328.1 | 336.2 | 203 | 195 | 1684 | 352.6 | 359.3 | 340.4 | 347.8 | 2.41 | 1.86 |
| 1.2 | 264 | 245 | 1278 | 315.4 | 330.4 | 211 | 203 | 1794 | 356.7 | 363.2 | 336.1 | 346.8 | 4.52 | 1.77 |
| 1.2 | 314 | 314 | 1567 | 321.5 | 321.5 | 199 | 199 | 1757 | 363.0 | 363.0 | 342.3 | 342.3 | 0.00 | 0.00 |
| 1.2 | 265 | 265 | 1356 | 326.5 | 326.5 | 190 | 190 | 1726 | 367.8 | 367.8 | 347.1 | 347.1 | 0.00 | 0.00 |

| $m_d$ (g) | $I_{U,M}$ (mV) | $I_{U,D}$ (mV) | $I_{o,U}$ (mV) | $C_{U,M}$ (g/m$^3$) | $C_{U,D}$ (g/m$^3$) | $I_{L,M}$ (mV) | $I_{L,D}$ (mV) | $I_{o,U}$ (mV) | $C_{L,M}$ (g/m$^3$) | $C_{L,D}$ (g/m$^3$) | $C_{Av.M}$ (g/m$^3$) | $C_{Av.D}$ (g/m$^3$) | $U_U$ (%) | $U_L$ (%) |
|---|---|---|---|---|---|---|---|---|---|---|---|---|---|---|
| 1.2 | 261 | 261 | 1600 | 362.6 | 362.6 | 124 | 124 | 972 | 343.2 | 343.2 | 352.9 | 352.9 | 0.00 | 0.00 |
| 1.2 | 255 | 260 | 1305 | 326.5 | 322.7 | 169 | 200 | 1406 | 353.1 | 325.0 | 339.8 | 323.8 | 1.20 | 8.64 |
| 1.2 | 197 | 205 | 1000 | 324.9 | 316.9 | 131 | 136 | 1084 | 352.2 | 346.0 | 338.6 | 331.5 | 2.51 | 1.80 |
| 1.2 | 199 | 207 | 1025 | 327.8 | 319.9 | 180 | 187 | 1514 | 354.9 | 348.6 | 341.4 | 334.3 | 2.46 | 1.82 |
| 1.2 | 194 | 202 | 1037 | 335.2 | 327.2 | 186 | 193 | 1624 | 361.2 | 355.0 | 348.2 | 341.1 | 2.47 | 1.73 |
| 1.1 | 394 | 383 | 1638 | 285.0 | 290.6 | 213 | 195 | 1373 | 310.6 | 325.3 | 297.8 | 308.0 | 1.95 | 4.52 |
| 1.1 | 306 | 288 | 1300 | 289.3 | 301.4 | 258 | 248 | 1707 | 314.9 | 321.5 | 302.1 | 311.5 | 4.02 | 2.05 |
| 1.1 | 230 | 221 | 1000 | 293.9 | 301.9 | 204 | 196 | 1308 | 309.7 | 316.4 | 301.8 | 309.1 | 2.64 | 2.11 |
| 1.1 | 351 | 331 | 1534 | 295.0 | 306.7 | 235 | 220 | 1511 | 310.2 | 321.1 | 302.6 | 313.9 | 3.83 | 3.42 |
| 1.1 | 298 | 286 | 1278 | 291.2 | 299.4 | 254 | 244 | 1597 | 306.4 | 313.1 | 298.8 | 306.3 | 2.75 | 2.14 |
| 1.1 | 230 | 230 | 985 | 290.9 | 290.9 | 248 | 248 | 1551 | 305.5 | 305.5 | 298.2 | 298.2 | 0.00 | 0.00 |
| 1.1 | 328 | 315 | 1376 | 286.8 | 294.9 | 210 | 195 | 1283 | 301.6 | 314.0 | 294.2 | 304.4 | 2.74 | 3.93 |
| 1.1 | 360 | 360 | 1476 | 282.2 | 282.2 | 247 | 247 | 1471 | 297.4 | 297.4 | 289.8 | 289.8 | 0.00 | 0.00 |
| 1.1 | 317 | 333 | 1300 | 282.2 | 272.4 | 197 | 211 | 1169 | 296.8 | 285.3 | 289.5 | 278.9 | 3.62 | 4.01 |
| 1.1 | 237 | 246 | 1000 | 287.9 | 280.5 | 185 | 192 | 1135 | 302.3 | 296.1 | 295.1 | 288.3 | 2.66 | 2.09 |
| 1 | 381 | 396 | 1534 | 278.6 | 270.8 | 276 | 287 | 1406 | 271.4 | 264.8 | 275.0 | 267.8 | 2.85 | 2.46 |
| 1 | 329 | 329 | 1278 | 271.4 | 271.4 | 372 | 372 | 1892 | 271.1 | 271.1 | 271.2 | 271.2 | 0.00 | 0.00 |
| 1 | 452 | 452 | 1720 | 267.3 | 267.3 | 180 | 180 | 894 | 267.1 | 267.1 | 267.2 | 267.2 | 0.00 | 0.00 |
| 1 | 353 | 353 | 1389 | 274.0 | 274.0 | 172 | 172 | 889 | 273.8 | 273.8 | 273.9 | 273.9 | 0.00 | 0.00 |
| 1 | 367 | 352 | 1487 | 279.8 | 288.2 | 171 | 164 | 919 | 280.3 | 287.2 | 280.1 | 287.7 | 2.90 | 2.43 |
| 1 | 328 | 315 | 1248 | 267.3 | 275.3 | 264 | 256 | 1315 | 267.6 | 272.7 | 267.4 | 274.0 | 2.94 | 1.88 |
| 1 | 452 | 434 | 1745 | 270.2 | 278.3 | 281 | 270 | 1414 | 269.3 | 276.0 | 269.7 | 277.1 | 2.92 | 2.41 |
| 1 | 298 | 286 | 1189 | 276.8 | 285.0 | 298 | 286 | 1559 | 275.8 | 282.6 | 276.3 | 283.8 | 2.88 | 2.42 |
| 1 | 349 | 337 | 1374 | 274.1 | 281.1 | 287 | 266 | 1475 | 272.8 | 285.5 | 273.5 | 283.3 | 2.49 | 4.44 |
| 1 | 367 | 367 | 1452 | 275.1 | 275.1 | 312 | 312 | 1614 | 273.9 | 273.9 | 274.5 | 274.5 | 0.00 | 0.00 |
| 0.9 | 412 | 412 | 1376 | 241.2 | 241.2 | 277 | 277 | 1167 | 239.7 | 239.7 | 240.4 | 240.4 | 0.00 | 0.00 |

| $m_d$ (g) | $I_{U,M}$ (mV) | $I_{U,D}$ (mV) | $I_{o,U}$ (mV) | $C_{U,M}$ (g/m$^3$) | $C_{U,D}$ (g/m$^3$) | $I_{L,M}$ (mV) | $I_{L,D}$ (mV) | $I_{o,U}$ (mV) | $C_{L,M}$ (g/m$^3$) | $C_{L,D}$ (g/m$^3$) | $C_{Av.M}$ (g/m$^3$) | $C_{Av.D}$ (g/m$^3$) | $U_U$ (%) | $U_L$ (%) |
|---|---|---|---|---|---|---|---|---|---|---|---|---|---|---|
| 0.9 | 334 | 334 | 985 | 216.3 | 216.3 | 288 | 288 | 1199 | 237.7 | 237.7 | 227.0 | 227.0 | 0.00 | 0.00 |
| 0.9 | 407 | 423 | 1376 | 243.6 | 235.9 | 259 | 275 | 1111 | 242.7 | 232.7 | 243.2 | 234.3 | 3.27 | 4.29 |
| 0.9 | 428 | 445 | 1476 | 247.6 | 239.8 | 292 | 304 | 1282 | 246.6 | 239.9 | 247.1 | 239.8 | 3.25 | 2.80 |
| 0.9 | 518 | 539 | 1845 | 254.1 | 246.1 | 300 | 312 | 1372 | 253.4 | 246.8 | 253.7 | 246.5 | 3.23 | 2.65 |
| 0.9 | 393 | 393 | 1389 | 252.5 | 252.5 | 299 | 299 | 1345 | 250.6 | 250.6 | 251.6 | 251.6 | 0.00 | 0.00 |
| 0.9 | 377 | 377 | 1300 | 247.6 | 247.6 | 326 | 326 | 1427 | 246.1 | 246.1 | 246.8 | 246.8 | 0.00 | 0.00 |
| 0.9 | 364 | 349 | 1278 | 251.2 | 259.6 | 304 | 292 | 1363 | 250.1 | 256.8 | 250.6 | 258.2 | 3.24 | 2.61 |
| 0.9 | 450 | 429 | 1567 | 249.5 | 259.1 | 354 | 337 | 1569 | 248.1 | 256.4 | 248.8 | 257.7 | 3.69 | 3.20 |
| 0.9 | 391 | 375 | 1356 | 248.7 | 257.1 | 278 | 267 | 1225 | 247.2 | 253.9 | 247.9 | 255.5 | 3.25 | 2.65 |
| 0.8 | 556 | 534 | 1720 | 225.9 | 233.9 | 316 | 303 | 1213 | 224.2 | 231.2 | 225.0 | 232.6 | 3.45 | 3.03 |
| 0.8 | 463 | 480 | 1389 | 219.7 | 212.5 | 357 | 371 | 1341 | 220.6 | 214.2 | 220.1 | 213.3 | 3.39 | 2.99 |
| 0.8 | 501 | 521 | 1487 | 217.6 | 209.8 | 337 | 350 | 1224 | 215.0 | 208.7 | 216.3 | 209.2 | 3.73 | 3.02 |
| 0.8 | 417 | 434 | 1248 | 219.2 | 211.3 | 510 | 530 | 1873 | 216.8 | 210.4 | 218.0 | 210.8 | 3.78 | 3.05 |
| 0.8 | 594 | 634 | 1745 | 215.5 | 202.5 | 467 | 486 | 1677 | 213.1 | 206.4 | 214.3 | 204.5 | 6.44 | 3.22 |
| 0.8 | 391 | 391 | 1189 | 222.4 | 222.4 | 454 | 454 | 1696 | 219.7 | 219.7 | 221.0 | 221.0 | 0.00 | 0.00 |
| 0.8 | 457 | 457 | 1374 | 220.2 | 220.2 | 468 | 468 | 1727 | 217.6 | 217.6 | 218.9 | 218.9 | 0.00 | 0.00 |
| 0.8 | 516 | 516 | 1452 | 206.9 | 206.9 | 490 | 490 | 1729 | 210.1 | 210.1 | 208.5 | 208.5 | 0.00 | 0.00 |
| 0.8 | 465 | 446 | 1376 | 217.0 | 225.3 | 445 | 427 | 1671 | 220.5 | 227.4 | 218.7 | 226.4 | 3.70 | 3.03 |
| 0.8 | 473 | 454 | 1389 | 215.4 | 223.6 | 369 | 354 | 1406 | 223.0 | 229.9 | 219.2 | 226.8 | 3.67 | 3.01 |
| 0.7 | 542 | 520 | 1300 | 175.0 | 183.3 | 521 | 500 | 1724 | 199.4 | 206.3 | 187.2 | 194.8 | 4.52 | 3.32 |
| 0.7 | 535 | 509 | 1278 | 174.2 | 184.1 | 441 | 423 | 1452 | 198.6 | 205.6 | 186.4 | 194.8 | 5.41 | 3.38 |
| 0.7 | 628 | 628 | 1567 | 182.9 | 182.9 | 452 | 452 | 1480 | 197.7 | 197.7 | 190.3 | 190.3 | 0.00 | 0.00 |
| 0.7 | 519 | 540 | 1320 | 186.7 | 178.8 | 356 | 370 | 1195 | 201.8 | 195.4 | 194.3 | 187.1 | 4.44 | 3.29 |
| 0.7 | 526 | 547 | 1345 | 187.8 | 179.9 | 356 | 370 | 1202 | 202.8 | 196.4 | 195.3 | 188.2 | 4.35 | 3.27 |
| 0.7 | 451 | 466 | 1086 | 175.8 | 169.2 | 459 | 472 | 1443 | 190.9 | 186.3 | 183.3 | 177.7 | 3.87 | 2.50 |
| 0.7 | 456 | 456 | 1093 | 174.8 | 174.8 | 444 | 444 | 1363 | 186.9 | 186.9 | 180.9 | 180.9 | 0.00 | 0.00 |

| $m_d$ (g) | $I_{U,M}$ (mV) | $I_{U,D}$ (mV) | $I_{o,U}$ (mV) | $C_{U,M}$ (g/m$^3$) | $C_{U,D}$ (g/m$^3$) | $I_{L,M}$ (mV) | $I_{L,D}$ (mV) | $I_{o,U}$ (mV) | $C_{L,M}$ (g/m$^3$) | $C_{L,D}$ (g/m$^3$) | $C_{Av.M}$ (g/m$^3$) | $C_{Av.D}$ (g/m$^3$) | $U_U$ (%) | $U_L$ (%) |
|---|---|---|---|---|---|---|---|---|---|---|---|---|---|---|
| 0.7 | 691 | 691 | 1634 | 172.1 | 172.1 | 447 | 447 | 1348 | 184.0 | 184.0 | 178.0 | 178.0 | 0.00 | 0.00 |
| 0.7 | 589 | 565 | 1419 | 175.9 | 184.2 | 463 | 444 | 1429 | 187.8 | 194.8 | 181.8 | 189.5 | 4.52 | 3.58 |
| 0.7 | 643 | 617 | 1566 | 178.0 | 186.3 | 496 | 476 | 1551 | 190.0 | 196.9 | 184.0 | 191.6 | 4.43 | 3.48 |
| 0.6 | 629 | 604 | 1310 | 146.7 | 154.8 | 495 | 475 | 1283 | 158.7 | 165.6 | 152.7 | 160.2 | 5.24 | 4.15 |
| 0.6 | 580 | 580 | 1267 | 156.3 | 156.3 | 536 | 536 | 1471 | 168.3 | 168.3 | 162.3 | 162.3 | 0.00 | 0.00 |
| 0.6 | 535 | 535 | 1114 | 146.7 | 146.7 | 408 | 408 | 1169 | 175.4 | 175.4 | 161.1 | 161.1 | 0.00 | 0.00 |
| 0.6 | 512 | 532 | 1103 | 153.5 | 145.8 | 380 | 395 | 1135 | 182.4 | 175.9 | 167.9 | 160.9 | 5.26 | 3.67 |
| 0.6 | 588 | 612 | 1219 | 145.8 | 137.8 | 511 | 531 | 1456 | 174.5 | 168.1 | 160.2 | 153.0 | 5.81 | 3.81 |
| 0.6 | 514 | 535 | 1113 | 154.5 | 146.5 | 494 | 514 | 1485 | 183.4 | 176.8 | 169.0 | 161.7 | 5.47 | 3.74 |
| 0.6 | 544 | 566 | 1189 | 156.4 | 148.5 | 422 | 439 | 1282 | 185.2 | 178.6 | 170.8 | 163.5 | 5.34 | 3.69 |
| 0.6 | 592 | 592 | 1161 | 134.7 | 134.7 | 515 | 515 | 1372 | 163.3 | 163.3 | 149.0 | 149.0 | 0.00 | 0.00 |
| 0.6 | 499 | 499 | 1013 | 141.6 | 141.6 | 513 | 513 | 1345 | 160.6 | 160.6 | 151.1 | 151.1 | 0.00 | 0.00 |
| 0.6 | 538 | 516 | 1052 | 134.1 | 142.5 | 550 | 529 | 1427 | 158.9 | 165.4 | 146.5 | 153.9 | 5.86 | 3.92 |
| 0.5 | 696 | 678 | 1096 | 90.8 | 96.1 | 680 | 653 | 1363 | 115.9 | 122.6 | 103.4 | 109.3 | 5.46 | 5.51 |
| 0.5 | 718 | 701 | 1226 | 107.0 | 111.8 | 710 | 682 | 1569 | 132.2 | 138.9 | 119.6 | 125.3 | 4.29 | 4.83 |
| 0.5 | 907 | 882 | 1467 | 96.2 | 101.8 | 683 | 656 | 1414 | 121.3 | 128.0 | 108.7 | 114.9 | 5.49 | 5.25 |
| 0.5 | 778 | 778 | 1247 | 94.4 | 94.4 | 772 | 772 | 1559 | 117.1 | 117.1 | 105.7 | 105.7 | 0.00 | 0.00 |
| 0.5 | 929 | 929 | 1776 | 129.6 | 129.6 | 704 | 704 | 1475 | 123.3 | 123.3 | 126.4 | 126.4 | 0.00 | 0.00 |
| 0.5 | 916 | 938 | 1783 | 133.2 | 128.5 | 754 | 777 | 1614 | 126.8 | 121.8 | 130.0 | 125.1 | 3.70 | 4.11 |
| 0.5 | 908 | 927 | 1728 | 128.7 | 124.6 | 826 | 850 | 1723 | 122.5 | 117.8 | 125.6 | 121.2 | 3.33 | 4.05 |
| 0.5 | 919 | 933 | 1703 | 123.4 | 120.3 | 901 | 928 | 1821 | 117.3 | 112.4 | 120.3 | 116.3 | 2.51 | 4.38 |
| 0.5 | 938 | 963 | 1715 | 120.7 | 115.4 | 809 | 831 | 1608 | 114.5 | 110.0 | 117.6 | 112.7 | 4.56 | 4.06 |
| 0.5 | 932 | 932 | 1542 | 100.7 | 100.7 | 814 | 814 | 1694 | 122.1 | 122.1 | 111.4 | 111.4 | 0.00 | 0.00 |
| 0.4 | 1178 | 1178 | 1570 | 57.5 | 57.5 | 1100 | 1100 | 1797 | 81.8 | 81.8 | 69.6 | 69.6 | 0.00 | 0.00 |
| 0.4 | 1153 | 1138 | 1572 | 62.0 | 64.6 | 930 | 912 | 1561 | 86.3 | 89.6 | 74.2 | 77.1 | 4.05 | 3.64 |
| 0.4 | 1121 | 1107 | 1519 | 60.8 | 63.3 | 1033 | 1019 | 1723 | 85.3 | 87.5 | 73.0 | 75.4 | 3.97 | 2.60 |

| $m_d$ (g) | $I_{U,M}$ (mV) | $I_{U,D}$ (mV) | $I_{o,U}$ (mV) | $C_{U,M}$ (g/m$^3$) | $C_{U,D}$ (g/m$^3$) | $I_{L,M}$ (mV) | $I_{L,D}$ (mV) | $I_{o,U}$ (mV) | $C_{L,M}$ (g/m$^3$) | $C_{L,D}$ (g/m$^3$) | $C_{Av.M}$ (g/m$^3$) | $C_{Av.D}$ (g/m$^3$) | $U_U$ (%) | $U_L$ (%) |
|---|---|---|---|---|---|---|---|---|---|---|---|---|---|---|
| 0.4 | 1201 | 1188 | 1642 | 62.6 | 64.7 | 855 | 838 | 1441 | 87.0 | 90.3 | 74.8 | 77.5 | 3.36 | 3.70 |
| 0.4 | 1116 | 1116 | 1696 | 83.7 | 83.7 | 934 | 934 | 1502 | 79.2 | 79.2 | 81.4 | 81.4 | 0.00 | 0.00 |
| 0.4 | 1201 | 1201 | 1613 | 59.0 | 59.0 | 847 | 847 | 1397 | 83.4 | 83.4 | 71.2 | 71.2 | 0.00 | 0.00 |
| 0.4 | 1224 | 1243 | 1645 | 59.1 | 56.0 | 722 | 736 | 1179 | 81.7 | 78.5 | 70.4 | 67.3 | 5.50 | 4.08 |
| 0.4 | 1149 | 1166 | 1564 | 61.7 | 58.7 | 730 | 741 | 1210 | 84.2 | 81.7 | 72.9 | 70.2 | 5.00 | 3.05 |
| 0.4 | 1071 | 1089 | 1678 | 89.8 | 86.5 | 715 | 730 | 1179 | 83.4 | 79.9 | 86.6 | 83.2 | 3.86 | 4.33 |
| 0.4 | 1248 | 1248 | 1627 | 53.0 | 53.0 | 975 | 975 | 1537 | 75.9 | 75.9 | 64.4 | 64.4 | 0.00 | 0.00 |
| 0.3 | 1186 | 1186 | 1688 | 70.6 | 70.6 | 964 | 964 | 1423 | 64.9 | 64.9 | 67.7 | 67.7 | 0.00 | 0.00 |
| 0.3 | 1278 | 1267 | 1534 | 36.5 | 38.2 | 1056 | 1039 | 1474 | 55.6 | 58.3 | 46.0 | 48.3 | 4.52 | 4.64 |
| 0.3 | 1379 | 1368 | 1619 | 32.1 | 33.7 | 1076 | 1067 | 1467 | 51.7 | 53.1 | 41.9 | 43.4 | 4.75 | 2.64 |
| 0.3 | 1373 | 1361 | 1633 | 34.7 | 36.4 | 1211 | 1203 | 1674 | 54.0 | 55.1 | 44.3 | 45.8 | 4.82 | 2.01 |
| 0.3 | 1234 | 1234 | 1730 | 67.6 | 67.6 | 1160 | 1160 | 1697 | 63.4 | 63.4 | 65.5 | 65.5 | 0.00 | 0.00 |
| 0.3 | 1220 | 1220 | 1503 | 41.7 | 41.7 | 1237 | 1237 | 1777 | 60.4 | 60.4 | 51.0 | 51.0 | 0.00 | 0.00 |
| 0.3 | 1245 | 1257 | 1615 | 52.0 | 50.1 | 1128 | 1140 | 1607 | 59.0 | 57.2 | 55.5 | 53.7 | 3.83 | 3.08 |
| 0.3 | 1167 | 1181 | 1461 | 44.9 | 42.6 | 1190 | 1204 | 1784 | 67.5 | 65.5 | 56.2 | 54.0 | 5.61 | 2.97 |
| 0.3 | 1234 | 1248 | 1622 | 54.7 | 52.4 | 1323 | 1341 | 1705 | 42.3 | 40.0 | 48.5 | 46.2 | 4.30 | 5.63 |
| 0.3 | 1230 | 1246 | 1550 | 46.2 | 43.7 | 1254 | 1271 | 1733 | 53.9 | 51.7 | 50.1 | 47.7 | 5.92 | 4.34 |
| 0.2 | 1445 | 1438 | 1575 | 17.2 | 18.2 | 1230 | 1217 | 1590 | 42.8 | 44.6 | 30.0 | 31.4 | 5.34 | 3.97 |
| 0.2 | 1343 | 1338 | 1445 | 14.6 | 15.4 | 1321 | 1309 | 1682 | 40.3 | 41.8 | 27.5 | 28.6 | 4.85 | 3.64 |
| 0.2 | 1289 | 1303 | 1630 | 46.9 | 44.8 | 1366 | 1379 | 1775 | 43.7 | 42.1 | 45.3 | 43.4 | 4.82 | 3.75 |
| 0.2 | 1234 | 1226 | 1490 | 37.7 | 39.0 | 1277 | 1265 | 1619 | 39.5 | 41.1 | 38.6 | 40.1 | 3.34 | 3.83 |
| 0.2 | 1456 | 1456 | 1640 | 23.8 | 23.8 | 1250 | 1250 | 1608 | 42.0 | 42.0 | 32.9 | 32.9 | 0.00 | 0.00 |
| 0.2 | 1359 | 1359 | 1711 | 46.1 | 46.1 | 1310 | 1310 | 1694 | 42.8 | 42.8 | 44.5 | 44.5 | 0.00 | 0.00 |
| 0.2 | 1413 | 1421 | 1684 | 35.1 | 34.0 | 1486 | 1501 | 1797 | 31.7 | 30.0 | 33.4 | 32.0 | 3.32 | 5.58 |
| 0.2 | 1423 | 1435 | 1686 | 33.9 | 32.2 | 1599 | 1605 | 1955 | 33.5 | 32.9 | 33.7 | 32.6 | 5.21 | 1.90 |
| 0.2 | 1499 | 1511 | 1756 | 31.6 | 30.1 | 1285 | 1300 | 1605 | 37.1 | 35.1 | 34.4 | 32.6 | 5.31 | 5.51 |

## B.2 Reliability of gas concentration

In this section complete data of gas concentration reliability experiments is presented (Section B.2.4). An explanation of the symbols used in Tables B.1 to B.4 along with the conversion formulae is given in following:

### B.2.1 Explanation of the data symbols

| Data Symbol | Explanation |
|---|---|
| $V°_{T}$ (ln/hr) | Volumetric flowrate of the gas mixture (methane +air) |
| $V°_{CH4}$ (ln/hr) | Volumetric flowrate of methane |
| $V°_{Air}$ (ln/hr) | Volumetric flow rate of air |
| $Conc._{CH4, S.D}$ | Software determined concentration of methane |
| $Conc._{CH4, G.A}$ | Concentration of methane measured with the gas analyser |
| Colour code green | Values outside the uncertainty lines of gas analyser in the negative direction |
| Colour code yellow | Values outside the uncertainty lines of gas analyser in the positive direction |

### B.2.2 Flow time calculation for gas analyser

Suction flow rate of the gas = 0.2 ln/min = $3.33 \times 10^{-5}$ $m^3/s$

Cross-sectional area of the tube (5mm) = $1.96 \times 10^{-5}$ $m^2$

Length of the tube = 2m

Gas analyser Flow time $= \frac{\text{length x Cross-sectional area}}{\text{volumetric flowrate}}$ = 11.7 sec

### B.2.3 Inherent uncertainties

***Gas analyser***

Measurement range for methane = 0-10 vol.-%

Uncertainty = ±1 vol.-% of the full scale = ± 0.1vol.-% $CH_4$

***Flow controllers***

measurement range for methane = 2-200 ln/hr

Uncertainty = 0.3 % of full scale plus 0.5 % of the measured value

Uncertainty = 0.003x200 = 0.6 ln/hr + 0.5 % of the measured value

Calculated uncertainty range for all the tested flow rates = 0.03 Vol.% – 0.12 Vol.%

### B.2.4 Gas concentration reliability data

| $V°_T$ (ln/hr) | $V°_{CH4}$ (ln/hr) | $V°_{Air}$ (ln/hr) | $Conc._{CH4, S.D}$ (Vol.-%) | $Con._{CH4, G.A}$ (Vol.-%) |
|---|---|---|---|---|
| 2500 | 150 | 2350 | 6 | 5.95 |
| 2500 | 150 | 2350 | 6 | 6.03 |
| 2500 | 150 | 2350 | 6 | 5.9 |
| 2500 | 125 | 2375 | 5 | 5.2 |
| 2500 | 125 | 2375 | 5 | 5.05 |
| 2500 | 125 | 2375 | 5 | 5.1 |
| 2500 | 100 | 2400 | 4 | 4.07 |
| 2500 | 100 | 2400 | 4 | 3.9 |
| 2500 | 100 | 2400 | 4 | 3.94 |
| 2500 | 75 | 2425 | 3 | 3 |
| 2500 | 75 | 2425 | 3 | 3.08 |
| 2500 | 75 | 2425 | 3 | 3.1 |
| 2500 | 50 | 2450 | 2 | 2.06 |
| 2500 | 50 | 2450 | 2 | 1.84 |
| 2500 | 50 | 2450 | 2 | 2.05 |
| 2500 | 25 | 2475 | 1 | 1.05 |
| 2500 | 25 | 2475 | 1 | 0.92 |
| 2500 | 25 | 2475 | 1 | 0.85 |
| 2000 | 120 | 1880 | 6 | 6.1 |
| 2000 | 120 | 1880 | 6 | 6.13 |
| 2000 | 120 | 1880 | 6 | 6 |
| 2000 | 100 | 1900 | 5 | 5.09 |
| 2000 | 100 | 1900 | 5 | 4.92 |
| 2000 | 100 | 1900 | 5 | 4.88 |
| 2000 | 80 | 1920 | 4 | 4.07 |
| 2000 | 80 | 1920 | 4 | 4.18 |
| 2000 | 80 | 1920 | 4 | 3.89 |
| 2000 | 60 | 1940 | 3 | 3.1 |
| 2000 | 60 | 1940 | 3 | 3.02 |
| 2000 | 60 | 1940 | 3 | 3 |
| 2000 | 40 | 1960 | 2 | 2.15 |
| 2000 | 40 | 1960 | 2 | 2 |
| 2000 | 40 | 1960 | 2 | 2.02 |
| 2000 | 20 | 1980 | 1 | 0.93 |
| 2000 | 20 | 1980 | 1 | 0.98 |
| 2000 | 20 | 1980 | 1 | 1.06 |
| 1600 | 96 | 1504 | 6 | 5.98 |
| 1600 | 96 | 1504 | 6 | 6.06 |
| 1600 | 96 | 1504 | 6 | 6.08 |
| 1600 | 80 | 1520 | 5 | 5.19 |
| 1600 | 80 | 1520 | 5 | 4.93 |
| 1600 | 80 | 1520 | 5 | 5.09 |

| $V°_{T}$ (ln/hr) | $V°_{CH4}$ (ln/hr) | $V°_{Air}$ (ln/hr) | $Conc._{CH4, S.D}$ (Vol.-%) | $Con._{CH4, G.A}$ (Vol.-%) |
|---|---|---|---|---|
| 1600 | 64 | 1536 | 4 | 3.86 |
| 1600 | 64 | 1536 | 4 | 3.97 |
| 1600 | 64 | 1536 | 4 | 4.02 |
| 1600 | 48 | 1552 | 3 | 3 |
| 1600 | 48 | 1552 | 3 | 3.01 |
| 1600 | 48 | 1552 | 3 | 3.08 |
| 1600 | 32 | 1568 | 2 | 1.98 |
| 1600 | 32 | 1568 | 2 | 1.9 |
| 1600 | 32 | 1568 | 2 | 2.05 |
| 1600 | 16 | 1584 | 1 | 0.81 |
| 1600 | 16 | 1584 | 1 | 1.05 |
| 1600 | 16 | 1584 | 1 | 0.96 |
| 1300 | 78 | 1222 | 6 | 6.12 |
| 1300 | 78 | 1222 | 6 | 6.07 |
| 1300 | 78 | 1222 | 6 | 5.9 |
| 1300 | 65 | 1235 | 5 | 5 |
| 1300 | 65 | 1235 | 5 | 4.96 |
| 1300 | 65 | 1235 | 5 | 4.88 |
| 1300 | 52 | 1248 | 4 | 3.91 |
| 1300 | 52 | 1248 | 4 | 4.04 |
| 1300 | 52 | 1248 | 4 | 4.11 |
| 1300 | 39 | 1261 | 3 | 3.04 |
| 1300 | 39 | 1261 | 3 | 2.94 |
| 1300 | 39 | 1261 | 3 | 2.98 |
| 1300 | 26 | 1274 | 2 | 1.94 |
| 1300 | 26 | 1274 | 2 | 2.07 |
| 1300 | 26 | 1274 | 2 | 2.2 |
| 1300 | 13 | 1287 | 1 | 0.89 |
| 1300 | 13 | 1287 | 1 | 1.03 |
| 1300 | 13 | 1287 | 1 | 1.08 |
| 1000 | 60 | 940 | 6 | 5.98 |
| 1000 | 60 | 940 | 6 | 5.8 |
| 1000 | 60 | 940 | 6 | 5.93 |
| 1000 | 50 | 950 | 5 | 5.2 |
| 1000 | 50 | 950 | 5 | 4.87 |
| 1000 | 50 | 950 | 5 | 5.12 |
| 1000 | 40 | 960 | 4 | 4.14 |
| 1000 | 40 | 960 | 4 | 4.02 |
| 1000 | 40 | 960 | 4 | 3.96 |
| 1000 | 30 | 970 | 3 | 3.01 |
| 1000 | 30 | 970 | 3 | 2.93 |
| 1000 | 30 | 970 | 3 | 3.1 |
| 1000 | 20 | 980 | 2 | 1.81 |

| $V°_{T}$ (ln/hr) | $V°_{CH4}$ (ln/hr) | $V°_{Air}$ (ln/hr) | $Conc._{CH4, S.D}$ (Vol.-%) | $Con._{CH4, G.A}$ (Vol.-%) |
|---|---|---|---|---|
| 1000 | 20 | 980 | 2 | 2.06 |
| 1000 | 20 | 980 | 2 | 2.08 |
| 1000 | 10 | 990 | 1 | 1.13 |
| 1000 | 10 | 990 | 1 | 0.94 |
| 1000 | 10 | 990 | 1 | 0.91 |
| 700 | 42 | 658 | 6 | 5.83 |
| 700 | 42 | 658 | 6 | 6.06 |
| 700 | 42 | 658 | 6 | 6.11 |
| 700 | 35 | 665 | 5 | 4.92 |
| 700 | 35 | 665 | 5 | 4.89 |
| 700 | 35 | 665 | 5 | 5.1 |
| 700 | 28 | 672 | 4 | 4.01 |
| 700 | 28 | 672 | 4 | 3.97 |
| 700 | 28 | 672 | 4 | 4 |
| 700 | 21 | 679 | 3 | 2.93 |
| 700 | 21 | 679 | 3 | 2.93 |
| 700 | 21 | 679 | 3 | 2.98 |
| 700 | 14 | 686 | 2 | 2 |
| 700 | 14 | 686 | 2 | 1.9 |
| 700 | 14 | 686 | 2 | 2.07 |
| 700 | 7 | 693 | 1 | 1.05 |
| 700 | 7 | 693 | 1 | 1.11 |
| 700 | 7 | 693 | 1 | 0.96 |

## B.3 MEC of dusts

### B.3.1 MEC of lycopodium

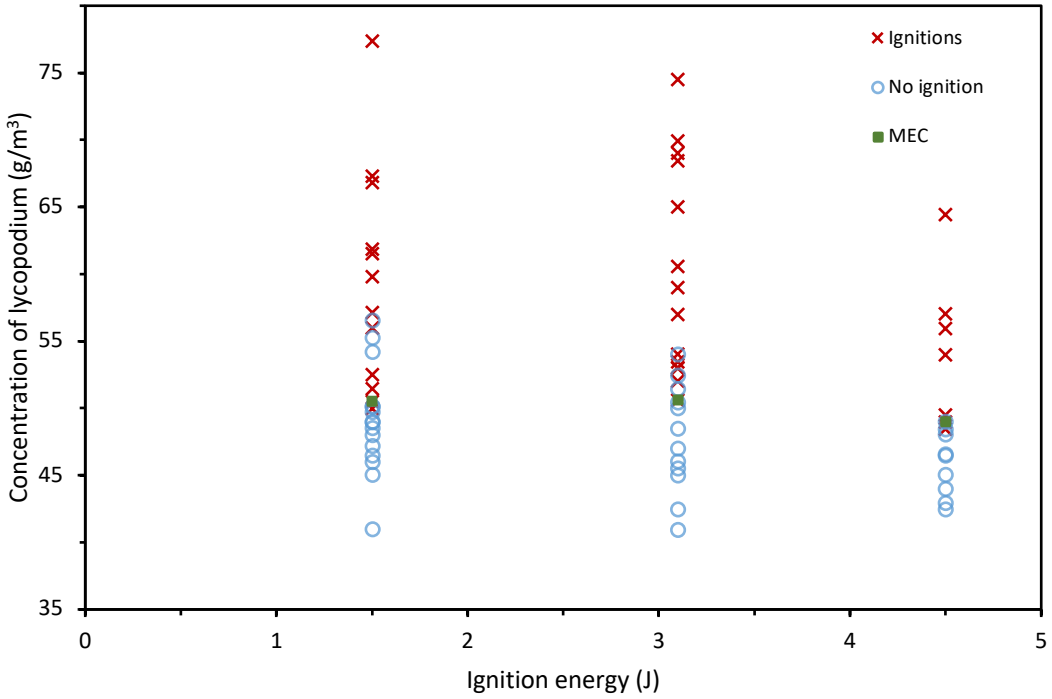


*Figure B.1: MEC of lycopodium at 13 cm/s*

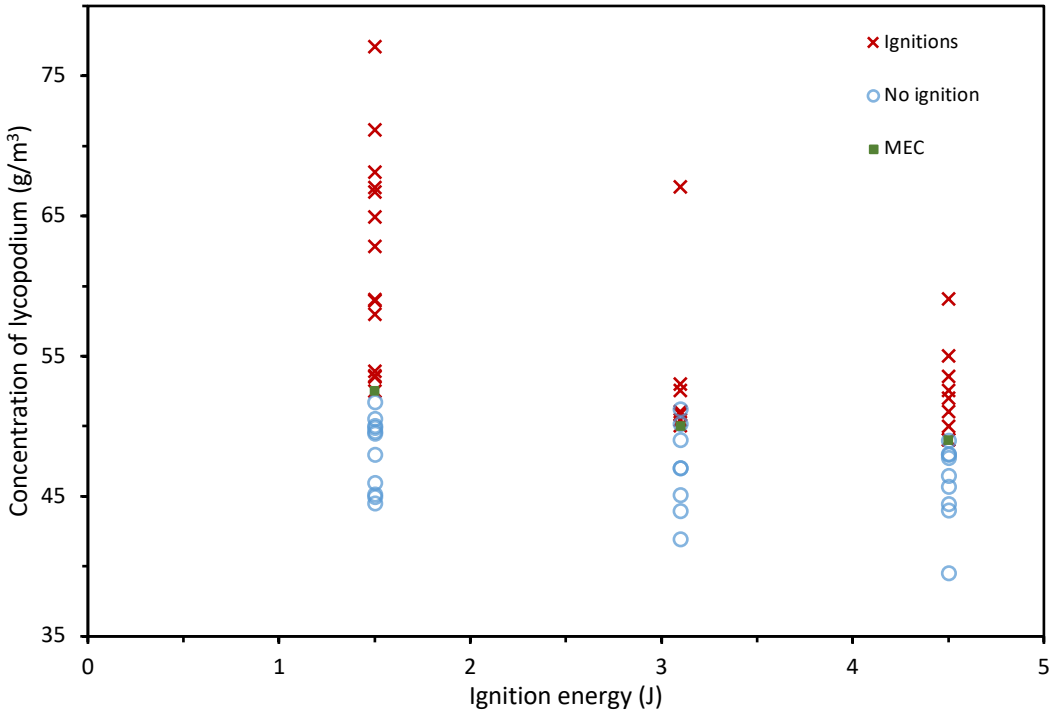


*Figure B.2: MEC of lycopodium at 9.5 cm/s*

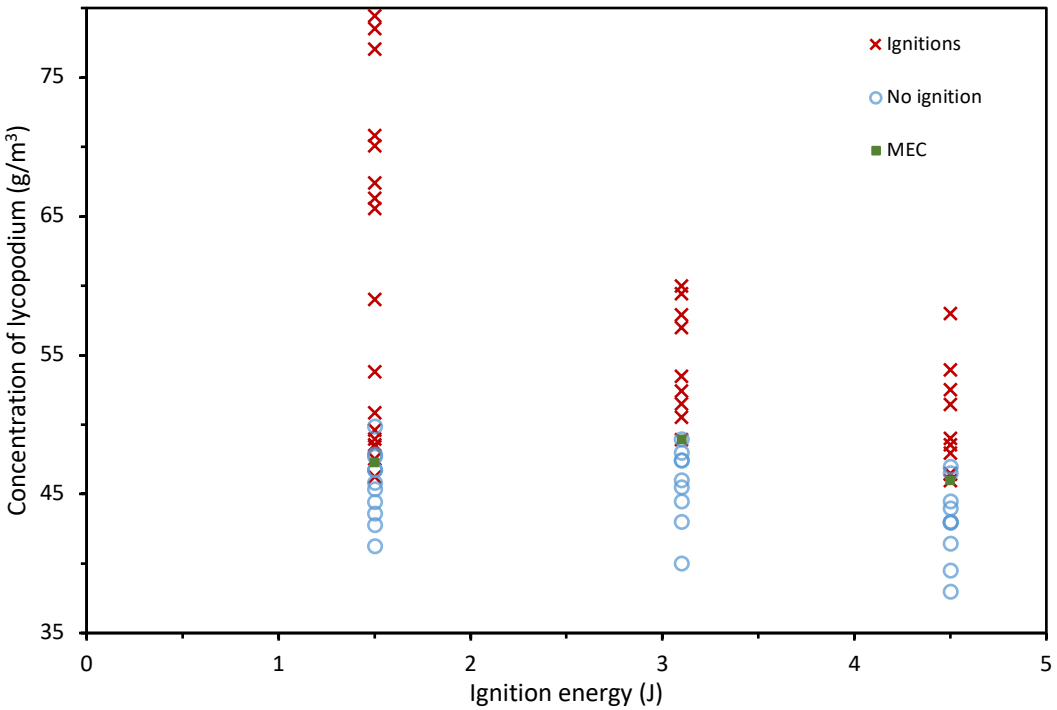


*Figure B.3: MEC of lycopodium at 7.14 cm/s*

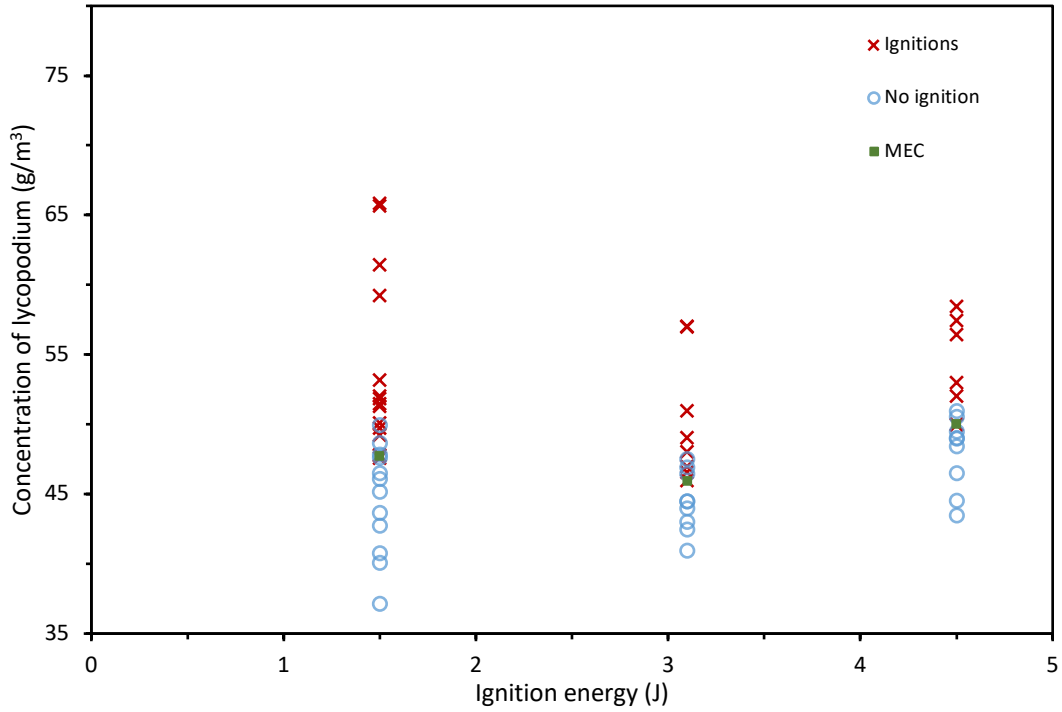


*Figure B.4: MEC of lycopodium at 4.8 cm/s*

### B.3.2 MEC of titanium

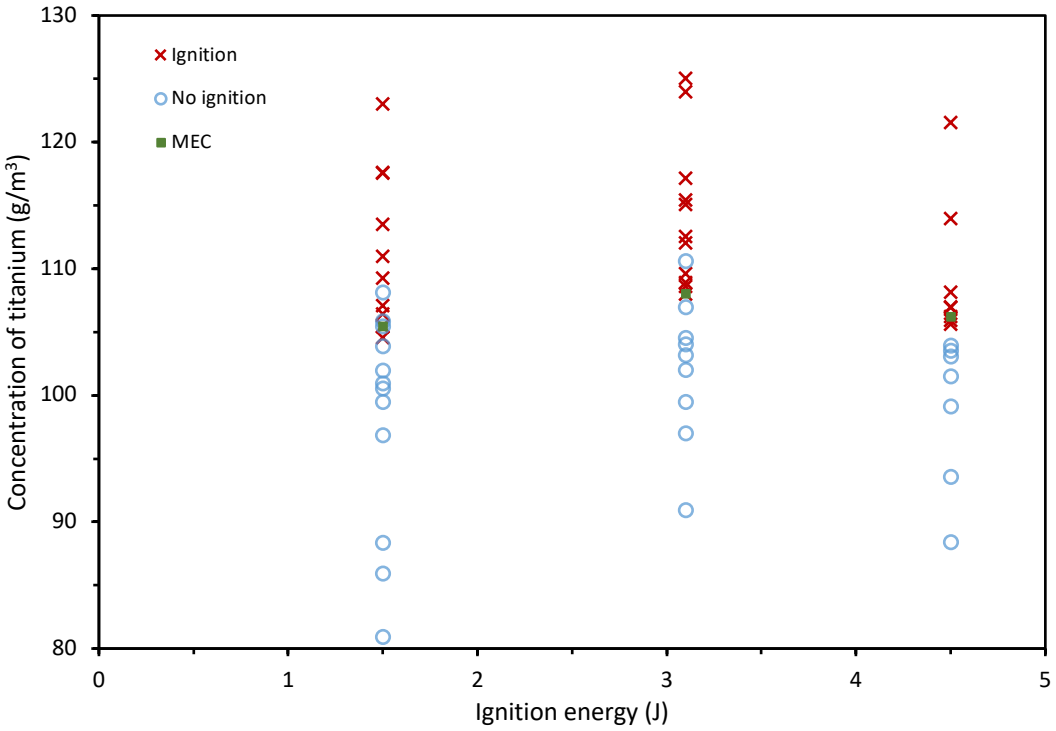


*Figure B.5: MEC of titanium at 20 cm/s*

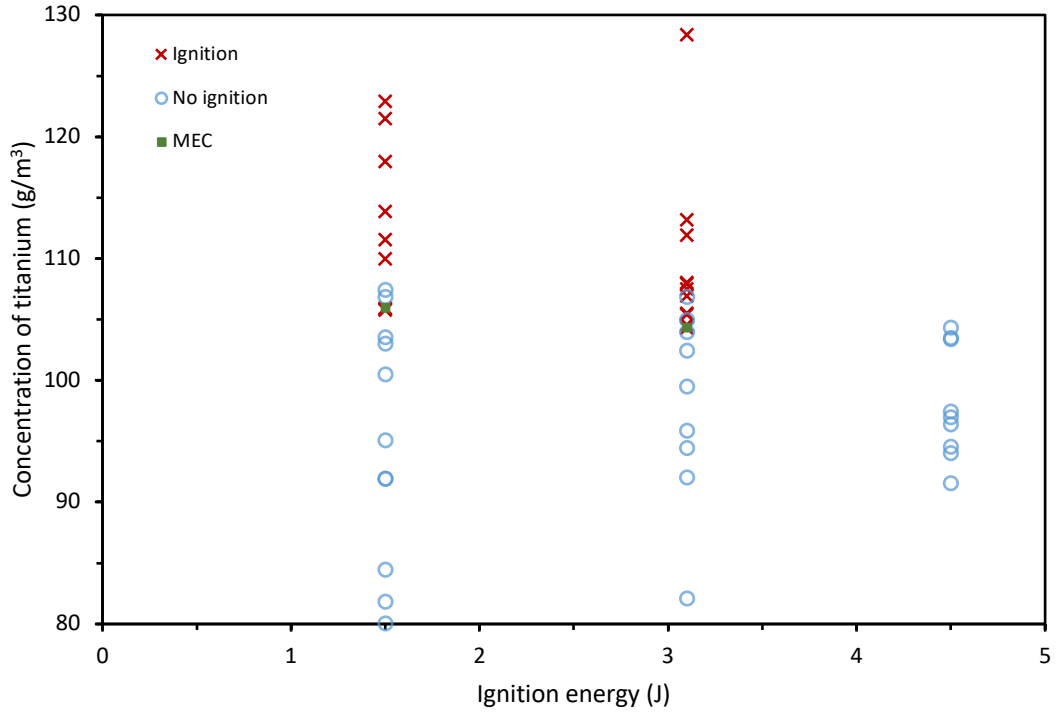


*Figure B.6: MEC of titanium at 16 cm/s*

## B.4 LEL of methane

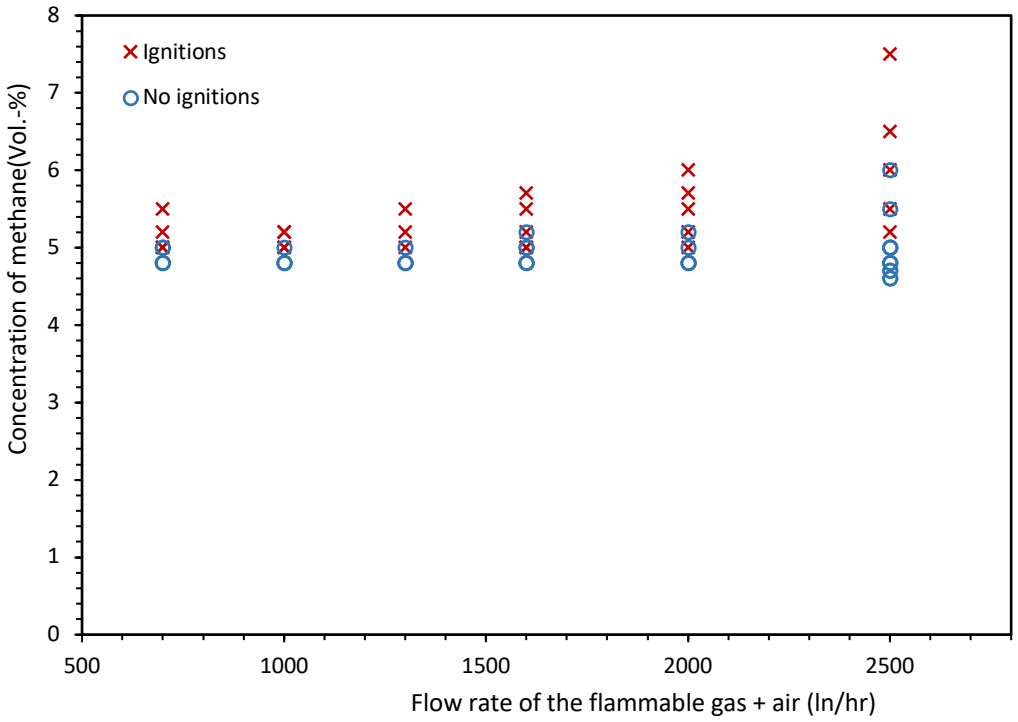

## B.5 LEL of hybrid mixture

### B.5.1 LEL of hybrid mixtures of lycopodium and methane

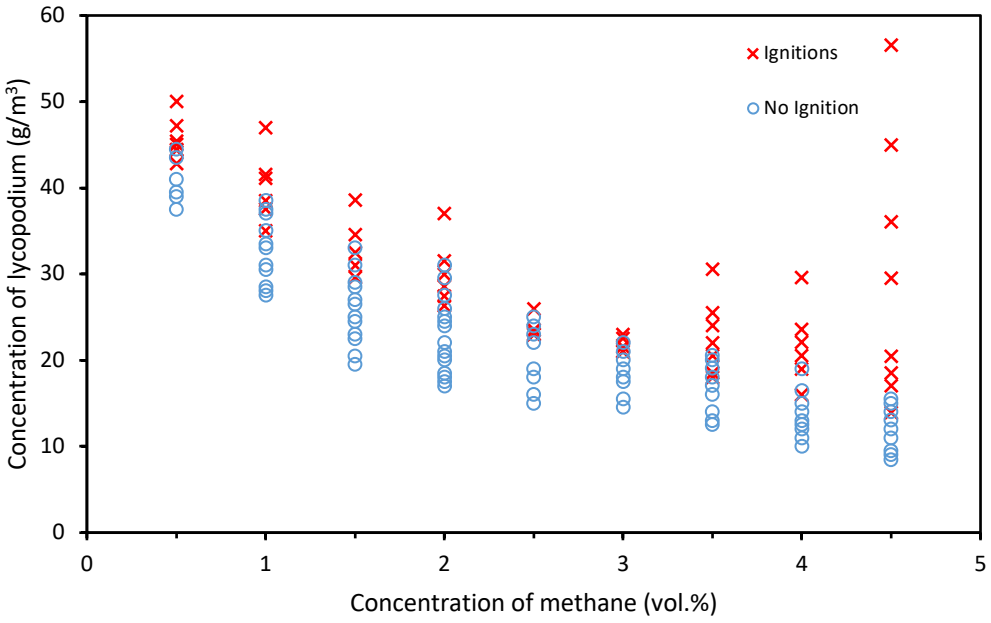


*Figure B.7: LEL of hybrid mixture of lycopodium and methane at flow velocity 13 cm/s and 50 ms spark duration*

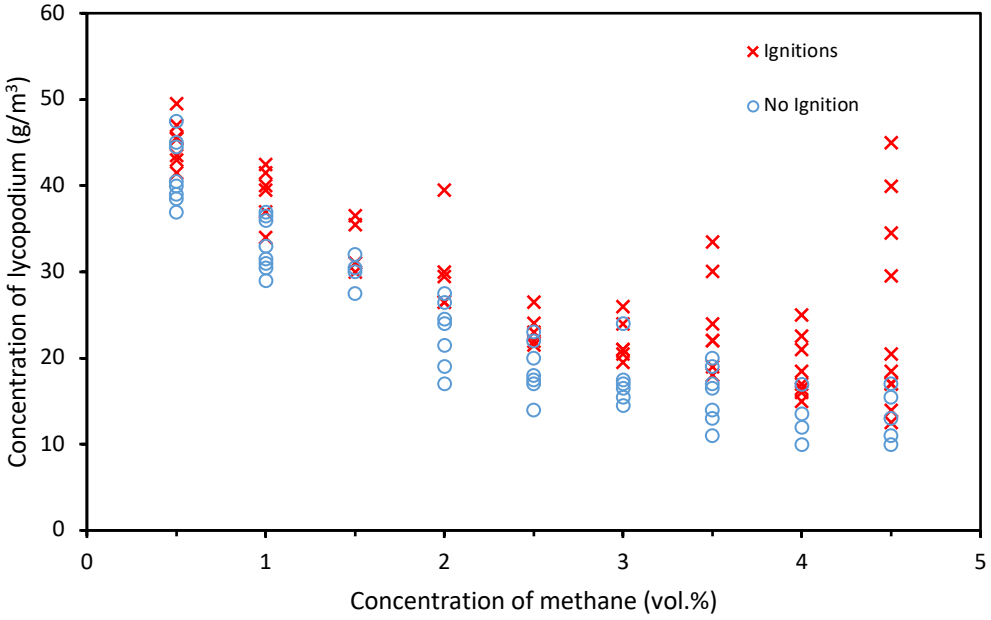


*Figure B.8: LEL of hybrid mixture of lycopodium and methane at flow velocity 13 cm/s and 100 ms spark duration*

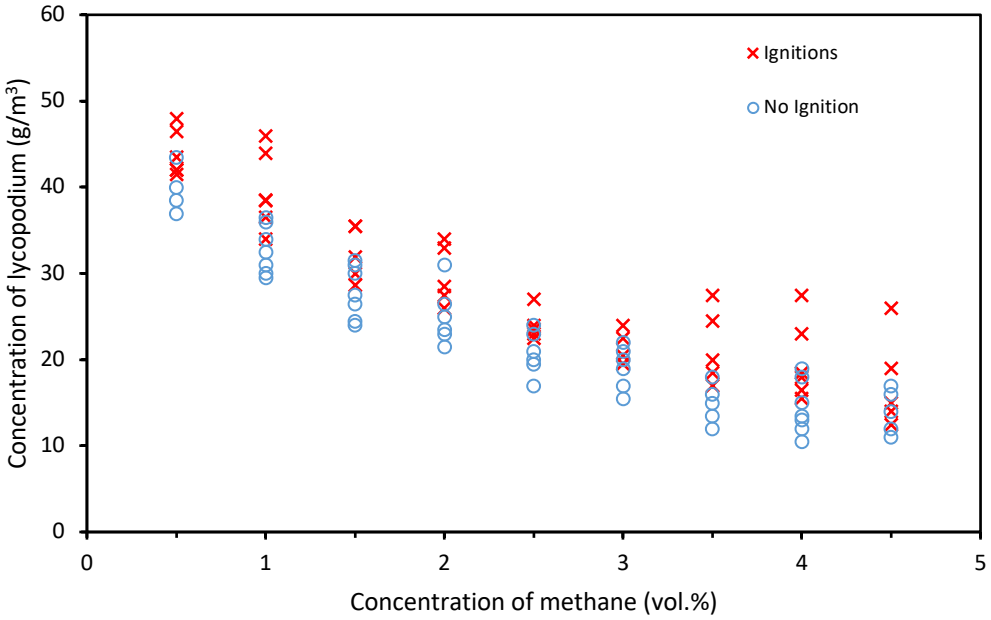


*Figure B.9: LEL of hybrid mixture of lycopodium and methane at flow velocity 13 cm/s and 150 ms spark duration*

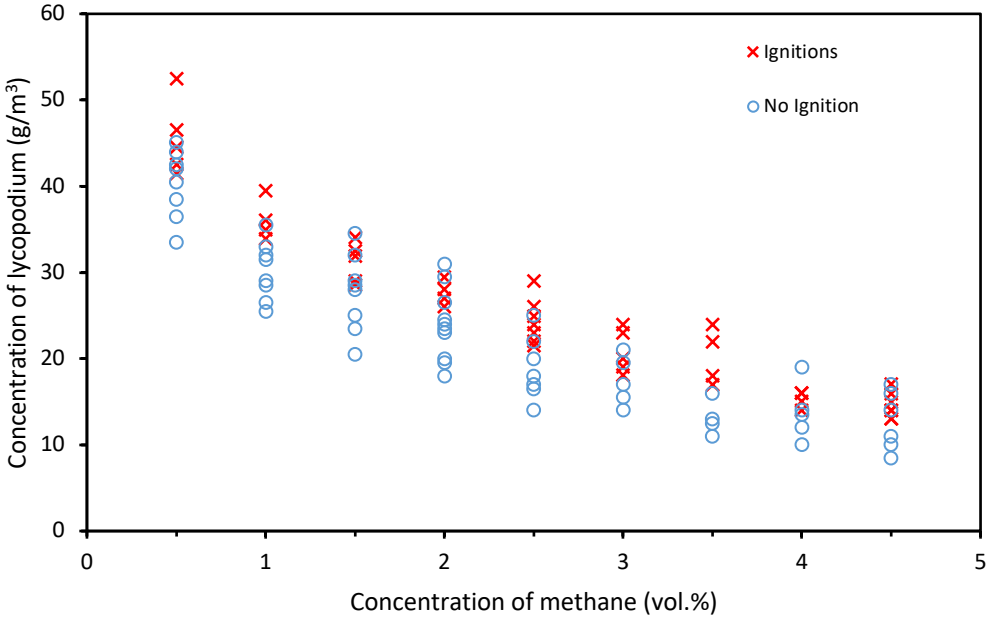


*Figure B.10: LEL of hybrid mixture of lycopodium and methane at flow velocity 9.5 cm/s and 50 ms spark duration*

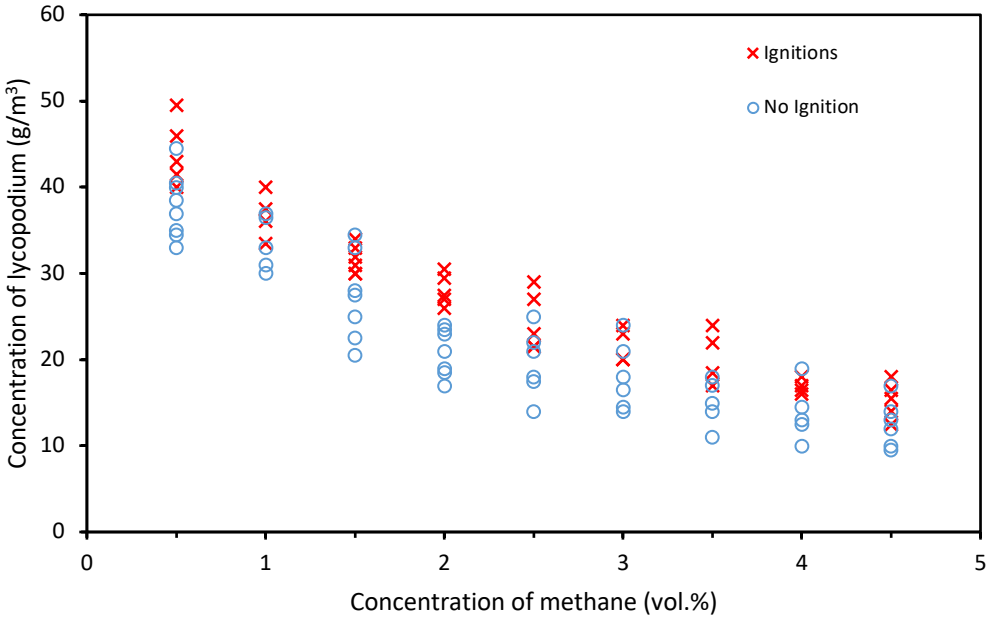


*Figure B.11: LEL of hybrid mixture of lycopodium and methane at flow velocity 9.5 cm/s and 100 ms spark duration*

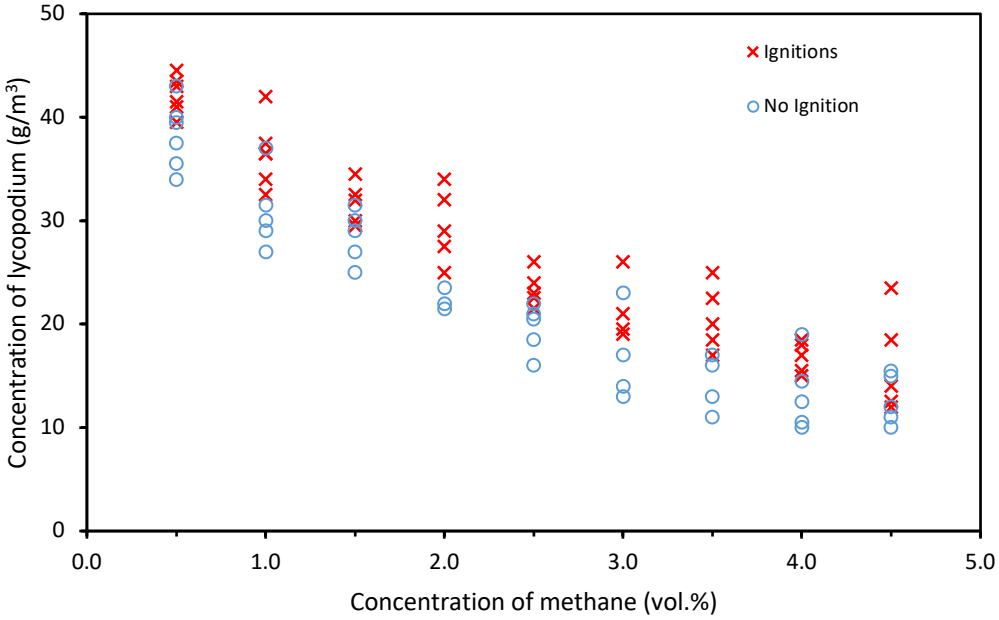


*Figure B.12: LEL of hybrid mixture of lycopodium and methane at flow velocity 9.5 cm/s and 150 ms spark duration*

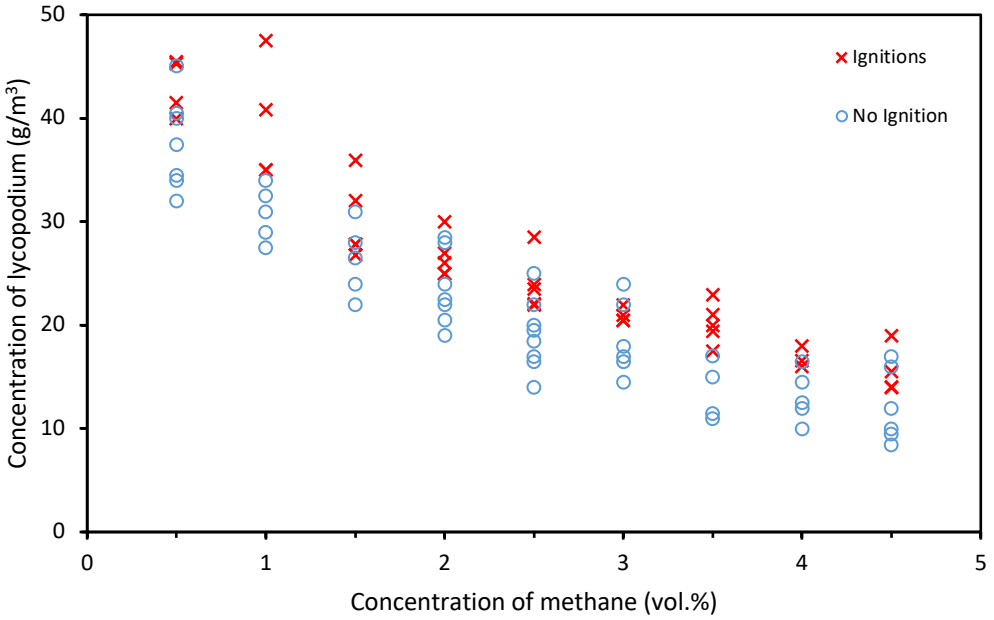


*Figure B.13: LEL of hybrid mixture of lycopodium and methane at flow velocity 7.14 cm/s and 50 ms spark duration*

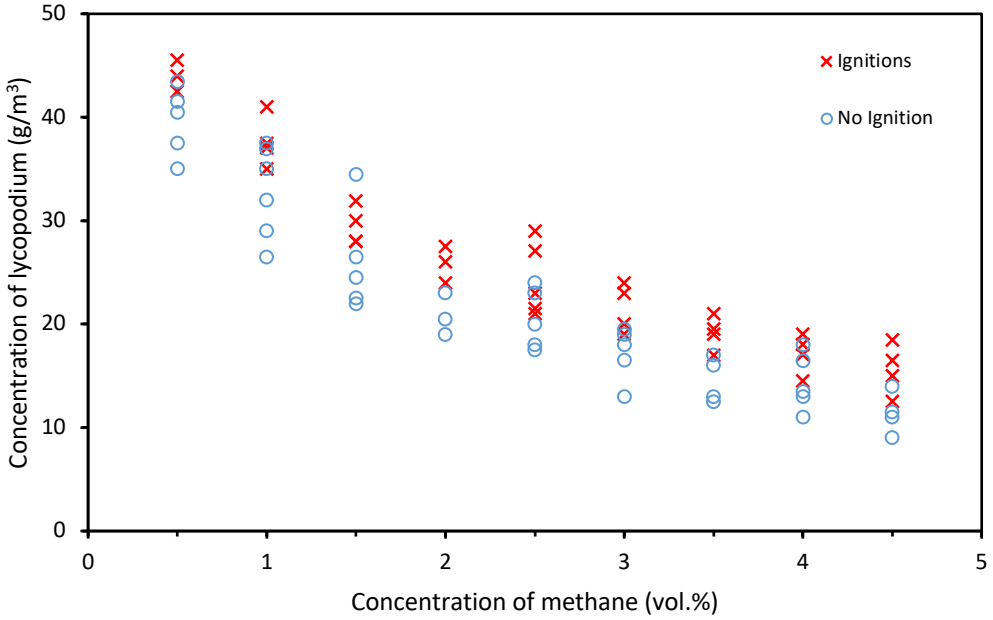


*Figure B.14: LEL of hybrid mixture of lycopodium and methane at flow velocity 7.14 cm/s and 100 ms spark duration*

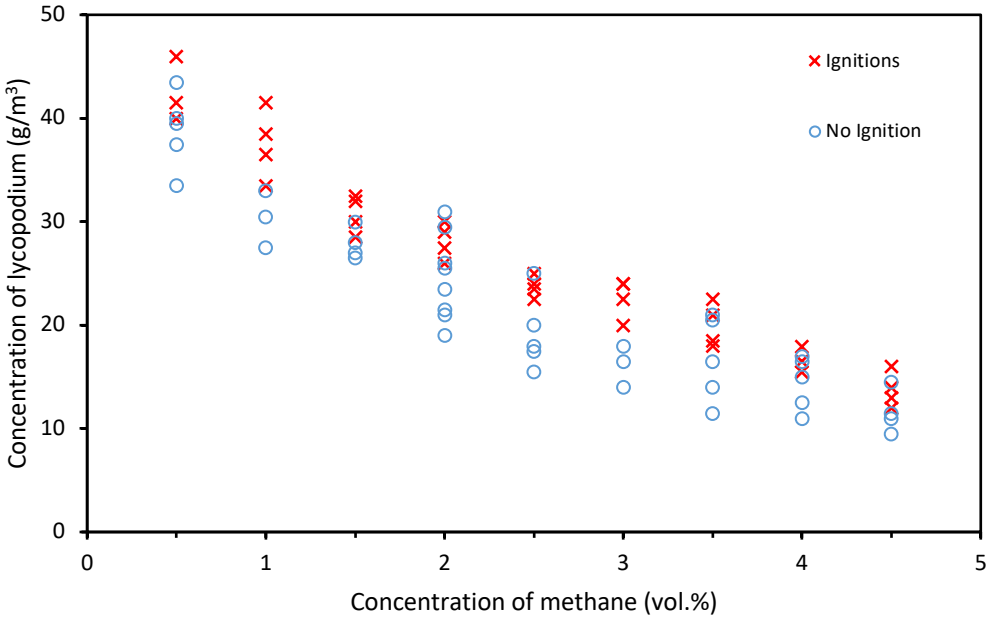


*Figure B.15: LEL of hybrid mixture of lycopodium and methane at flow velocity 7.14 cm/s and 150 ms spark duration*

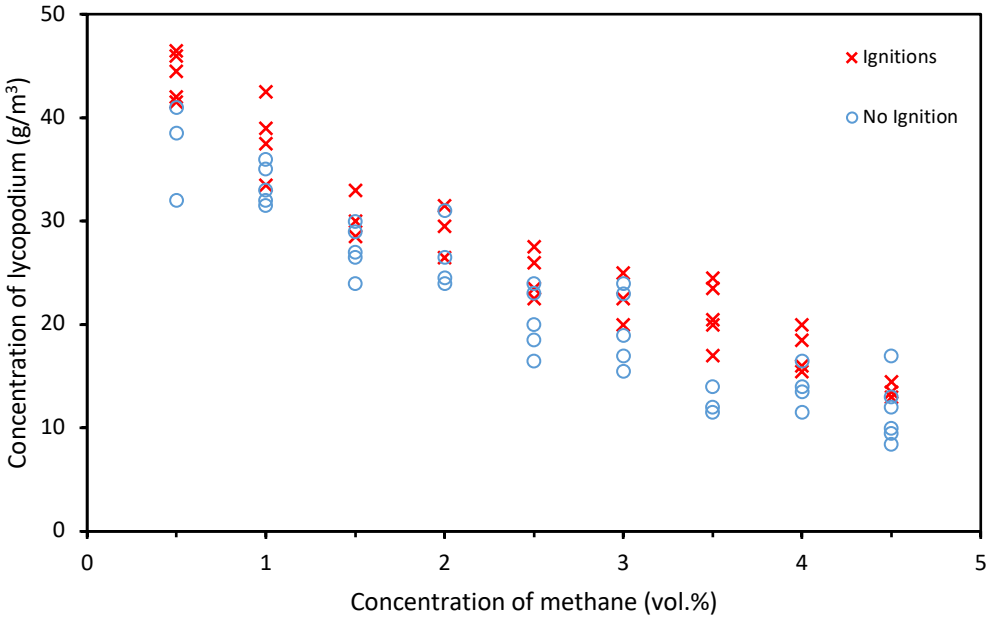


*Figure B.16: LEL of hybrid mixture of lycopodium and methane at flow velocity 4.8 cm/s and 50 ms spark duration*

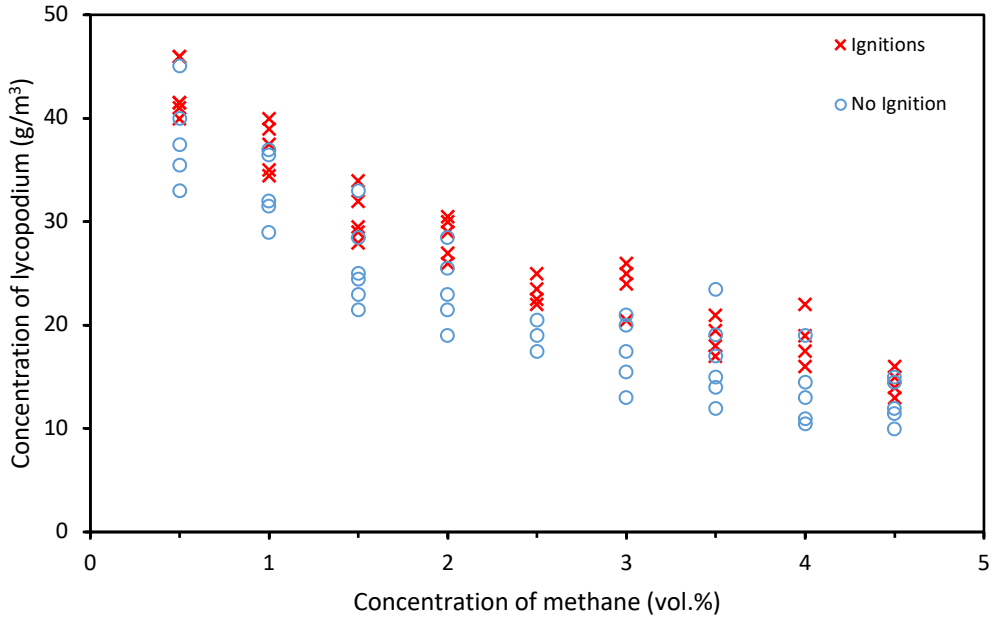


*Figure B.17: LEL of hybrid mixture of lycopodium and methane at flow velocity 4.8 cm/s and 100 ms spark duration*

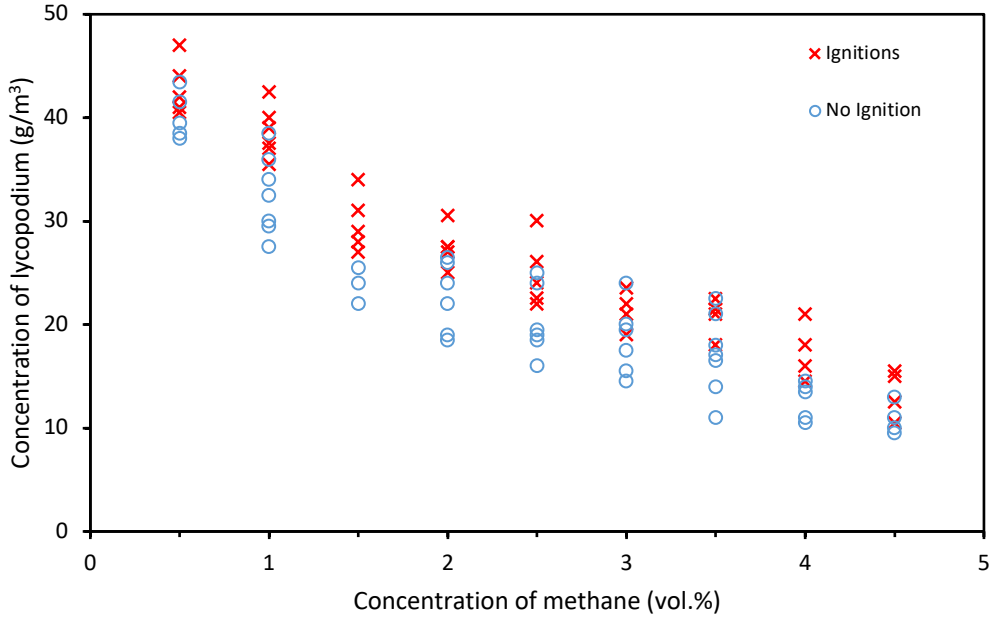


*Figure B.18: LEL of hybrid mixture of lycopodium and methane at flow velocity 4.8 cm/s and 150 ms spark duration*

## B.5.2 Uncertainties associated with the LEL of hybrid mixtures of lycopodium and methane

*Table B.1: LEL of hybrid mixtures of lycopodium and methane*

| | **Concentration of lycopodium (g/m$^3$) ±Uncertainty (g/m$^3$)** | | | | | | | | | | | | |
|---|---|---|---|---|---|---|---|---|---|---|---|---|---|
| **Flow velocity** | 4.8 cm/s | | | 7.14 cm/s | | | 9.5 cm/s | | | 13 cm/s | | | |
| **Ignition energy** | 1.5 J | 3.1 J | 4.5 J | 1.5 J | 3.1 J | 4.5 J | 1.5 J | 3.1 J | 4.5 J | 1.5 J | 3.1 J | 4.5 J | **Gas** |
| | 13 ±3 | 13 ±4 | 11 ±3 | 14 ±4 | 13 ±3 | 12 ±4 | 13 ±3 | 13 ±3 | 12 ±3 | 14 ±2 | 13 ±2 | 13 ±3 | **4.5** |
| | 15 ±4 | 16 ±2 | 15 ±4 | 16 ±3 | 15 ±4 | 15 ±4 | 15 ±3 | 16 ±4 | 15 ±3 | 16 ±4 | 15 ±4 | 15 ±3 | **4** |
| | 17 ±4 | 17 ±3 | 18 ±3 | 18 ±4 | 17 ±4 | 18 ±3 | 17 ±4 | 17 ±4 | 17 ±3 | 18 ±3 | 18 ±4 | 17 ±4 | **3.5** |
| | 20 ±4 | 21 ±3 | 19 ±2 | 20 ±4 | 19 ±4 | 20 ±4 | 19 ±2 | 20 ±3 | 19 ±4 | 21 ±3 | 20 ±3 | 20 ±4 | **3** |
| | 23 ±3 | 22 ±3 | 22 ±4 | 22 ±3 | 21 ±5 | 23 ±4 | 22 ±3 | 22 ±3 | 22 ±4 | 23 ±4 | 22 ±5 | 23 ±4 | **2.5** |
| | 27 ±4 | 26 ±2 | 25 ±4 | 25 ±4 | 24 ±5 | 26 ±3 | 26 ±3 | 26 ±5 | 25 ±5 | 26 ±2 | 27 ±4 | 26 ±3 | **2** |
| | 29 ±2 | 28 ±3 | 27 ±5 | 28 ±3 | 28 ±2 | 29 ±2 | 29 ±4 | 30 ±5 | 30 ±4 | 30 ±3 | 30 ±5 | 29 ±4 | **1.5** |
| | 34 ±4 | 35 ±3 | 36 ±4 | 35 ±5 | 35 ±4 | 34 ±5 | 35 ±4 | 34 ±5 | 33 ±4 | 35 ±4 | 34 ±4 | 34 ±5 | **1** |
| | 42 ±4 | 40 ±5 | 41 ±5 | 40 ±4 | 43 ±5 | 40 ±4 | 42 ±4 | 40 ±6 | 40 ±5 | 43 ±4 | 42 ±4 | 42 ±6 | **0.5** |
| | 48 ±5 | 46 ±5 | 50 ±4 | 46 ±3 | 49 ±6 | 46 ±4 | 52 ±4 | 50 ±5 | 49 ±5 | 50 ±5 | 51 ±5 | 49 ±6 | **0** |

### B.5.3 LEL of hybrid mixtures of titanium and methane

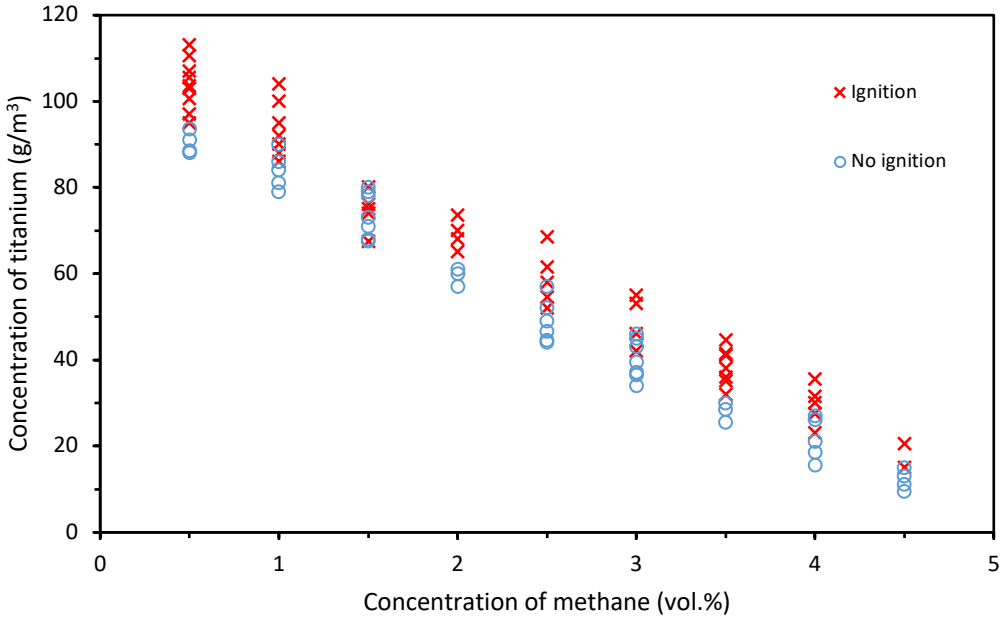


*Figure B.19: LEL of hybrid mixtures of titanium and methane at flow velocity 20 cm/s and 50 ms spark duration*

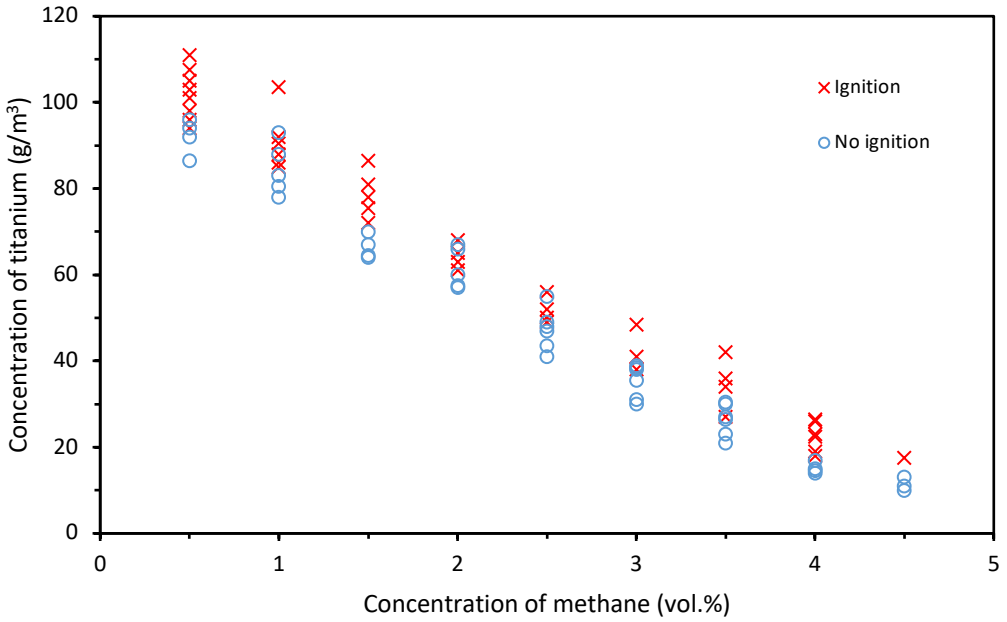


*Figure B.20: LEL of hybrid mixtures of titanium and methane at flow velocity 20 cm/s and 100 ms spark duration*

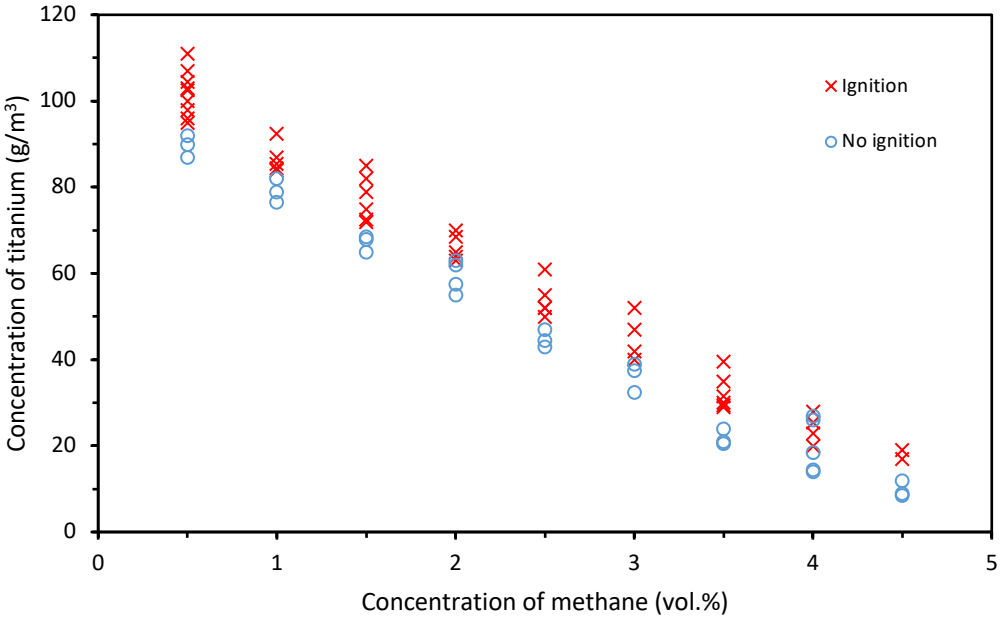


*Figure B.21: LEL of hybrid mixtures of titanium and methane at flow velocity 20 cm/s and 150 ms spark duration*

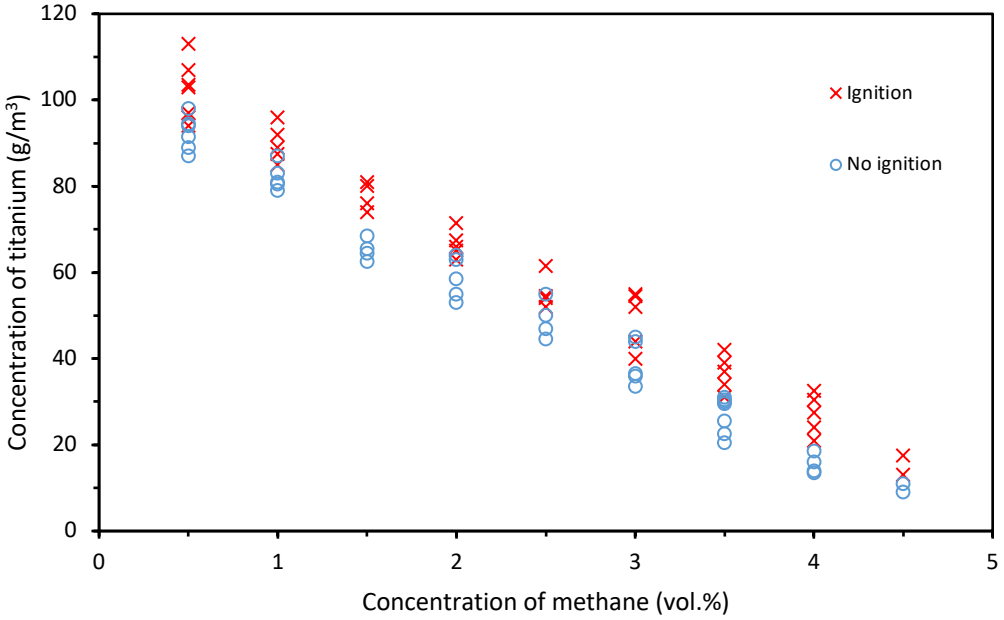


*Figure B.22: LEL of hybrid mixtures of titanium and methane at flow velocity 16 cm/s and 50 ms spark duration*

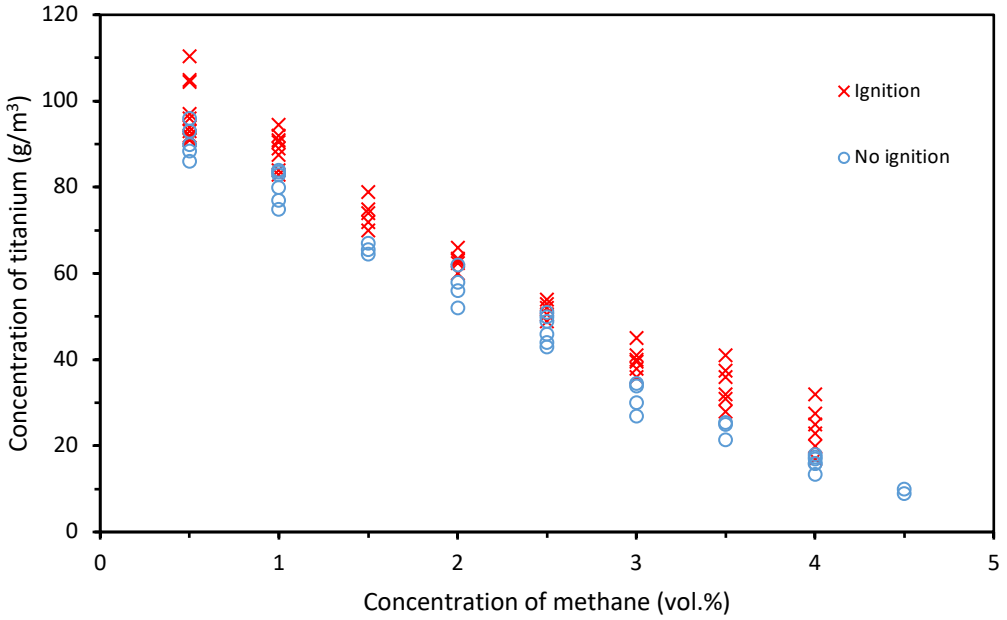


*Figure B.23: LEL of hybrid mixtures of titanium and methane at flow velocity 16 cm/s and 100 ms spark duration*

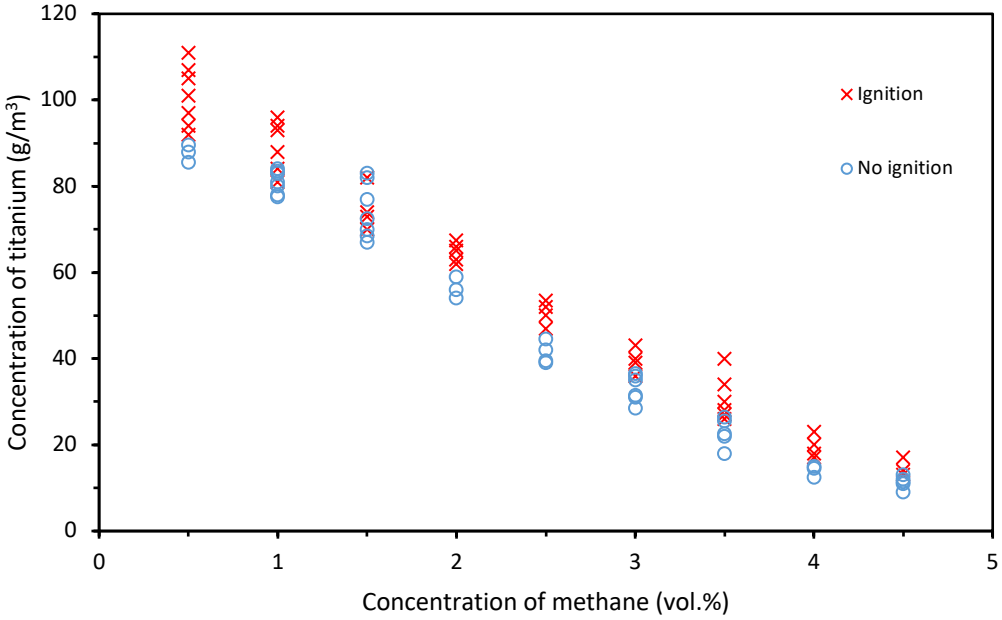


*Figure B.24: LEL of hybrid mixtures of titanium and methane at flow velocity 16 cm/s and 150 ms spark duration*

### B.5.4 Uncertainties associated with the LEL of hybrid mixtures of titanium and methane

*Table B.2: LEL of hybrid mixtures of titanium and methane*

| | **Concentration of titanium (g/m$^3$) ±Uncertainty (g/m$^3$)** | | | | | | |
|---|---|---|---|---|---|---|---|
| **Flow velocity** | 16 cm/s | | | 20 cm/s | | | |
| **Ignition energy** | 1.5 J | 3.1 J | 4.5 J | 1.5 J | 3.1 J | 4.5 J | **Gas** |
| | 13 ±2 | 11 ±4 | 12 ±4 | 15 ±6 | 13 ±4 | 13 ±4 | **4.5** |
| | 21 ±7 | 17 ±4 | 17 ±3 | 23 ±5 | 18 ±5 | 20 ±4 | **4** |
| | 31 ±6 | 28 ±4 | 26 ±5 | 32 ±6 | 27 ±5 | 29 ±4 | **3.5** |
| | 40 ±5 | 36 ±5 | 36 ±3 | 42 ±6 | 38 ±5 | 40 ±5 | **3** |
| | 52 ±5 | 49 ±5 | 47 ±4 | 52 ±7 | 49 ±4 | 50 ±5 | **2.5** |
| | 63 ±8 | 60 ±4 | 62 ±4 | 65 ±8 | 61 ±7 | 63 ±4 | **2** |
| | 74 ±6 | 70 ±5 | 70 ±5 | 75 ±8 | 73 ±6 | 72 ±6 | **1.5** |
| | 85 ±8 | 83 ±5 | 81 ±6 | 86 ±7 | 86 ±5 | 84 ±5 | **1** |
| | 94 ±6 | 91 ±5 | 92 ±5 | 95 ±9 | 94 ±5 | 95 ±7 | **0.5** |
| | 106 ±6 | 104 ±8 | 102 ±8 | 105 ±6 | 108 ±7 | 106 ±9 | **0** |

## B.6 Conversion formulas for concentration of dust and gas in the hybrid mixture

**Mass per unit volume to mole percent**

This was used to convert experimentally determined values of LEL of hybrid mixtures, where the dust concentration is measured in g/m$^3$ and gas concentration in vol. %. Starting with the experimentally determined concentrations of dust and gas, LEL of hybrid mixture could be expressed in mol. % using the conversion formulas listed in this section. Moreover, the values calculated by Bartknecht's formula and Le Chatelier's model were also converted in molar units using these formulas.

To express the LEL of hybrid mixtures in molar units, the values of $x_d$, $x_g$ and LEL (mol%) are required. Known parameters are concentration of dust $c_d$ (g/m$^3$) and concentration of gas $y_g$ (vol.%).

$$x_d = \frac{n_d}{n_f} \qquad\qquad x_g = \frac{n_g}{n_f}$$

Where $n_d$, $n_g$ and $n_f$ are molar densities (mol/m$^3$) of dust, gas and total fuel content and are given by:

$$n_d = \frac{c_d}{M.wt_d} \qquad n_g = \frac{y_g\ (vol.\%)}{100} \cdot \frac{\delta_g}{M.wt_g} \qquad n_f = n_d + n_g$$

Where $M.wt_d$ is the molecular weight of the dust and $\delta_g$ and $M.wt_g$ are the density and molecular weight of gas respectively. Since $c_d$, $M.wt_d$, $y_g$, $\delta_g$ and $M.wt_g$ are known $x_d$ and $x_g$ can be calculated.

To calculate the LEL of hybrid mixture in mol. % following formulas were used.

$$LEL_{hybrid} = \frac{n_f}{n_f + n_{air}}$$

Where $n_{air}$ is the molar density of air and is given by

$$n_{air} = \frac{(1 - y_g\ (vol.\%))}{100} \cdot \frac{\delta_{air}}{M.wt_{air}}$$

**Mole percent to mass per unit volume**

Equation 5.15 calculated the LEL of hybrid mixtures in mole percent of the total fuel content, where $x_d$ and $x_g$ are predefined by the user. In order to express the concentration of dust in g/m$^3$ and the concentration of gas in vol. % following formulas were used.

$$c_d = n_d.M.wt_d$$

$$n_d = n_f.x_d$$

$$n_f = \frac{n_{air} LEL_{hybrid}}{1 - LEL_{hybrid}}$$

$$n_{air} = \frac{(1 - y_g\ (vol.\%))}{100} . \frac{\delta_{air}}{M.wt_{air}}$$

Merging all these equations:

$$c_d = \frac{(1 - y_g\ (vol.\%))}{100} . \frac{\delta_{air}}{M.wt_{air}} . \frac{LEL_{hybrid}}{1 - LEL_{hybrid}} . x_d . M.wt_d$$

All the parameters on the right hand side of the above equation are known except $y_g$. $y_g$ is calculated as following:

$$LEL_{hybrid} = \frac{n_f}{n_f + n_{air}}$$

$$n_{air} = \frac{n_f\ (1 - LEL_{hybrid})}{LEL_{hybrid}}$$

Where $n_f = \frac{n_g}{x_g} = \frac{y_g\ (vol.\%)}{100} . \frac{\delta_g}{M.wt_g.x_g}$ and $n_{air} = \frac{(1 - y_g\ (vol.\%))}{100} . \frac{\delta_{air}}{M.wt_{air}}$. Combining these equations and solving for $y_g$ yields:

$$y_g\ (vol.\%) = \frac{1}{\left\{\frac{\delta_g M.wt_{air}}{M.wt_g x_g \delta_{air}} \left(\frac{1 - LEL_{hybrid}}{LEL_{hybrid}}\right)\right\} + 1}$$

Since all the parameters on the right hand side of above equation are known, $y_g$ can be calculated.